CONTROL DESIGN AND APPLICATION OF D-STATCOM FOR LOAD VOLTAGE CONTROL

Kittaya Somsai

A Thesis Submitted in Partial Fulfillment of the Requirements for the

Degree of Doctor of Philosophy in Electrical Engineering

Suranaree University of Technology

Academic Year 2012

การออกแบบระบบควบคุมและการประยุกต์ใช้งานอุปกรณ์ชดเชยซิงโครนัสแบบสถิตของระบบจำหน่ายสำหรับการรักษาระดับแรงดันไฟฟ้าที่โหลดบัส

นายกฤตยา สมสัย

วิทยานิพนธ์นี้เป็นส่วนหนึ่งของการศึกษาตามหลักสูตรปริญญาวิศวกรรมศาสตรดุษฎีบัณฑิต
สาขาวิชาวิศวกรรมไฟฟ้า
มหาวิทยาลัยเทคโนโลยีสุรนารี
ปีการศึกษา 2555

CONTROL DESIGN AND APPLICATION OF D-STATCOM FOR LOAD VOLTAGE CONTROL

Suranaree University of Technology has approved this thesis submitted in partial fulfillment of the requirements for the Degree of Doctor of Philosophy.

Thesis Examining Committee

(Dr.Nimit Chomnawang)
Chairperson

(Assoc. Prof. Dr.Thanatchai Kulworawanichpong)
Member (Thesis Advisor)

(Dr. Nitus Voraphonpiput)
Member

(Asst. Prof. Dr. Kongpan Areerak)
Member

(Dr. Pradit Fuangfoo)
Member

(Prof. Dr. Sukit Limpijumnong)
Vice Rector for Academic Affairs

(Assoc. Prof. Flt. Lt. Dr. Kontorn Chamniprasart)
Dean of Institute of Engineering

กฤตยา สมสัย : การออกแบบระบบควบคุมและการประยุกต์ใช้งานอุปกรณ์ชดเชยซิงโครนัสแบบสถิตของระบบจำหน่ายสำหรับการรักษาระดับแรงดันไฟฟ้าที่โหลดบัส (CONTROL DESIGN AND APPLICATION OF D-STATCOM FOR LOAD VOLTAGE CONTROL) อาจารย์ที่ปรึกษา : รองศาสตราจารย์ ดร.ธนัดชัย กุลวรวานิชพงษ์, 329 หน้า

งานวิจัยนี้นำเสนอแบบจำลองของระบบจำหน่ายและอุปกรณ์ชดเชยซิงโครนัสแบบสถิตบนแกนอ้างอิงซิงโครไนซ์ (*dq* Synchronous Rotating Reference Frame) โดยเลือกแกนอ้างอิงซึ่งเหมือนกับการควบคุมสนามแม่เหล็กหมุนที่ใช้สำหรับควบคุมมอเตอร์ไฟฟ้ากระแสสลับสามเฟส แบบจำลองในรูปแบบสมการปริภูมิสถานะถูกหาและถูกนำมาใช้ในการวิเคราะห์ผลกระทบต่อสมรรถนะเชิงพลวัตของระบบจากพารามิเตอร์ต่างๆ ของระบบจำหน่ายและอุปกรณ์ชดเชยซิงโครนัสแบบสถิตพร้อมทั้งนำไปสู่การวิเคราะห์ความสัมพันธ์ของพารามิเตอร์และสมรรถนะในสภาวะคงตัวอีกด้วย สมการปริภูมิสถานะยังนำไปใช้สำหรับการออกแบบระบบควบคุมสำหรับการควบคุมกระแสและการควบคุมแรงดันไฟฟ้าทั้งแรงดันไฟฟ้ากระแสตรงและแรงดันไฟฟ้ากระแสสลับ เทคนิคการควบคุมแบบแยกผลกระทบระหว่างกระแสจริงและกระแสรีแอกตีฟถูกใช้สำหรับการควบคุมกระแส พารามิเตอร์ของตัวควบคุมนี้ถูกหาโดยใช้วิธีการของ Symmetrical Optimum และการค้นหาแบบ Genetic Algorithms ซึ่งการควบคุมแบบแยกผลกระทบบนหลักการค้นหาแบบ Genetic Algorithms ให้ผลตอบสนองเชิงพลวัตดีที่สุดที่ส่วนเผื่อเสถียรภาพอัตราขยายและเฟสเท่ากันกับวิธีการของ Symmetrical Optimum ในขณะที่การควบคุมแบบลดผลกระทบของกระแสรีแอคตีฟถูกนำเสนอสำหรับการควบคุมแรงดันไฟฟ้ากระแสตรง พารามิเตอร์ของตัวควบคุมแรงดันไฟฟ้ากระแสตรงถูกหาโดยใช้วิธีการของ Symmetrical Optimum และการค้นหาแบบ Genetic Algorithms ซึ่งการควบคุมที่นำเสนอนี้บนหลักการหาค่าพารามิเตอร์ด้วยวิธีการ Symmetrical Optimum ให้ผลตอบสนองเชิงพลวัตที่ดีและให้ส่วนเผื่อเสถียรภาพอัตราขยายมากที่สุด สำหรับการควบคุมแรงดันไฟฟ้ากระแสสลับ การออกแบบตัวควบคุมโดยการกำหนดสมรรถนะของระบบให้มีเสถียรภาพด้วยเทคนิค Loop Shaping ถูกนำมาใช้ แบบจำลองและวิธีการควบคุมที่ได้นำเสนอในงานวิจัยนี้ถูกตรวจสอบโดยการจำลองบนคอมพิวเตอร์โดยใช้ SIMULINK/MATLAB งานวิจัยนี้ได้ทำการศึกษาการประยุกต์ใช้งานอุปกรณ์ชดเชยซิงโครนัสแบบสถิตของระบบจำหน่ายในการรักษาระดับแรงดันไฟฟ้าของระบบที่มีโหลดแบบความต้านทานเพียงอย่างเดียว แบบความต้านทานต่ออนุกรมกับความเหนี่ยวนำ และระบบที่ต่อร่วมกับเครื่องกำเนิดไฟฟ้าระบบจำหน่าย ผลจากการจำลองแสดงให้เห็นว่า วิธีการควบคุมที่นำเสนอสามารถควบคุม

กระแสทั้งสองแยกอิสระต่อกันและสามารถลดทอนการพุ่งเกินของแรงดันไฟฟ้ากระแสตรงได้ นอกจากนี้ผลตอบสนองการควบคุมแรงดันไฟฟ้ากระแสสลับได้ผลเป็นที่น่าพอใจ

สาขาวิชาวิศวกรรมไฟฟ้า ลายมือชื่อนักศึกษา _____

ปีการศึกษา 2555 ลายมือชื่ออาจารย์ที่ปรึกษา_____

ลายมือชื่ออาจารย์ที่ปรึกษาร่วม_____

KITTAYA SOMSAI : CONTROL DESIGN AND APPLICATION OF D-STATCOM FOR LOAD VOLTAGE CONTROL. THESIS ADVISOR : ASSOC. PROF. THANATCHAI KULWORAWANICHPONG, Ph.D., 329 PP.

D-STATCOM/CURRENT CONTROL/DC VOLTAGE CONTROL/AC VOLTAGE CONTROL

In this research, the *dq* synchronous rotating reference frame similar to that used for the field oriented control of three phase AC machines was applied to model the distribution system and the D-STATCOM. The state equations can be obtained and were used to analyze the effect of different parameters of the distribution system with D-STATCOM on dynamic system performance, and also to investigate the relation between the parameters and the steady state performance. These equations were used to design the current, DC voltage and AC voltage control system. In the current control system, the decoupling technique was exploited. Their controller parameters were obtained by using the symmetrical optimum and genetic algorithms. The decoupling current control based on the genetic algorithms gives the best dynamic response with the same gain and phase stability margins. In the DC voltage control, the elimination of the effects of the reactive current was proposed. Similar to the current control, their controller parameters were also obtained by the symmetrical optimum and genetic algorithms. The proposed control based on the symmetrical optimum gives good dynamic response and the best gain stability margin. In the outer loop, the AC voltage control system, the loop shaping technique was employed to

stabilize the system performances and to ensure the gain margin within the desired specification. The proposed D-STATCOM and its control were verified by SIMULIK/MATLAB simulation. The applications of the D-STATCOM for the load voltage regulation in the distribution system with purely resistive, inductive loads and distributed generators were presented. The research results indicated that the D-STATCOM with the proposed control can regulate both active and reactive currents separately. In addition, it can reduce the overshoot of the DC voltage responses. Furthermore, the satisfactory of the responses of the AC voltage control was found.

School of Electrical Engineering

Academic Year 2012

Student's signature _____

Advisor's signature _____

Co-Advisor's signature _____

ACKNOWLEDGEMENTS

I would like to acknowledge with gratitude the help, support and co-operation I received from many people during my research work. I would like to start with a tribute to my supervisor, Assoc. Prof. Dr Thanatchai Kulworawanichpong and co-supervisor, Dr Nitus Voraphonpiput, for their great supervision throughout the course of this study. Through their supervision, I have learned a lot especially how to be more prudent, selective, reasonable, non-judgmental, and critical. Their valuable feedback, comments, and suggestions have always been a source of guidance for me to improve my work.

I would like to express my grateful thanks to the Office of the Higher Education Commission, Thailand for the financial support under the Strategic Scholarships for Frontier Research Network for the Joint Ph.D. Program Thai Doctoral degree for this study.

I am deeply grateful to the committee members of both the proposal and thesis defense for their useful comments and suggestions. Many thanks go to the School of Electrical Engineering, Institute of Engineering, SUT, for the assistance, support, and the provision of facilities. I am also deeply indebted to staffs at RMUTI Sakon Nakhon Campus for giving their time and enthusiastic participation through my study. Without these, my work could not have been done successfully.

My heartfelt thanks go to my parents and brothers to their fantastic moral support and active encouragement. I also wish to express my appreciation and

indebtedness to Mrs. Surapa Somsai, my wife, Master Kittapat Somsai, my son, for their marvelous support and help during my study.

Last but absolutely not least, my appreciation also goes out to my friends at SUT; RMUTI, Sakon Nakhon Campus for any of their kind help.

Kittaya Somsai

TABLE OF CONTENTS

Page

TABLE OF CONTENTS (Continued)

Page

TABLE OF CONTENTS (Continued)

Page

TABLE OF CONTENTS (Continued)

Page

TABLE OF CONTENTS (Continued)

Page

TABLE OF CONTENTS (Continued)

Page

LIST OF TABLES

Table **Page**

LIST OF TABLES (Continued)

Table **Page**

LIST OF TABLES (Continued)

Table **Page**

LIST OF FIGURES

Figure **Page**

LIST OF FIGURES (Continued)

Figure **Page**

LIST OF FIGURES (Continued)

Figure **Page**

LIST OF FIGURES (Continued)

Figure **Page**

LIST OF FIGURES (Continued)

Figure **Page**

LIST OF FIGURES (Continued)

Figure **Page**

LIST OF FIGURES (Continued)

Figure **Page**

LIST OF FIGURES (Continued)

Figure **Page**

LIST OF FIGURES (Continued)

Figure **Page**

LIST OF FIGURES (Continued)

Figure **Page**

LIST OF FIGURES (Continued)

Figure **Page**

CHAPTER I

INTRODUCTION

In recent years, the main concern of consumers of electricity was the reliability of supply. The reliability is defined as the continuity of the electric supply. Even though the power generation in most developed countries is fairly reliable, the distribution is not always so. It is not only reliability that the consumers require in these days, bus also power quality is very important to them. For example, the consumers that are connected to the same bus that supplies a large motor load may have to face a severe voltage sags or dips in their supply. In some extreme cases, they may have to tolerate with blackouts. This is unacceptable to most customers. There are also very sensitive loads such as hospitals (life support, operation theatre and patient database system), processing plants (semiconductor, food, rayon and fabrics), air traffic control, financial institutions and many other data processing and service providers that require clean and uninterrupted power. In several processes such as semiconductor manufacturing or food processing plants, the products can be destroyed by voltage sag of very short duration. Such customers are very wary of such voltage sags since each such interruption cost them a substantial amount of money. Thus in this changed scenario in which the customers increasingly demand quality power, the term power quality (PQ) attains increased significance.

1.1 Power Quality Problems

Power quality problems are classified into six categories as transients, short duration voltage variation, long duration voltage variation, voltage imbalance, waveform distortion and voltage flicker. A brief description of the characteristics of category power quality problems is given next.

The transient is that part of change in a system variable that disappears during transition from one steady-state operating condition to another. Transients can be classified into two categories as impulsive transient and oscillatory transients. Impulsive transients do not travel very far from their point of entry. However an impulsive transient can give rise to an oscillatory transient. The oscillatory transient can lead to transient overvoltage and consequent damage to the power line insulators. Impulsive transients are usually suppressed by surge arresters.

Any variation in the supply voltage for duration not exceeding one minute is called a short duration voltage variation. Short duration variations are further classified as voltage sags, voltage swells and interruptions. Short duration voltage variations have varied effects on consumers. Voltage sags (also known as dips) can cause loss of production in automated processes since the voltage sag can trip a motor or cause its controller to malfunction. For semiconductor manufacturing industries such a loss can be substantial. The voltage sag can also force a computer system or data processing system to damage. Also voltage swells can put stress on computers and many home appliances, thereby shortening their lives. A temporary interruption lasting a few seconds can cause a loss of production, erasing of computer data etc. The case of such an interruption during peak hours can cost lots of money.

The long during voltage variations are defined as the RMS variations in the supply voltage at the fundamental frequency for periods exceeding 1 minute. These variations are classified into overvoltages, undervoltages and sustained interruptions. The impact of long duration voltage variations is greater than those of short duration variations. A sustained overvoltage lasting for few hours can cause damage to household appliances without their owner knowing it, until it is too late. The undervoltage has the same effect as that of the voltage sag. In the case of the voltage sag the termination of process is sudden. But normal operation can be resumed after the normal voltage is restored. However in the case of a sustained undervoltage, the process cannot even be started or resumed. The sustained interruption is usually caused by faults. Since the loss to customers due to any sustained interruption can cost lots of money, it is necessary for the utility to have a good preventive maintenance schedule and to have agreements or regulations to encourage high supply reliability.

Voltage imbalance is the condition in which the voltages of the three phases of the supply are not equal in magnitude. Furthermore, they may not even be equally displaced in time. The voltage imbalance can cause temperature rise in motors and can even cause a large motor to trip.

Waveform distortion is the steady-state deviation in the voltage or current waveform from an ideal sine wave. These distortions are classified as DC offset, harmonics and notching. DC offsets can cause saturation in the power transformer magnetic circuits. Harmornics can cause malfunction of ripple control or traffic control system, losses and heating in transformers, electromagnetic interference (EMI) and interference with the communication system. So, unwanted harmonic

currents flowing through the distribution network can causes needless losses. The notch is a periodic transient that rides on the supply voltage. It can damage capacitive components connected in shunt due to high rate of voltage rise at the notches.

A very rapid change in the supply voltage is called voltage flicker. This is caused by rapid variations in current magnitude of loads such as arc furnaces, arc discharge lamps, starting of large motors, arc welding machines etc. Therefore other customers that are supplied by the same feeder face regular severe voltage drops unless the supply bus is very stiff. The voltage flickers can cause the light intensity from incandescent lamps to vary and can have adverse effects on human health. The voltage flicker can also reduce the life span of electronic equipment, lamps etc.

1.2 Custom power devices (CPD)

The flexible AC transmission technology (FACT) allows a greater control of power flow. Since these devices provide very fast power swing damping, the power transmission lines can be securely loaded up to their thermal limits. In a similar way power electronic devices can be applied to the power distribution systems to increase the reliability and the quality of power supplied to the customers. The technology of the application of power electronics to power distribution system for the benefit of customers is called custom power devices (CPDs). The concept of CPDs was introduced by Hingorani and Gyugyi (1995). Since, through this technology the utilities can supply value-added power to these specific customers. Other applications of CPDs are to improve the power quality to general customers in a region. The CPD provides an integrated solution to the present problems that are faced by the utilities and power distributions. Through this technology the reliability of the power

delivered can be improved in terms of reduced interruptions and reduced voltage variations. The proper use of this technology will benefit all the industrial, commercial and domestic customers.

The CPDs are basically of two types as network reconfiguring type and compensating type. The network reconfiguring equipment can be GTO based or thyristor based. They are usually used for fast current limiting and current breaking during faults. They can also prompt a fast load transfer to an alternate feeder to protect a load from voltage sag / swell or fault in the supplying feeder. The members of the family of network reconfiguring devices are such as a solid state current limiter (SSCL), solid state circuit breaker (SSCB) and solid state transfer switch (SSTS). The compensating devices are used for active filtering, load balancing, power factor correction and voltage regulation. The active filters, which eliminate the harmonic currents, can be connected in both shunt and series. However, the shunt filters are more popular than the series filters because of greater ease of protection. Some others are operated to provide balanced, harmonic free voltage to the customers. Some of these devices are used as load compensators, i.e., correct the unbalance and distortions in the load currents and load voltage regulation. The family of compensating devices has the members are distribution STATCOM (D-STATCOM), dynamic voltage restorer (DVR) and unified power quality conditioner (UPQC). The D-STATCOM is connected parallel to the load and in shunt to the power system. The DVR is connected in series with the power supply lines. It adds a voltage to the supply voltage which is opposite to the line voltage drop. There by decreasing the effective length of the line. The UPQC is a combination of both series and shunt compensators.

The concept of compensation has its genesis to reactive power compensation (Miller, 1982), which initially was conceived with fixed or passive capacitors. Later, Static Var Compensator (SVC) came into use for Var compensation and voltage regulation at the load end. These systems suffered from the following drawbacks: suffered from granularity or the minimum amount of Var compensation possible; they exhibited poor dynamic performances; they had to be supplemented with filters as they injected harmonics into the network; they failed under low voltage conditions; and they did not provide for load balancing and load leveling. The answer to the above was found in the D-STATCOM, which was conceived from the concept of STATCOM (Tan, 1999; Gonzalez and Cerrada, 2000; Singh et al., 2009) used for transmission line compensation. A D-STATCOM is basically a shunt connected bidirectional converter based device which can act as a generalized impedance converter to realize either inductive or capacitive reactance by changing its output voltage levels (Bhattacharya et al., 1997). By proper tracking of the load current, the converter can generate such voltages and currents so that the harmonics and oscillations generated by the load current do not get transmitted to the supply side. A state of art D-STATCOM is capable of cancelling or suppressing; the effect of poor load power factor, the effect of poor voltage regulation, the harmonics introduced by the load, the DC offset in loads such that the current drawn from the source has no offset, the effect of unbalanced loads such that the current drawn from the source is balanced, and if provided with an energy storage system, it can perform load leveling when the source fails. Therefore, the D-STATCOM can solve most of the customer's load related to power quality problems. Furthermore, the major attributes of D-STATCOM are quick response time, less space requirement, optimum voltage

platform higher operational flexibility and excellent dynamic characteristics under various operating conditions.

1.3 Aim of Research

One of the main power quality problems is voltage sag or dip. The voltage sags are the most important power quality problems facing industrial and large commercial customers (Dugan et al., 1996). It contributes more than 80% of power quality (PQ) problems that exist in power systems (Ghosh and Ledwich, 2002). By definition, the voltage sag is a short time (10 ms to 1 minute) event during which a reduction in RMS voltage magnitude occurs. The voltage sag magnitude is ranged from 10% to 90% of nominal voltage and with duration from half a cycle to 1 min. The voltage sag is caused by a fault in the utility system, a fault within the customer's facility or a large increase of the load current, like starting a motor or transformer energizing. Voltage sag causes problem on various types of utilization equipment. Especially computers, adjustable-speed drives and process-control equipment are well-known for their sensitivity to supply voltage sags. Equipment used in modern industrial plants are actually becoming more sensitive to voltage sags as the complexity of the equipment increases and the equipments are interconnected in sophisticated processes. Even thought power interruptions are also common in power systems, they mostly occur when a protective device operates and isolates the circuit serving a user. This normally occurs only when there is a fault in a circuit that supplies a particular user. Meanwhile, short interruptions are also known to be a troublesome and costly type of power quality problem for most customers. However, occurrence of voltage sags is much more frequent compared to interrupt. Since

voltage sag can occur due to the faults in a wide part of a power system whereas, interrupt usually occur only when there is a fault on a particular circuit. If equipment is sensitive to these sags, the frequency of problems experienced will be much higher than if the equipment would be only sensitive to interruptions. Over the last ten years, voltage sags have become one of the main topics concerning power quality among utilities, customers and equipment manufacturers. Several international standards and working group documents have been produced to improve the understanding of voltage sag or dip problems.

In a power distribution system, fast load voltage regulation is required to compensate for source voltage variations and time varying loads such as electric arc furnaces, fluctuating output power of wind generation systems and transients on parallel connected loads. Controlled reactive power sources are commonly used for load voltage regulation in presence of disturbances. Due to their high control bandwidth and attributes, D-STATCOMs, based on three-phase pulse width modulation voltage source converters, have been proposed for this application. In this thesis, the load voltage regulation of the distribution system by using the D-STATCOM is considered. The aim of the research was to carry out load voltage regulation analyses based on computer modeling and simulation. The modeling strategy similar to that used for the field oriented control of three phase AC machines is employed. This work derives a set of dynamic equations of the power distribution system equipped with an installed D-STATCOM. Here, theses dynamic equations are used to investigate the impact of dynamic system modeling on load voltage regulation. In addition, the steady-state equations can be obtained from these equations. Then the steady-state performance of the D-STATCOM in electric power

distribution systems is investigated. Furthermore, the dynamic equations of the D-STATCOM are used to designing the current and DC voltage controllers. Meanwhile, the D-STATCOM model and its control were integrated with the power distribution system for designing the load voltage controller. The application of the D-STATCOM with the proposed design control technique for load voltage regulation were verified using computer simulation performed in SIMULINK/MATLAB.

The major objectives of this thesis are as follows:

1. Develop a mathematical model of the distribution system with the D-STATCOM and its control on the synchronously rotating reference frame.

2. Investigate steady state and dynamic performance of the distribution system with the D-STATCOM.

3. Design size and component rating of D-STATCOM for using to load voltage regulation when the source voltage and load power are varied.

4. Design appropriate control scheme for practical use of the D-STATCOM for load voltage regulation.

5. Implementation of D-STATCOM model with the proposed design control technique for load voltage regulation in the distribution system on the SIMULINK/MATLAB to verify steady state and dynamic performance.

6. Cost estimation of the D-STATCOM installation to regulate the load voltage.

1.4 Structure of thesis

This thesis presents the load voltage regulation in the distribution system by using the D-STATCOM. It is also arranged into 10 chapters as follows.

Chapter 1 introduces power quality problems and discusses the importance of the power quality problems in the distribution system especially the voltage sags or dips. The brief review of custom power devices is presented. The aim of research is also included in this chapter.

Chapter 2 proposes a review of the D-STATCOM and its application. The working principle and several configurations of the D-STATCOM are discussed. The heart of the D-STACOM used for compensation of the power system is its control system that the D-STATCOM control strategies will be presented in this chapter. In addition, the example of the applications and installations of the D-STATCOM for compensation of the distribution system are proposed.

Chapter 3 proposes the mathematical modeling of the distribution system based on the synchronously rotating reference frame. Steady state characteristic is obtained from state equation of the distribution system with the D-STATCOM which leads to analysis of the steady state performance. The size of the D-STATCOM for voltage regulation with only injecting the reactive power into the system is presented in this chapter.

Chapter 4 analyzes the dynamic performance of the distribution system with the D-STATCOM by using root locus and frequency response methods. In this chapter, the power circuit of the D-STATCOM is modeled by a controlled current source. The linear approximation is applied to investigating the dynamic performance of the distribution system with the D-STATCOM.

Chapter 5, the designing component rating and modeling of the D-STATCOM are presented. A modeling strategy similar to that used for the field oriented control of three phase AC machines is used in this chapter. The steady state characteristics and

dynamic performance of the D-STATCOM are analyzed in which of the parameters variations.

Chapter 6 presents the current and DC voltage control design strategies. The tuning of the PI controller parameters based on symmetrical optimum and genetic algorithms are proposed and compared.

Chapter 7 presents the AC voltage control design for load voltage regulation of the distribution system. This design is considered in two cases as the distribution system with the R and RL loads. In this chapter, the D-STATCOM model and its control were integrated with the power distribution system for designing the load voltage controller. The mathematical modeling of the distribution system with the D-STATCOM and its control based on the synchronously rotating reference frame is presented. To investigate the dynamic performance of these systems, linear approximation is applied. The classical loop shaping method is presented and applied to the load voltage controller design in this chapter.

Chapter 8, this chapter presents the application of the D-STATCOM with the proposed design control technique for load voltage regulation. The applications of the D-STATCOM for load voltage regulation for the distribution system with the R and RL loads are discussed. In addition, the applications of the D-STATCOM for the system with the distribution generators are presented. Dynamic performances of the D-STATCOM in distribution system voltage regulation are simulated using SIMULINK/MATLAB are presented.

Chapter 9 discusses cost estimation of the D-STATCOM installation to regulate the load voltage.

Chapter 10, this chapter presents summary of this thesis. The contributions of the research are presented and future works are also discussed.

CHAPTER II

REVIEW OF D-STATCOM AND ITS APPLICATIONS

When the STATCOM is applied to the distribution system it is called D-STATCOM (Distribution-STACOM). Its configuration is the same or with small modifications of the STATCOM that is applied to the distribution network at low and medium voltage. It operates in a similar manner as the STATCOM, with the active power flow controlled by the angle between the AC system and AC output converter voltages and the reactive power flow controlled by the difference between the magnitudes of these voltages. However, some of the control algorithms and applications of these devices are different. This chapter proposes a review of the D-STATCOM and its applications. The working principle and several configurations of the D-STATCOM are discussed. The heart of the D-STACOM used for compensation of the power system is its control system that the D-STATCOM control strategies will be presented in this chapter. In addition, the example of the applications and installations of the D-STATCOM for compensation of the distribution system are proposed.

2.1 Working Principle and Configuration of D-STATCOM

The voltage related power quality problems, such as sags and swells, voltage dips, harmonic distortions due to nonlinear loads and voltage unbalancing in electrical

power distribution systems, have been a major concern for the voltage sensitive loads. Load voltage regulation using a voltage source converter (VSC) for different grid connected applications has been recently attempted in (Mohamed and Saadany, 2009; Samuel et al., 2009; Selvajyothi and Janakiraman, 2010). D-STATCOM is one of VSC-based compensators which has been commonly used for the mitigation of the voltage sags and swells and regulating the load bus voltage. The D-STATCOM is most widely used for power factor correction, to eliminate current based distortion and load balancing, when connected at the load terminals. It can also perform voltage regulation when connected to a distribution bus. The schematic diagram for load compensation using the D-STATCOM is shown in Figure 2.1. A current controlled voltage source converter is assumed at the heart of the D-STATCOM. Hence for an ideal case, the D-STATCOM is replaced by an ideal current source i_f. Further, as is generally the case, the load is assumed to be reactive, nonlinear and unbalanced. First, assume the load is without a compensator. Hence, i_s flowing through the feeder is also unbalanced and distorted and consequently, the voltage on PCC bus will also be unbalanced and distorted.

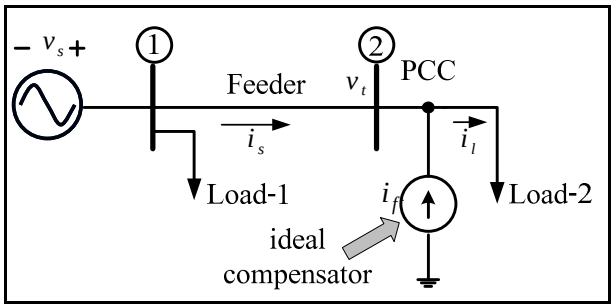

Figure 2.1 Distribution systems with the installed D-STATCOM

Ideally, the utility would like to see a load drawing unity power factor with fundamental and positive sequence current. Without the compensator, i_s will be the same as i_l i.e. reactive, unbalanced and distorted. To mitigate the problem, the compensator must inject current such that i_s becomes fundamental, positive sequence and in-phase with the PCC voltage. From Figure 2.1, applying KCL to the PCC that is

$$i_s + i_f = i_l \tag{2.1}$$

hence $i_s = i_l - i_f$

Thus, the compensator must generate a current i_f such that it cancels the reactive, harmonic and the unbalance components of the load current.

The schematic diagram of an ideal D-STATCOM acting as a voltage regulator is shown in Figure 2.2(a). In this the ideal D-STATCOM is represented by a voltage source and it is connected to the PCC. However it is rather difficult to realize this circuit and the alternate structure is shown in Figure 2.2(b). It can be seen that this like structure as used for load compensation. However, it has the advantage that the harmonics can be bypassed by the filter capacitor *C*. The basic idea here is to inject the current i_f in such a way that the voltage v_t follows a specified reference. The ideal D-STATCOM must be operated such that it does not inject or absorb any real power in the steady state.

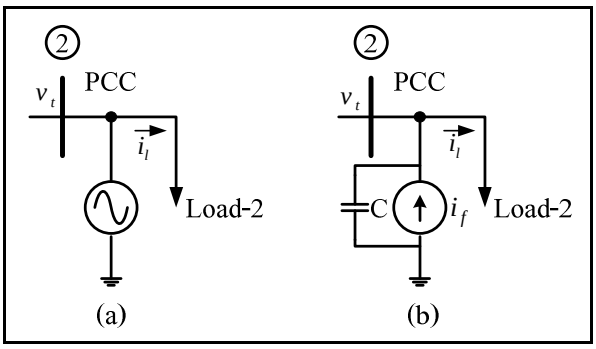

Figure 2.2 Schematic diagram of an ideal D-STATCOM acting as a voltage regulator

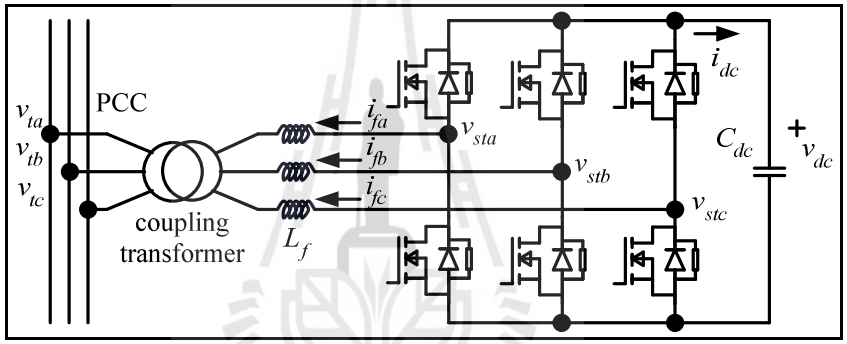

Figure 2.3 Basic Two-Level VSC bridge

In practice however the current source is implemented using the voltage source converter which is schematically depicted in Figure 2.3. It consists of a three phase voltage source converter, interfacing inductors and a DC link capacitor. The VSC is connected to the network through the transformer and the interfacing inductors which are used to filter high-frequency components of compensating currents. The VSC is the backbone of D-STATCOM and it is a combination of self-commutating solid-state turn-off devices (i.e. the metal oxide semiconductor field effect transistor, MOSFET and integrated gate bipolar transistor, IGBT) with a

reverse diode connected in parallel to it. For the D-STATCOM, the solid-state switches operate in pulse width modulation (PWM) mode employing high switching frequencies in a cycle of operation. A DC voltage source on the input side of VSC is generally achieved by a DC capacitor. The turn-off device makes the converter action, whereas diode handles rectifier action. The primary objective of D-STATCOM is to obtain almost harmonic neutralized and controllable three-phase AC output voltage waveforms at the point of common coupling to regulate the reactive current flow by generation and absorption of controllable reactive power by the solid-state switching algorithm. As D-STATCOM has inherent characteristics of real power exchange with a support of the proper energy storage system, the operation of such controller is possible in all four quadrants of *QP* plane and it is governed by the following power flow relation

$$S = 3\frac{V_t V_{st}}{X_f}\sin\delta - j3\left(\frac{V_t V_{st}}{X_f}\cos\delta - \frac{V_t^2}{X_f}\right) = P - jQ \tag{2.2}$$

where S is the apparent power flow, P the active power flow, Q the reactive power flow, V_t the terminal AC phase voltage to neutral (rms) at PCC, V_{st} the D-STATCOM fundamental output AC phase voltage (rms), X_f (ωL_f, where, $\omega = 2\pi f$), the leakage reactance, L_f the leakage inductance, f the system frequency and δ the phase angle between V_t and V_{st}. Active power flow is influenced by the variation of δ and reactive power flow is greatly varied with the magnitude of the voltage variation between V_t and V_{st}. For $\delta = 0$, the P is zero and Q is derived from (2.2) as follows

$$Q = \frac{V_t}{X_f}(V_{st} - V_t) \tag{2.3}$$

The AC voltage output (V_{st}) of D-STATCOM can be controlled through the PWM switching method.

Functionally, D-STATCOM injects an almost sinusoidal current (I_f) in quadrature (lagging or leading) with the terminal voltage (V_t), and emulates as an inductive or a capacitive reactance at the point of connection with the electrical system for reactive power control, and it is ideally the situation when amplitude of V_t is controlled from full leading (capacitive) to full lagging (inductive) for δ equals to zero (i.e. both V_{st} and V_t are in the same phase). The magnitude and phase angle of the injected current (I_f) are determined by the magnitude and phase difference (δ) between V_t and V_{st} across the leakage inductance (L_f), which in turn controls reactive power flow and DC voltage, V_{dc} across the capacitor. Figure 2.4 shows the phasor diagrams on the operating principle at the fundamental frequency for capacitive and inductive modes. The terminal voltage (V_t) is equal to the sum of the converter AC output voltage (V_{st}) and the voltage across the coupling transformer and interfacing inductor reactive (V_{L_f}) in both capacitive and inductive modes. I_f mean that if output voltage of D-STATCOM (V_{st}) is in-phase with bus terminal voltage (V_t) and V_{st} is greater than V_t ($V_{st} > V_t$), the D-STATCOM is considered to be operating in a capacitive mode that it provides reactive power to system. If V_{st} is smaller than V_t ($V_{st} < V_t$), it is operating in an inductive mode that it absorbs reactive

power from the power system. And for V_{st} is equal V_t ($V_{st} = V_t$), it is no reactive power exchange takes place.

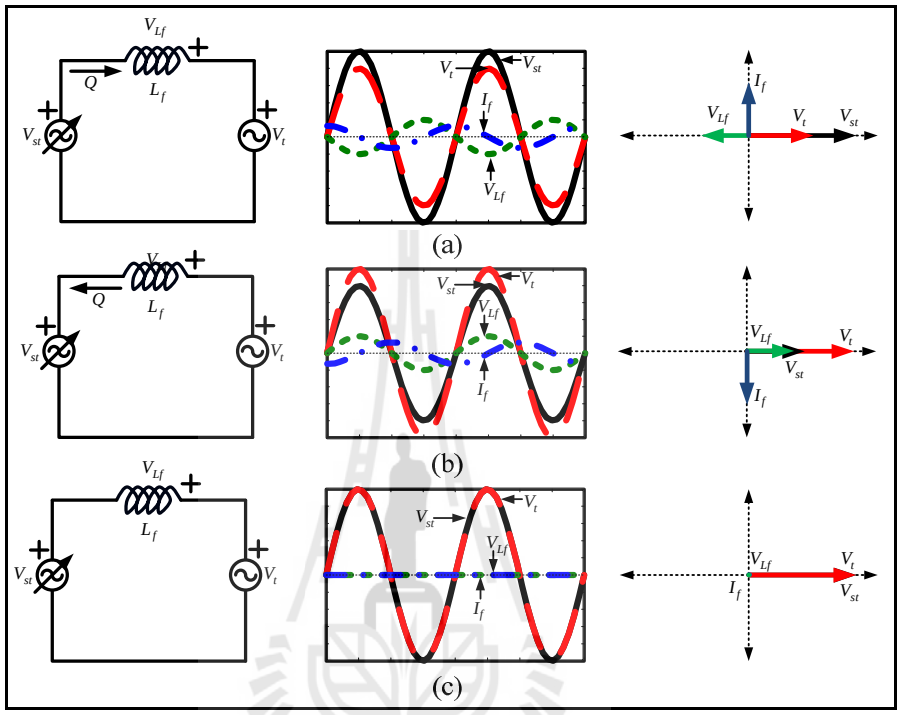

Figure 2.4 Phasor diagrams on the operating principle at the fundamental frequency for (a) capacitive, (b) inductive and (c) no reactive power exchange modes

Ideally, V_t and V_{st} have the same phase, but actually they have a little phase difference to component the loss of the transformer winding, interfacing inductor and inverter switching, so absorbs some active power from system. Figure 2.5 shows D-STATCOM absorbs or produces active power with V_t and V_{st} having phase lagging or leading ($\mp\delta$). For lagging ($-\delta$), power (P) flows from V_t to V_{st} that the active power is transferred from the AC terminal to the DC capacitor and causes the DC voltage to

rise. For leading ($+\delta$), power (P) flows from V_{st} to V_t that the active power is transferred from the DC capacitor to the AC terminal and causes the DC voltage to reduce. In any practical D-STATCOM there are losses in the transformer windings, interfacing inductor and in the converter switches. These losses consume active power from the AC terminals. Accordingly, a small phase difference always exists between the VSC AC output voltage and the AC system voltage. A summary of the power exchanges between the D-STATCOM and the AC system as a function of the D-STATCOM AC output voltage V_{st} and the AC terminal voltage V_t.

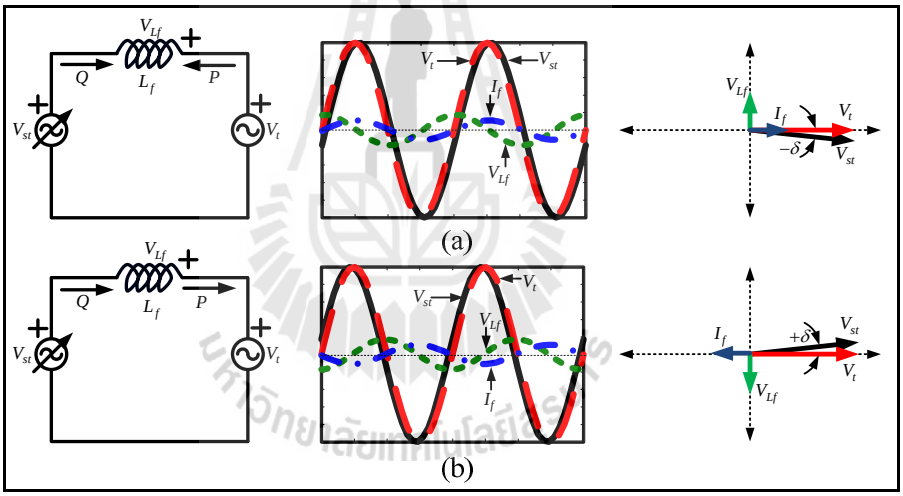

Figure 2.5 D-STATCOM (a) absorbs active power with V_t and V_{st} having phase lagging $-\delta$ and (b) produces active power with V_t and V_{st} having phase leading $+\delta$

For power quality improvement the voltage source converter (VSC) bridge structure is generally used for the development of custom power devices, while the use of the current source converter (CSC) is less reported. The current source

converter topology finds its application for the development of active filters (Akagi et al., 2007), D-STATCOM (Routimo et al., 2007). Figure 2.6 shows basic three-phase three-wire D-STATCOM based on the CSC, which is connected in shunt with distribution system. The CSC D-STATCOM PWM bridge is built with six controllable unidirectional switches. The semiconductor devices are under bipolar voltage stresses and the maximum values of these are the peak value of the supply filter capacitor line-to-line voltage (Mohamed and Saadany, 2009), which in steady state is nearly equal to supply line-to-line voltage. Figure 2.6 shows the anti-parallel diodes of the commercial power switch modules (i.e. the metal oxide semiconductor field effect transistor, MOSFET and integrated gate bipolar transistor, IGBT). Because of these and the very low reverse voltage blocking capability of the switch, additional diodes have to be connected in series with the power switch module. The PWM bridge of the CSC D-STATCOM is connected to the power system through the second order filter (*LC*), which filters the carrier frequency components from the PWM currents. As the energy storage of the CSC D-STATCOM there is an inductor (L_{dc}) with a DC current (i_{dc}) flowing through it. The current should be at least as high as the peak value of the compensating current.

In addition, the D-STATCOM can be classified based on the supply and / or the load system having single-phase (two wire) and three-phase (three-wire or four-wire) systems. There are many nonlinear loads, such as domestic appliances, connected to single-phase supply systems. Some three-phase nonlinear loads are without neutral, such as adjustable speed drive (ASD), fed from three-wire supply systems. There are many nonlinear single-phase loads distributed on four-wire three-phase supply systems, such as computers, commercial lighting, etc. Hence, the D-

STATCOM may also be classified accordingly as two-wire, three-wire, and four-wire types.

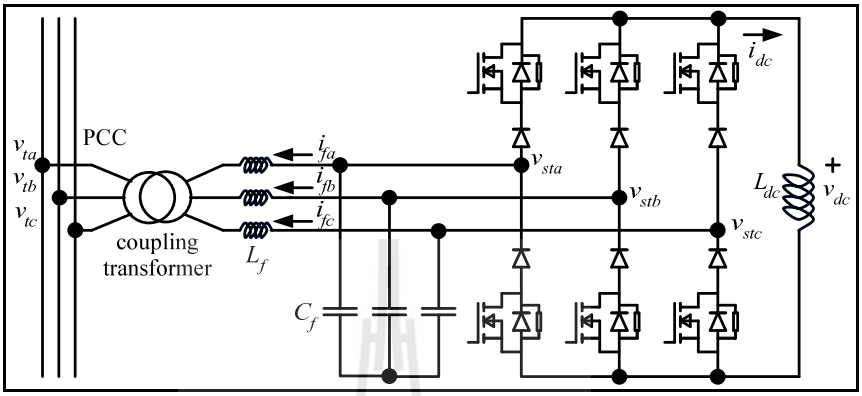

Figure 2.6 Basic three-phase three-wire D-STATCOM based on the CSC

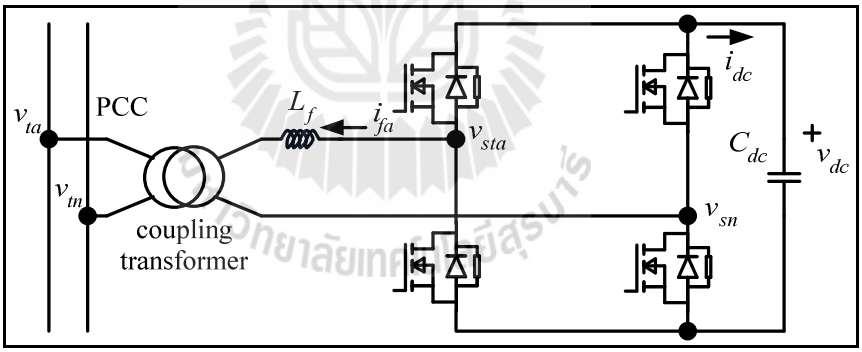

Figure 2.7 Two-wire (single-phase) H-bridge D-STATCOM

The most common voltage source PWM bridge with DC capacitive bus energy storage elements, is used to form two-wire (single phase) D-STATCOM that the configuration is shown in Figure 2.7. In Figure 2.7, it is called an H-bridge as it looks like the eighth letter of the English alphabet. The converter contains four switches that

each comprising a power semiconductor device and an anti-parallel diode as also indicated in the figure. The power semiconductor device can be a power MOSFET or IGBT for distribution system applications.

Three-phase three-wire non-linear loads, such as ASD's, are major applications of solid-state power converters. A large number of publications have appeared in three-phase D-STATCOM (Singh et al., 2006; Singh et al., 2005; Xiao-ping Yang et al., 2008; Sao et al., 2002; Singh et al., 2005), with three wires on AC side and two wires on DC side that is shown in Figure 2.3. At medium voltage level this device is developed with voltage fed type having single stage VSC and for enhanced voltage and power handling capacity multilevel VSC is used. In the multilevel VSC, the number of possible operating states increases and as a consequence, the flexibility of the converter improves. As all the devices are individually controlled, better control over the voltage magnitude and harmonic suppression can be achieved. Use of a multilevel VSC reduces the required transformer voltage ratio and sometimes even makes possible direct connection of the compensator to the increased voltage supply systems. Three different multilevel VSC topologies are considered currently. These are 1) diode-clamped multilevel converter (DCMC); 2) flying capacitor multilevel converter (FCMC); and 3) cascade multilevel converter (CMC).

Figure 2.8 shows a three-phase, five-level diode-clamped VSC. The diode-clamped multilevel converter uses capacitors in series to divide up the DC bus voltage into a set of voltage levels. To produce a *m*-level phase voltage, a diode-clamped convertor needs *m*-1 capacitors on the DC bus.

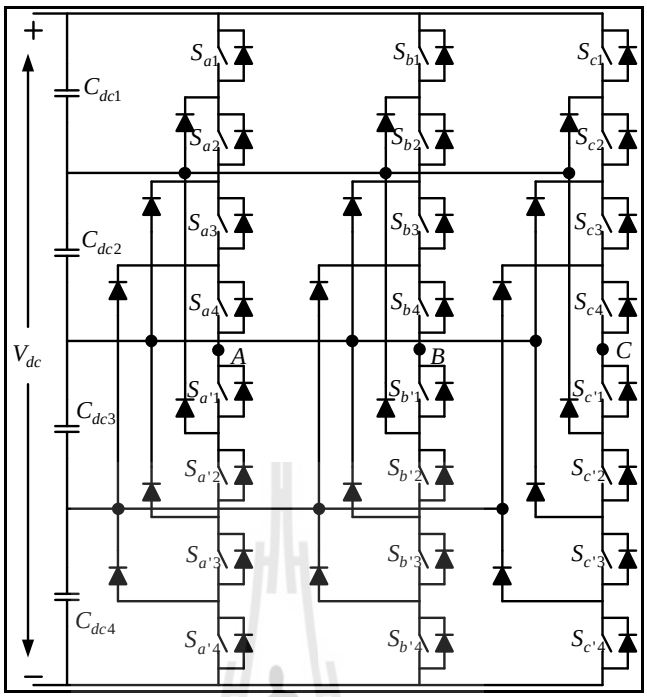

Figure 2.8 A three-phase, five-level diode-clamped VSC

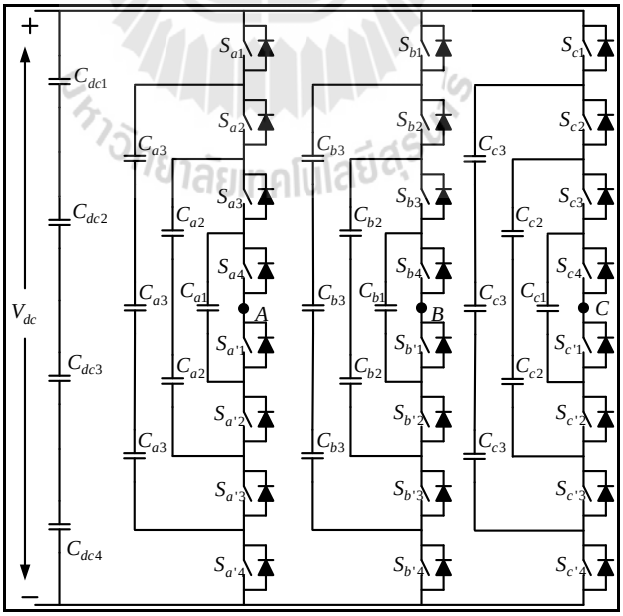

Figure 2.9 A three-phase, five-level flying-capacitor VSC

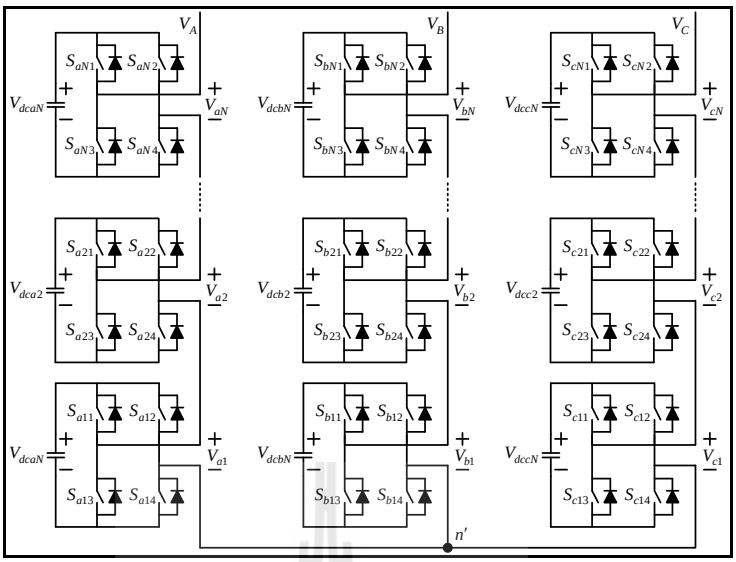

Figure 2.10 A three-phase, *m*-level configuration of the CMC

A flying-capacitor multilevel converter (FCMC), as shown in Figure 2.9, uses a ladder structure of DC capacitors for which the voltage on each capacitor differs from that on the next capacitor. To generate a *m*-level staircase output voltage, *m*-1 capacitors in the DC bus are needed. Each phase leg has an identical structure. The size of the voltage increment between two capacitors determines the size of the voltage levels in the output waveform. It is obvious that the three inner-loop balancing capacitors for phase leg A are independent from those for phase leg B. All phase legs share the same DC-link capacitors.

The cascaded-multilevel converter (CMC) uses cascaded converters with separate DC sources (SDCSs). The general function of this multilevel converter is the same as that of the two previous converters. The CMC synthesizes a desired voltage from several independent sources of DC voltages, which may be obtained from batteries, fuel cells or solar cells. This converter can avoid extra clamping diodes or

voltage-balancing capacitors. A three-phase, *m*-level configuration of the CMC is shown in Figure 2.10. Each SDCS is associated with a single-phase H-bridge converter. The AC outputs of different full-bridge converters in the same phase are connected in series such that the synthesized voltage waveform is the sum of the individual converter outputs. In the three-phase system, the output voltage of the three cascaded converters can be connected in either wye or delta configurations. For example, a wye-configured *m*-level converter using a CMC with separated capacitors is illustrated in Figure 2.10.

A large number of single-phase loads may be supplied from three-phase mains with neutral conductor. They cause excessive neutral current, harmonics and reactive power burden, and unbalance. To reduce these problems, four-wire D-STATCOM has been attempted. To develop the D-STATCOM device for three-phase, four-wire distribution system different configuration of VSC having capacitor mid-point, three single-phase H-bridge VSC configurations, and four legs VSC, are used.

The capacitor mid-point VSC that allows the injection of three independent currents including any DC current that the load may draw is proposed in (Mishra et al., 2006). This configuration is used for small ratings as the entire neutral current flows through the DC bus capacitor. A three-phase, four-wire capacitor mid-point VSC configuration is shown in Figure 2.11. In this figure, the converter is supplied by two equal DC sources, the neutral point of which is denoted by n'. A three-phase load is connected at the PCC. The load neutral is denoted by *n* and this point is connected to the neutral point n' of the converter. This neutral clamped topology allows a path for the zero sequence current and therefore the three injected currents can be independently controlled.

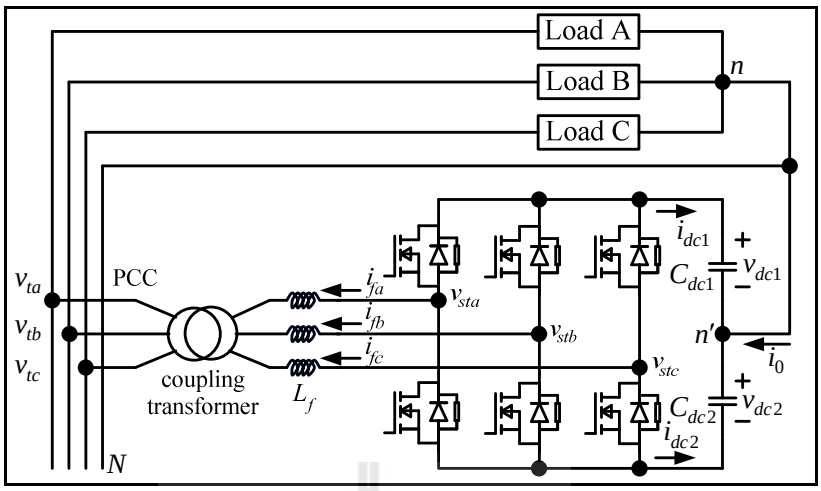

Figure 2.11 A three-phase four-wire capacitor mid-point VSC configuration

Three single-phase H-bridges scheme is popular as it allows the proper voltage matching for solid state devices and enhances the reliability of the devices. Figure 2.12 shows the three-phase, four-wire configurations of the D-STATCOM. It contains three H-bridge VSCs connected to a common DC storage capacitor. This topology allows three independent current injections, as this contains three separate H-bridge converters. Each VSC is connected to the network though a transformer and interfacing inductors. Six output terminals of the transformer are connected in wye. The purpose of including the transformers is to provide isolation between the converters. This prevents the DC storage capacitor from being short-circulated through switches in different converters. The neutral point of the three transformers is connected to the load neutral.

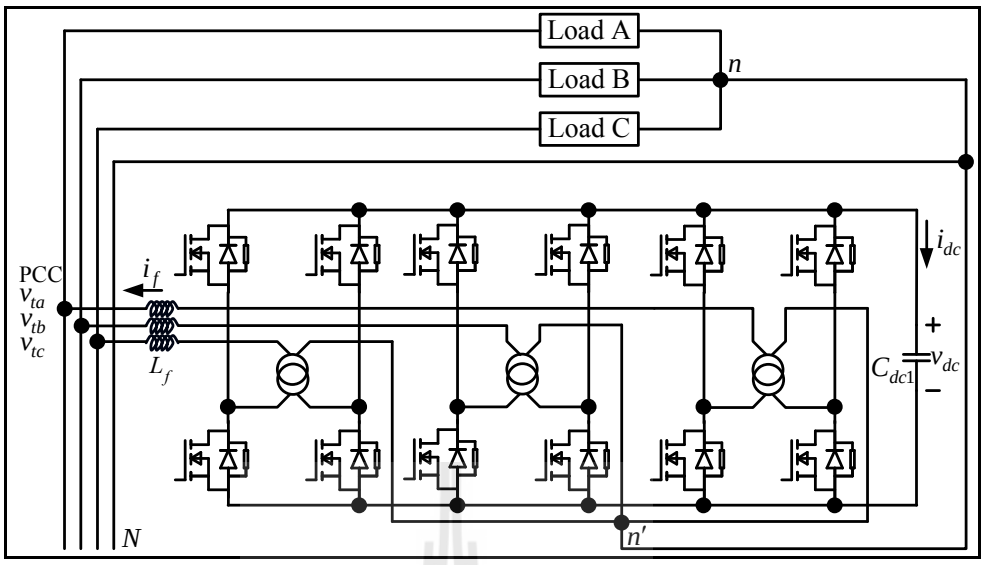

Figure 2.12 H-bridge three-phase four-wire configurations of the D-STATCOM

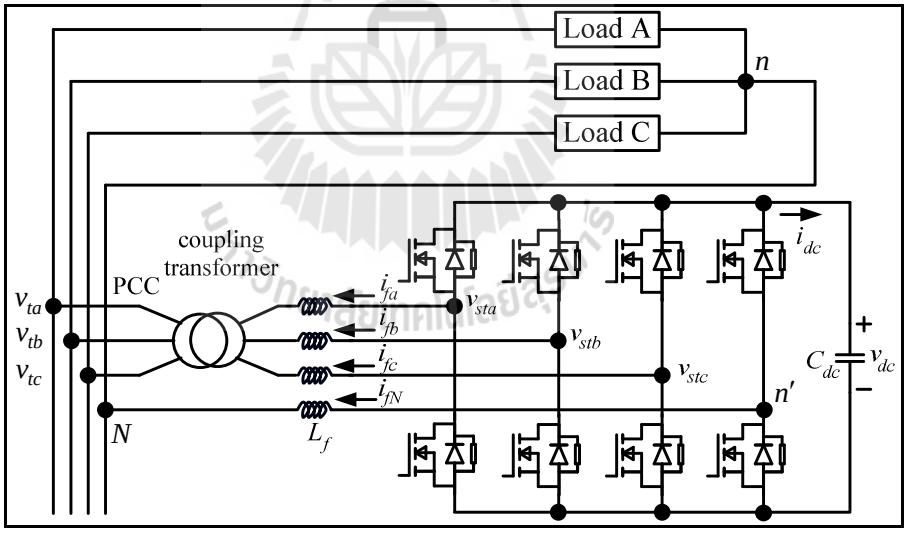

Figure 2.13 Four-leg VSC configuration

An alternate topology is shown in Figure 2.13 in which a VSC with four legs are used. This requires only one DC storage unit. Three of its legs are used for phase

connection while the fourth leg is connected to the load neutral and the system neutral, if available, through a resistance (Quinn et al., 1992; Quinn et al., 1993; Hoffman and Ledwich, 1994). The fourth leg is used to stabilize the neutral of D-STATCOM. The scheme utilizes a four legs voltage source converter topology and fourth leg is connected to the neutral which serves the purpose of compensating neutral current. The reference current for the fourth leg is the negative sum of three phase load currents. This nullifies the effect of DC component of load current. To maintain the adequate charge on the DC side capacitor the flow of active power from AC side is controlled towards the DC side of the converter.

2.2 D-STATCOM Control Strategies

The heart of the D-STACOM used for compensation of the power system is its control system and its response to the dynamic change of the load depends on the methodology used for its control. Usually, the control of the D-STATCOM power circuit in general is achieved in four stages. The first stage involves sensing the essential AC and DC voltages and currents using PTs, CTs, Hall-effect sensors, etc. to gather information about the dynamic condition of the load and the system. Based on this information some signals are synthesized using techniques like *dq* synchronous rotating axis transformation (Freitas et al., 2002; Jazayeri and Fendereski, 2007), $\alpha - \beta$ stationary reference frame transformations (Singh and Jitendra, 2006; Correa et al., 2005) and so on in the second stage. A reference signal is generated from this signal. Further the converter AC output voltage needs to be synchronized with the power system voltage. A phase locked loop (PLL) is generally used to gather phase and frequency information of the fundamental positive sequence component of the

system voltage. The basic PLL block diagram is illustrated in Figure 2.14. Then using the control methodology, the compensating commands in terms of current or voltage levels are generated in the third stage. The control methodology used in this stage can be categorized into linear (Freitas et al., 2002; Jazayeri and Fendereski, 2007; Singh and Jitendra, 2006; Correa et al., 2005), nonlinear (Shukla et al., 2005) and special control techniques (Singh et al., 2005; Xiao-ping Yang et al., 2008). Then depending on the device configurations of the VSC, the gating signal for the solid state devices of the VSC are produced in the fourth stage.

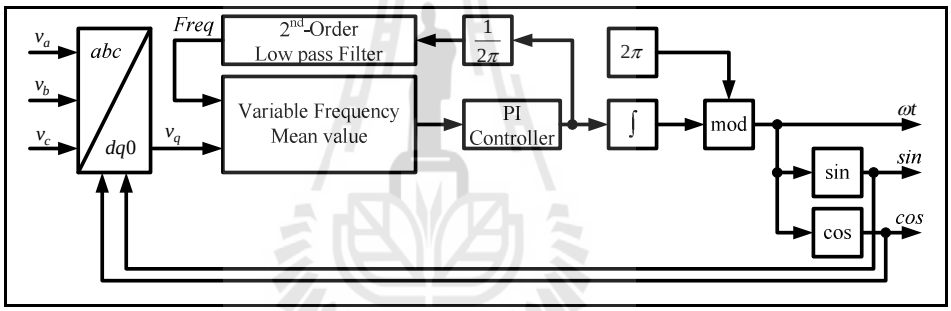

Figure 2.14 Basic PLL block diagram

The development of the compensating signals plays an important part in deciding the rating and transient as well as the steady - state performance of the D-STATCOM. The control methodologies used for generation of the compensating commands generally involve frequency domain and time domain control techniques. The D-STATCOM using the time-domain methodologies senses the time-domain signals of instantaneous voltage and / or current vectors and synthesizes the *dq* signals using the popular *dq* synchronous rotating axis transformation (Freitas et al., 2002;

Jazayeri and Fendereski, 2007; Singh and Jitendra, 2006; Correa et al., 2005). Control techniques like PI or PID are then used to process the transformed signals to derive the compensating signals. In addition to this symmetrical component transformation and unit vector control are some of the other popular control schemes to extract the reference signals in time domain. In the PWM mode of control two popular control techniques, voltage control (VC) and current control (CC) are adopted (Ledwich and Ghosh 2002). The CC technique is widely reported in literature for linear and nonlinear control strategies. Under the linear control methodologies are reported control schemes using a stationary PI controller, synchronous vector PI control, state feedback control, predictive control and dead-beat controls. The nonlinear control schemes encompass hysteresis control, delta modulation (DM) or pulse DM current control and online optimized controller.

Generation of proper triggering pulses for the switches of the VSC is very crucial for proper implementation of the load compensation. The advent of the low switching loss has enabled the designers to shift from fundamental frequency switching (FFS) to pulse width modulation (PWM). Further, custom power being a relatively low power application, PWM methods offer a more flexible option than fundamental frequency switching methods favored in FACTS applications. Though various topologies of VSC have been reported, single three-phase bridge with six switches is widely reported in D-STATCOM. From time to time, various schemes were reported to generate the pulses for turning on the converter switches, with each scheme having some or the other advantages. It has been observed that all the schemes broadly fall into the following categories: phase shift control, carrier based PWM control, and carrier less hysteresis control.

2.2.1 Phase Shift Control

The phase shift control scheme is simple. The objective is to maintain a constant voltage at the load terminal. The control algorithm exerts a voltage angle control and generates a phase shift in the output voltage of the VSC with respect to the AC terminal voltage. An error signal is generated by comparing the measured PCC voltage with the desired or the reference voltage. The error signal is fed to a PI controller to generate an angle δ to drive the voltage error to zero. Thus the PCC voltage is regulated at the desired value. The PWM generator phase modulates the sinusoidal voltage signal by angle δ and generates the switching signals for the VSC switches by comparing it with a triangular carrier signal. The DC side voltage is maintained by a separate DC source. A schematic diagram for phase shift control of D-STATCOM is shown in Figure 2.15.

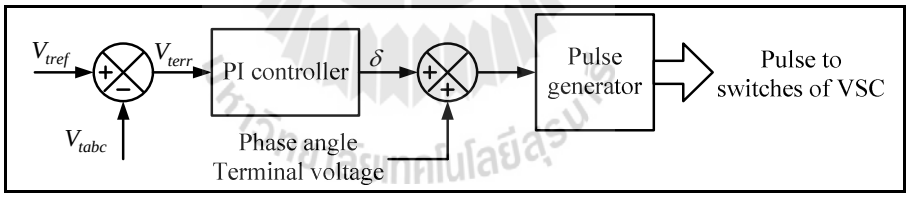

Figure 2.15 A schematic diagram for phase shift control of D-STATCOM

The positive aspects of this type of control are: this control algorithm is easy to implement and is sufficiently robust, and requires only voltage measurement. Current and reactive power measurements are not required. However, it suffers from the following disadvantages:

- It does not have a self supporting DC bus and requires a separate DC source to pre-charge the DC side capacitor and maintain its voltage during the operation of D-STATCOM.

- It assumes that the AC terminal voltage is balanced and without harmonics, since the fundamental waveform is used to obtain the phase angles of the AC terminal waveform.

- There is no provision for harmonic suppression in case the load connected to PCC is nonlinear.

- This method results in generation of active power by the VSC along with the reactive power.

2.2.2 Carrier Based PWM Control

The schematic diagram for the carrier based PWM control is shown in Figure 2.16. A fixed frequency carrier based sinusoidal PWM is used for generating the switching pulses for the switch of the VSC. This algorithm is based on the instantaneous reactive power theory. The instantaneous voltage and current of the system and the load are measured. The three-phase system is transformed to a *dq* synchronously rotating reference frame using Park's transformation. Compensation is achieved by control of active and reactive currents (i_d and i_q). The active power *p* and the reactive power *q* injected into the system by the D-STATCOM, under the *dq* reference frame are given by:

$$p = v_{td} i_d + v_{tq} i_q \tag{2.4}$$

$$q = v_{tq} i_d - v_{td} i_q \tag{2.5}$$

For a balanced three-phase system $v_{tq} = 0$. Thus the i_d and i_q completely describes the instantaneous value of real and reactive power produced by the D-STATCOM.

$$p = v_{td} i_d \text{ and } q = -v_{td} i_q \tag{2.6}$$

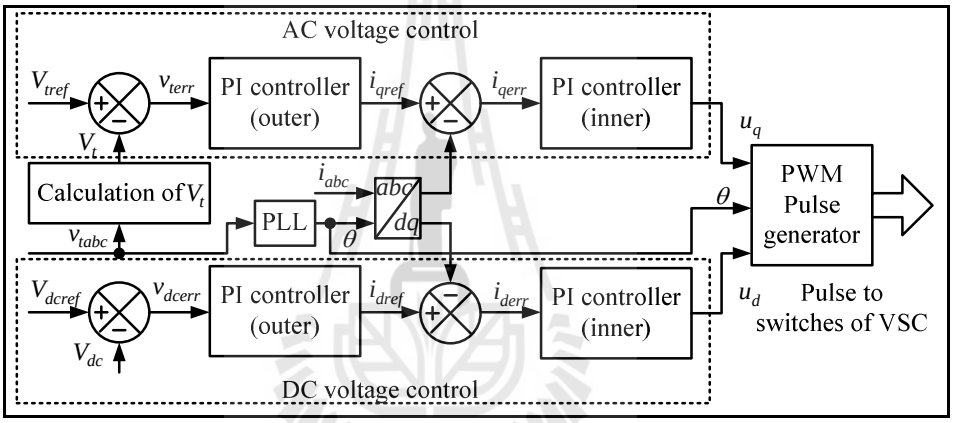

Figure 2.16 Schematic diagram for the carrier based PWM control

The instantaneous i_d reference current is generated by PI regulation of the DC terminal voltage with respect to a reference DC voltage. Similarly, i_q reference current is generated by PI regulation of the AC terminal voltage of the VSC with respect to a reference AC terminal voltage. In case the only power factor correction is desired, the reference i_q is set to zero. The decoupled i_d and i_q components obtained from *abc* to *dq* transformation of the measured instantaneous three-phase current, is then regulated with two separate PI regulators with respect to the reference i_d and i_q

currents obtained earlier. In order to synchronize *abc* to *dq0* transformation, a Phase Locked Loop (PLL) is used.

As can be seen in Figure 2.16, the three phase terminal voltages (v_{ta}, v_{tb} and v_{tc}) are considered sinusoidal and hence their amplitudes (RMS) are computed as:

$$V_t = \sqrt{\frac{2}{3}\left(v_{ta}^2 + v_{tb}^2 + v_{tc}^2\right)} \tag{2.7}$$

The value of V_t computed above is compared with the desired terminal voltage V_{tref}. The AC voltage error v_{terr} is

$$v_{terr} = \left(V_{tref} - V_t\right) \tag{2.8}$$

where V_t is the amplitude of the sensed three phase AC voltages at the PCC terminal. The error v_{terr} is fed to an outer PI controller, using time integration, to generate the i_{qref}.

$$i_{qref} = K_{Pac} v_{terr} + K_{Iac} \int v_{terr} dt \tag{2.9}$$

where K_{Pac} and K_{Iac} are the proportional and integral gain constants of the outer PI controller of the AC terminal voltage at the PCC. The actual value of i_q is generated

by an *abc* to *dq* convertor using Park's transformation over the D-STATCOM current. The i_{qref} and i_q components are compared and the error i_{qerr} is fed to an inner PI current controller to generate u_q.

$$i_{qerr} = \left(i_{qref} - i_q\right) \tag{2.10}$$

$$u_q = K_{Piq} i_{qerr} + K_{Iiq} \int i_{qerr} dt \tag{2.11}$$

where K_{Piq} and K_{Iiq} are the proportional and integral gain constants of the inner PI controller of the AC terminal voltage at the PCC.

For control of the voltage at the DC bus of the D-STATCOM, the V_{dc} of the DC bus is compared with the desired DC bus voltage V_{dcref}. The DC voltage error v_{dcerr} is

$$v_{dcerr} = \left(V_{dcref} - V_{dc}\right) \tag{2.12}$$

where V_{dc} is the sensed DC voltage at the DC bus of the D-STATCOM. The error is then fed to an outer PI controller to generate i_{dref}.

$$i_{dref} = K_{Pdc} v_{dcerr} + K_{Idc} \int v_{dcerr} dt \tag{2.13}$$

where K_{Pdc} and K_{Idc} are the proportional and integral gain constants of the outer PI controller of the DC bus voltage. The actual i_d is generated by an *abc* to *dq* convertor using Park's transformation over the D-STATCOM current. The signals i_{dref} and i_d are compared and the error i_{derr} is fed to an inner PI current controller to generate u_d.

$$i_{derr} = \left(i_{dref} - i_d \right) \tag{2.14}$$

$$u_d = K_{Pid} i_{derr} + K_{Iid} \int i_{derr} dt \tag{2.15}$$

where K_{Pid} and K_{Iid} are the proportional and integral gain constants of the inner PI controller of the DC bus voltage.

In PWM current controller, u_d and u_q signals generated above are converted into a modulation index *m* and phase angle δ which are then used by the PWM modulator for producing the required pulses for triggering the switches of the VSC. This causes the VSC to maintain the AC terminal voltage of the system at the PCC by generating / absorbing the required reactive current and supplying / absorbing active power from the system to maintain the DC side voltage of the converter.

The advantageous features of this scheme include:

- It incorporates a self supporting DC bus.

- The active and reactive power control achieved through i_d and i_q control are decoupled from each other. The DC bus control / regulation is decoupled from the AC bus control like voltage regulation or power factor correction and load balancing.

- Switching of devices of VSC is done at a fixed frequency. Thus switching losses can be limited within the rating of the devices.

- This type of control is inherently linear and robust and uses PI or PID controls, which are very easy to implement in real time and are less complex in hardware.

However it suffers from the following disadvantages:

- Very little harmonic suppression is achieved. Additional series and shunt filters need to be connected for removal of harmonics.

- As four PI controllers are used, response time is more.

- The scheme is based on synchronization with the fundamental frequency using a PLL. In the case of distorted mains the PLL may produce errors.

- The scheme is applicable for balanced three-phase, three-wire system. It cannot be used for single-phase systems.

- During transient conditions, the supply current shoots up to a very high value.

- A larger series filter can be connected on the AC side to limit transients and harmonics. However it shall reduce the reactive power generating capacity of the VSC.

2.2.3 Carrier Less Hysteresis Control

This compensation scheme is very versatile and is widely reported for power factor correction and voltage regulation, in addition to load balancing, harmonic suppression and load leveling. Various methods are reported for deciding the magnitude of the reference active and reactive current to be generated by the D-STATCOM. Simplest method reported is with the use of PI controller. Figure 2.17

shows the control scheme for PI controller based carrier less hysteresis controller. The unit vectors for the in-phase and the quadrature voltages are obtained from the terminal voltage. The in-phase unit vectors (u_{ta}, u_{tb} and u_{tc}) are computed by dividing the AC terminal voltages (v_{ta}, v_{tb} and v_{tc}) by their amplitude V_t. Another set of vectors called the quadrature unit vectors (w_{ta}, w_{tb} and w_{tc}) is a sinusoidal function, obtained from the in-phase unit vector set (u_{ta}, u_{tb} and u_{tc}). To regulate the PCC AC terminal voltage, its amplitude V_t is compared with the desired voltage V_{tref} and the error v_{terr} is processed by a PI controller. The output of the PI controller i^*_{smq} decides the amplitude of the reactive current to be generated by the D-STATCOM. Multiplication of the quadrature unit vectors (w_{ta}, w_{tb} and w_{tc}) with i^*_{smq} yields the quadrature component of the reference current (i^*_{saq}, i^*_{sbq} and i^*_{scq}).

To provide self supporting DC bus for the D-STATCOM, the charging current must be provided from the PCC. In order to achieve this, the DC bus voltage V_{dc} is sensed and compared with the DC reference voltage V_{dcref}. The DC voltage error v_{dcerr} is processed by a second PI controller. The output of the PI controller i^*_{smd} decides the amplitude of the active power component of the D-STATCOM. Multiplication of the in-phase vectors (u_{ta}, u_{tb} and u_{tc}) with i^*_{smd} yields the in-phase component of the reference currents (i^*_{sad}, i^*_{sbd} and i^*_{scd}). The reference currents (i^*_{sa}, i^*_{sb} and i^*_{sc}) are obtained by adding the corresponding in-phase and the quadrature components. The hysteresis controller adds a hysteresis band ± h around the calculated reference current. When ($i_{sa} - i^*_{sa}$) > +h, pulses are generated for the lower

level switches and when ($i_{sa} - i_{sa}^{*}$) < -*h*, pulses are generated for the upper level switches of the VSC. As can be seen in Figure 2.17, the three phase voltages at the PCC (v_{ta}, v_{tb} and v_{tc}) are sinusoidal and hence their magnitude (RMS) is computed as shown in (2.16). The unit vectors u_{ta}, u_{tb} and u_{tc} are derived as shown in (2.17).

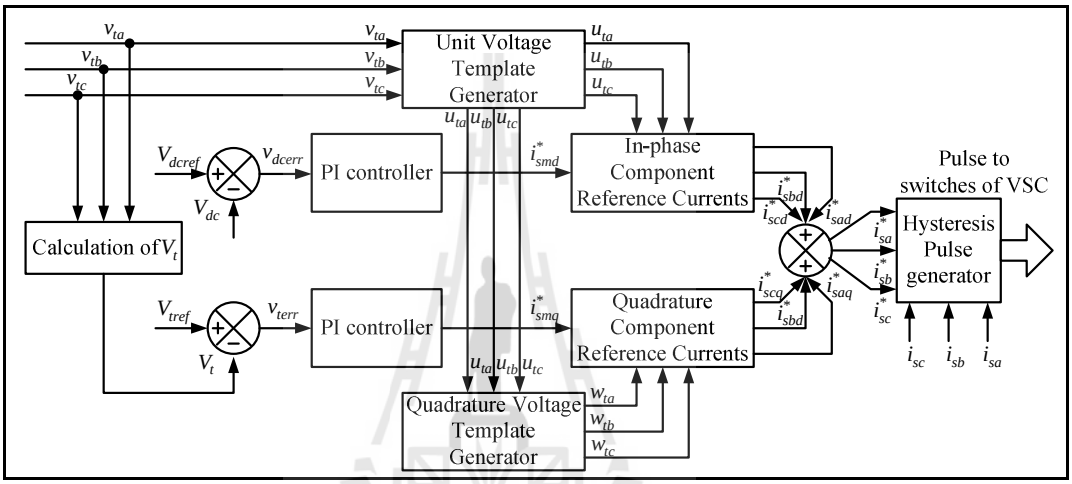

Figure 2.17 Control scheme for PI controller based carrier less hysteresis controller

$$V_t = \sqrt{\frac{2}{3}\left(v_{ta}^2 + v_{tb}^2 + v_{tc}^2\right)} \tag{2.16}$$

$$u_{ta} = \frac{v_{ta}}{V_t}$$
$$u_{tb} = \frac{v_{tb}}{V_t} \tag{2.17}$$
$$u_{tc} = \frac{v_{tc}}{V_t}$$

The unit vectors in quadrature (w_{ta} , w_{tb} and w_{tc}), are derived from the in-phase unit vectors (u_{ta} , u_{tb} and u_{tc}), using the following transformation

$$w_{ta} = -\frac{u_{tb}}{\sqrt{3}} + \frac{u_{tc}}{\sqrt{3}} \tag{2.18}$$

$$w_{tb} = \frac{\sqrt{3}}{2} u_{ta} + \left(u_{tb} - u_{tc}\right)\frac{\sqrt{3}}{2} \tag{2.19}$$

$$w_{tc} = -\frac{\sqrt{3}}{2} u_{ta} + \left(u_{tb} - u_{tc}\right)\frac{\sqrt{3}}{2} \tag{2.20}$$

The error of the AC terminal voltage at the PCC is

$$v_{terr} = \left(V_{tref} - V_t\right) \tag{2.21}$$

where V_{tref} is the amplitude of the reference AC terminal voltage at PCC and V_t is the amplitude of the sensed three phase AC terminal voltages at PCC. The amplitude i^*_{smq} of the quadrature component of the reference D-STATCOM current is derived as the output of the PI controller for maintaining AC terminal voltage constant and can be expressed as:

$$i^*_{smq} = K_{Pismq} v_{terr} + K_{Iismq} \int v_{terr} dt \tag{2.22}$$

In the above, K_{Pismq} and K_{Iismq} are the proportional and integral gain constants of the PI controller, v_{terr} is the AC voltage error. The quadrature components of the reference D-STATCOM currents are estimated as:

$$\begin{aligned} i_{saq}^{*} &= i_{smq}^{*} w_{ta} \\ i_{sbq}^{*} &= i_{smq}^{*} w_{tb} \\ i_{scq}^{*} &= i_{smq}^{*} w_{tc} \end{aligned} \tag{2.23}$$

For in-phase component of reference D-STATCOM current, the DC bus voltage error v_{dcerr} is

$$v_{dcerr} = \left(V_{dcref} - V_{dc} \right) \tag{2.24}$$

where V_{dcref} is the reference DC voltage and V_{dc} is the sensed DC link voltage of the D-STATCOM. The output of the PI controller for maintaining the DC bus voltage of the D-STATCOM is expressed as

$$i_{smd}^{*} = K_{Pismd} v_{dcerr} + K_{Iismd} \int v_{dcerr} dt \tag{2.25}$$

i_{smd}^{*} is considered as the amplitude of the active power component of the D-STATCOM current. K_{Pismd} and K_{Iismd} are the proportional and integral gain constants of the DC bus voltage PI controller, respectively. In-phase components of the reference D-STATCOM currents are estimated as:

$$\begin{aligned} i_{sad}^{*} &= i_{smd}^{*} u_{ta} \\ i_{sbd}^{*} &= i_{smd}^{*} u_{tb} \\ i_{scd}^{*} &= i_{smd}^{*} u_{tc} \end{aligned} \tag{2.26}$$

The total reference D-STATCOM current is the sum of in-phase and quadrature components of the reference D-STATCOM currents.

$$\begin{aligned} i_{sa}^{*} &= i_{saq}^{*} + i_{sad}^{*} \\ i_{sb}^{*} &= i_{sbq}^{*} + i_{sbd}^{*} \\ i_{sc}^{*} &= i_{scq}^{*} + i_{scd}^{*} \end{aligned} \tag{2.27}$$

The reference D-STATCOM currents (i_{sa}^{*}, i_{sb}^{*} and i_{sc}^{*}) are compared with the sensed D-STATCOM currents (i_{sa}, i_{sb} and i_{sc}). The on / off switching patterns of the gate drive of the switches are generated from the hysteresis controller. The hysteresis controller adds a hysteresis band ± *h* around the calculated reference current. If the sensed current corresponding to phase *a* signal is greater than the reference current added to the hysteresis band ($i_{sa} > i_{sa}^{*} + h$), the lower switch of the phase *a* leg of VSC is made ON, upper switch of the phase *a* leg of VSC is made OFF. If the sensed current is less than the reference current subtracted with the hysteresis band ($i_{sa} < i_{sa}^{*} - h$), upper switch is made ON and lower switch is made OFF. A similar logic applies to the other two phases *b* and *c*.

Some of the positive factors of this scheme are:

- The algorithm has built-in property of the self supporting DC bus.

- It is very simple, robust and has the automatic current limiting capability.

- Low the THD of D-STATCOM current.

- It has two PI controllers. It also does not require a PLL and the complex *abc* to *dq* transformation. This enhances its dynamic response.

- The algorithm can be easily modified to incorporate advanced control methods in place of the two PI controllers to enable quicker estimation of reference currents, resulting in better response for the D-STATCOM.

- Compensation for three-phase, four-wire systems can be easily achieved with the addition of a fourth leg to the VSC and a separate control for the same.

However, the negative aspects of this scheme are:

- The ripples on the DC side are high and needs proper filtering.

- Switching of the converters, depending on the dynamics of the system, may be at a considerable high frequency, causing excessive switching losses in the devices.

- And hardware implementation of the control is complex and more difficult to configure.

2.3 Application and Installation of D-STATCOM

In a distributed system, domestic and industrial loads induce harmonics, produce voltage dips, draw large reactive currents, cause imbalance in the supply current etc. The voltage of a particular bus can be distorted or unbalanced if the loads on any part of the system are nonlinear or unbalanced. The customers connected to that bus would be supplied by a set of unbalanced and distorted voltages, even when their loads are not contributing to the bus voltage pollution. The D-STATCOM has

emerged as a promising CPD to provide not only for voltage sag mitigation but a host of other PQ solutions. Important applications of it include voltage regulation, load balancing, power factor correction, harmonic filtering, and flicker mitigation. Applications of D-STATCOM in distribution level to improve power quality are well reported in many references.

2.3.1 Application of D-STATCOM for Load Compensation

For the load compensation, D-STATCOM is most widely used for harmonics mitigation, power factor correction, reactive power compensation and load balancing when connected at the load terminals. As the circuit configuration of shunt active filter is similar to D-STATCOM hence it can be used in the context of D-STATCOM. The function of shunt active filter is dependent on injection of current harmonics in phase with the load current harmonics, hence removing the harmonic content of the line current. Active filters provide an opportunity to choose the current harmonics to be filtered and the degree of attenuation. The VSC size can be reduced by using selective filtering and eliminating only those current harmonics that violate the limits given in IEEE Std. 519-1992 (IEEE 519, 1992). Active filtering also provides a control on the power factor by injecting or absorbing reactive power from the load. Moreover, Active filters can be also used to compensate nonlinear as well as unbalanced load (Akagi et al., 2007). Figure 2.18 illustrates the principle of the D-STATCOM acting as the active filter. As can be seen in this figure, the load is assumed to be reactive, nonlinear and unbalanced that can be written as (2.28).

$$i_l = i_{lp} + i_{lq} + i_{lh} \tag{2.28}$$

$$i_f = i_{lq} + i_{lh} \tag{2.29}$$

$$i_{lp} = i_s \tag{2.30}$$

$$i_s + i_f = i_l \tag{2.31}$$

where i_{lp}, i_{lq} and i_{lh} are active, reactive and harmonic load currents, respectively. First, assume the load is without a compensator. Hence, line current i_s flowing through the feeder is also unbalanced and distorted. The function of D-STATCOM is dependent on injection of reactive and harmonic currents (2.29) in-phase with the load reactive and harmonic currents, hence removing the reactive and harmonic content of the line current i_s. Therefore, the line current i_s becomes active current (2.30) and in-phase with the system voltage v_t.

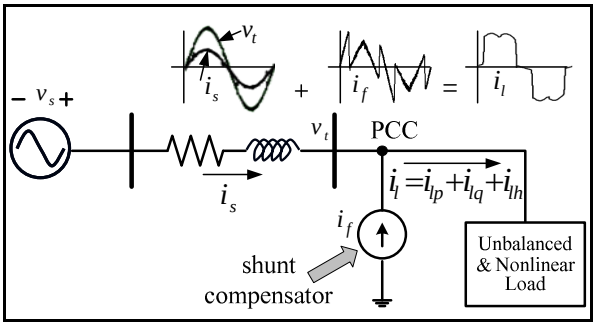

Figure 2.18 Principle of the D-STATCOM acting as the active filter

In practice however the current source is implemented using the voltage source converter which can control the compensation current i_f to extract the reference current signal. The method of generating reference currents for the D-STATCOM is interested and presented in many references. Akagi and his coworkers have described an instantaneous *pq* theory of generating reference currents for the D-STATCOM in (Akagi et al., 1984; Akagi et al., 1986). Since then various interpretations of this method have been presented in (Furuhashi et al., 1990; Willems, 1992; Watanabe et al., 1993; Ferrero and Superti-Furga, 1991). This method is applicable to the three-phase, four-wire system. To begin with, transformation of the three phase voltages from *abc* to $\alpha\beta 0$ frame and vice versa using the following invariant transformation

$$\begin{bmatrix} v_0 \\ v_\alpha \\ v_\beta \end{bmatrix} = \sqrt{\frac{2}{3}} \begin{bmatrix} 1/\sqrt{2} & 1/\sqrt{2} & 1/\sqrt{2} \\ 1 & -1/2 & -1/2 \\ 0 & \sqrt{3}/2 & -\sqrt{3}/2 \end{bmatrix} \begin{bmatrix} v_a \\ v_b \\ v_c \end{bmatrix} \tag{2.32}$$

Similarly, the currents can be also transformed by using the same transform matrix. Three instantaneous powers: the instantaneous zero sequence power p_0, the instantaneous active power p, and the instantaneous reactive power q are defined from the instantaneous phase voltages and line currents on the $\alpha\beta 0$ axes as

$$\left[\begin{array}{c} p_0 \\ \hdashline p \\ q \end{array}\right] = \left[\begin{array}{c|cc} v_0 & 0 & 0 \\ \hdashline 0 & v_\alpha & v_\beta \\ 0 & v_\beta & -v_\alpha \end{array}\right] \left[\begin{array}{c} i_0 \\ \hdashline i_\alpha \\ i_\beta \end{array}\right] \tag{2.33}$$

The relation between the conventional concepts of powers and the new powers defined in the *pq* theory is better visualized if the powers *p*, *q* and p_0 are separated in their average values $\bar{p}$, $\bar{q}$, $\bar{p}_0$ and their oscillating parts $\tilde{p}$, $\tilde{q}$, $\tilde{p}_0$.

$$\begin{aligned} &\text{Active power:} && p = \bar{p} + \tilde{p} \\ &\text{Reactive power:} && q = \bar{q} + \tilde{q} \\ &\text{Zero sequence power:} && p_0 = \bar{p}_0 + \tilde{p}_0 \end{aligned} \tag{2.34}$$

Average powers — Oscillating powers

There are no zero sequence current components in three-phase, three-wire systems, that is, $i_0 = 0$. In this case, only the instantaneous powers defined on the $\alpha\beta$ axes exist, because the product $v_0 i_0$ is always zero. Hence, (2.33) can be rewritten as

$$\begin{bmatrix} p \\ q \end{bmatrix} = \begin{bmatrix} v_\alpha & v_\beta \\ v_\beta & -v_\alpha \end{bmatrix} \begin{bmatrix} i_\alpha \\ i_\beta \end{bmatrix} \tag{2.35}$$

These two powers have constant values and a superposition of oscillating components. Therefore, it is interesting to separate *p* and *q* into two parts:

$$\begin{aligned} &\text{Active power:} && p = \bar{p} + \tilde{p} \\ &\text{Reactive power:} && q = \bar{q} + \tilde{q} \end{aligned} \tag{2.36}$$

Average powers Oscillating powers

The idea is to compensate all undesirable power components generated by nonlinear loads that can damage or make the power system overloaded or stressed by harmonic pollution. In this way, it would be desirable for a three-phase balanced power generating system to supply only the average active power $\bar{p}$ of the load. Thus, all other power components required by the nonlinear load, that is, $\tilde{p}$, $\bar{q}$, $\tilde{q}$, $\bar{p}_0$ and $\tilde{p}_0$, should be compensated by a D-STATCOM connected as close as possible to this load. This algorithm is called constant instantaneous power control strategy (Akagi et al., 2007). If there is no zero sequence current to be compensated, the zero sequence power p_0 is always zero. In this case, a D-STATCOM should be controlled to compensate the oscillating active power $\tilde{p}$ and the whole reactive power $q = \bar{q} + \tilde{q}$.

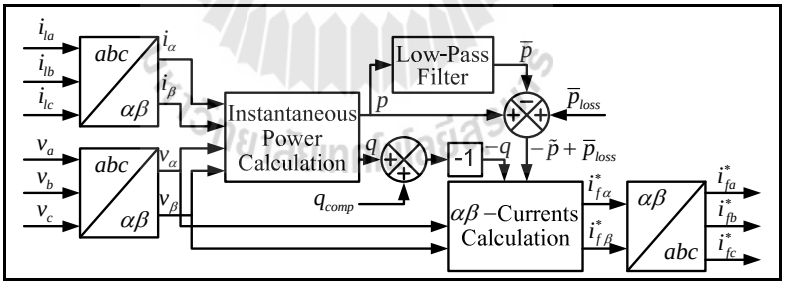

Figure 2.19 Algorithm of constant instantaneous power control strategy

Figure 2.19 shows the algorithm of a controller for a three-phase three-wire D-STATCOM that compensates the oscillating active power and the reactive power for the load. This guarantees constant instantaneous power $\bar{p}$ drawn from the

source with reduced losses in the distribution system, since the reactive power of the load is also being compensated. This is done by selecting the powers $\tilde{p}$ and q of the load to be compensated. The compensating current can be calculated as

$$\begin{bmatrix} i^*_{f\alpha} \\ i^*_{f\beta} \end{bmatrix} = \frac{1}{v_\alpha^2 + v_\beta^2} \begin{bmatrix} v_\alpha & v_\beta \\ v_\beta & -v_\alpha \end{bmatrix} \begin{bmatrix} -\tilde{p} + \bar{p}_{loss} \\ -q \end{bmatrix} \tag{2.37}$$

$$\begin{bmatrix} i^*_{fa} \\ i^*_{fb} \\ i^*_{fc} \end{bmatrix} = \sqrt{\frac{2}{3}} \begin{bmatrix} 1 & 0 \\ -1/2 & \sqrt{3}/2 \\ -1/2 & -\sqrt{3}/2 \end{bmatrix} \begin{bmatrix} i^*_{c\alpha} \\ i^*_{c\beta} \end{bmatrix} \tag{2.38}$$

Additionally, the DC voltage regulator determines an extra amount of active power, represented by $\bar{p}_{loss}$ in Figure 2.19 that causes an additional flow of energy to (from) the DC capacitor in order to keep its voltage around a fixed reference value. In order to control the compensation current i_f to extract the reference current signal i^*_f the PWM or hysteresis current control can be used.

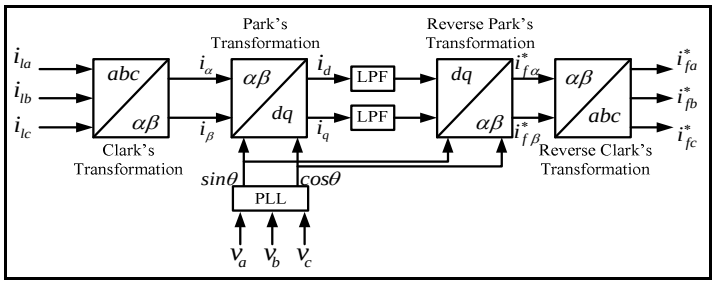

Figure 2.20 Algorithm of the synchronous reference frame of generating reference currents

The applications of the instantaneous *pq* theory with the hysteresis current control are investigated and presented in (Singh et al., 2006; Singh and Jitendra, 2006). The performances of the three-phase, four-wire D-STATCOM (Singh et al., 2006) and three-phase, three-wire D-STATCOM (Mishra et al., 2006) for load compensation are proposed. In addition, a comparative study of control algorithms between the instantaneous *pq* theory and synchronous reference frame to generate reference currents of D-STATCOM for load compensation are presented in (Singh and Jitendra, 2006). The algorithm of synchronous reference frame of generating reference currents is shown in Figure 2.20. As the results, the dynamic performances of both the instantaneous *pq* theory and synchronous reference frame are similar. However, these performances have a delay time because of the effect of the low pass filters and PLL (in case of synchronous reference frame).

Another method for generating the reference currents that are instantaneous symmetrical components is proposed in (Ghosh and Ledwich, 2002). This compensation scheme can be applied to either a three-phase, three-wire system or a three-phase, four-wire system. The loads can be either connected in wye or in delta. The objective in either three or four wires system compensation is to provide balance supply current such that its zero-sequence component is zero.

$$i_{sa} + i_{sb} + i_{sc} = 0 \tag{2.39}$$

In the method discussed in above, there is no direct control over the power factor angle from the source and the algorithm forces the source current to be unity power factor. In the method under consideration, this angle can be set to have

desired value. The current references of compensating wye and delta connected loads by using the instantaneous symmetrical components theory are shown in (2.40) and (2.41), respectively (Ghosh and Joshi, 2000).

$$\begin{aligned} i_{fa}^{*} &= i_{la} - \frac{v_{ta} + (v_{tb} - v_{tc})\beta}{v_{ta}^2 + v_{tb}^2 + v_{tc}^2} p_{lav} \\ i_{fb}^{*} &= i_{lb} - \frac{v_{tb} + (v_{tc} - v_{ta})\beta}{v_{ta}^2 + v_{tb}^2 + v_{tc}^2} p_{lav} \\ i_{fc}^{*} &= i_{lc} - \frac{v_{tc} + (v_{ta} - v_{tb})\beta}{v_{ta}^2 + v_{tb}^2 + v_{tc}^2} p_{lav} \end{aligned} \tag{2.40}$$

$$\begin{aligned} i_{fab}^{*} &= i_{lab} - \frac{v_{tab} - 3\beta v_{tc}}{(v_{ta} - v_{tb})^2 + (v_{tb} - v_{tc})^2 + (v_{tc} - v_{ta})^2} p_{lav} \\ i_{fbc}^{*} &= i_{lbc} - \frac{v_{tbc} - 3\beta v_{ta}}{(v_{ta} - v_{tb})^2 + (v_{tb} - v_{tc})^2 + (v_{tc} - v_{ta})^2} p_{lav} \\ i_{fca}^{*} &= i_{lca} - \frac{v_{tca} - 3\beta v_{tb}}{(v_{ta} - v_{tb})^2 + (v_{tb} - v_{tc})^2 + (v_{tc} - v_{ta})^2} p_{lav} \end{aligned} \tag{2.41}$$

where $\beta \equiv \tan\phi/\sqrt{3}$, ϕ is the desired phase angle between system voltage and source current. p_{lav} is the average power drawn by the load. For $\beta = 0$, the source currents are to be in-phase of PCC voltages. It implies that the reactive power demand of the load is supplied by the D-STATCOM. For non-zero of β, the system supplies or absorbs the reactive power corresponding to the β.

Applications of the instantaneous symmetrical components to generate the reference currents for D-STATCOM are well reported in many references. Hasanzadeh et al. (2005) have proposed the instantaneous symmetrical components to generate the reference currents of a D-STATCOM for the load balancing and power

factor correction. Two topologies such as H-bridge and three-phase, four-wire capacitor mid-point VSC have been investigated. The PWM and hysteresis current control schemes are used to control the compensation current to extract the reference current signal. The performance of the D-STATCOM topology for compensating AC loads in the three-phase, four-wire system as well as supplying DC load from its DC link is presented in (Mishra and Karthikeyan, 2008). In this paper, the instantaneous symmetrical components method to generate the reference currents and the hysteresis current control are applied. The DC load is supplied from the DC link of the D-STATCOM. Due to the transients on the load side, the DC bus voltage is significantly affected. To regulate this voltage, the DC voltage control is proposed. Which consideration the DC voltage control, the current reference in (2.40) is modified as (2.42).

$$
\begin{aligned}
i_{fa}^{*} &= i_{la} - \frac{v_{ta} + (v_{tb} - v_{tc})\beta}{v_{ta}^2 + v_{tb}^2 + v_{tc}^2}(p_{lav} + p_{loss}) \\
i_{fb}^{*} &= i_{lb} - \frac{v_{tb} + (v_{tc} - v_{ta})\beta}{v_{ta}^2 + v_{tb}^2 + v_{tc}^2}(p_{lav} + p_{loss}) \\
i_{fc}^{*} &= i_{lc} - \frac{v_{tc} + (v_{ta} - v_{tb})\beta}{v_{ta}^2 + v_{tb}^2 + v_{tc}^2}(p_{lav} + p_{loss})
\end{aligned}
\tag{2.42}
$$

where p_{loss} is the power supplied to the DC load and losses in the converter. To generate p_{loss}, two controllers such as conventional and fast acting DC voltage controller are used and compared. PI controller is used in both conventional and fast acting DC voltage control. However, control algorithm especially PI parameter tuning is not discussed in detail in the paper.

Mishra and Karthikeyan (2008) present four legs VSC based D-STATCOM with modified instantaneous symmetrical component theory based on the control algorithm for load compensation. The performance of D-STATCOM is studied for the compensation of reactive power, harmonic currents and load balancing along with power factor correction in three-phase four-wire distribution system. To regulate the DC and PCC voltages the PI controller is used. However, the PI parameter tuning is not presented. In addition, Ghosh and Ledwich (2003) have discussed the three H-bridge VSCs that are connected to a common DC storage capacitor with instantaneous symmetrical components theory control of a D-STATCOM for load compensation at a weak AC bus. The operation of a D-STATCOM for weak AC buses will result in distortions in the line current or the voltage at the point of common coupling. The line current distortion has been eliminated using the fundamental voltage of the PCC, but the distortion in voltage cannot be eliminated without adding a filter capacitor in parallel with the D-STATCOM. However, the addition of the filter capacitor generates control issues and complicates the tracking problem, as standard controls are not appropriate to be used in this situation. A switching control scheme was then proposed that depends on the extraction of the reference signals to solve the tracking problem. To implement the switching control the references for compensator current are computed using modified instantaneous symmetrical components theory as shown in (2.43).

$$
\begin{aligned}
i_{fa}^{*} &= i_{la} - \frac{v_{ta} - v_0}{\left(v_{ta}^2 + v_{tb}^2 + v_{tc}^2\right) - v_0^2}\left(p_{lav} + p_{loss}\right) \\
i_{fb}^{*} &= i_{lb} - \frac{v_{tb} - v_0}{\left(v_{ta}^2 + v_{tb}^2 + v_{tc}^2\right) - v_0^2}\left(p_{lav} + p_{loss}\right) \\
i_{fc}^{*} &= i_{lc} - \frac{v_{tc} - v_0}{\left(v_{ta}^2 + v_{tb}^2 + v_{tc}^2\right) - v_0^2}\left(p_{lav} + p_{loss}\right)
\end{aligned}
\tag{2.43}
$$

Where $v_0 = \frac{1}{3}\left(v_{ta} + v_{tb} + v_{tc}\right)$ and p_{loss} is the power loss due to the converter. The correction p_{loss} must be generated through a suitable feedback control such that the DC voltage across the storage capacitor is maintained. In the simplest form of feedback, The PI controller is used to correct the DC voltage. However, the design of PI controller parameters is not proposed.

Furthermore, many literatures have been discussing various topologies of a D-STATCOM for the load compensation. The performances of D-STATCOM connected to feeding four–wire linear and nonlinear load for power factor correction and load balancing are presented in (Singh et al., 2006; Mishra and Karthikeyan, 2008; Vechiu et al., 2010). In these papers, a four leg voltage source converter configuration is chosen as D-STATCOM. Meanwhile, the D-STATCOM of three-phase, three-wire distribution system for unbalanced load compensation is proposed in (Shukai Xu et al., 2005). As D-STATCOM has an inherent characteristic of real power exchange with a support of the proper energy storage system such as a battery. If a battery is connected to the DC capacitor, the power regulation ability of a common D-STATCOM can be expanded to both reactive and active power compensation. The D-STATCOM with battery energy storage system for load

compensation such as the harmonic elimination, load balancing and load leveling are investigated in (Singh et al., 2007; Bhatia et al., 2004).

2.3.2 Application of D-STATCOM for Voltage Regulation

For voltage regulation, the D-STATCOM can be also applied to the voltage regulation, mitigate voltage sag / swell, voltage flicker and voltage fluctuations when connected to a distribution bus. In steady state analysis, the schematic diagram of a D-STATCOM for voltage regulation is shown in Figure 2.21. In this diagram, the D-STATCOM injected current $\bar{I}_f$ regulates the voltage by adjusting the voltage drop across the system impedance $\bar{Z}_{th}$. The injected current $\bar{I}_f$ can be written as

$$\bar{I}_f = \bar{I}_l - \bar{I}_s = \bar{I}_l - \frac{\bar{V}_{th} - \bar{V}_t}{\bar{Z}_{th}}$$

$$\text{or, } I_f \angle \gamma = I_l \angle -\theta - \frac{V_{th} \angle (\alpha - \beta)}{Z_{th}} + \frac{V_t \angle -\beta}{Z_{th}} \tag{2.44}$$

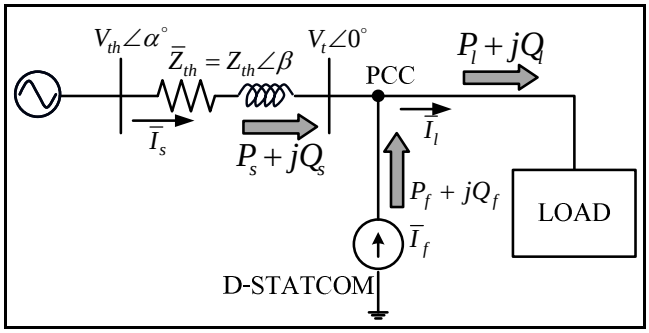

Figure 2.21 Schematic diagram of a D-STATCOM for voltage regulation

It may be mentioned here that the effectiveness of the D-STATCOM in regulating voltage depends on the value of $\bar{Z}_{th}$ or fault level of the PCC bus. When the injected current $\bar{I}_f$ is kept in quadrature with $\bar{V}_t$, the desired voltage regulation can again be achieved without injecting any active power into the system. In this case, the entire load active power P_l must be provided by the system. The active power flow through the Thevenin impedance of Figure 2.21 (at load side) can be written as

$$P_l = \frac{V_{th}V_l}{Z_{th}}\cos(\beta-\alpha) - \frac{V_l^2}{Z_{th}}\cos\beta \tag{2.45}$$

From (2.45), the angle α can be expressed as

$$\alpha = \beta - \cos^{-1}\left[\frac{V_t}{V_{th}}\cos\beta + \frac{Z_{th}P_l}{V_{th}V_t}\right] \tag{2.46}$$

For a feasible value of α, the condition in (2.47) must be satisfied.

$$\frac{V_t}{V_{th}}\cos\beta + \frac{Z_{th}P_l}{V_{th}V_t} \le 1 \tag{2.47}$$

The above constraint can be rewritten as

$$V_{th} \ge (V_l\cos\beta + \frac{Z_{th}P_l}{V_t}) \tag{2.48}$$

Thus, when the system voltage magnitude satisfies as (2.48), the D-STATCOM can regulate the voltage without injecting any active power into the system. However, the D-STATCOM can regulate the voltage with minimum apparent power injection into the system. The apparent power injection of the D-STATCOM can be expressed as

$$\overline{S}_f = \overline{V}_t \overline{I}_f^* \tag{2.49}$$

Thus the condition of minimum apparent power injection is

$$\frac{\partial \overline{I}_f}{\partial \alpha} = 0 \tag{2.50}$$

An analytical expression of $\overline{I}_f$ can readily be obtained from (2.44), and solution of (2.50) provides the following

$$\alpha = \tan^{-1}\left[\frac{Z_{th} I_l \sin(\beta - \theta)}{V_t + Z_{th} I_l \cos(\beta - \theta)}\right] \tag{2.51}$$

Thus for a given load, the value of α can easily be found from (2.51). Once the value of α is known, the complex current and apparent power injection of the D-STATCOM can again be obtained from (2.44) and (2.49), respectively (Haque, 2001).

In actuality, the current source is implemented using the VSC connected to the network through the transformer and the interfacing inductors which the DC voltage source on the input side of VSC that is generally achieved by a DC

capacitor. Therefore, the magnitude and phase angle of the injected current $\bar{I}_f$ in Figure 2.21 can be determined by the magnitude and phase angle of the AC output voltage of VSC (V_{st} and δ). In this case, the D-STATCOM can regulate the terminal voltage by injecting only reactive power into the system which consuming some active power from the system to control DC capacitor voltage.

Power flows of the voltage regulation with the D-STATCOM can be illustrated in Figure 2.22. At the normal operation point (t = 0 – 0.05s), the load voltage is as the desired magnitude, the D-STATCOM does not inject the reactive power into the system to regulate load voltage. As, in this point, the load powers are supplied by the source through feeder. When the source voltage sags (t = 0.05 – 0.25s), this results in the decrease of the load voltage that can be seen in Figure 2.22(a). However, the load voltage can be regulated by injecting the reactive power of the D-STATCOM into the system. When the source voltage swells (t = 0.25 – 0.35s), the load voltage is above the desired magnitude. Therefore, the D-STATCOM regulates the load voltage by absorbing the reactive power resulting in being the negative of D-STATCOM reactive power. The reactive powers for the load voltage regulation are show in Figure 2.22(b).

In practice, the semiconductor switches of the converter are not lossless, so the energy stored in the DC capacitor is eventually used to meet the internal losses of the convertor, and the DC capacitor voltage diminishes. However, when the D-STATCOM is used to generate or absorb reactive power, the converter itself can keep the capacitor charged to the required voltage level. This task is accomplished by making the output voltages of the converter lag behind the AC system voltages by a small angle. In this way, the converter absorbs a small amount of

active power from the AC system to meet its internal losses and keep the capacitor voltage at the desired level. The same mechanism can be used to increase or decrease the capacitor voltage. The active power and DC capacitor voltage for the load voltage regulation are show in Figure 2.22(c) and Figure 2.22(d), respectively.

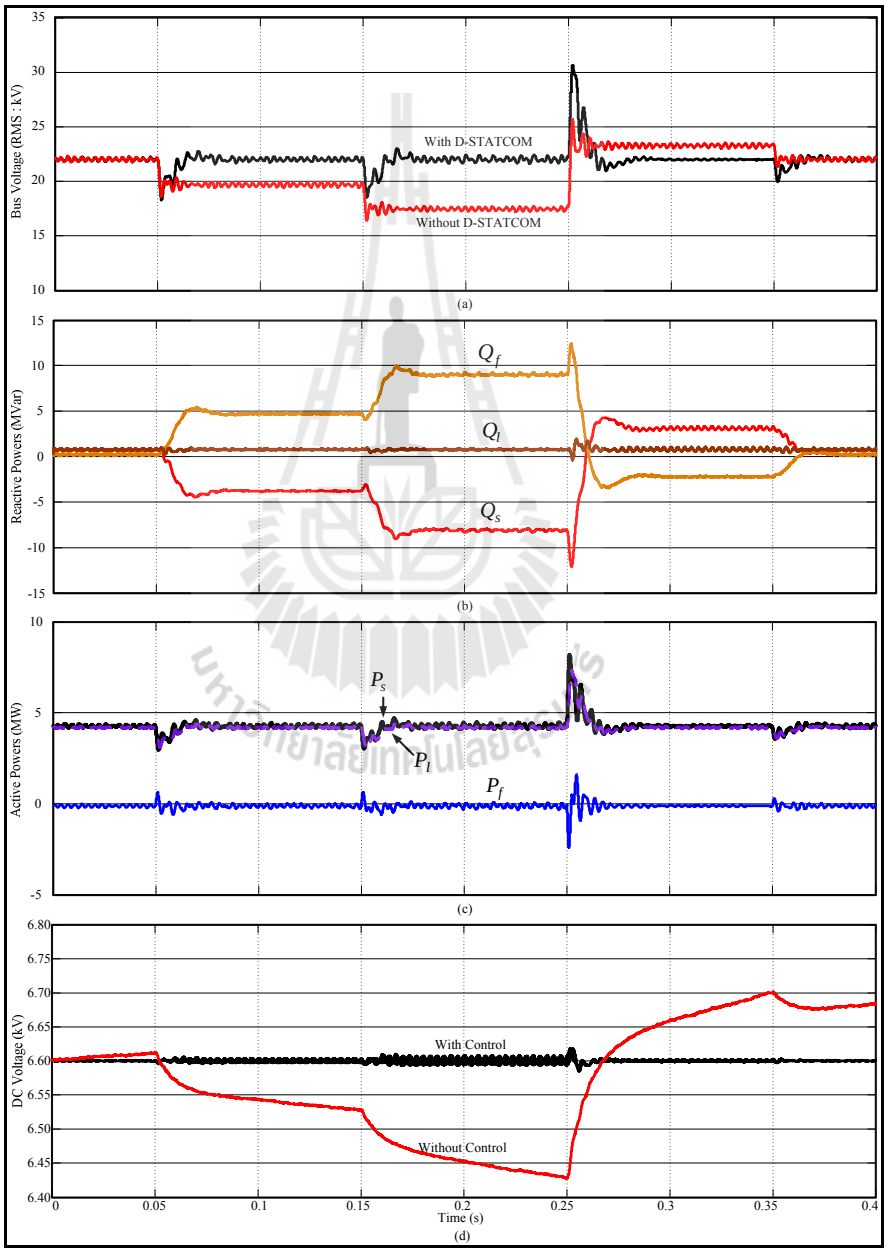

Figure 2.22 Power flow of the voltage regulation with the D-STATCOM

Many literatures have been proposed applications of the D-STATCOM for AC voltage control. Anaya-Lara and Acha (2002) and Somsai and Kulworawanichpong (2008) have presented a method to operate D-STATCOM as a voltage regulator to maintain the voltage of a distribution bus. A three-phase, three-wire distribution system has been assumed in this investigation. D-STATCOM is realized by a three-phase bridge VSC circuit that is supplied by a DC storage capacitor. Since the AC output voltage of VSC is proportional the DC voltage, the AC terminal voltage can be controlled through the DC voltage. However, the DC voltage can be controlled by adjusting the phase angle δ of the AC output voltage of VSC. Thus the AC output voltage references can be written as

$$\begin{aligned} v_{staref} &= V_{tm}\sin(\omega t - \delta) \\ v_{stbref} &= V_{tm}\sin(\omega t - \delta - 120^{\circ}) \\ v_{stcref} &= V_{tm}\sin(\omega t - \delta + 120^{\circ}) \end{aligned} \tag{2.52}$$

where V_{tm} is the amplitude of the reference AC terminal voltage at PCC. The phase angle δ of the AC output voltage of VSC is derived as output of the PI controller for maintaining AC terminal voltage constant and can be expressed as:

$$\delta = K_{Pac}(V_{rmsref} - V_{rms}) + K_{Iac}\int (V_{rmsref} - V_{rms})dt \tag{2.53}$$

This algorithm is called the phase shift control of D-STATCOM for AC voltage regulation.

Mishra et al. (2002) have proposed the D-STATCOM with modified phase shift control to maintain the voltage of a distribution system. A three-phase, four-wire distribution system has been assumed in this investigation. D-STATCOM is realized by a three-phase bridge VSC circuit that is supplied by two neutral-clamped DC storage capacitors. Three filter capacitors, one for each phase; have been connected in parallel with the D-STATCOM to eliminate high-frequency switching components. The control scheme realized by a dead-beat controller for the VSC has been used to control the voltage across the filter capacitor to maintain the AC bus voltage. The control scheme consists of an outer DC capacitor voltage control loop and an inner phase angle control loop. The P controller is applied to the outer DC capacitor voltage control loop whereas the inner phase angle control loop the PI controller is used. Block diagram of closed loop voltage control is shown in Figure 2.23. The load bus voltage magnitude is chosen as nominal value, i.e., 1.0 p.u., while its phase angle is attained through a feedback loop that regulates the voltage across the DC storage capacitors. It has been shown through detailed simulation and experimental results, that the D-STATCOM is capable of regulating the PCC voltage against any unbalance and distortion in either on the load or supply side. However, the employed dead-beat control scheme for the VSC to maintain the AC bus voltage is very sensitive to system parameters and it must be carefully used even if it has a very fast convergence property.

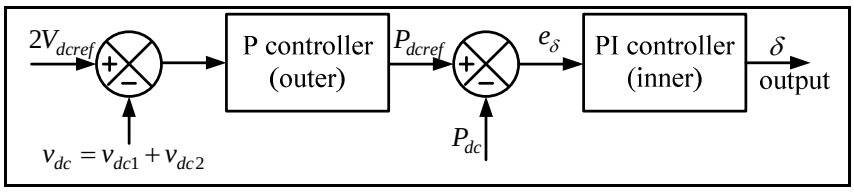

Figure 2.23 Modified phase shift control to maintain the voltage of a distribution system

The control algorithm based on the developed mathematical model in the *dq* synchronously rotating reference frame of the D-STATCOM for voltage regulation has been proposed in (Jain et al., 2006). In this paper, a modeling strategy similar to that used for the field oriented control of three phase AC machines is used. This gives a clearer representation of instantaneous load bus voltage magnitude and D-STATCOM reactive current without any restriction on the dynamics. The control problem of load voltage regulation using reactive current as the control input was shown to be the non-minimum phase for certain operating condition, thereby limiting dynamic response using linear output feedback. A linear controller with output feedback and a nonlinear controller with state feedback for load voltage control were designed and compared. Results show that the nonlinear controller has a better transient response for load changes and leads to better mitigation of flicker arising from time varying loads. However, the system considered in this paper is a simplified model of an only real resistance load supplied on a distribution system.

Freitas et al. (2005) have presented a dynamic study about the simultaneous usage of AC generators and D-STATCOM devices on the dynamic behavior of distribution networks. The performance of a D-STATCOM as a power

factor controller or a voltage controller has been analyzed. D-STATCOM voltage controller is shown in Figure 2.24. The controllers' impact on the stability performance and protection system of distribution networks with distributed generators has been determined. Simulation results have shown that a D-STATCOM voltage controller can improve the stability performance of induction generators significantly. Whereas, a D-STATCOM power factor controller may adversely affect the stability performance of synchronous generators. Moreover, simulation results show that although load bus is maintained at constant value but the D - STATCOM response to stabilize load voltage is poor and it took 35 cycles to attain steady-state value. This shows that D-STATCOM controller performance needs to be improved.

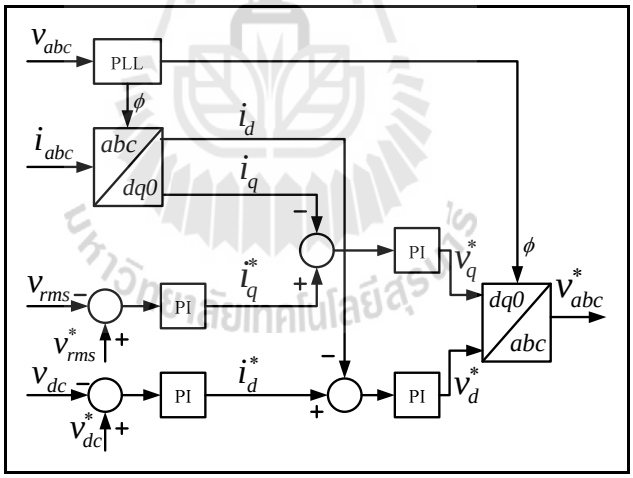

Figure 2.24 D-STATCOM Voltage Controller

Blazic and Papic (2006) have proposed a new D-STATCOM control algorithm that enables separate control of positive- and negative-sequence currents and decoupled control of *dq* axes current components. The proposed control algorithm

is based on the developed mathematical model in the *dq* synchronously rotating reference frame for a D-STATCOM operating under unbalanced conditions. The problem of DC-side voltage ripple and AC side harmonics generation due to unbalanced voltages / currents is solved with an appropriate modulation of switching function so that a DC capacitor does not have to be overrated. The proposed control scheme is also suitable for high-power applications using multi-pulse VSCs. The algorithm has been tested by carrying out detailed simulation using PSCAD. Simulation results have shown good dynamic performance especially in the case of unbalanced load compensation. However, as the *dq* synchronously rotating reference frame method is used for sag detection in the control algorithm, it provides good results for balanced voltage sag.

In addition, the fast response of the D-STATCOM makes it the efficient solution for improving voltage flicker phenomena in distribution systems that are presented in (Chong et al., 2007; Sun et al., 2002). The performances of the D-STATCOM used for mitigating voltage sag and swell are investigated and compared with the series compensator as presented in (Anaya-Lara and Acha, 2002; Gupta et al., 2011; Ravi Kumar and Siva Nagaraju, 2007). The multi level D-STATCOM for voltage sag and swell reduction is proposed in (Sharmeela et al., 2005). Isolated distribution systems are comparatively not as stiff as grid systems; so large starting currents and objectionable voltage drop during starting of an induction motor could be critical to the entire system. The application of D-STATCOM to industrial systems for mitigation of the voltage dip problem during the starting of an induction motor is presented in (Singh et al., 2006).

2.3.3 Application of D-STATCOM with Distributed Generator

Furthermore, current power distribution systems are experiencing increased installation of distributed generators and application of custom power devices. The most common type of distributed generation employs AC rotating machines. The D-STATCOM has been adopted for the purpose of improving power quality and reliability of the power distribution systems with installation of distributed generators. The dynamic study about the influences of AC generators (induction and synchronous machines) and D-STATCOM device on the dynamic behavior of distribution networks is presented in (Freitas et al., 2005). The performance of the D-STATCOM as a voltage controller or a power factor controller is analyzed. Induction generators (IG) have received more attention, which have been employed in thermal, small-hydro and wind generation plants. Induction generators have some technical advantages when compared with synchronous generators; for example: increased robustness reduced size, decreased cost, greater electromechanical damping. However, it is well known that induction generators draw very large reactive currents during the fault occurrence, depressing the network voltage further and leading the system to voltage instability. An alternative for solving this problem is to adopt local dynamic reactive power compensation. Freitas et al. (2002) investigate the use of the D-STATCOM to improve the voltage stability performance of distribution systems with induction generators based on three-phase non-linear dynamic simulations.

In addition, self excited induction generators (SEIGs) have regained importance in supplying electricity to the remotely located communities (where grid supply is not applicable) using available renewable energy sources like wind, hydro and bio-mass. It is well known that for maintaining constant voltage at the terminals

of IG under the condition of varying loads and speed, a continuous demand of reactive power is needed. In case of the constant speed prime mover like bio-gas, diesel, gasoline engines, the speed of the isolated induction generator (IIG) remains constant while voltage at the generator terminal varies under varying consumer loads because of increased reactive power requirement. The applications of the D-STATCOM for regulating terminal voltage of the isolated induction generators have been proposed in (Kansal and Singh, 2008; Singh and Kansal, 2008).

2.3.4 Status of Installations of D-STATCOM Device

Status of the installations of the D-STATCOM device is not very well documented. It is thus rather difficult to get the current installation status. The status given below is reported in (IEEE P1409, 1999) and by no means presents the complete picture.

American Electric Power (AEP) has installed a distribution static shunt voltage compensator at a rock crushing facility. This facility has two existing rocks crushing operations with a third going into service. The rating of the device installed at the facility to control the voltage flicker is ±2*MVA* at 12.47*kV*. It was placed online in January 1998 and commissioned on February 12, 1998. The unit utilizes two 1*MVAr* capacitor banks that allow operation with output from 0 to 4*MVAr* capacitive.

The D-STATCOM device has successfully completed the one-year demonstration project at the Adams Lake Lumber Company in Chase, British Columbia where it provided voltage regulation and voltage flicker mitigation caused by a large whole log chipping operation. This device is capable of adjusting the line voltage +/- 4.2%. Field experience has shown that overall flicker was reduced from 5-8% to 2.5-4%. The ±2*MVA* inverter-based trailer unit is now being readied by BC

Hydro for relocation to another site where voltage flicker is creating major problems for customers on the 25kV distribution system.

In October 1990 the 20*MVAr* GTO inverter D-STATCOM device was implemented for arc furnace flicker compensation on a 22*kV* feeder. The successful operation and experience of this first installation encouraged the steel manufacturer to further increase arc furnace operation, and was followed by another D-STATCOM device installation using a 21*MVAr* GTO inverter for the same purpose in May 1995. The GTO inverter cubicles of the second D-STATCOM device were specifically designed to be more compact in size in order to provide benefits for industrial application use.

A static var compensator of 3.5*MVAr* capacities using a bipolar transistor inverter for arc furnace flicker compensation was installed on the Mitsubishi Steel Co. 33*kV* feeder on December 1989. This installation was implemented in conjunction with an existing 60*MVAr* SVC that had been installed in April 1984. The additional 3.5*MVAr* D-STATCOM enabled an increase in steel productivity of the arc furnace without any increase in the previous flicker level.

Oglethorpe Power Corporation and Oconee Electric Membership Corporation, a member system of Oglethorpe Power, are host utilities to an installation of D-STATCOM installed on a 12.47*kV* feeder serving a building products plant in Dudley, Georgia. The plant uses many large induction motors that cause flicker when starting and operating. In addition to flicker, a low power factor is present when the motors are idling, which is often the case. This installation continues to mitigate flicker as designed.

The installation of a 5*MVA*, 4.16*kV* D-STATCOM was completed in July, 1999 at the Seattle Iron & Metals Corporation's new steel recycling facility in Seattle, Washington. The D-STATCOM was selected as the preferred option for voltage flicker compensation of a 4,000*Hp* shredder motor, which is being operated at the new facility. The D-STATCOM has a rated output capacity of +/-2*MVAr* (continuous rating) and +/-3*MVAr* (overload rating for 1 minute). In this application, the D-STATCOM is operating at 4.16*kV* and provides reliable power quality for both the new steel recycling facility and the interconnecting utility, Seattle City Light, which provides power to the plant at 26.4*kV*. Final field testing and commissioning of the D-STATCOM was completed in February, 2000.

2.4 Summary

This chapter proposes a review of the D-STATCOM and its application. The working principle and several configurations of the D-STATCOM are presented. The principle of D-STATCOM based on ideal current source and voltage source converter are discussed in detail. For power quality improvement the voltage source converter (VSC) bridge structure is generally used for the development of the D-STATCOM. Several configurations of VSC-based D-STATCOM such as single-phase H-bridge, three-phase three-wire, three-phase four-wire and multilevel VSC are proposed. The performance of the D-STATCOM depends on the control algorithm. Many control strategies of the D-STATCOM have been reported and presented in various literatures. However, a brief review of the D-STATCOM control strategies is presented in this chapter. In addition, the generation of proper triggering pulses for the switches of the VSC is very crucial. It has been observed that all the schemes broadly

fall into three categories such as phase shift control, carrier-based PWM control and carrier less hysteresis control. Furthermore, the examples of the applications and installations of the D-STATCOM for compensation in the distribution system are proposed. Applications of the D-STATCOM in distribution level to improve power quality are well reported in many references. Three categories of applications such as load compensation, voltage regulation and application with distributed generators are also presented. For load compensations, the methods of generating reference currents of the D-STATCOM i.e. instantaneous *pq* theory, synchronous reference frame and instantaneous symmetrical components and their applications are presented. Meanwhile, the phase shift and the *dq* synchronous rotating reference frame control algorithm are discussed in the applications of the D-STATCOM for voltage regulation. In terms of the applications with the distributed generator, the D-STATCOM has applied for reactive compensation and maintaining constant voltage at the terminals of distributed generator. Regarding the applications of the D-STATCOM, the performances depend on the control algorithm. Of all the mentioned applications, the most common type of controllers employs the PI controller. However, the details of the strategy to tune the PI controller parameters have not been widely presented and discussed by various researchers, especially in terms of the applications for voltage regulation which is significant and interesting.

CHAPTER III

MODELING AND STEADY STATE ANALYSIS OF THE DISTRIBUTION SYSTEM WITH D-STATCOM

This chapter presents the mathematical modeling of the distribution system with an ideal D-STATCOM. The D-STATCOM modeled as an ideal controllable current source. For control design and dynamic analysis, the mathematical modeling of the distribution system was derived by transforming the equivalent system impedance to a *dq* frame that is presented in Section 3.1. In Section 3.2, a modeling strategy similar to that used in the field oriented control of three phase AC machines is used. However, the steady state characteristic can be obtained from state equation of the distribution system with an ideal D-STATCOM that leads to analysis of the steady state performance in Section 3.3. In this section, the maximum load power and the minimum source voltage that the D-STATCOM can regulate the load voltage with injecting only the reactive power into the system are obtained and discussed. Furthermore, the effects of system parameters on size of the D-STATCOM for voltage regulation when the source voltage sags and load power variations are investigated. A summary of this chapter is presented in Section 3.4.

3.1 Modeling of the Distribution System

The system considered here is a simplified model of a load served by an electric power distribution system. It assumes that a D-STATCOM is connected in parallel with the load to perform power compensation in a medium-voltage distribution feeder. The distribution system with the D-STATCOM is shown in Figure 3.1. For simplification, a model of an ideal current source is employed. The system consists of the source modeled as an infinite bus with inductive source impedance, the load modeled by a series of resistance and inductance, the D-STATCOM modeled as a controllable current source, and coupling capacitor. The coupling capacitor is included for two reasons: (i) a real compensator may have an L-C filter at its output or have fixed compensation capacitors connected in parallel, and (ii) if the capacitor is not included, then the line current and the D-STATCOM output current are not independent and the *dq* transformation is not well defined. Per-phase equivalent circuit of the model is shown in Figure 3.2. It assumes that the source, the load and the D-STATCOM are balanced. Hence, the system dynamics can be described as:

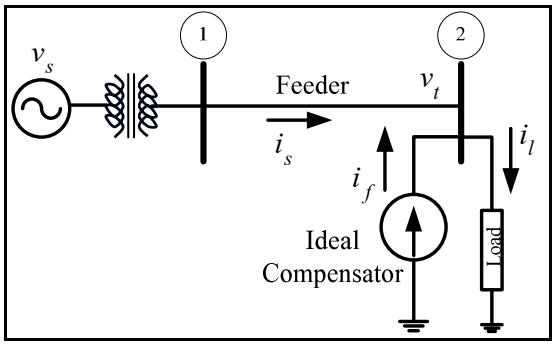

Figure 3.1 Distribution system with the D-STATCOM

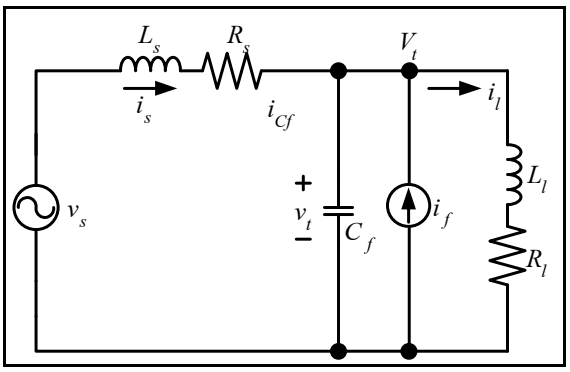

Figure 3.2 Per-phase equivalent circuits

$$L_s \frac{di_{s,abc}}{dt} = -R_s i_{s,abc} - v_{t,abc} + v_{s,abc} \tag{3.1}$$

$$C_f \frac{dv_{t,abc}}{dt} = -i_{l,abc} + i_{s,abc} + i_{f,abc} \tag{3.2}$$

$$L_l \frac{di_{l,abc}}{dt} = -R_l i_{l,abc} + v_{t,abc} \tag{3.3}$$

Here, $i_{s,abc}$, $i_{f,abc}$, $v_{s,abc}$ and $v_{t,abc}$ are vectors consisting of individual phase quantities denoted in Figure 3.2, R_l is a load resistance, L_l is a load inductance, L_s is a source inductance, R_s is a source resistance, and C_f is a coupling capacitor. Under the assumption that zero sequence components are not present, (3.1) – (3.3) can be transformed into an equivalent two-phase system by applying the following three-to-two phase transformation:

$$v_{s,xy} = v_{sa}e^{j0} + v_{sb}e^{j2\pi/3} + v_{sc}e^{j4\pi/3} \tag{3.4}$$

where the complex number $v_{s,xy} \equiv v_{sx} + jv_{sy}$. This is followed by the following rotational transformation:

$$v_{s,dq} \equiv v_{sd} + jv_{sq} = e^{-j\theta}v_{s,xy} \tag{3.5}$$

Applying the transformations, (3.1) – (3.3) can be written as:

$$L_s \frac{di_{s,dq}}{dt} = -\left(R_s + j\omega L_s\right)i_{s,dq} - v_{t,dq} + v_{s,dq} \tag{3.6}$$

$$C_f \frac{dv_{t,dq}}{dt} = -\left(j\omega C_f\right)v_{t,dq} + i_{s,dq} + i_{f,dq} - i_{l,dq} \tag{3.7}$$

$$L_l \frac{di_{l,dq}}{dt} = -\left(R_l + j\omega L_l\right)i_{l,dq} + v_{t,dq} \tag{3.8}$$

where $\omega \equiv \frac{d\theta}{dt}$ is to be designed and also be a function of time. The equivalent circuit corresponding to the real (*d*-axis) and imaginary (*q*-axis) components of the equation are shown in Figure 3.3.

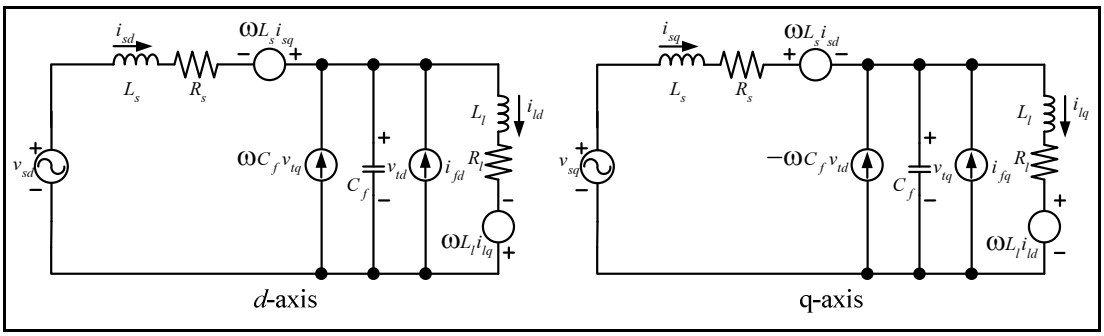

Figure 3.3 *d*-axis and *q*-axis equivalent circuit

3.2 Choice of Reference Frame

We choose the *dq* reference frame which is similar to that used for field-oriented control of three phase AC machines. Thus, the angle θ used in (3.5) is defined by $\theta = \tan^{-1}\left(v_{ty}/v_{tx}\right)$. This implies,

$$v_{tq} \equiv 0 \rightarrow \frac{dv_{tq}}{dt} = 0 \tag{3.9}$$

Defining $\alpha = \theta - \omega_s t$ where ω_s is the angular speed of the infinite bus phase voltages, we get $v_{s,dq} = V_s.e^{-j\alpha}$, where V_s is the magnitude of the supply voltage. The relative orientation of the vectors $v_{t,dq}$, $v_{s,dq}$ and the reference frame are shown in Figure 3.4. The system equations can now be rewritten as:

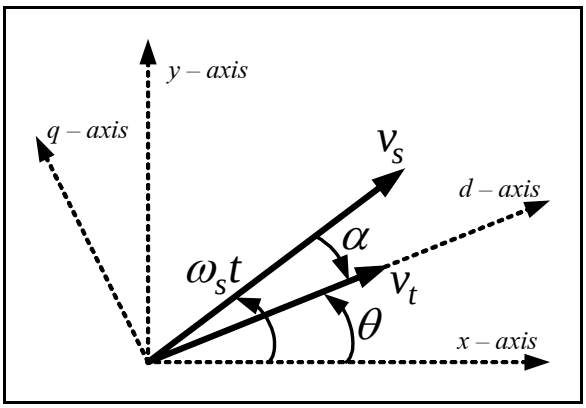

Figure 3.4 Orientation of reference frames

$$\frac{di_{sd}}{dt} = -\frac{1}{T_s} i_{sd} + \omega i_{sq} - \frac{1}{L_s} v_{td} + \frac{V_s}{L_s} \cos\alpha \tag{3.10}$$

$$\frac{di_{sq}}{dt} = -\frac{1}{T_s} i_{sq} - \omega i_{sd} - \frac{V_s}{L_s} \sin\alpha \tag{3.11}$$

$$\frac{dv_{td}}{dt} = -\frac{1}{C_f} i_{ld} + \frac{1}{C_f} i_{sd} + \frac{1}{C_f} i_{fd} \tag{3.12}$$

$$\frac{di_{ld}}{dt} = -\frac{1}{T_l} i_{ld} + \omega i_{lq} + \frac{1}{L_l} v_{td} \tag{3.13}$$

$$\frac{di_{lq}}{dt} = -\frac{1}{T_l} i_{lq} - \omega i_{ld} \tag{3.14}$$

$$\frac{d\alpha}{dt} = \omega - \omega_s \tag{3.15}$$

$$\omega = \frac{-i_{lq} + i_{sq} + i_{fq}}{C_f v_{td}} \tag{3.16}$$

Where T_s is the time constant of the source and feeder, $T_s = \frac{L_s}{R_s}$

T_l is the time constant of the load, $T_l = \frac{L_l}{R_l}$

The (3.16) is derived using (3.9). This should be noted that ω varies with time and is different from ω_s. Since $v_{tq} \equiv 0$, v_{td} represents the instantaneous magnitude of the phase voltages $v_{t,abc}$, while i_{fq} denotes the instantaneous reactive current supplied by the D-STATCOM. In addition, in the absence of negative sequence components, all the state variables in (3.10) – (3.15) are constants in steady states. Thus, a balanced three-phase system is effectively transformed into an equivalent DC system and its control problem is therefore simplified. From the system equations on *dq*-axis in (3.10) – (3.16), the block diagram can be derived as shown in Figure 3.5.

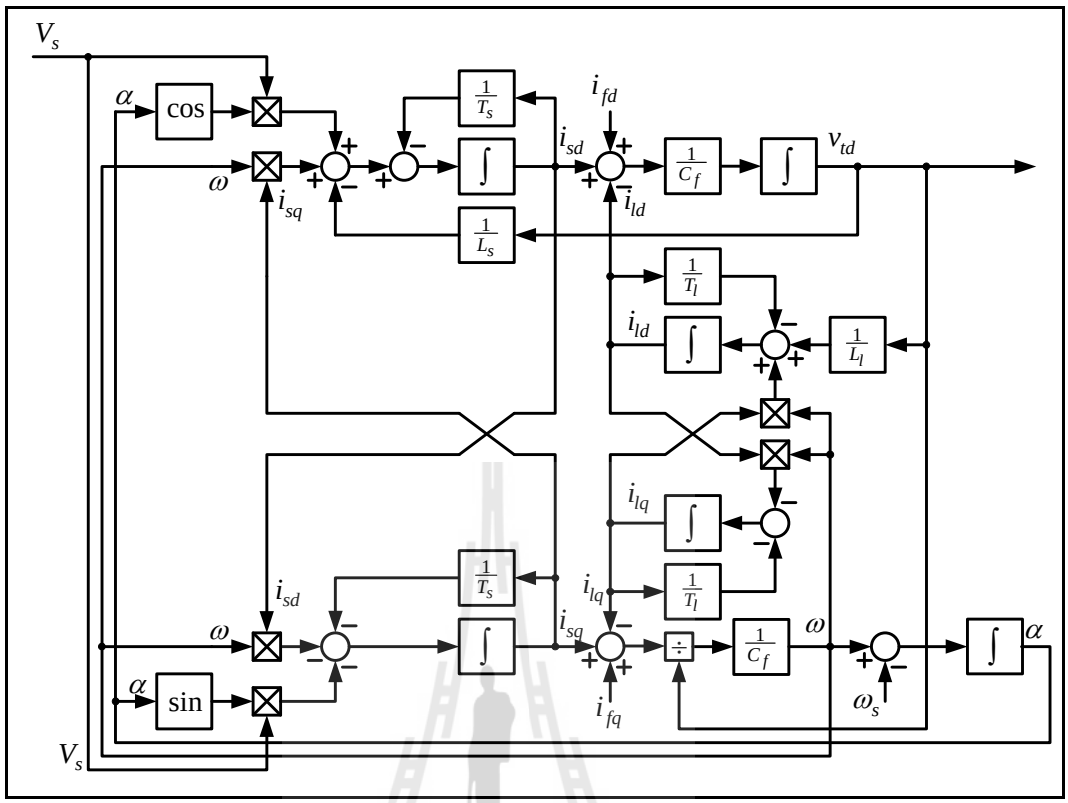

Figure 3.5 System equations on *dq*-axis

The block diagram in Figure 3.5 represents the model of the distribution system with D-STATCOM on the synchronously rotating reference frame (*dq*-axis). This system has three inputs that are the magnitude of the source voltage (V_s), the active and reactive current supplied by the D-STATCOM (i_{fd} and i_{fq}). The source active current (i_{sd}), source reactive current (i_{sq}), load voltage (v_{td}), load active current (i_{ld}), load reactive current (i_{lq}) and source voltage angle (α) are the state variable while the load voltage (v_{td}) is chosen as the output of this system.

3.3 Steady State Analysis of the Distribution System with the D-STATCOM

The equations in the previous section are dynamic equations. However, the equation for the steady state operation of the system can be obtained from (3.11) – (3.16) by giving all derivative terms of (3.11) – (3.15) as zero. After transformation into synchronously rotating reference frame, voltages and currents become DC quantities, i.e. $i_{sd} = I_{sd}$, $i_{sq} = I_{sq}$, $v_{td} = V_{td}$, $i_{ld} = I_{ld}$, $i_{lq} = I_{lq}$. The steady state equations can now be as follows:

$$0 = -\frac{1}{T_s} I_{sd} + \omega I_{sq} - \frac{1}{L_s} V_{td} + \frac{V_s}{L_s} \cos\alpha \tag{3.17}$$

$$0 = -\frac{1}{T_s} I_{sq} - \omega I_{sd} - \frac{V_s}{L_s} \sin\alpha \tag{3.18}$$

$$0 = -\frac{1}{C_f} I_{ld} + \frac{1}{C_f} I_{sd} + \frac{1}{C_f} I_{fd} \tag{3.19}$$

$$0 = -\frac{1}{T_l} I_{ld} + \omega I_{lq} + \frac{1}{L_l} V_{td} \tag{3.20}$$

$$0 = -\frac{1}{T_l} I_{lq} - \omega I_{ld} \tag{3.21}$$

$$0 = \omega - \omega_s \tag{3.22}$$

Where

$$\omega = \frac{-I_{lq} + I_{sq} + I_{fq}}{C_f V_{td}} \tag{3.23}$$

The load voltage regulation by using the D-STATCOM can be done by either injecting only reactive power or injecting both active and reactive power into the system. However, the injecting only reactive power is the focal point in this thesis. In this section, the size of D-STATCOM ($S_{D-STATCOM}$) for load voltage regulation by injecting only reactive power is investigated. Figure 3.2 shows the load voltage regulation with injecting only the reactive power into the system. Thus, the entire load active power (P_l) must be provided by the source. The P_l can be written as:

$$P_l = V_{td} I_{ld} = V_{td} I_{sd} \tag{3.24}$$

Since the D-STATCOM injects only the reactive power into the system, a load active and a source active currents are equal, ($I_{ld} = I_{sd}$). The source active current shown in (3.25) can be obtained by solving (3.17) – (3.18).

$$I_{sd} = -\frac{R_s}{R_s^2 + \omega_s^2 L_s^2}\left(V_{td} - V_s \cos\alpha\right) - \frac{\omega_s L_s}{R_s^2 + \omega_s^2 L_s^2} V_s \sin\alpha \tag{3.25}$$

Substituting (3.24) with (3.25), the P_l can be written as:

$$P_l = \frac{V_{td}V_s}{\sqrt{R_s^2+\omega_s^2L_s^2}}\left(\frac{R_s}{\sqrt{R_s^2+\omega_s^2L_s^2}}\cos\alpha - \frac{\omega_s L_s}{\sqrt{R_s^2+\omega_s^2L_s^2}}\sin\alpha\right) - \frac{V_{td}^2R_s}{R_s^2+\omega_s^2L_s^2} \tag{3.26}$$

If $\frac{R_s}{\sqrt{R_s^2+\omega_s^2L_s^2}} = \cos\beta$ and $\frac{\omega_s L_s}{\sqrt{R_s^2+\omega_s^2L_s^2}} = \sin\beta$ where β is an angle of source impedance,

$$\begin{aligned} P_l &= \frac{V_{td}V_s}{\sqrt{R_s^2+\omega_s^2L_s^2}}\left(\cos\beta\cos\alpha - \sin\beta\sin\alpha\right) - \frac{V_{td}^2R_s}{R_s^2+\omega_s^2L_s^2} \\ &= \frac{V_{td}V_s}{\sqrt{R_s^2+\omega_s^2L_s^2}}\left(\cos\left(\beta-\alpha\right)\right) - \frac{V_{td}^2R_s}{R_s^2+\omega_s^2L_s^2} \end{aligned} \tag{3.27}$$

From (3.27), α is an angle of the source voltage and can be expressed as:

$$\alpha = \beta - \cos^{-1}\left(\frac{V_{td}}{V_s}\frac{R_s}{\sqrt{R_s^2+\omega_s^2L_s^2}} + \frac{P_l\sqrt{R_s^2+\omega_s^2L_s^2}}{V_{td}V_s}\right) \tag{3.28}$$

For a feasible value of α, the condition (3.29) must be satisfied.

$$\frac{V_{td}}{V_s}\frac{R_s}{\sqrt{R_s^2+\omega_s^2L_s^2}} + \frac{P_l\sqrt{R_s^2+\omega_s^2L_s^2}}{V_{td}V_s} \le 1 \tag{3.29}$$

In (3.29), if the load voltage magnitude is regulated at a desired value ($V_{td,desired}$) with D-STATCOM, the load active power at the desired load voltage magnitude ($P_{l,desired}$) and the source voltage can be expressed as (3.30) and (3.31), respectively.

$$P_{l,desired} \le \left(\frac{V_s \sqrt{R_s^2 + \omega_s^2 L_s^2} - V_{td,desired} R_s}{R_s^2 + \omega_s^2 L_s^2} \right) V_{td,desired} \tag{3.30}$$

$$V_s \ge V_{td,desired} \frac{R_s}{\sqrt{R_s^2 + \omega_s^2 L_s^2}} + \frac{P_{l,desired} \sqrt{R_s^2 + \omega_s^2 L_s^2}}{V_{td,desired}} \tag{3.31}$$

Thus, when the $P_{l,desired}$ satisfies (3.30), the D-STATCOM can regulate the load voltage at a desired value without injecting any active power into the system. Similarly, when the source voltage satisfies (3.31), the D-STATCOM can regulate the load voltage at a desired value without injecting any active power into the system as well.

As seen in (3.30) and (3.31), the $P_{l,desired}$ and V_s are a function of the resistance R_s and inductance L_s when the $V_{td,desired}$ is kept constant. To investigate the effect of system parameters on the maximum value of the load active power at the desired load voltage magnitude, $P_{l,desired}(\max)$, and minimum value of the source voltage, $V_s(\min)$, the parameters of the system as shown in Table 3.1 are employed.

Table 3.1 Parameters of the distribution power system

Parameters	Value
Nominal magnitude source voltage (V_s)	12.10 *kV*
Desired load voltage magnitude ($V_{td,desired}$)	11.00 *kV*
Nominal source resistance and inductance (R_s and L_s)	1 Ω and 10 *mH*
Nominal load power (P_l and Q_l)	12.0*MW* and 0 *MVar*
System frequency (f_s)	50 *Hz*
Coupling capacitor (C_f)	50 μF

Plots of the $P_{l,desired}(\max)$ as a function of the resistance R_s and inductance L_s for different values of the V_s are shown in Figure 3.6 and 3.7. In Figure 3.6, the inductance L_s is varied from 5 to 15*mH* while the V_s are 3.63, 6.05, 9.08 and 12.10 *kV*. The time constant T_s and the $V_{td,desired}$ are kept constant as 3.14 and 11.00 *kV*, respectively. It is seen that the $P_{l,desired}(\max)$ increases as the inductance L_s decreases.

The effect of the time constant T_s is shown in Figure 3.7. In this case, the inductance L_s is kept constant as 10*mH* whilst the time constant T_s is varied from 3.14 to 31.42 with 2 step increments. It can be observed from Figure 3.7 that increasing of the time constant T_s results in increasing of the $P_{l,desired}(\max)$.

Trends of the $P_{l,desired}(\max)$ as a function of the inductance L_s and V_s are shown in Figure 3.8 while trends of the $P_{l,desired}(\max)$ as a function of the time constant T_s and V_s can be seen from Figure 3.9. In these Figures, the $P_{l,desired}(\max)$ surface is a linearly increasing graph with respect to the V_s, e.g. AB in Figure 3.8 and 3.9 corresponding to plot at $V_s = 12.10kV$ in Figure 3.6 and 3.7, respectively.

The effect of the time constant T_s and the inductance L_s with different values of the load active power on the $V_s(\min)$ are shown in Figure 3.10 and 3.11. In Figure 3.10, the inductance L_s is varied from 5 to 15mH while the load active powers are 1.20, 6.00, 12.00, 18.00 and 24.00MW. The time constant T_s and $V_{td,desired}$ are kept constant as 3.14 and 11.00kV, respectively. As seen from this Figure, the $V_s(\min)$ is decreasing with respect to the inductance L_s .

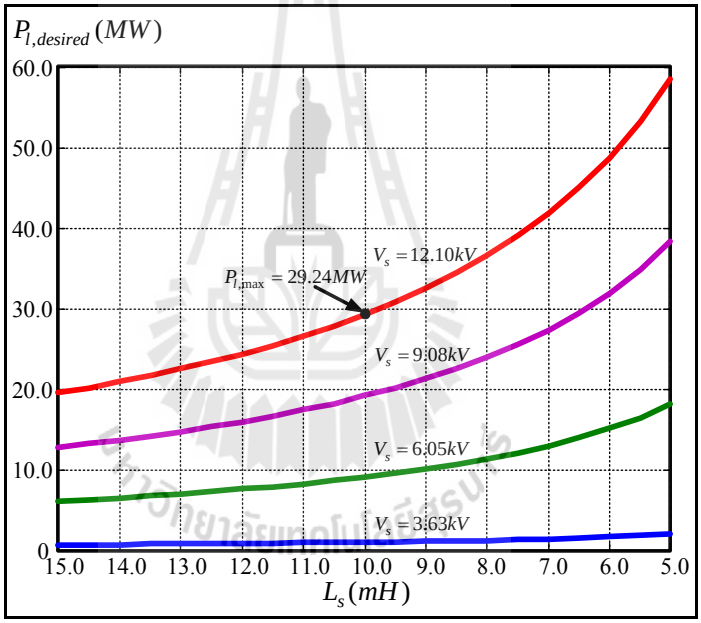

Figure 3.6 Maximum load active powers with source inductance L_s variation while fixed T_s

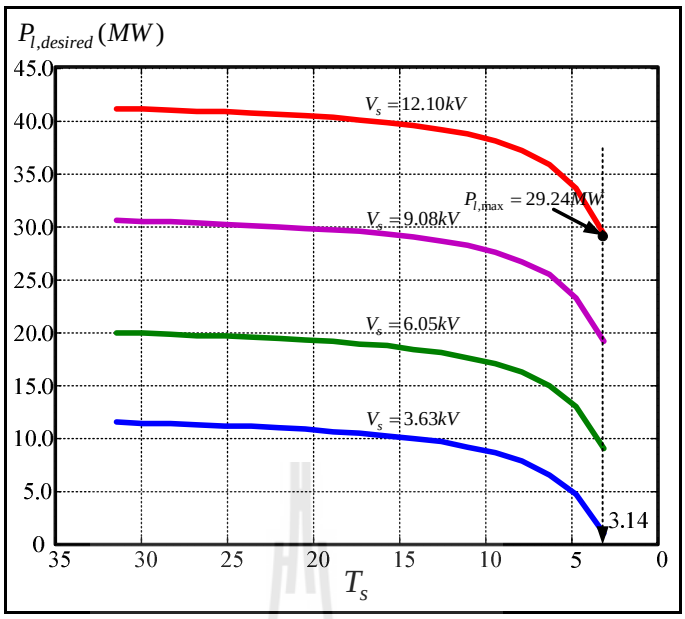

Figure 3.7 Maximum load active powers with T_s variation while fixed source inductance L_s

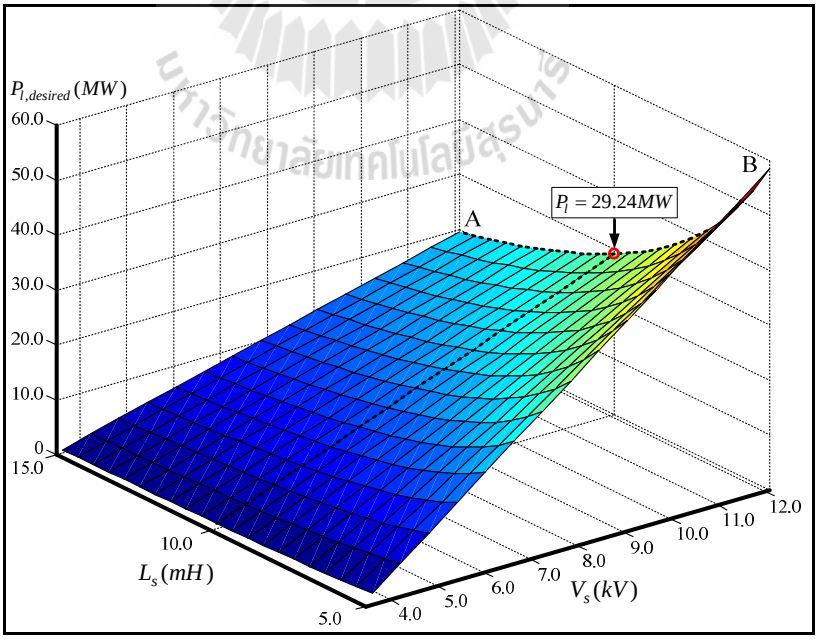

Figure 3.8 Effect of L_s and source voltage on the maximum load active power

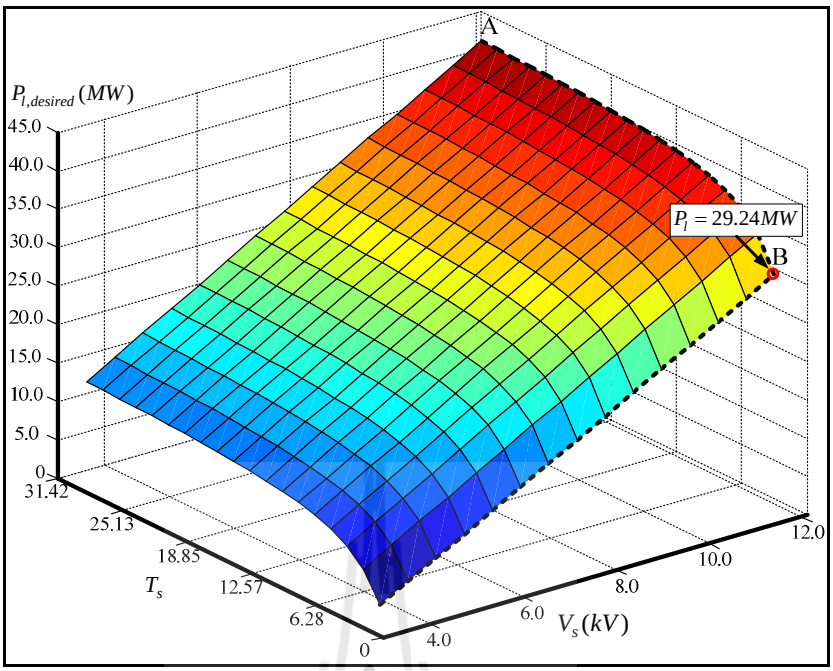

Figure 3.9 Effect of T_s and source voltage on the maximum load active power

The effect of time constant T_s is shown in Figure 3.11. The inductance L_s is kept constant as $10mH$ while the time constant T_s is varied from 3.14 to 31.42 with 2 step increments in this case. It can be observed from Figure 3.11 that decreasing of the time constant T_s results in increasing of the $V_s(\min)$. Trends of the $V_s(\min)$ as a function of the inductance L_s and load active power are shown as Figure 3.12 whilst trends of the $V_s(\min)$ as a function of the time constant T_s and load active power can be seen from 3.13. It is seen that the minimum source voltage surface is a linearly increasing graph with respect to the load active power, e.g. AB in Figure 3.12 and 3.13 corresponding to plot at $P_l = 12.00MW$ in Figure 3.10 and 3.11, respectively.

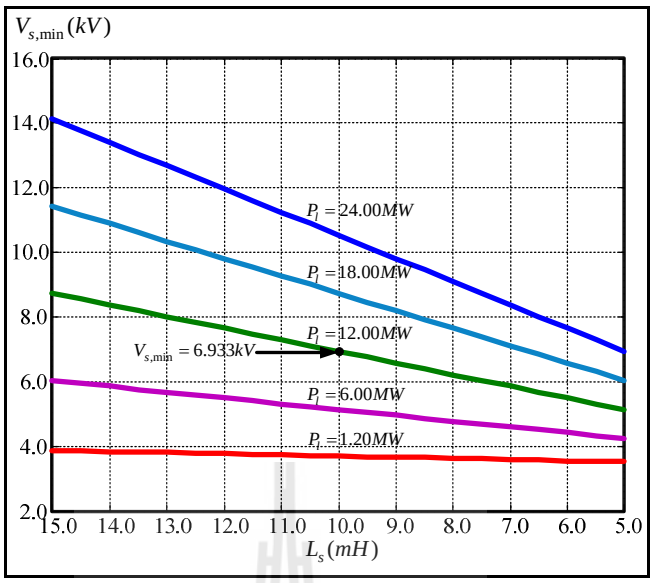

Figure 3.10 Minimum source voltages with source inductance L_s variation while fixed T_s

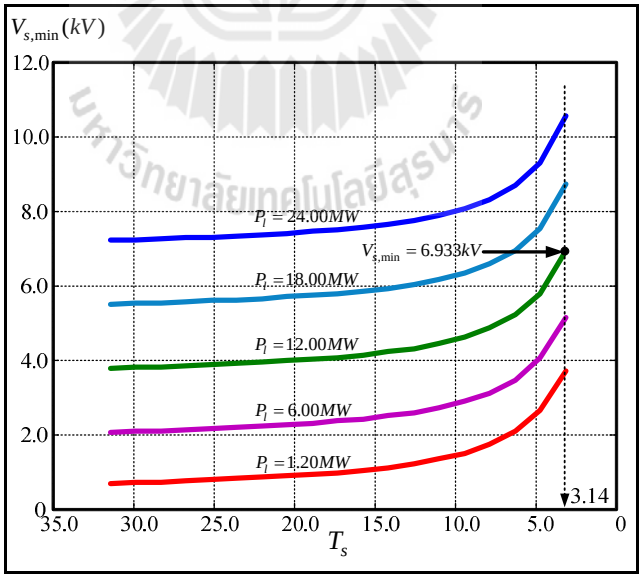

Figure 3.11 Minimum source voltages with T_s variation while fixed source inductance L_s

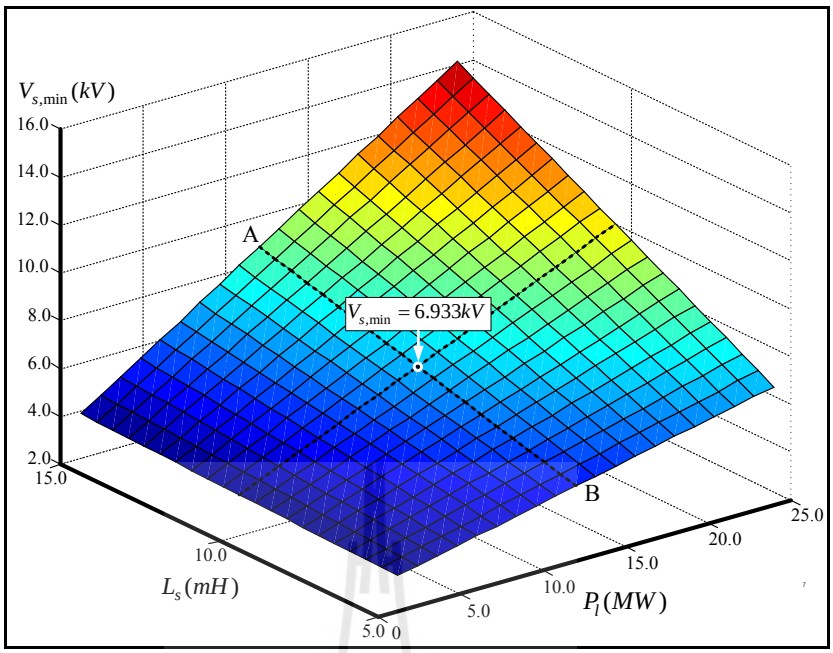

Figure 3.12 Effect of L_s and load active power on the maximum source voltage

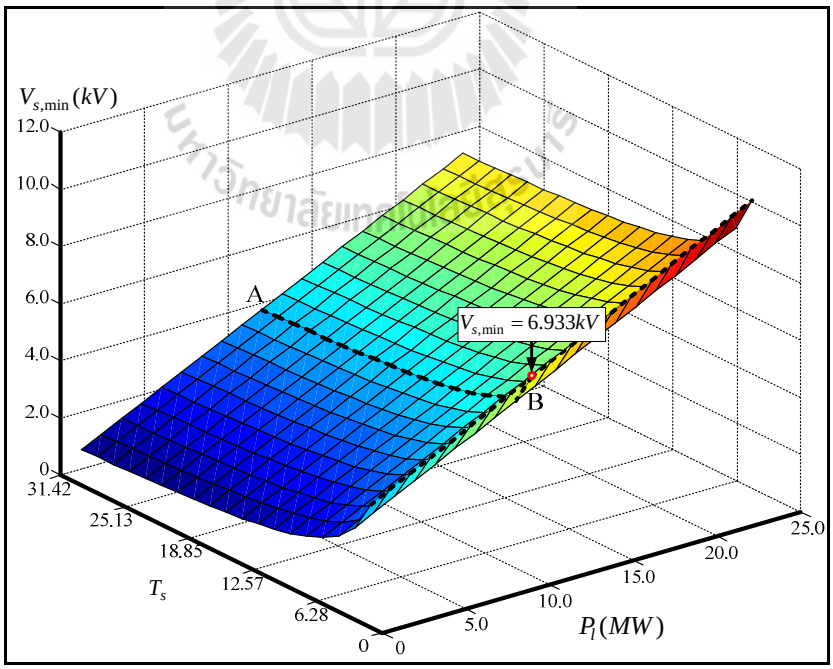

Figure 3.13 Effect of T_s and load active power on the maximum source voltage

To determine the maximum value of the load active power at the desired load voltage magnitude: $P_{l,desired}(\max)$ and minimum value of the source voltage: $V_s(\min)$ for nominal operating condition, the nominal parameters of the system as shown in Table 3.1 are used. The $P_{l,desired}(\max)$ at nominal operating condition is 29.24 *MW* as shown in Figure 3.8 and 3.9 while the $V_s(\min)$ is 6.933 *kV* indicating in Figure 3.12 and 3.13.

In addition, comparing between the maximum load active power and PV curve are demonstrated in Figure 3.14. In this Figure, the distribution power system with the loads containing unity power factor ($P_l = 12.0MW$ and $Q_l = 0MVar$), 0.9 lag power factor ($P_l = 12.0MW$ and $Q_l = 5.8MVar$) and 0.8 lag power factor ($P_l = 12.0MW$ and $Q_l = 9.0MVar$) are presented. However, the coupling capacitor (C_f) is included with the system, so the load voltage at no load ($P_l \approx 0MW$) is above the nominal source voltage.

The collapse power of unity, 0.9 lag and 0.8 lag power factors are 17.7 *MW*, 12.36 *MW* and 10.24 *MW*, respectively. Meanwhile, the maximum load active powers of three load power factor are the same value i.e. 29.24*MW*. Although the load power factor dose isn't affecting the maximum value of load active power, it affects the load voltage of the system. The maximum load active power point of unity and 0.9 lag power factors are $P_l = 29.24MW$ with $V_{td} = 8.51kV$ and $P_l = 29.24MW$ with $V_{td} = 7.15kV$, that correspond to the load power at 17.5 *MW* and 12.34 *MW* on the PV curve, respectively. These points are above the collapsing point of the PV curves. For the maximum load active power point of 0.8 lag power factors, it is

$P_l = 29.24MW$ with $V_{td} = 6.51kV$ corresponding to the load power at 10.23 MW on the PV curve which is under the collapsing point of the PV curve. Although the maximum load active power point is not the same as exactly the collapse point in PV curve, it is around the collapsing point.

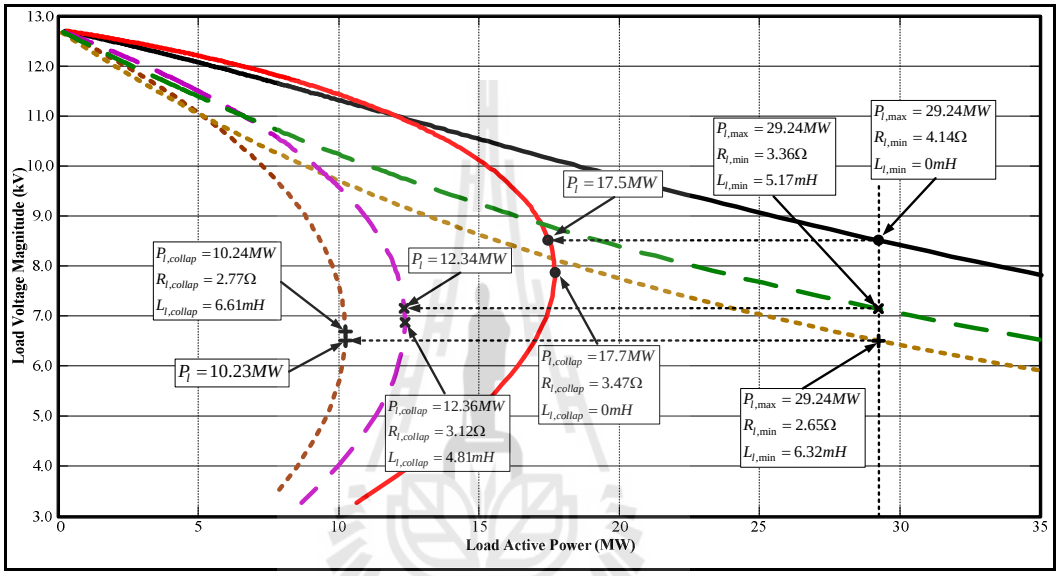

Figure 3.14 Relation between the maximum load active power and PV curve

Regarding the $S_{D-STATCOM}$ for the load voltage regulation, loads in power distribution systems are commonly used in the power model. To simplify this calculation, linearized load impedance derived from the load power and its bus corresponding voltage so the R_l and L_l can be obtained by solving (3.32) – (3.33). Since losses in the D-STATCOM are ignored, the D-STATCOM active current is zero ($I_{fd} = 0$). Subsequently, the reactive current (I_{fq}) can be obtained by solving

(3.17) – (3.23) when the given V_{td} is $V_{td,desired}$. Thus, the $S_{D-STATCOM}$ is the reactive power of D-STATCOM as (3.34).

$$V_{td,desired}^2 \frac{R_l}{R_l^2 + \omega_s^2 L_l^2} - P_{l,desired} = 0 \tag{3.32}$$

$$V_{td,desired}^2 \frac{\omega_s L_l}{R_l^2 + \omega_s^2 L_l^2} - Q_{l,desired} = 0 \tag{3.33}$$

$$S_{D-STATCOM} = V_{td} I_{fq} = Q_{D-STATCOM} \tag{3.34}$$

when $V_{td} = V_{td,desired}$.

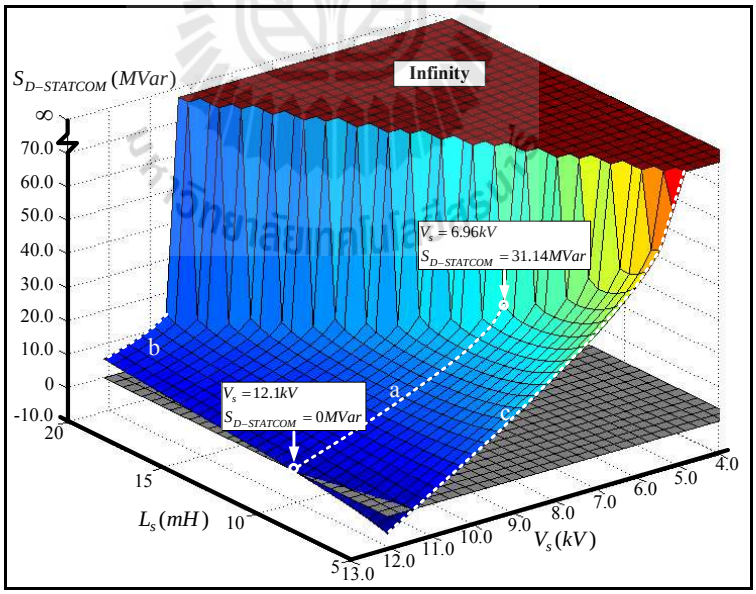

Figure 3.15 $S_{D-STATCOM}$ with L_s and V_s variation for unity power factor ($P_l = 12.0MW$ and $Q_l = 0MVar$)

The $S_{D-STATCOM}$ is a function of the system parameters i.e. V_s, R_s, L_s and load power. To study the effect of system parameters on $S_{D-STATCOM}$ when the source voltage sags, the system parameters i.e. L_s and T_s are varied. When the load power is unity power factor at $P_l = 12.0MW$ and $Q_l = 0MVar$, the surface of $S_{D-STATCOM}$ as a function of the inductance L_s and time constant T_s for different values of the source voltage are shown in Figure 3.15 and 3.16 while the load power is 0.9 lag power factor at $P_l = 12.0MW$ and $Q_l = 5.8MVar$, the surface of $S_{D-STATCOM}$ are shown in Figure 3.17 and 3.18.

In Figure 3.15, the inductance L_s is varied from 5 to 20mH while the source voltage is varied from 3.63 to 12.10 kV. The time constant T_s and the $V_{td,desired}$ are kept constant as 3.14 and 11.00kV, respectively. At the nominal operation point ($L_s = 10mH$ and $V_s = 12.10kV$) that corresponds $V_{td} = 11.00kV$, the load voltage is at the desired load voltage magnitude, the D-STATCOM does not inject any power into the system to regulate load voltage.

The minimum source voltage that can regulate the load voltage magnitude only injecting reactive power into the system, $V_s(\min)$, can be obtained from (3.31). From (3.31), the $V_s(\min) = 6.93kV$ causes the $V_{td} = 6.30kV$. From the nominal operation point to $V_s(\min)$, V_s decreases from 12.10kV to 6.93kV, this results in the decrease of the V_{td} from 11.00kV to 6.30kV. However, the load voltage can be regulated by injecting only the reactive power of the D-STATCOM until the V_s is less than 6.93kV. The $S_{D-STATCOM}$ for load voltage regulation in this case is a dash line as shown in Figure 3.15.

When the inductance L_s is higher, i.e. L_s is $20mH$, the $V_s(\min) = 10.53kV$ causes the $V_{td} = 8.23kV$. In this case, V_s decreases from 12.10 to 10.53kV, this results in the decrease of the V_{td} from 9.46 to 8.23kV. The load voltage can be regulated by injecting only the reactive power of the D-STATCOM until the V_s is less than 10.53kV. The $S_{D-STATCOM}$ in this case is a dash line b. On the other hand when the inductance L_s is lower, i.e. L_s is $5mH$, the $V_s(\min) = 5.14kV$ that corresponds the $V_{td} = 4.95kV$. If V_s decreases from 12.10 to 5.14kV, this results in the decrease of the V_{td} from 11.66 to 4.95kV. The load voltage can be regulated by absorbing or injecting only the reactive power of the D-STATCOM until the V_s is less than 5.14kV with the $S_{D-STATCOM}$ is shown as a dash line c. At the nominal source voltage ($V_s = 12.10kV$), the V_{td} is above the desired load voltage magnitude. In this point, the load voltage can be regulated by absorbing only the reactive power of the D-STATCOM that corresponds the $S_{D-STATCOM}$ is a negative value.

The effect of time constant T_s on the $S_{D-STATCOM}$ is shown in Figure 3.16. In this case, the inductance L_s and the $V_{td,desired}$ are kept constant as $10mH$ and 11.00kV, respectively. The time constant T_s is varied from 3.14 to 31.42 with 2 step increments while the source voltage is varied from 3.63 to 12.10 kV. At the time constant $T_s = 3.14$, when the source voltage decreases from the nominal operating point to $V_s(\min)$, V_s decreases from 12.10kV to 6.93kV, this results in the decrease of the V_{td} from 11.00kV to 6.30kV. The load voltage can be regulated by injecting only the

reactive power of the D-STATCOM until the V_s is less than 6.93kV. The $S_{D-STATCOM}$ for this case (seen as dash line a) is the same value as dash line a in Figure 3.15.

Whereas the time constant T_s is higher, i.e. T_s is 31.42, the $V_s(\min) = 3.78kV$ causes the V_{td} is 3.74kV. In this case, V_s decreases from 12.10 to 3.78kV, this results in the decrease of the V_{td} from 11.98 to 3.74kV. The load voltage can be regulated by absorbing or injecting only the reactive power of the D-STATCOM until the V_s is less than 3.78kV. The $S_{D-STATCOM}$ for this case is a dash line b as shown in Figure 3.16. However, at the nominal source voltage ($V_s = 12.10kV$), the V_{td} is above the desired load voltage magnitude. In this point, the load voltage can be regulated by absorbing only the reactive power that corresponds the $S_{D-STATCOM}$ is a negative value.

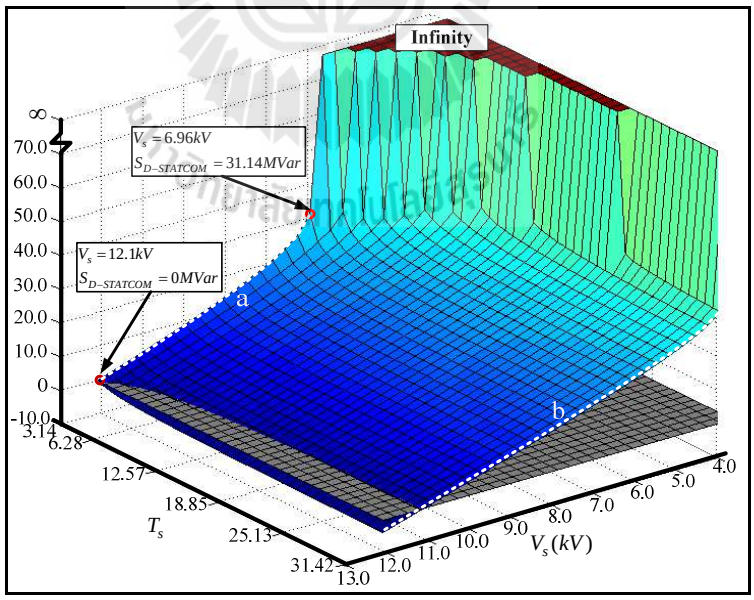

Figure 3.16 $S_{D-STATCOM}$ with T_s and V_s variation for unity power factor ($P_l = 12.0MW$ and $Q_l = 0MVar$)

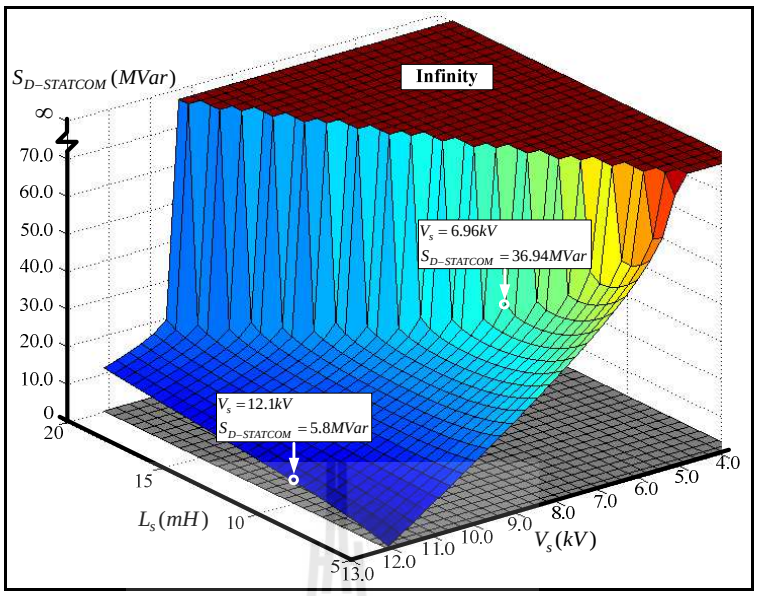

Figure 3.17 $S_{D-STATCOM}$ with L_s and V_s variation for 0.9 lagging power factor ($P_l = 12.0MW$ and $Q_l = 5.8MVar$)

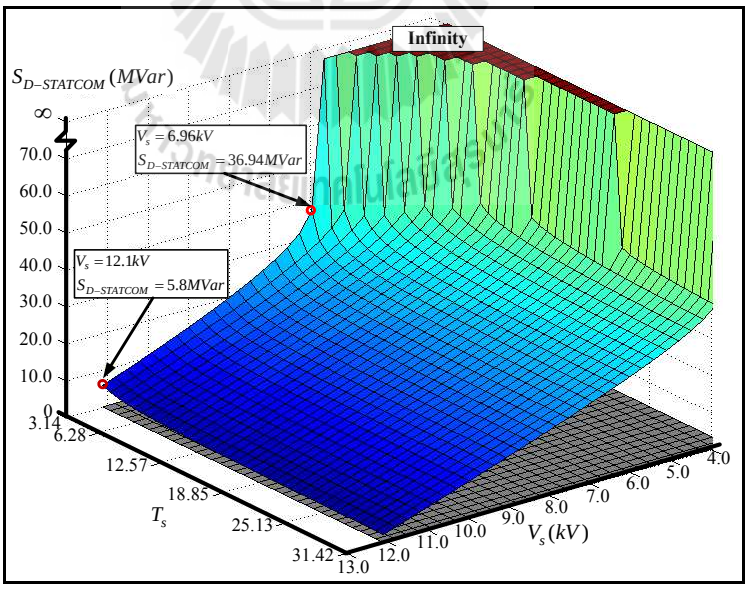

Figure 3.18 $S_{D-STATCOM}$ with T_s and V_s variation for 0.9 lagging power factor ($P_l = 12.0MW$ and $Q_l = 5.8MVar$)

When the load power is 0.9 lag power factor, the surface of $S_{D-STATCOM}$ as a function of the inductance L_s and time constant T_s for different values of the source voltage are shown in Figure 3.17 and 3.18. As seen from these Figures, the load power factor does not affect $V_s(\min)$. However, the load power factor dose affects the load voltage, this results in the decreasing of the load voltage than case of unity power factor. For example, the source voltage at 12.10*kV*, the load voltage in case of unity power factor is 11.00*kV* while in case of 0.9 lag power factor is 9.82*kV*. Since for the same variation of the source voltage, i.e. V_s decreases from 12.10*kV* to 6.93*kV*, the $S_{D-STATCOM}$ for load voltage regulation in case of 0.9 lag power factor is more than as the same value of the load reactive power (Q_l).

The $S_{D-STATCOM}$ for the load voltage regulation in case of the load power variation are shown in Figure 3.19 – 3.22. In this case, the P_l, R_s and L_s are varied while the source voltage is kept constant as 12.10*kV*. To study the effect of system parameters on $S_{D-STATCOM}$ when the load power variation, the system parameters i.e. the inductance L_s and time constant T_s are varied. When the load power is unity power factor, the surface of $S_{D-STATCOM}$ as a function of the inductance L_s and time constant T_s for different values of the load active power are shown in Figure 3.19 and 3.20 while the load power is 0.9 lag power factor, the surface of $S_{D-STATCOM}$ are shown in Figure 3.21 and 3.22.

As seen from Figure 3.19, the inductance L_s is varied from 5 to 20*mH* while the load active power is varied from 10.0 to 50.0 *MW*. The time constant T_s and the $V_{td,desired}$ are kept constant as 3.14 and 11.00*kV*, respectively. At the nominal operation

point ($L_s = 10mH$ and $P_l = 12.00MW$) that corresponds $V_{td} = 11.00kV$, the load voltage is at the desired load voltage magnitude, the D-STATCOM does not inject any power into the system to regulate load voltage.

The maximum load active power that can regulate the load voltage magnitude only injecting reactive power into the system, $P_{l,desired}(\max)$, can be obtained from (3.30). From (3.30), the $P_{l,desired}(\max) = 29.24MW$ causes the $V_{td} = 8.51kV$. From the nominal operation point to $P_{l,desired}(\max)$, P_l increases from 12.00*MW* to 29.24*MW*, this results in the decrease of the V_{td} from 11.00*kV* to 8.51*kV*. The load voltage can be regulated by injecting only the reactive power of the D-STATCOM until the P_l is more than 29.24*MW*. However, at the active load power lower than the nominal active load power, the load voltage is over than the desired value. In this point, the load voltage can be regulated by absorbing only the reactive power of the D-STATCOM that corresponds the $S_{D-STATCOM}$ is a negative value.

When the inductance L_s is higher, i.e. L_s is 20*mH*, the $P_{l,desired}(\max) =$ 12.78*MW* causes the $V_{td} = 9.22kV$. In this case, P_l increases from 12.00 to 12.78*MW*, this results in the decrease of the V_{td} from 9.46 to 9.22*kV*. The load voltage can be regulated by injecting only the reactive power of the D-STATCOM until the P_l is more than 12.78*MW*. On the other hand when the inductance L_s is lower, i.e. L_s is 5*mH*, the $P_{l,desired}(\max) = 51.13MW$ that corresponds the $V_{td} = 8.87kV$. If P_l increases from 12.00 to 51.13*MW*, this results in the decrease of the V_{td} from 11.66 to 8.87*kV*. The load voltage can be regulated by absorbing or injecting only the reactive power of the D-STATCOM until the P_l is more than 51.13*MW*. However, at the nominal active

load power ($P_l = 12.00MW$), the V_{td} is above the desired load voltage magnitude. In this point, the load voltage can be regulated by absorbing only the reactive power of the D-STATCOM that corresponds the $S_{D-STATCOM}$ is a negative value.

The effect of the time constant on the $S_{D-STATCOM}$ is shown in Figure 1.30. In this case, the inductance L_s and the load voltage magnitude are kept constant as $10mH$ and $11.00kV$, respectively. The time constant T_s is varied from 3.14 to 31.42 with 2 step increments while the source voltage is varied from 3.63 to 12.10 kV. At the $T_s = 3.14$, when the active load power increases from the nominal operating point to $P_{l,desired}(\max)$, P_l increases from $12.00MW$ to $29.24MW$, this results in the decrease of the V_{td} from $11.00kV$ to $8.51kV$. The load voltage can be regulated by injecting only the reactive power of the D-STATCOM until the P_l is more than $29.24MW$. The $S_{D-STATCOM}$ for this case is the same value in Figure 1.29.

When the time constant (T_s) is higher, i.e. T_s is 31.42, the $P_{l,desired}(\max) = 37.27MW$ causes the V_{td} about $8.77kV$. In this case, P_l increases from 12.00 to $37.27MW$, this results in the decrease of the V_{td} from 11.98 to $8.77kV$. The load voltage can be regulated by absorbing or injecting only the reactive power of the D-STATCOM until the P_l is more than $37.27MW$. However, at the nominal source voltage ($P_l = 12.00MW$), the V_{td} is above the desired load voltage magnitude. In this point, the load voltage can be regulated by absorbing only the reactive power of the D-STATCOM that corresponds the $S_{D-STATCOM}$ is a negative value.

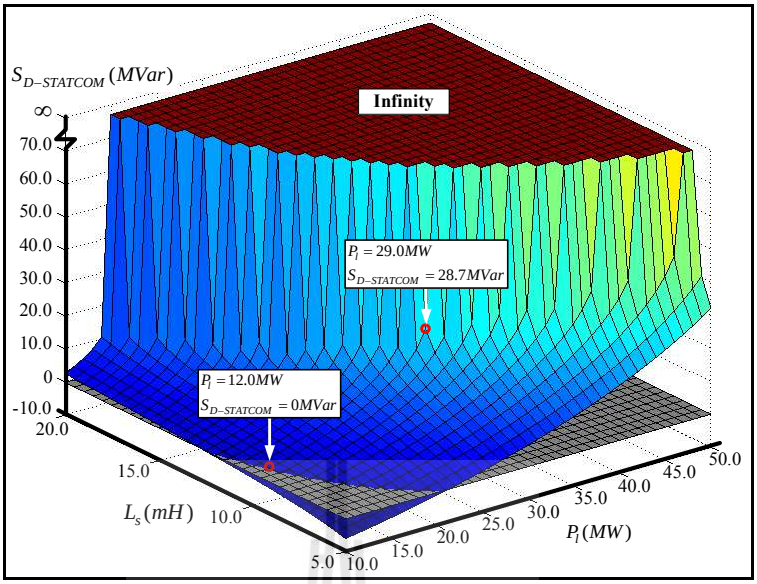

Figure 3.19 $S_{D-STATCOM}$ with L_s and P_l variation for unity power factor

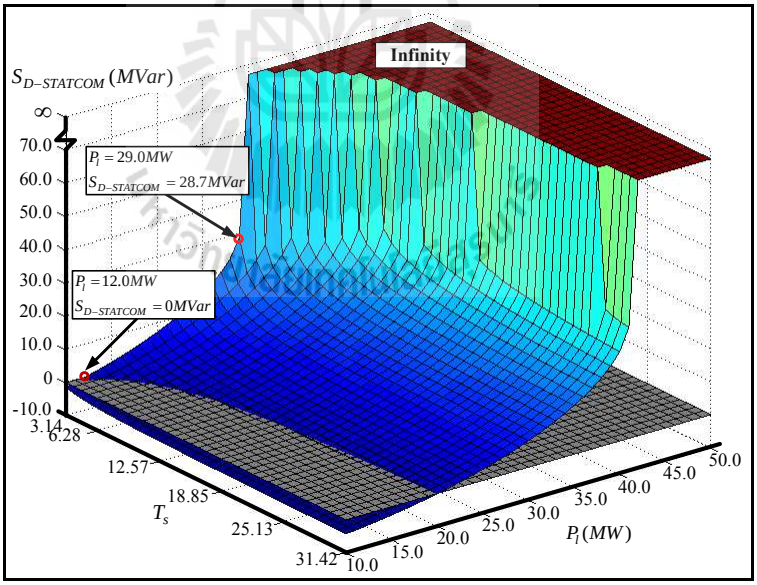

Figure 3.20 $S_{D-STATCOM}$ with T_s and P_l variation for unity power factor

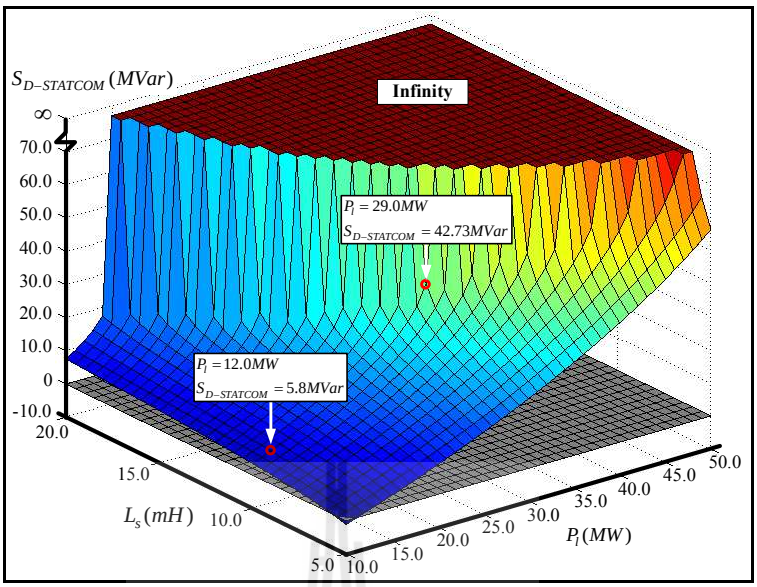

Figure 3.21 $S_{D-STATCOM}$ with L_s and P_l variation for 0.9 lagging power factor

When the load power is 0.9 lag power factor, the surface of $S_{D-STATCOM}$ as a function of the L_s and T_s for different values of the active load power (P_l) are shown in Figure 3.21 and 3.22. As seen from these Figures, the load power factor does not affect $P_{l,desired}(\max)$. However, the load power factor dose affects the load voltage, this results in the decreasing of the load voltage than case of unity power factor. For example, the active load power at 12.00*MW*, the load voltage in case of unity power factor is 11.00*kV* while in case of 0.9 lag power factor is 9.82*kV*. Whereas for the same variation of the active load power, i.e. P_l increases from 12.00*MW* to 29.24*MW*, the $S_{D-STATCOM}$ for load voltage regulation in case of 0.9 lag power factor is more than with the same value of the load reactive power (Q_l).

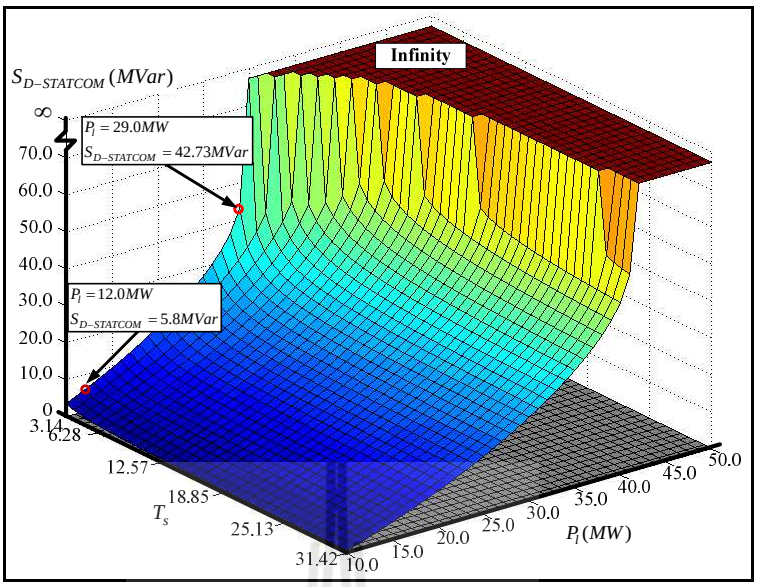

Figure 3.22 $S_{D-STATCOM}$ with T_s and P_l variation for 0.9 lagging power factor

3.4 Summary

In this chapter, the modeling of the distribution system with an ideal D-STATCOM is proposed. The D-STATCOM modeled as an ideal controllable current source. The small signal model of the distribution system was derived by transforming the equivalent system impedance to a *dq* frame. The modeling strategy similar to that used for the field oriented control of three phase AC machines is used in this chapter. Than, the steady state characteristic can be obtained from the state equation of the distribution system with an ideal D-STATCOM.

As this characteristic, the maximum load power and the minimum source voltage that the D-STATCOM can regulate the load voltage with injecting only the active power into the system are obtained and discussed. It is seen that the maximum load power ($P_{l,desired}\,(\max)$) increases as the source inductance (L_s) decreases while

the increasing of the source time constant (T_s) results in increasing of the maximum load power $P_{l,desired}(\max)$. For the effect of the source time constant (T_s) and the source inductance (L_s) on the minimum source voltage $V_s(\min)$, the increasing of the source inductance (L_s) results in linearly increasing the minimum source voltage $V_s(\min)$ while the increasing of the source time constant (T_s) results in decreasing the minimum source voltage $V_s(\min)$.

In addition, the comparison between the maximum load active power and PV curve is demonstrated in this chapter. The collapse power of the system with the unity and 0.9 lagging load power factors are above the collapsing point of the PV curve while the collapse power of the system with the unity and 0.8 lagging under the collapsing point of the PV curve. Although the maximum load active power point is not the same as exactly the collapsing point in the PV curve, it is around the collapsing point.

Furthermore, the effects of system parameters on the size of the D-STATCOM ($S_{D-STATCOM}$) for the voltage regulation when the source voltage sags and the load power vary are investigated. The size of the D-STATCOM ($S_{D-STATCOM}$) is a function of the system parameters e.g. source resistance (R_s), source inductance (L_s).

CHAPTER IV

DYNAMIC ANALYSIS OF THE DISTRIBUTION SYSTEM WITH D-STATCOM

This chapter proposes a small signal model and analysis of the distribution system with an ideal D-STATCOM. The proposed non-linear model in Chapter 3 can be linearized around some initial state conditions. Therefore, the state-transition matrix representing the linearized model can be obtained. By applying with stability criteria, dynamic stability or small signal stability of the linearized systems can be evaluated by means of eigenvalues. In this chapter, a simplified 11-kV, 2-bus test power system that described in Chapter 3 is employed for the simulation. Variation of some parameters, e.g. location of an installed D-STATCOM, the time constant of feeder section, initial state conditions, etc., is investigated to exhibit the dynamic system stability.

4.1 Linearization of the Power System with D-STATCOM

In this section, an illustration of the basic methods of the linearization of non-linear state equations representing the dynamics of electric power distribution systems is presented. This concerns basic problems of mathematical models dealing with the linearization of the non-linear dynamic systems. The problems presented here can be also used in control theory. In many considerations concerning system dynamics, the

physical systems are treated as a linearized system. This follows from assuming simplified statements that say that the characteristics of system elements are linear in character, or that the equation linearized by Taylor's series expansion occurs for some small deviations of state variables around the equilibrium point. However, in many cases, it is impossible to accept such assumptions. The first part of this section introduces the basic concepts concerning the linearization of dynamic systems. In the later section, linearization of the electric power distribution system equipped with D-STATCOM is derived.

4.1.1 Linearization of Non-linear Dynamic Systems

For this analysis, it assumes the following system of non-linear equations.

$$\dot{x} = f(x,u,t)\,;\;\; x(0) = x_0 \tag{4.1}$$

Where $f(x,u,t)$ is the vector of non-linear functions, $x(t) \in \Re^n$ and $u(t) \in \Re^m$ are the vector of the state variables and the input vector, respectively. x_0 represents the set of initial conditions. Assume that under usual working circumstances this system operates along the initial state x_0 while it is driven by the system input $u_0 = u(0)$. It further assumes that the motion of the nonlinear system driven by a small change, $\Delta u(t)$, in the system input u is in the neighborhood of the initial state x_0, that is

$$x(t) = x_0 + \Delta x(t) \tag{4.2}$$

$$u(t) = u_0 + \Delta u(t) \tag{4.3}$$

Where $\Delta x(t)$ represents a small change of the state variable x.

$$\dot{x}(t) + \Delta\dot{x}(t) = f(x_0 + \Delta x(t), u_0 + \Delta u(t), t_0 + \Delta t) \tag{4.4}$$

For the system variables in close proximity to the initial state, (4.4) can be expanded into a Taylor's series around the initial state x_0 and the initial input u_0, which produces

$$\begin{aligned}\dot{x}(t) + \Delta\dot{x}(t) = {} & f(x_0, u_0) + \left\{\frac{\partial f}{\partial x}(x_0, u_0)\right\}\Delta x(t) + \left\{\frac{\partial f}{\partial u}(x_0, u_0)\right\}\Delta u(t) \\ & + high-order\ terms\end{aligned} \tag{4.5}$$

By cancelling higher-order terms which contain very small quantities, the linear differential equation can be obtained as follows.

$$\Delta\dot{x}(t) = \left\{\frac{\partial f}{\partial x}(x_0, u_0)\right\}\Delta x(t) + \left\{\frac{\partial f}{\partial u}(x_0, u_0)\right\}\Delta u(t) \tag{4.6}$$

The partial derivatives in the linearization are evaluated at the initial points. The coefficients A_0 and B_0 can be solved and expressed as (4.7) – (4.8). Therefore the linearized system of the dynamic system can be represented as (4.9).

$$A_0 = \frac{\partial f}{\partial x}(x_0, u_0) \tag{4.7}$$

$$B_0 = \frac{\partial f}{\partial u}(x_0, u_0) \tag{4.8}$$

$$\Delta\dot{x}(t) = A_0\Delta x(t) + B_0\Delta u(t) \tag{4.9}$$

4.1.2 Linearized System of the Distribution System with the Ideal D-STATCOM

The dynamic equations of the distribution system with the ideal D-STATCOM are described in chapter 3 as shown in (3.10) – (3.16) that are non-linear differential equations. To investigate the dynamic performance of this system, linear approximation is applied as described previously. Linearization of this system around a specific operating point gives a set of linearized equations as shown in (4.9). The state variables and the input variables of the D-STATCOM are defined as given in (4.10) and (4.11), respectively. With the currents of the D-STATCOM and thus applying (4.7) – (4.8), the coefficients A_0 and B_0 can be calculated as described in (4.12) and (4.13).

$$\Delta x = \begin{bmatrix} \Delta i_{sd} \\ \Delta i_{sq} \\ \Delta v_{td} \\ \Delta i_{ld} \\ \Delta i_{lq} \\ \Delta \alpha \end{bmatrix} \tag{4.10}$$

$$\Delta u = \begin{bmatrix} \Delta i_{fd} \\ \Delta i_{fq} \\ \Delta V_s \end{bmatrix} \tag{4.11}$$

$$A_0 = \begin{bmatrix} -\frac{1}{T_s} & \left(\omega_0 + \frac{k_{isq}}{C_f}\right) & -\left(\omega_0 \frac{k_{isq}}{C_f} + \frac{1}{L_s}\right) & 0 & -\frac{k_{isq}}{C_f} & -\frac{k_{vsin}}{L_s} \\ -\omega_0 & -\left(\frac{1}{T_s} + \frac{k_{isd}}{C_f}\right) & -\omega_0 k_{isd} & 0 & \frac{k_{isd}}{C_f} & -\frac{k_{vcos}}{L_s} \\ \frac{1}{C_f} & 0 & 0 & -\frac{1}{C_f} & 0 & 0 \\ 0 & \frac{k_{ilq}}{C_f} & -\omega_0 k_{ilq} + \frac{1}{L_l} & -\frac{1}{T_l} & \left(\omega_0 - \frac{k_{ilq}}{C_f}\right) & 0 \\ 0 & -\frac{k_{ild}}{C_f} & \omega_0 k_{ild} & -\omega_0 & -\frac{1}{T_l} + \frac{k_{ild}}{C_f} & 0 \\ 0 & \frac{k_{vtd}}{C_f} & -\omega_0 k_{vtd} & 0 & -\frac{k_{vtd}}{C_f} & 0 \end{bmatrix} \tag{4.12}$$

$$B_0 = \begin{bmatrix} 0 & \frac{k_{isq}}{C_f} & \frac{1}{L_s}\cos(\alpha_0) \\ 0 & -\frac{k_{isd}}{C_f} & -\frac{1}{L_s}\sin(\alpha_0) \\ \frac{1}{C_f} & 0 & 0 \\ 0 & \frac{k_{ilq}}{C_f} & 0 \\ 0 & -\frac{k_{ild}}{C_f} & 0 \\ 0 & \frac{k_{vtd}}{C_f} & 0 \end{bmatrix} \tag{4.13}$$

Where

$$\omega_0 = \left(\frac{-i_{lq0} + i_{sq0} + i_{fq0}}{C_f v_{td0}} \right)$$

$$k_{isq} = \frac{i_{sq0}}{v_{td0}}$$

$$k_{v\sin} = V_{s0} \sin \alpha_0$$

$$k_{isd} = \frac{i_{sd0}}{v_{td0}}$$

$$k_{v\cos} = V_{s0} \cos \alpha_0$$

$$k_{ilq} = \frac{i_{lq0}}{v_{td0}}$$

$$k_{ild} = \frac{i_{ld0}}{v_{td0}}$$

$$k_{vtd} = \frac{1}{v_{td0}}$$

4.2 Stability Criteria via the State-Transition Matrix

There is an analytical method of solving a set of time-invariant linear equations in which the state matrix, A_0, is constant. The analytical solution can be obtained by the following expression.

$$\Delta x(t) = \Delta x_0 e^{A_0(t-\tau)} + \int_{t_0}^{t} e^{A_0(t-\tau)} B_0(\tau) d\tau; t \geq t_0 \qquad (4.14)$$

(4.14) has two terms on the right-hand side. The first term depends upon the initial condition. This term is called the initial response of the system. The second term, the integral term, is independent of the initial conditions but depends upon the state input. This integral form exhibits a so-called steady-state response. The combination of all the system responses to state input functions is called the dynamic response of the system. As can be seen, the matrix exponential, $e^{A_0(t-\tau)}$, performs a linear transformation and it is also known as the state-transition matrix. Thus, using this state-transition matrix, the state at any time t can be predicted if the state at the previous time $t_0 (t > t_0)$ is known. The state-transition matrix enables determination of the stability criteria of the dynamic system. The elements of $e^{A_0(t-\tau)}$ are linear combinations of $e^{\lambda_k(t-\tau)}$, where $\lambda_k = \alpha_k + j\beta_k$ are distinct eigenvalues of the system for k = 1, 2, …, n. The following criteria can apply to judge whether a system is stable or not.

(1) A system is said to be *asymptotically stable* if all eigenvalues λ_k of the state-transition matrix have negative real parts. This is the first stability criterion.

(2) A system is said to be *unstable* if any eigenvalue λ_k of the state-transition matrix has a positive real part. This is the second stability criterion.

(3) A system is said to be *unstable* if any eigenvalue λ_k of the state-transition matrix has zero real part. This is the third stability criterion.

4.3 Analysis of the Power System with D-STATCOM

To investigate the dynamic stability analysis of the D-STATCOM in electric power distribution system, the parameters of a simplified test power system in

Chapter 3 that shown in Table 3.1 are used. In this case, the nominal reactive load power is assumed to be zero ($Q_l = 0MVar$). These state equations can be reduced as fourth order. The state variables i_{ld} and i_{lq} can be neglected. This test power system produces four characteristic roots, the base-case eigenvalues, comprising of two pairs of complex conjugate roots, which are $-1041.93 \pm j1369.22$ and $-1041.93 \pm j740.90$. All the base-case eigenvalues of the test power system are negative real part.

The work described in this section can be divided into four sub-sections. The first part is to study the effect of D-STATCOM's location and feeder's time constant on the dynamic system stability (small signal stability). The second describes the effect of filter capacitance. The third part illustrates the stability limit with respect to the initial state conditions. The last part presents the frequency responses of the D-STATCOM's transfer functions.

4.3.1 Location of the D-STATCOM and Feeder Line Time Constant

The D-STATCOM can be installed in any position in the feeder line. To evaluate the effect of its location, variations of L_s while fixed T_s is considered. The location of the D-STATCOM in Table 3.1 is at 10 *km* away from the power substation. This implies the resistance and inductance (per *km*) of the feeder line are 0.1 *Ω/km* and 1 *mH/km*, respectively. When T_s is fixed, the variation of L_s is from 20% to 200% of its base-case value, which correspond to the D-STATCOM's location varied from 2 km to 20 km, respectively.

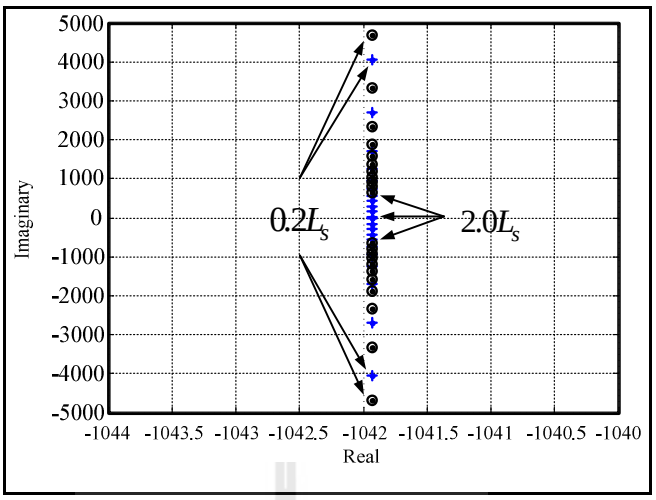

Figure 4.1 Root locus with the variation of L_s while fixed T_s $(12.00 + j0.00MVA)$

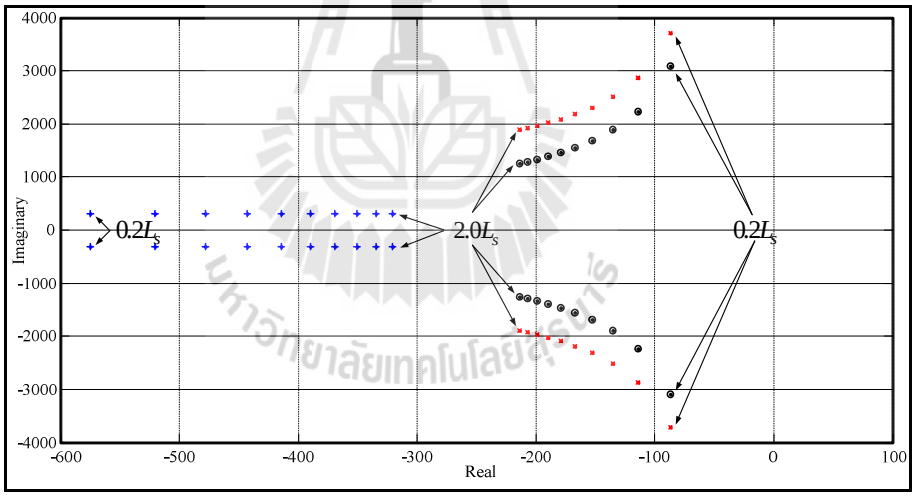

Figure 4.2 Root locus with the variation of L_s while fixed T_s $(12.00 + j5.8MVA)$

The effect of inductance L_s on the system performance is shown by the root locus diagram in Figure 4.1. L_s is varied from 20% to 200% with 20% increment per steps while the time constant T_s and capacitance C_f are kept constant. The

inductance L_s causes two pairs of the complex roots to reduce their imaginary values with constant real values at -1041.93.

When the load power is changed from $12.00 + j0.00MVA$ to $12.00 + j5.8MVA$, the state variables i_{ld} and i_{lq} are considered. This system produces six characteristic roots that the root locus diagram is shown in Figure 4.2. As can be seen from this figure, the increasing inductance causes two pairs of the complex roots move away from the imaginary axis with reducing their imaginary values while another pair of the complex root moves towards the imaginary axis and its imaginary values remains constant.

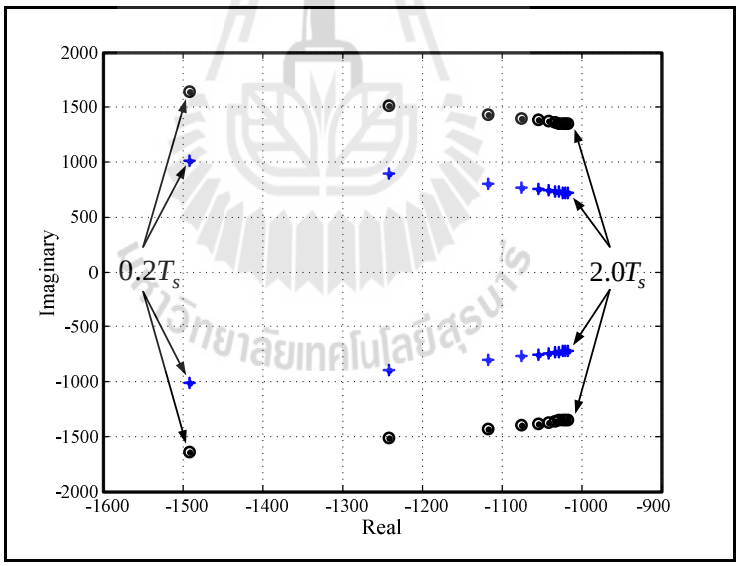

Figure 4.3 Root locus with the variation T_s while fixed L_s $(12.00 + j0.00MVA)$

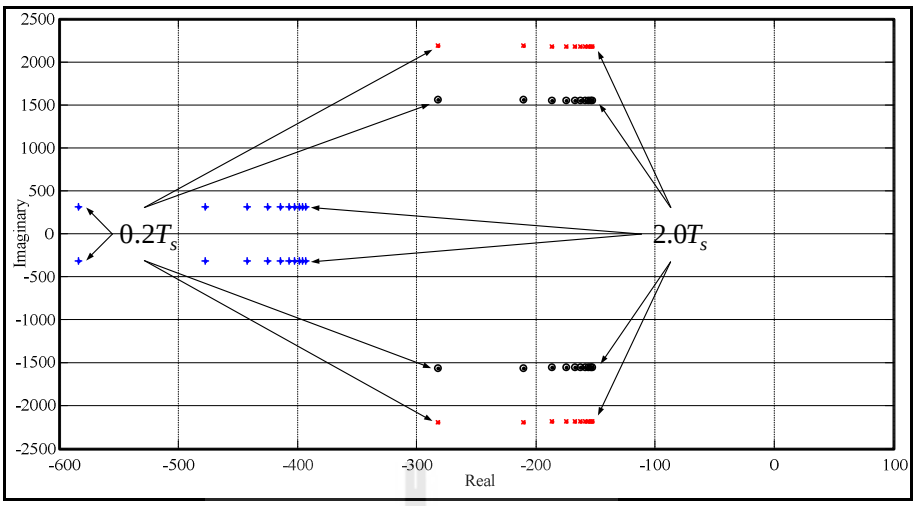

Figure 4.4 Root locus with the variation of T_s while fixed L_s $(12.00 + j5.8MVA)$

The effect of time constant T_s on the transient performance is shown in Figure 4.3. In this figure, T_s is varied from 20% to 200% with 20% increment per step while L_s and C_f are kept constant. When time constant increases, two pairs of the complex roots move towards the imaginary axis with reducing its imaginary values. When the load power is changed from $12.00 + j0.00MVA$ to $12.00 + j5.8MVA$, the increasing time constant causes all the complex roots moves towards the imaginary axis with constant imaginary values as described by the root locus diagram in Figure 4.4.

4.3.2 Effect of Filter Capacitance

When the source inductance L_s and the feeder time constant T_s are fixed, the filter capacitance C_f is varied from 10% to 200%. The root loci are shown in Figure 4.5 and Figure 4.6. In Figure 4.5, the load is given at $12.00 + j0.00MVA$. As can be seen in this figure, there are two pairs of complex conjugate roots. These pairs

start at *A* in Figure 4.5 when $C_f = 10\%$. As the capacitance C_f increases, one of these pairs moves towards the imaginary axis with the constant imaginary values at $\pm j314.159$ whilst the other pair of the complex roots moves away from the imaginary axis and imaginary values remains constant at $\pm j314.159$. However, when the capacitance C_f further increases to some specific value more than 47.9% (see *B* in Figure 4.5), the two pairs of the complex conjugate roots tend to move towards the imaginary axis, after they reach *C* when $C_f = 200\%$.

When the load is $12.00 + j5.8MVA$, the effect of filter capacitance C_f on the system dynamic performance is shown in Figure 4.6. The increasing filter capacitance C_f causes two pair complex roots move slightly towards the imaginary axis with reducing imaginary values. However, another pair of the complex roots moves away from the imaginary axis while imaginary values remain constant at $\pm j314.159$.

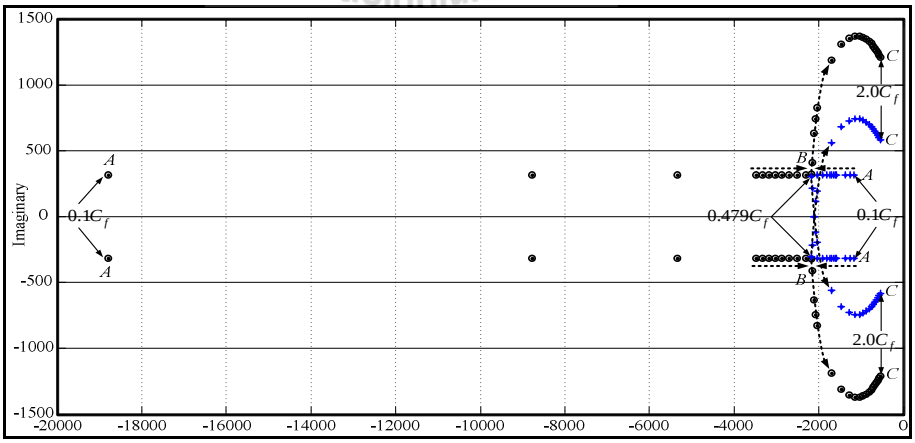

Figure 4.5 Root locus with the variation of C_f $(12.00 + j0.00MVA)$

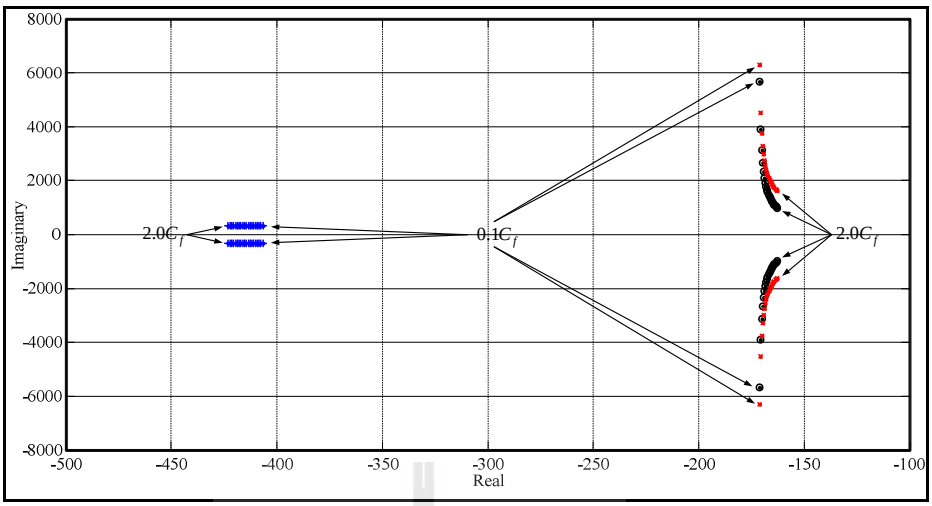

Figure 4.6 Root locus with the variation of the capacitance C_f $(12.00 + j5.8MVA)$

4.3.3 Effect of the Initial Conditions

The initial state conditions can be varied by various means. Firstly, the variation of load active power is studied under two specified power factors, 1.0 and 0.9, respectively. When all parameters of the distribution system (i.e. the source inductance L_s, source resistance R_s and the filter capacitance C_f) are fixed, the load active power P_l is varied from 20% to 200%. The root loci with load active power P_l variation for the two load power factor as 1.0 and 0.9 are shown in Figure 4.7 and Figure 4.8, respectively. As can be seen in Figure 4.7, there are two pairs of complex conjugate roots. These two pairs start at A when $P_l = 20\%$. As the load active power P_l increases, they move away from the imaginary axis with reducing their imaginary values. However, when the load active power P_l further increases to the value greater than 147.6% (see B in Figure 4.7), one of two pairs moves towards the imaginary axis

and its imaginary values remains constant at $\pm j314.159$. Whilst, the other moves away from the imaginary axis with the constant imaginary values at $\pm j314.159$.

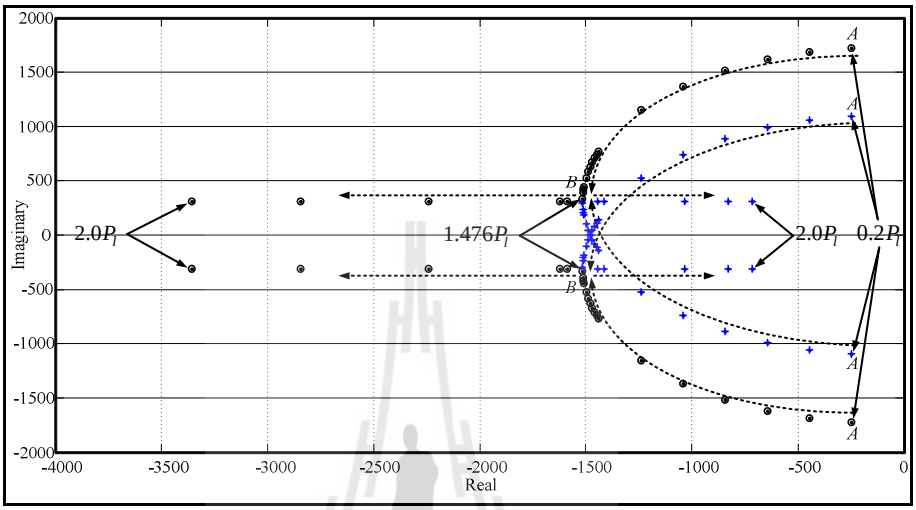

Figure 4.7 Root locus with the variation of active power load P_l (PF = 1.0)

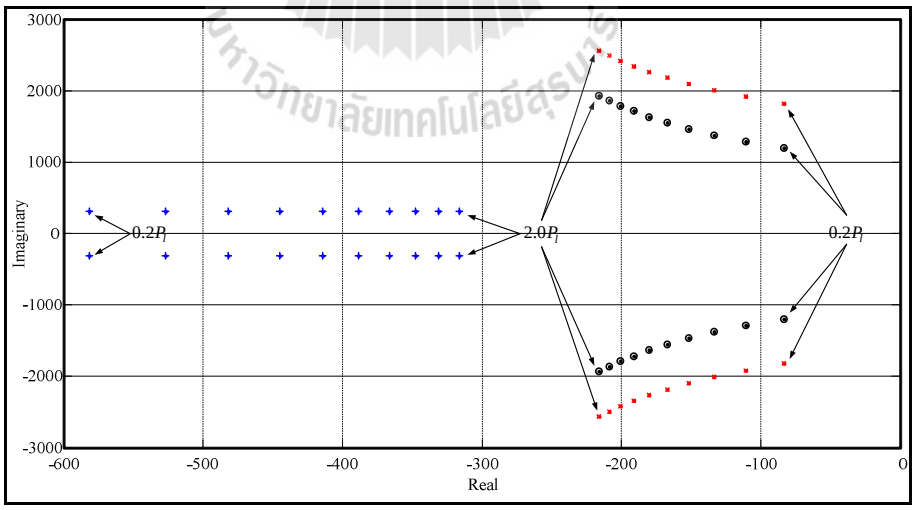

Figure 4.8 Root locus with the variation of active power load P_l (PF = 0.9)

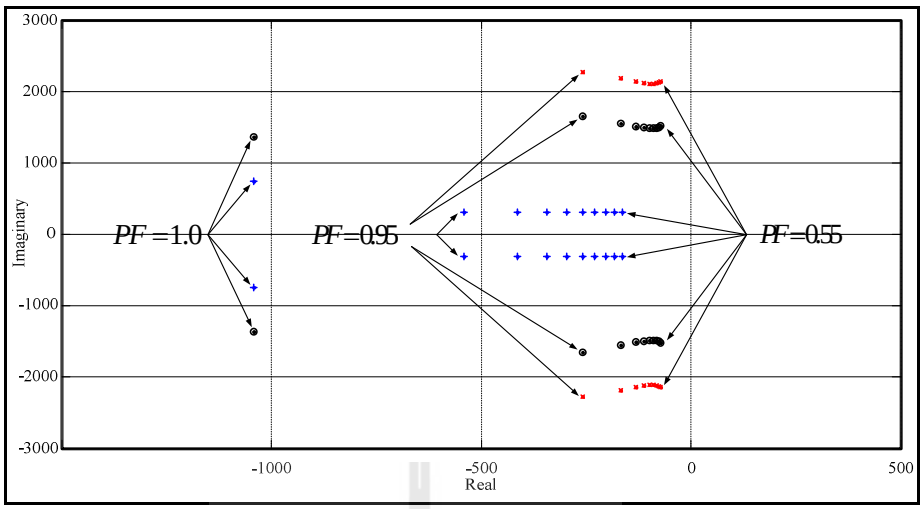

Figure 4.9 Root locus with the variation of load power factor (PF)

When the load power factor is 0.9, the increasing load active power P_l causes two pairs of complex roots move away from the imaginary axis with increasing their imaginary values. The other pair of the complex root, however, moves towards the imaginary axis and its imaginary values remains constant at $\pm j314.159$ as shown in Figure 4.8.

In Figure 4.9, the root locus with the variation of the load power factor is presented. In this figure, PF is varied from 1.0 to 0.55 lagging which 0.05 decrement per step. As can be seen in this figure, there are three pairs of complex conjugate roots which one pair of the complex conjugate roots does not appear when PF=1.0. However, the decreasing load power factor PF causes all complex roots moving towards the imaginary axis.

Secondly, the effects of the compensating currents (i_{fd0}, i_{fq0}) on the dynamic system performances are investigated. When all parameters of the test power

system are fixed and the D-STATCOM's active and reactive currents (i_{fd0} and i_{fq0}) are varied. The root loci with the variation of i_{fd0} and i_{fq0} for two difference load conditions are shown in Figure 4.10 – Figure 4.13. In Figure 4.10, the load is given at $12.00 + j0.00MVA$ (PF= 1.0) and i_{fd0} is varied from +1,000*A* to -1,000*A* while the i_{fq0} is kept constant at 0*A*. From the calculation, there are two pairs of complex conjugate roots as can be seen in Figure 4.10. This figure illustrates the behavior of the two pairs of the complex conjugate roots. They start at point *A* in the figure when $i_{fd0} = +1,000A$ and reach the point *B* when $i_{fd0} = -1,000A$. However, one pair of the complex conjugate roots becomes real at i_{fd0} about $-443.6A$ and then it reaches point *B* when $i_{fd0} = -1,000A$.

When the load power is $12.00 + j5.8MVA$ (PF= 0.9), there are three pairs of the complex conjugate roots which one pair starts on the RHP when $i_{fd0} = +1,000A$. As i_{fd0} decreases, this complex conjugate pair moves towards the imaginary axis and cross to the LHP when i_{fd0} is about $+307A$. When i_{fd0} further decreases continually, the complex conjugate pair moves deeply into the LHP. Meanwhile, the other two pairs of the complex conjugate roots start on the LHP when $i_{fd0} = +1,000A$. One of them moves slightly towards the imaginary axis when the i_{fd0} decreases while the other moves elliptically when i_{fd0} is varied. The behavior of these pairs of complex conjugate roots when the load power is $12.00 + j5.8MVA$ are illustrated in Figure 4.11.

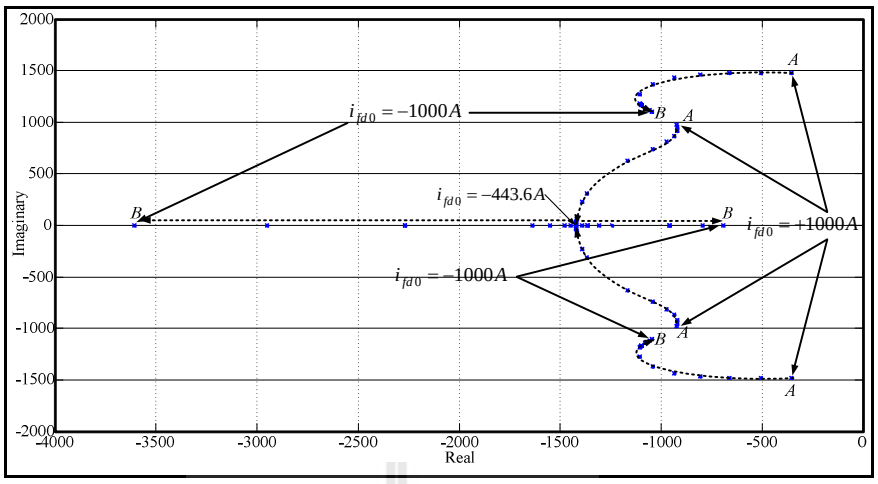

Figure 4.10 Root locus with the variation of i_{fd0} $(12.00 + j0.00MVA)$

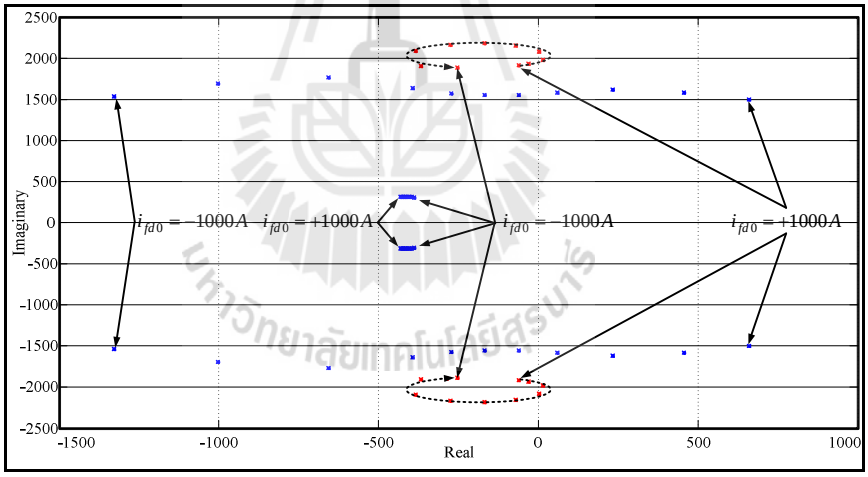

Figure 4.11 Root locus with the variation of i_{fd0} $(12.00 + j5.8MVA)$

The root loci with the variation of i_{fq0} for the load at $12.00\,j0.00MVA$ (PF= 1.0) are shown in Figure 4.12. In this Figure, i_{fq0} is varied from +1,000A to -1,000A while the i_{fd0} is kept constant at 0A. There are two pairs of complex conjugate

roots. As i_{fq0} decreases, one of the two pairs move towards while the other moves away from the imaginary axis.

When the load power is $12.00 + j5.8MVA$ (PF= 0.9), there exist three pairs of the complex conjugate roots. One pair of the complex conjugate roots starts on the RHP when $i_{fq0} = +1,000A$. As i_{fq0} decreases, this complex pair moves towards the imaginary axis and cross to the LHP when $i_{fq0} = +354A$. When the i_{fq0} further decreases continually, this pair moves away from the imaginary axis and deeply into the LHP. Meanwhile two pairs of the complex conjugate roots start on the LHP when $i_{fd0} = +1,000A$. One of them moves towards the imaginary axis when i_{fd0} decreases. Whereas the imaginary values of another pair left reduces slightly when i_{fq0} decreases. The behavior of these three pairs of complex conjugate roots when the load power is $12.00 + j5.8MVA$ are illustrated in Figure 4.13.

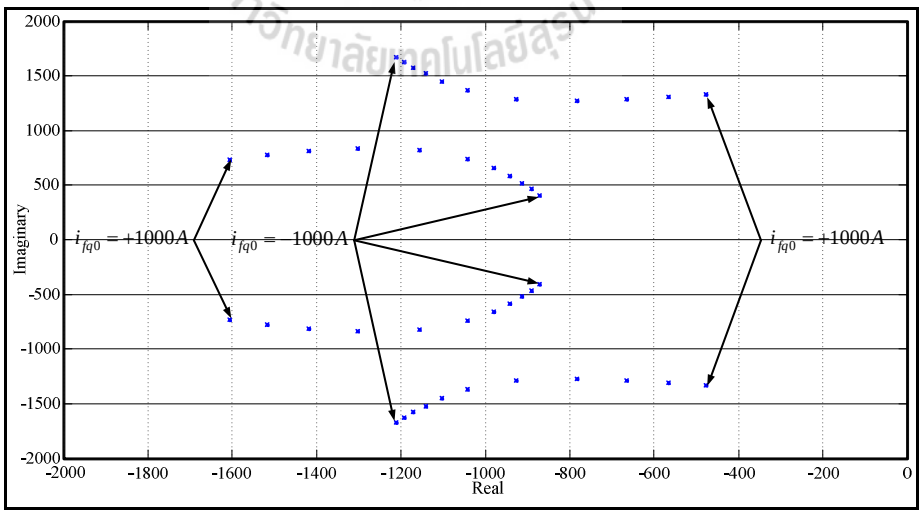

Figure 4.12 Root locus with the variation of i_{fq0} $(12.00 + j0.00MVA)$

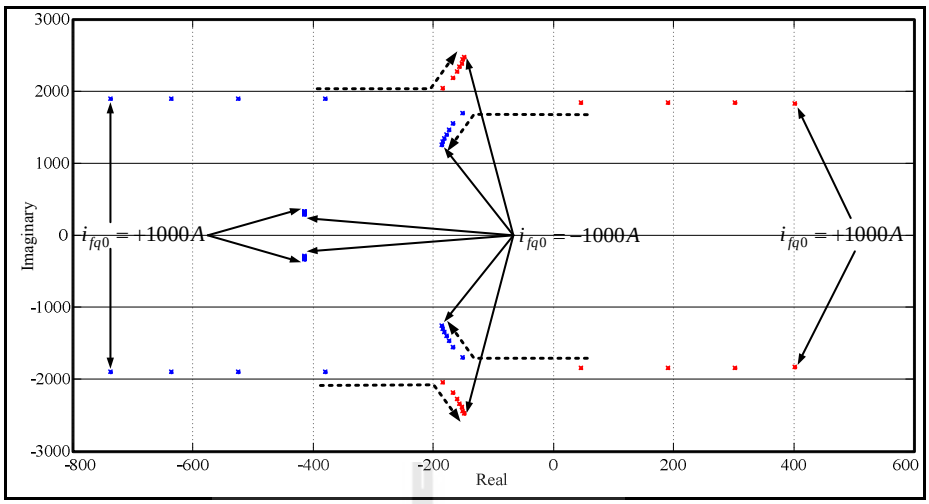

Figure 4.13 Root locus with the variation of $i_{fq0}\,(12.00 + j5.8MVA)$

4.3.4 Frequency Responses of the System with D-STATCOM

The D-STATCOM reactive current affect not only the characteristic roots, but also the Zeros of the system. The effect of the D-STATCOM reactive current can be described by the frequency response of the bode diagram. The bode plot in Figure 4.14 and Figure 4.15 illustrate the frequency responses of the D-STATCOM's active current, reactive current and the magnitude of the source voltage of the magnitude and phase of load voltage when the load powers are $12.0 + j0.0MVA$ and$12.0 + j5.8MVA$, respectively. The D-STATCOM's reactive current is varied from +1,000*A* to -1,000*A* with 200-*A* decrement per step. The Zeros in each step are calculated and shown in Table 4.1 and Table 4.2 when the load powers are $12.0 + j0.0MVA$and $12.0 + j5.8MVA$, respectively

When the D-STATCOM reactive current is varied from +1,000*A* to 0*A* with

200*A* per step, the transfer function of the load voltage with respect to the active compensating current is shown in Figure 4.14-a whereas Figure 4.14-d shows the transfer function when the D-STATCOM reactive current is varied from 0*A* to -1,000*A* with 200-*A* per step. This transfer function consists of one real Zero and one complex conjugate pair Zeros. All Zeros are located on the LHP and they do not move even the D-STATCOM reactive current is changed largely.

The transfer function of the load voltage with respect to the reactive current are shown in Figure 4.14-b and Figure 4.14-e when the D-STATCOM reactive current is varied from +1,000*A* to 0*A* and from 0*A* to -1,000*A* with 200-*A* per step, respectively. The Zeros of the transfer function are one complex conjugate pair located on the LHP when the D-STATCOM reactive current is varied from +1,000*A* to 0*A*. Real parts of the Zeros do not change during this variation of the reactive current. The Zeros become two real Zeros when the reactive current is in a range of +200*A* to -1,000*A*. One of these locates on the RHP whereas the other Zeros are on the LHP. In this consideration, the transfer function is a non-minimum phase system in a larger phase and a longer time delay than that of the minimum-phase system with the identical magnitude of frequency responses.

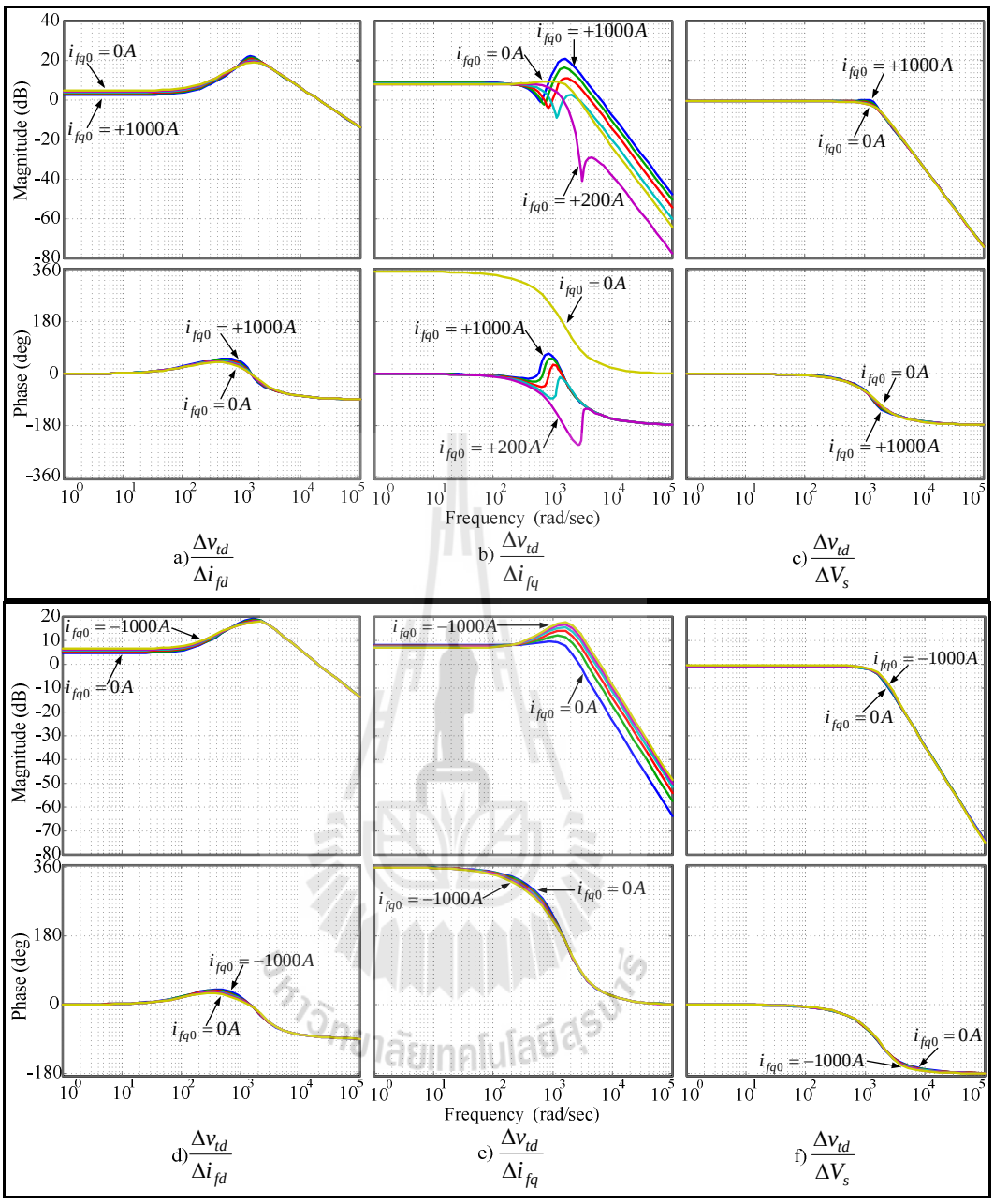

Figure 4.14 Bode plots of the system with D-STATCOM $(12.0 + j0.0MVA)$

The bode plot of the transfer function of the load voltage with respect to the magnitude of the source voltage are shown in Figure 4.14-c and Figure 4.14-f when the D-STATCOM's reactive current is varied from +1,000A to 0A and from 0A

to -1,000*A* with 200-*A* per step, respectively. This transfer function consists of one pair of complex conjugates Zeros that is located on the LHP. These zeros move slightly away from the imaginary axis and become two real Zeros when the D-STATCOM's reactive current varies in a range of -600*A* to -1,000*A*.

When the load power is $12.0 + j5.8MVA$, transfer function of the load voltage with respect to the active compensating current are shown in Figure 4.15-a and Figure 4.15-d. This transfer function consists of one real Zero and two complex conjugate pairs of Zeros. All the Zeros are located on the LHP and do not move even the D-STATCOM reactive current is changed largely.

The transfer function of the load voltage with respect to the reactive current are shown in Figure 4.15-b and Figure 4.15-e when the D-STATCOM reactive current is varied from +1,000*A* to 0*A* and from 0*A* to -1,000*A* with 200-*A* per step, respectively. The Zeros of the transfer function are two complex conjugate pairs in which one pair of these located on the LHP and move slightly towards the imaginary axis when the D-STATCOM reactive current is changed. Meanwhile, the other pair located on the LHP and then moves away the imaginary axis when the D-STATCOM reactive current is varied in a range of +1,000*A* to +200*A*. However, these Zeros become two real Zeros when the D-STATCOM reactive current varies in a range of +200*A* to -1,000*A*. One of these is located on the RHP while the other Zero is on the LHP. In this consideration, the transfer function is also a non-minimum phase system.

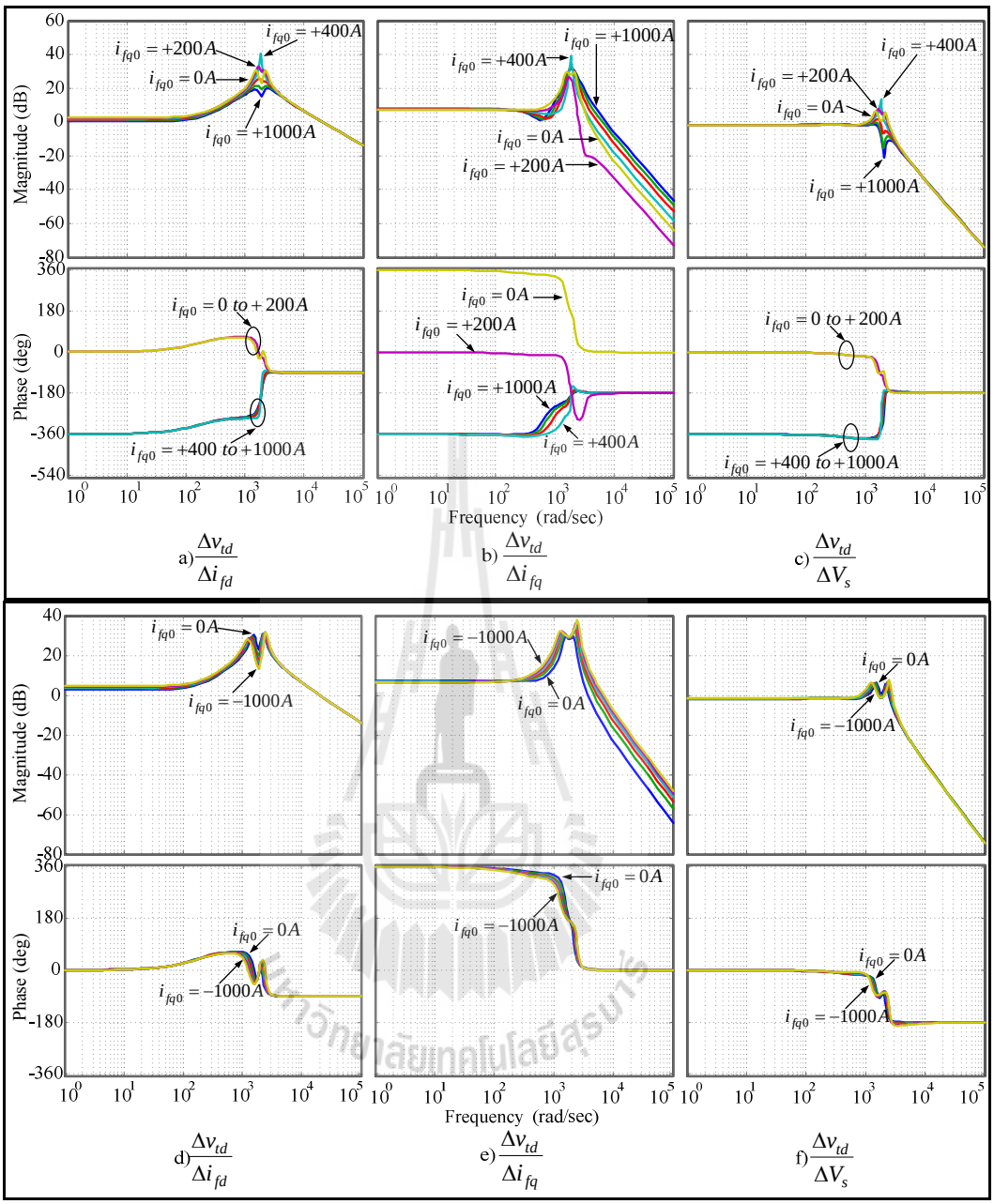

Figure 4.15 Bode plots of the system with D-STATCOM $(12.0 + j5.8MVA)$

The bode plot of the transfer function of the load voltage with respect to the magnitude of the source voltage are shown in Figure 4.15-c and Figure 4.16-f when the D-STATCOM reactive current is varied from +1,000*A* to 0*A* and from 0*A* to -1,000*A* with 200-*A* per step, respectively. This transfer function consists of two

complex conjugate pairs Zeros that all the Zeros are located on the LHP. One of them moves away from the imaginary axis while the other pair moves towards the imaginary axis when the D-STATCOM reactive current is varied from +1,000*A* to -1,000*A*.

Table 4.1 Zeros of the test power system when the load power is $12.0 + j0.0 MVA$

i_{fq0} **(A)**	**Zeros of** $\frac{\Delta v_{td}(s)}{\Delta i_{fd}(s)}$	**Zeros of** $\frac{\Delta v_{td}(s)}{\Delta i_{fq}(s)}$	**Zeros of** $\frac{\Delta v_{td}(s)}{\Delta V_s(s)}$
+1000	$-993.68 \pm j1062.04$ -196.51	$-100 \pm j634.96$	$-913.84 \pm j1439.84$
+800	$-993.68 \pm j1062.04$ -196.51	$-100 \pm j724.69$	$-938.29 \pm j1366.17$
+600	$-993.68 \pm j1062.04$ -196.51	$-100 \pm j871.19$	$-974.53 \pm j1288.31$
+400	$-993.68 \pm j1062.04$ -196.51	$-100 \pm j1179.67$	$-1020.93 \pm j1204$
+200	$-993.68 \pm j1062.04$ -196.51	$-100 \pm j3087.22$	$-1076.31 \pm j1110.20$
0	$-993.68 \pm j1062.04$ -196.51	-1479.02 1279.02	$-1139.86 \pm j1002.43$
-200	$-993.68 \pm j1062.04$ -196.51	-1022 822	$-1211.04 \pm j873.42$
-400	$-993.68 \pm j1062.04$ -196.51	-835.3 635.3	$-1289.53 \pm j708.92$
-600	$-993.68 \pm j1062.04$ -196.51	-726.37 526.37	$-1375.17 \pm j468.75$
-800	$-993.68 \pm j1062.04$ -196.51	-652.35 452.35	-1768.54 -1167.42
-1000	$-993.68 \pm j1062.04$ -196.51	-597.48 397.48	-2226.07 -910.21

Table 4.2 Zeros of the test power system when the load power is $12.0 + j5.8 MVA$

i_{fq0} **(A)**	**Zeros of** $\frac{\Delta v_{td}(s)}{\Delta i_{fd}(s)}$	**Zeros of** $\frac{\Delta v_{td}(s)}{\Delta i_{fq}(s)}$	**Zeros of** $\frac{\Delta v_{td}(s)}{\Delta V_s(s)}$
+1000	$-171.08 \pm j1891.13$ $-464.78 \pm j222.21$ -225.6	$-571.22 \pm j511.00$ $-177.44 \pm j580.34$	$-54.54 \pm j2048.79$ $-552.19 \pm j316.14$
+800	$-171.08 \pm j1891.13$ $-464.78 \pm j222.21$ -225.6	$-507.17 \pm j541.33$ $-241.49 \pm j670.42$	$-69.72 \pm j1995.84$ $-547.2 \pm j318.61$
+600	$-171.08 \pm j1891.13$ $-464.78 \pm j222.21$ -225.6	$-430.39 \pm j498.52$ $-318.27 \pm j903.62$	$-98.32 \pm j1949.44$ $-542.00 \pm j321.06$
+400	$-171.08 \pm j1891.13$ $-464.78 \pm j222.21$ -225.6	$-413.04 \pm j452.38$ $-335.62 \pm j1329.21$	$-138.32 \pm j1908.25$ $-536.57 \pm j323.47$
+200	$-171.08 \pm j1891.13$ $-464.78 \pm j222.21$ -225.6	$-406.80 \pm j422.21$ $-341.85 \pm j3130.10$	$-188.25 \pm j1871.05$ $-530.81 \pm j325.79$
0	$-171.08 \pm j1891.13$ $-464.78 \pm j222.21$ -225.6	-2268.48 1578.34 $-403.59 \pm j399.66$	$-247.04 \pm j1836.68$ $-524.68 \pm j327.99$
-200	$-171.08 \pm j1891.13$ $-464.78 \pm j222.21$ -225.6	-1650.60 956.60 $-401.66 \pm j381.47$	$-313.94 \pm j1804.04$ $-518.11 \pm j329.99$
-400	$-171.08 \pm j1891.13$ $-464.78 \pm j222.21$ -225.6	-1420.09 723.58 $-400.40 \pm j366.09$	$-388.41 \pm j1772.10$ $-511.05 \pm j331.71$
-600	$-171.08 \pm j1891.13$ $-464.78 \pm j222.21$ -225.6	-1291.22 593.02 $-399.56 \pm j352.67$	$-470.09 \pm j1739.85$ $-503.47 \pm j333.05$
-800	$-171.08 \pm j1891.13$ $-464.78 \pm j222.21$ -225.6	-1206.02 506.66 $-398.98 \pm j340.67$	$-558.75 \pm j1706.27$ $-495.34 \pm j333.87$
-1000	$-171.08 \pm j1891.13$ $-464.78 \pm j222.21$ -225.6	-1144.12 443.98 $-398.59 \pm j329.75$	$-654.29 \pm j1670.27$ $-486.66 \pm j334.03$

4.4 Summary

This chapter describes the analysis of the distribution system with ideal D-STATCOM. A simplified model of D-STATCOM in power distribution systems in the *dq* frame of reference is used to investigate. The power circuit of D-STATCOM is modeled by a controlled current source. The compensating current from the D-STATCOM is assumed to be purely sinusoidal. Therefore, a set of equations in the transformed domain can be collected and therefore used to develop the state-space dynamic system equations. The proposed non-linear model can be linearized around some initial state conditions. Thus, the state-transition matrix representing the linearized model can be obtained. Dynamic system stability of the linearized systems can be evaluated by means of eigenvalues. In this chapter, a simplified 11-kV, 2-bus test power system is employed for the simulation. Variation of some parameters, e.g. location of an installed D-STATCOM, the time constant of feeder section, initial state conditions, etc., is investigated to exhibit the dynamic system stability.

As a result shows that the variations of the location of an installed D-STATCOM (L_s), time constant of feeder section (T_s), filter capacitance (C_f) and the variation of the initial state condition e.g. load active power (P_l), load power factor and currents of the D-STATCOM (i_{fd} and i_{fq}) have effect on the dynamic performance especially in the system with the RL load. In addition, all variations not to involve the instability of the system with R load. However, some of positive active and reactive currents of the D-STATCOM involved the instability of the system with RL loads.

Furthermore, the frequency responses of the transfer function of the load voltage with respect to the reactive current shows that the negative reactive currents cause some of Zeros locates on the RHP. In this consideration, the transfer function is a non-minimum phase system in a larger phase and a longer time delay than that of the minimum-phase system with the identical magnitude of frequency responses.

CHAPTER V

DESIGN OF COMPONENT RATING AND MODELING OF D-STATCOM

This chapter presents the design of component rating of the D-STATCOM for the load voltage regulation. From the required reactive power for the load voltage regulation and the load voltage rating, the component rating of the D-STATCOM such as the compensation current, DC voltage and energy transfer of the capacitor are obtained. Then, the D-STATCOM parameters in each case of the load voltage regulation e.g. the AC inductor and DC capacitor are designed. In addition, the dynamic equations of the D-STATCOM based on synchronously rotating reference frame are proposed. The steady state characteristic of the D-STATCOM can be derived from these dynamic equations. To analyze the steady state performance, the effect of the control signal (u_d , u_q) and parameters of an AC inductor (L_f , R_f) on the active current, reactive current and DC voltage of the D-STATCOM are investigated. To investigate the dynamic performance of the D-STATCOM, linear approximation is applied.

5.1 Design of Component Rating of D-STATCOM

The D-STATCOM consists of switching devices, electrolytic capacitor at DC and filtering AC inductors. Normally insulated gate bipolar transistors (IGBT) or metal-oxide-semiconductor field effect transistors (MOSFETs) are used as switching devices in D-STATCOM. Reactive power to be supplied by the D-STATCOM to the system for load voltage regulations when the source voltage sag and load power vary is the deciding factor designing component rating of the D-STATCOM. To calculate the component rating, a design example is presented for the parameters of the distribution power system in Table 3.1.

As can be seen in Chapter 3, Figure 3.16 and Figure 3.18 shows the variation of required reactive power for load voltage regulation when the source voltage sags with the load as unity and 0.9 lag power factor, respectively. The required reactive power for different source voltage is given in Table 5.1. Meanwhile, Figure 3.19 and Figure 3.21 shows the variation of required reactive power for load voltage regulation when the load power varies with the load as unity and 0.9 lag power factor, respectively. The required reactive power for different load power is given in Table 5.2.

Table 5.1 Required reactive power for different source voltage

Source voltage (*kV*)	**Load as PF= 1.0**	**Load as PF= 0.9 lag**
	Required reactive power (*MVar*)	**Required reactive power (*MVar*)**
12.10 (1.0 p.u.)	0.00	5.80
10.89 (0.9 p.u.)	5.05	10.85
9.68 (0.8 p.u.)	10.53	16.33
8.47 (0.7 p.u.)	16.83	22.63

Table 5.2 Required reactive power for different load power

Load active power (*MW*)	Load as PF= 1.0	Load as PF= 0.9 lag
	Required reactive power (*MVar*)	Required reactive power (*MVar*)
12.00 (1.0 p.u.)	0.00	5.80
14.40 (1.2 p.u.)	1.80	8.77
16.80 (1.4 p.u.)	3.92	12.05
19.20 (1.6 p.u.)	6.43	15.72

If the converter losses are neglected, the current rating of the D-STATCOM corresponds to reactive power required for load voltage regulation is calculated from this equation

$$Q_{D-STATCOM}\,(MVar) = \sqrt{3}V_t I_f \tag{5.1}$$

where V_t is the desired load line voltage and I_f is the D-STATCOM line current. For example, the required reactive power for load voltage regulation when the source voltage sags as 8.47 *kV* with the load power factor as 0.9 lag is used. After substituting the value of reactive power ($Q_{D-STATCOM}$) and V_t (11.00 *kV*), the current rating of the D-STATCOM is $I_f = 1187.77A$. When the desired load line voltage is rated voltage of 11.00 *kV*, the DC bus voltage must be more than the peak load line voltage for satisfactory PWM control, as (Singh et al., 2004)

$$V_{dc} = \frac{2\sqrt{2}\left(\frac{V_t}{\sqrt{3}}\right)}{m_a} \tag{5.2}$$

where m_a is the modulation index normally with maximum value of 1. However, the modulation index should be varied from 0.2 to 0.9. If we choose the nominal modulation index m_a as 0.55, the nominal DC bus voltage obtained from (5.2) is:

$$V_{dc,\text{nominal}} = 32{,}659.86V \approx 33{,}000V \text{ (selected).}$$

If current ripple ($i_{cr(p-p)}$) through the AC inductor is allowed to be 10%, the inductance can be calculated as (Singh et al., 2004)

$$L_f = \frac{\left(\frac{\sqrt{3}}{2}\right) m_a V_{dc}}{6.a.f_s i_{cr(p-p)}} \tag{5.3}$$

where f_s is the switching frequency which is taken as 10kHz, in this case. During transients, the current rating is likely to vary from 120% to 180% of the steady state value. In inductance calculation current rating of 170% (a = 1.7) of steady state current is taken during transients. After substituting the value of V_{dc}, f_s and current ripple $i_{cr(p-p)}$ in (5.3), the inductance value is $L_f = 1.3mH$. The voltage drop across the AC inductor is calculated by

$$V_{Lf} = 2\pi f L_f I_f = 485.09V \approx 4.4\% \text{ of } 11.00kV. \tag{5.4}$$

The rating of the DC bus capacitor of D-STATCOM is a very important factor as it should provide the instantaneous energy at sudden source voltage sag or loading of the system. It also provides energy instantaneous to the system under transient operation. The response time of D-STATCOM is around 200 to 350 μs (Hingorani and Gyugyi, 2000). If the DC voltage dip during load voltage regulation is considered during transients then energy transfer from the capacitor to the system to provide reactive power is calculated as

$$\text{Energy transfer} = \frac{1}{2} C_{dc} \left(V_{dc}^2 - V_{dc,min}^2 \right) \eta = \left(3 V_{t,ph} I_f \right) t \tag{5.5}$$

where $V_{dc,min}$ is chosen minimum value of the DC voltage, t is hold-up time in seconds and η is the energy efficiency of the D-STATCOM. It is assumed the dip in DC bus voltage to 8% means that it varies from 33,000 to 30,360V ($V_{dc,min}$). After substituting the value of V_{dc}, $V_{dc,min}$, $V_{t,ph}$, I_f, t (350 μ sec) and η ($\approx$80%) into (5.5), the value of the DC bus capacitance is $C_{dc} = 118.38 \mu F$. The nearest commercially available value of $150 \mu F$ is selected in place of $118.38 \mu F$ (calculated value). It should be noted that for a given capacitance, the capacitor volume is roughly proportional to the voltage rating, and the maximum energy storage capability is proportional to the square of the voltage rating.

Table 5.3 Rating D-STATCOM parameters for different source voltage sag

Source voltage (*kV*)	Load as PF = 1.0				Load as PF= 0.9 lag			
	DC bus Voltage (*kV*)	Current Rating (*A*)	AC Inductance (*mH*)	DC bus Capacitance (μF)	DC bus Voltage (*kV*)	Current Rating (*A*)	AC Inductance (*mH*)	DC bus Capacitance (μF)
12.10	-	-	-	-	33.00	304.42	5.07	33
10.89	33.00	265.06	5.82	33	33.00	569.48	2.71	68
9.68	33.00	552.68	2.79	68	33.00	857.10	1.80	100
8.47	33.00	883.35	1.75	100	33.00	1187.77	1.30	150

Table 5.4 Rating D-STATCOM parameters for different load power

Load active power (*MW*)	Load as PF= 1.0				Load as PF= 0.9 lag			
	DC bus Voltage (*kV*)	Current Rating (*A*)	AC Inductance (*mH*)	DC bus Capacitance (μF)	DC bus Voltage (*kV*)	Current Rating (*A*)	AC Inductance (*mH*)	DC bus Capacitance (μF)
12.00	-	-	-	-	33.00	304.42	5.07	33
14.40	33.00	94.48	16.33	10	33.00	460.31	3.35	50
16.80	33.00	205.75	7.50	22	33.00	632.46	2.44	68
19.20	33.00	337.49	4.57	33	33.00	825.09	1.87	100

All selected values (DC bus voltage, D-STATCOM current rating, AC inductance, and DC bus capacitance) are given in Table 5.3 and 5.4, corresponding to source voltage sag and load power variations, respectively.

Voltage and current ratings of the solid-state devices (IGBTs or MOSFETs) are decided based on the maximum voltage across the devices and current through the devices. Under dynamic conditions, change in the terminal load voltage of the system to be 10%. The maximum ac voltage is calculated as

$$\text{The maximum ac voltage} = \sqrt{2}\left(V_t + V_{Lf} + V_d\right) \tag{5.6}$$

where V_{Lf} is the voltage drop across the AC inductor and V_d is 10% of V_t for dynamic conditions. After substituting the value of V_t, the voltage drop across inductor from

(5.4) and 10% of V_t (1100V) in (5.6), the maximum voltage is $\approx 17.80kV$. The rated current through the D-STATCOM is 1187.77A. The peak value of the D-STATCOM current is ($\sqrt{2} \times 1187.77A$) = 1679.76A. Considering the safety factor, the maximum line current can be calculated as

$$\text{The maximum line current} = 1.25\left(I_{cr(p-p)} + I_{f(peak)}\right) \tag{5.7}$$

After substituting the value of the peak-to-peak ripple in (5.7), the D-STATCOM maximum instantaneous line current is 2248.17A.

5. 2 Modeling of D-STATCOM

The basic circuit diagram and control of the D-STATCOM system are shown in Figure 5.1. It consists of a three phase voltage source converter (VSC), interfacing inductors, DC link capacitor, and control systems. In this Figure each switch represents a power semiconductor device and anti-parallel diode combination. The VSC is connected to the network through the transformer and the interfacing inductors which are used to filter high-frequency components of compensating currents. The inductance L_f in this Figure represents the leakage inductance of the transformer and the interfacing inductors. The copper loss of the connecting transformer and loss of the interfacing inductor is represented by a resistance R_f. In this thesis, the D-STATCOM is used for the load voltage regulation by injecting the reactive power. Therefore, the control systems of the D-STATCOM consist of a current control, DC voltage control, and AC voltage control. The primary control

objective is to rapidly regulate the D-STATCOM currents to the reference values that are generated by the voltage controllers. A secondary control objective is to keep the DC voltage around a desired value.

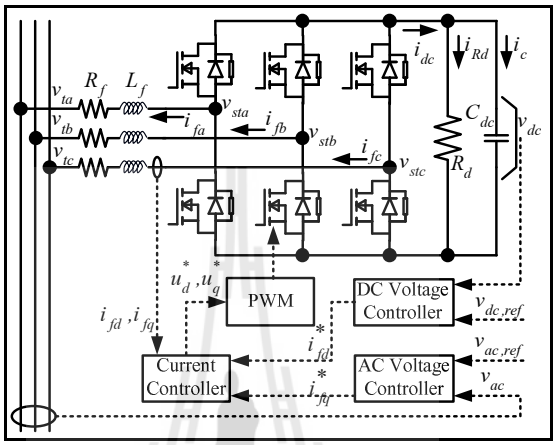

Figure 5.1 Basic circuit diagram and control of the D-STATCOM system

As can be seen in Figure 5.1, the D-STATCOM output AC voltage is represented by $v_{st,abc}$. This voltage is generated by the converter and is assumed to be quasi-sinusoidal voltage waveform. Therefore, the voltage equation of AC system can be written as

$$L_f \frac{di_{f,abc}}{dt} = -R_f i_{f,abc} - v_{t,abc} + v_{st,abc} \tag{5.8}$$

Consider the DC system in Figure 5.1, the DC current (i_{dc}) consists of capacitor current (i_c) and resistor current (i_{Rd}). The resistor R_d represents losses in the

converter. The power flow into the converters equals to the instantaneous power of the DC capacitor which can be described as

$$p_{dc} = v_{dc} i_{dc} = v_{dc}(i_c + i_{Rd}) = p_{ac} = v_{st,abc}^{T} i_{f,abc} \tag{5.9}$$

Here, v_{dc} is the D-STATCOM DC voltage, i_f is the D-STATCOM output current, v_t is the load voltage, while the subscript "*abc*" implies vectors consisting of individual phase quantities. From Figure 5.1, the DC current can be expressed as

$$i_{dc} = C_{dc} \frac{dv_{dc}}{dt} + \frac{v_{dc}}{R_{dc}} \tag{5.10}$$

where C_{dc} is the DC link capacitance. From Figure 5.1, the relation between DC power and AC power can be expressed as

$$v_{dc}\left(C_{dc} \frac{dv_{dc}}{dt} + \frac{v_{dc}}{R_{dc}} \right) = -\left(v_{st,abc}^{T} i_{f,abc} \right) \tag{5.11}$$

After applying the three-phase to two-phase transformation given by (3.4) followed by the rotational transformation of (3.5) with the chosen *dq* reference frame in Chapter 3, the D-STATCOM dynamics in (5.8) and (5.11) can be rewritten as:

$$\frac{di_{fd}}{dt} = -\frac{1}{T_f} i_{fd} + \omega i_{fq} - \frac{1}{L_f} v_{td} + \frac{1}{L_f} k_p u_d v_{dc} \tag{5.12}$$

$$\frac{di_{fq}}{dt} = -\frac{1}{T_f} i_{fq} - \omega i_{fd} + \frac{1}{L_f} k_p u_q v_{dc} \tag{5.13}$$

$$\frac{dv_{dc}}{dt} = -\frac{v_{dc}}{T_{dc}} - \frac{3}{2}\frac{1}{C_{dc}} k_p u_d i_{fd} - \frac{3}{2}\frac{1}{C_{dc}} k_p u_q i_{fq} \tag{5.14}$$

where T_f is the time constant of the transformer and interfacing inductor, $T_f = \frac{L_f}{R_f}$

T_{dc} is the time constant of the DC system, $T_{dc} = C_{dc} R_{dc}$

Here, $k_p u_d v_{dc}$ and $k_p u_q v_{dc}$ represent the D-STATCOM output AC voltage on *d*-axis and *q*-axis ($v_{st,d}$ and $v_{st,q}$), respectively. Meanwhile, the ω has been previously defined in (3.16), v_{dc}, i_{fd} and i_{fq} represent the state variables of the D-STATCOM, k_p is a constant value depending on the type of converter and transformer ratio (Marian et al., 2002). The D-STATCOM output AC voltage can be generated by controlling the converter. Therefore, AC voltage command on *dq*-axis (u_d and u_q) are the control inputs of the D-STATCOM.

Block diagram of the D-STATCOM can be modified from the equation (5.12) to (5.13) as shown in Figure 5.2. This block diagram represents the model of the AC system and the converter of the D-STATCOM on the synchronously rotating reference frame (*dq*-axis). This system has two inputs that are the AC voltage command on *dq*-axis (u_d and u_q). The active current, reactive current and DC capacitor voltage are the state variables of this system. Therefore, the state equation of the D-STATCOM can be derived from equation (5.12) to (5.14) as shown in (5.15).

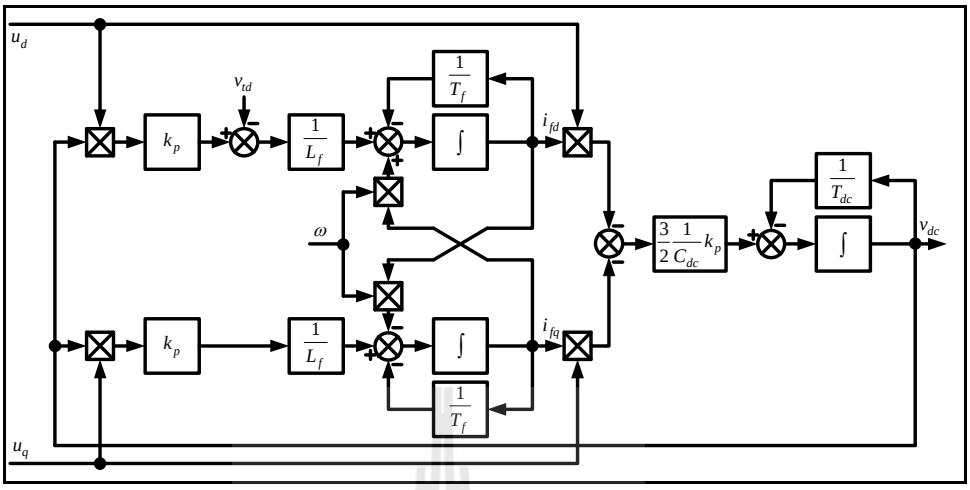

Figure 5.2 Block diagram of the D-STATCOM system

$$\frac{d}{dt}\begin{bmatrix} i_{fd} \\ i_{fq} \\ v_{dc} \end{bmatrix} = \begin{bmatrix} -\frac{1}{T_f} & \omega & \frac{1}{L_f}k_p u_d \\ -\omega & -\frac{1}{T_f} & \frac{1}{L_f}k_p u_q \\ -\frac{3}{2}\frac{1}{C_{dc}}k_p u_d & -\frac{3}{2}\frac{1}{C_{dc}}k_p u_q & -\frac{1}{T_{dc}} \end{bmatrix}\begin{bmatrix} i_{fd} \\ i_{fq} \\ v_{dc} \end{bmatrix} + \begin{bmatrix} -\frac{1}{L_f} \\ 0 \\ 0 \end{bmatrix}\begin{bmatrix} v_{td} \end{bmatrix} \tag{5.15}$$

5.3 Steady State Analysis of the D-STATCOM

The equation in (5.15) is a set of dynamic equations. However, the equation for the steady state operation of the system can be obtained from (5.15) by setting all derivative terms to zero. After transformation into synchronously rotating reference frame, voltages and currents become DC quantities, i.e. $v_{td} = V_{td}$, $v_{dc} = V_{dc}$, $i_{fd} = I_{fd}$, $i_{fq} = I_{fq}$. The steady state equations can now be as follows:

$$\begin{bmatrix} -R_f & X_f & k_p u_d \\ -X_f & -R_f & k_p u_q \\ -3k_p u_d & -3k_p u_q & -\dfrac{2}{R_{dc}} \end{bmatrix} \begin{bmatrix} I_{fd} \\ I_{fq} \\ V_{dc} \end{bmatrix} = \begin{bmatrix} V_{td} \\ 0 \\ 0 \end{bmatrix} \tag{5.16}$$

Where X_f is $\omega_s L_f$. Solving for I_{fd}, I_{fq} and V_{dc}, the solution are

$$I_{fd} = -\frac{R_f + \frac{3}{2}k_p^2 u_q^2 R_{dc}}{R_f^2 + X_f^2 + \frac{3}{2}k_p^2 R_f R_{dc}\left(u_d^2 + u_q^2\right)} V_{td} \tag{5.17}$$

$$I_{fq} = \frac{X_f + \frac{3}{2}k_p^2 u_d u_q R_{dc}}{R_f^2 + X_f^2 + \frac{3}{2}k_p^2 R_f R_{dc}\left(u_d^2 + u_q^2\right)} V_{td} \tag{5.18}$$

$$V_{dc} = \frac{\frac{3}{2}k_p R_{dc}\left(u_d R_f - u_q X_f\right)}{R_f^2 + X_f^2 + \frac{3}{2}k_p^2 R_f R_{dc}\left(u_d^2 + u_q^2\right)} V_{td} \tag{5.19}$$

As considered in (5.17) to (5.19), the expression for active current (I_{fd}), reactive current (I_{fq}) and DC capacitor voltage (V_{dc}) do not include DC capacitor. Therefore, the size of DC capacitor does not affect steady state performance of the system. Especially, the reactive current (I_{fq}) does not depend on the size of DC

capacitor. Although the DC capacitor does not affect the steady state performance, it is used for maintaining the DC voltage on the DC bus. Additionally, the DC capacitor value has no relation to the produced reactive power. However, the DC capacitor acts as a DC voltage source which can exchange reactive power between the power system and the converter.

According to (5.17) to (5.19) the steady state performances are calculated with parameters in Table 1.8. The active current I_{fd}, reactive current I_{fq}, and DC voltage V_{dc} as a function of the AC voltage command on *q*-axis u_q for different values of the AC voltage command on *d*-axis u_d are plotted as shown in Figure 5.3. The AC voltage command on *q*-axis u_q is varied from -0.1×10^{-3} to $+0.1\times10^{-3}$ while the AC voltage commands on *d*-axis u_d are three steps as 0.4, 0.6 and 0.8.

Table 5.5 D-STATCOM parameters

The D-STATCOM parameters	
Interfacing resistance and inductance (R_f and L_f)	0.01 Ω and 5.07 *mH*
Constant value of converter (k_p)	$\frac{1}{2U_t} \approx 0.5$
DC link capacitance (C_{dc})	150 μF
Capacitor leakage resistance (R_{dc})	61.273 $k\Omega$
Switching frequency (f_{sw})	5 *kHz*

At steady state, the reactive current (I_{fq}) is a linear function of the AC voltage command on *q*-axis (u_q) within this operating range of -1×10^{-3} to $+1\times10^{-3}$. The reactive current (I_{fq}) flows into the converter when the AC voltage command on *q*-

axis (u_q) is negative and flows out to the AC system when the AC voltage command on q-axis (u_q) is positive.

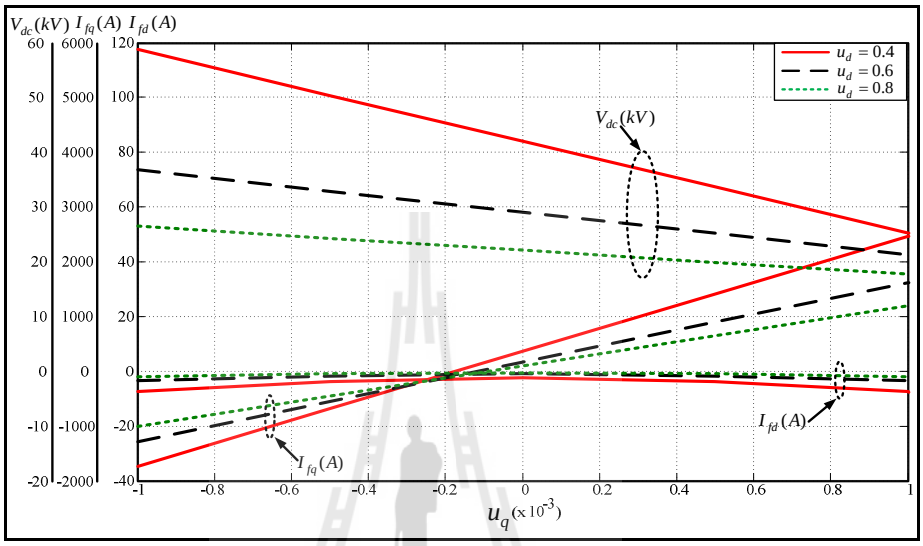

Figure 5.3 Steady state performance of the D-STATCOM connected to the distribution system

The DC voltage (V_{dc}) decreases linearly with the AC voltage command on q-axis (u_q) when the AC voltage command on q-axis varies from negative to positive. The active current (I_{fd}) is very small and is a quadratic function of the AC voltage command on q-axis (u_q). This is because it only furnishes the power losses in the converter.

It can be seen from Figure 5.3 that increasing of the AC voltage command on d-axis u_d results in decreasing of the active current (I_{fd}) and increasing of the slop of reactive current (I_{fq}). The AC voltage command on d-axis u_d has significantly

changed with the of DC voltage. The DC voltage decreases when the AC voltage commands on *d*-axis u_d increase and vise versa.

Trends of the active current (I_{fd}), reactive current (I_{fq}) and DC voltage (V_{dc}) as a function of the AC voltage command on *dq*-axis (u_d and u_q) are shown in Figure 5.4 to 5.6, respectively. At high AC voltage commands on *d*-axis u_d, the active current (I_{fd}), reactive current (I_{fq}) and DC voltage (V_{dc}) surfaces are very small changed while very high changed at low AC voltage commands on *d*-axis u_d, with respect to the AC voltage command on *q*-axis u_q varies from negative to positive.

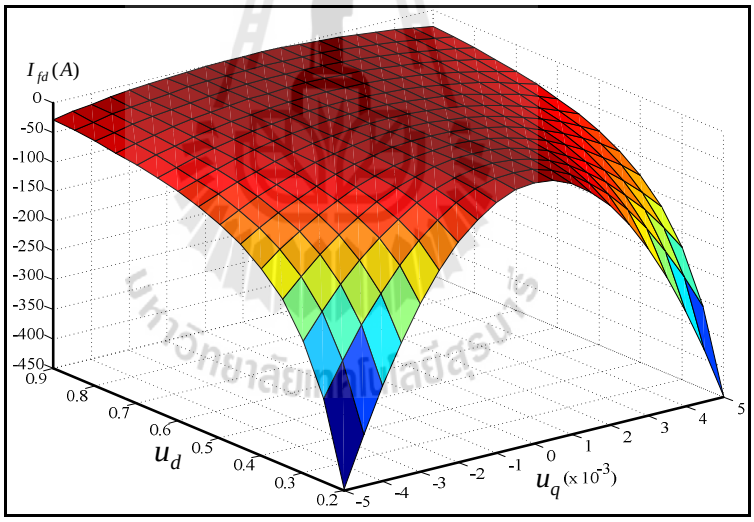

Figure 5.4 Effect of u_d and u_q on the active current (I_{fd})

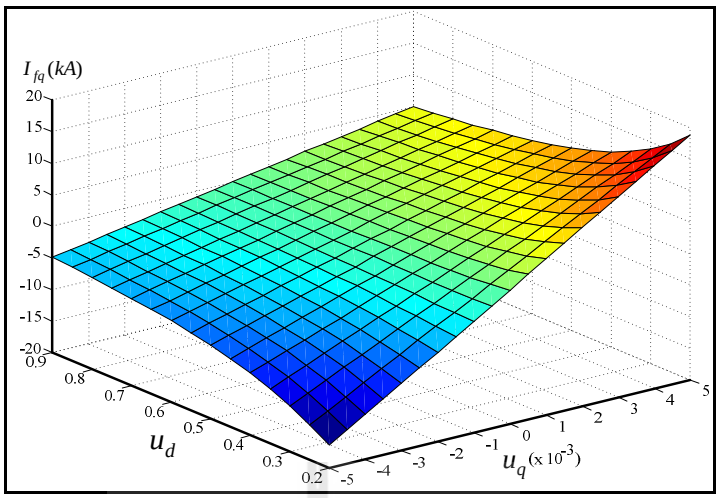

Figure 5.5 Effect of u_d and u_q on the Reactive Current (I_{fq})

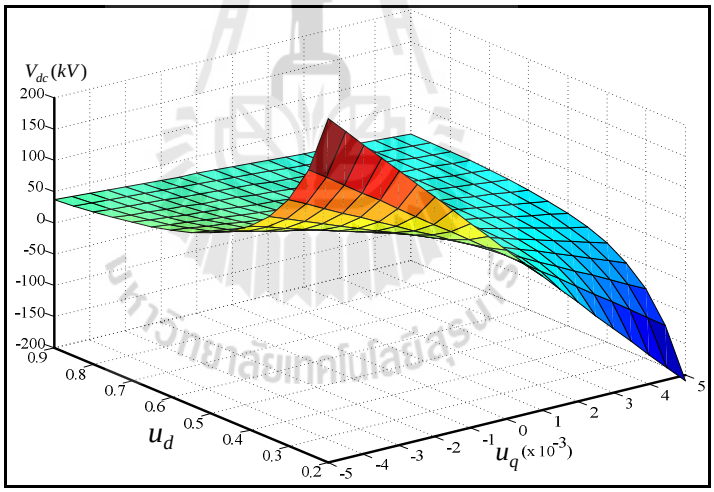

Figure 5.6 Effect of u_d and u_q on the DC voltage (V_{dc})

The effect of the inductance L_f on the active current (I_{fd}), reactive current (I_{fq}) and DC voltage (V_{dc}) are shown in Figure 5.7 to 5.9. In this case, the inductance L_f is varied from 1 to 15mH. The time constant T_f and the AC voltage commands on

d-axis u_d are kept constant as 15.93 and 0.6, respectively. As can be observed from Figure 5.7 and Figure 5.8, the active current (I_{fd}) and reactive current (I_{fq}) are very small changed at high inductance L_f while very high changed when the inductance L_f is lower, with respect to the AC voltage command on *q*-axis u_q varies from negative to positive. However, the DC voltage (V_{dc}) is changed very closely for each inductance L_f as shown in Figure 5.9.

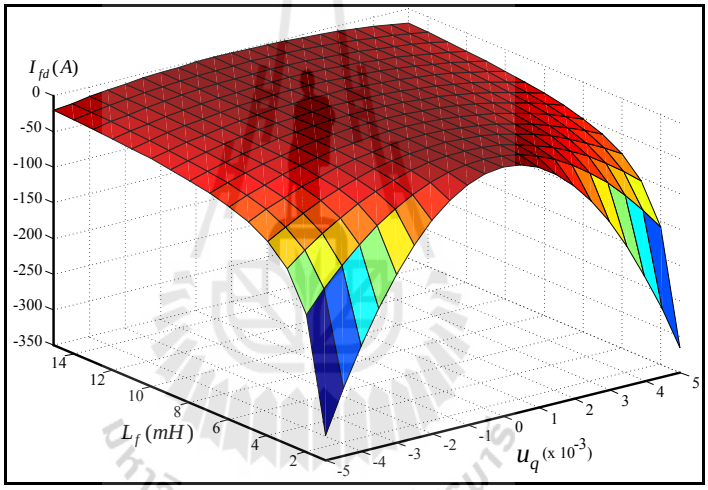

Figure 5.7 Effect of the inductance L_f on the active current (I_{fd})

The effect of time constant T_f on the active current (I_{fd}), reactive current (I_{fq}) and DC voltage (V_{dc}) are shown in Figure 5.10 to Figure 5.12. The inductance L_f is kept constant at $5.07mH$ while the time constant T_f is varied from 15.71 to 314.16 with 15.71 step increment in this case. It can be observed from these figures that the active current (I_{fd}), reactive current (I_{fq}) and DC voltage (V_{dc}) are very

small changed at low time constant T_f while they are highly changed when the time constant T_f is higher, with respect to the AC voltage command on q-axis u_q varies from negative to positive.

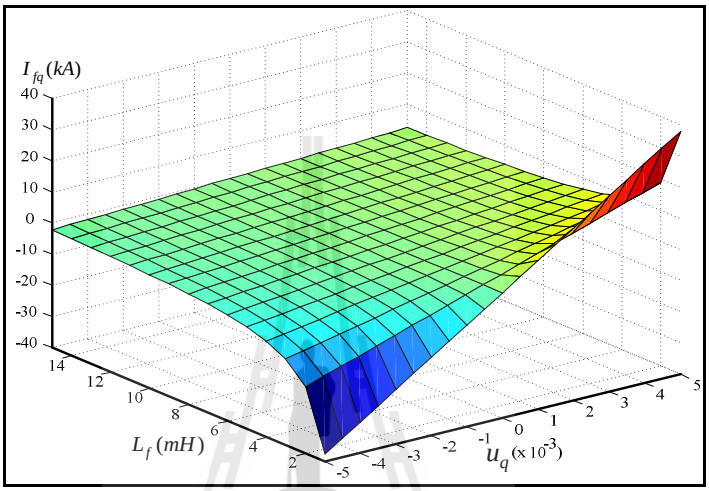

Figure 5.8 Effect of the inductance L_f on the reactive current (I_{fq})

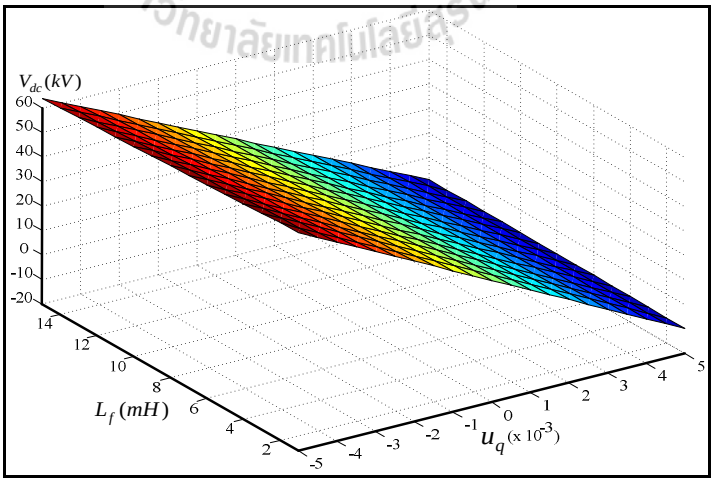

Figure 5.9 Effect of the inductance L_f on the DC voltage (V_{dc})

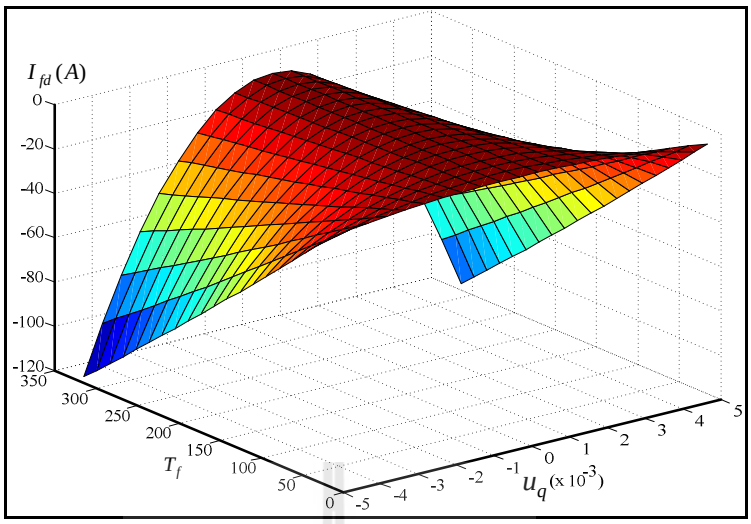

Figure 5.10 Effect of the time constant T_f on the active current (I_{fd})

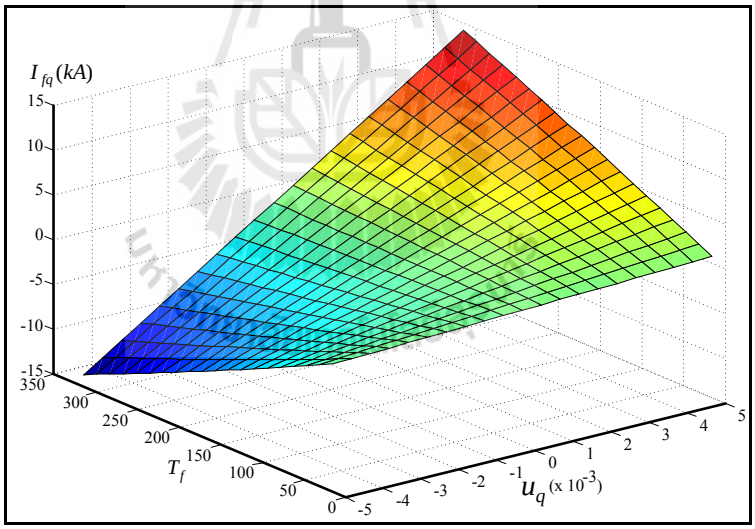

Figure 5.11 Effect of the time constant T_f on the reactive current (I_{fq})

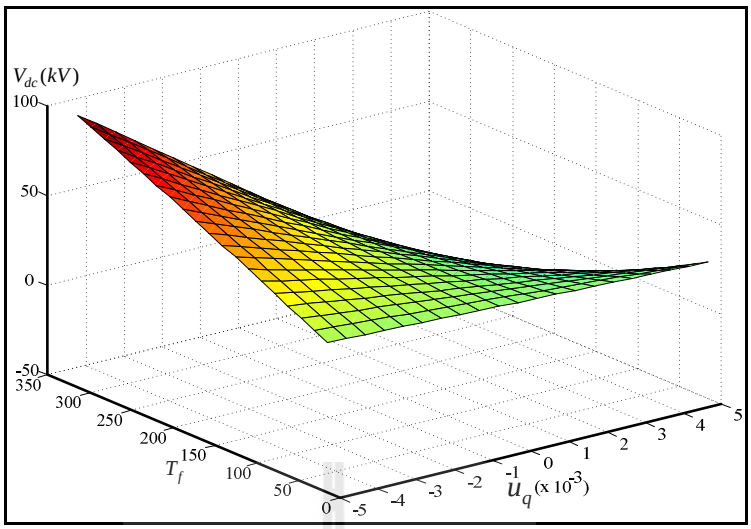

Figure 5.12 Effect of the time constant T_f on the DC voltage (V_{dc})

5.4 Dynamic Analysis of the D-STATCOM

The state equations in (5.15) are a set of nonlinear differential equations. To investigate the dynamic performance of this system, linear approximation is applied. Linearization of these systems around the operating point, i.e. the AC voltage command on *dq*-axis (u_{d0} and u_{q0}) and terminal voltage (v_{td0}), gives a set of linear equations as shown in (5.20).

$$\frac{d}{dt}\begin{bmatrix}\Delta i_{fd}\\ \Delta i_{fq}\\ \Delta v_{dc}\end{bmatrix}=\begin{bmatrix}-\frac{1}{T_f} & \left(\omega_0+\frac{k_{ifq}}{C_f}\right) & \frac{1}{L_f}k_p u_{d0}\\ -\omega_0 & -\left(\frac{1}{T_f}+\frac{k_{ifd}}{C_f}\right) & \frac{1}{L_f}k_p u_{q0}\\ -\frac{3}{2}\frac{1}{C_{dc}}k_p u_{d0} & -\frac{3}{2}\frac{1}{C_{dc}}k_p u_{q0} & -\frac{1}{T_{dc}}\end{bmatrix}\begin{bmatrix}\Delta i_{fd}\\ \Delta i_{fq}\\ \Delta v_{dc}\end{bmatrix}$$
$$+\begin{bmatrix}-\left(\omega_0 k_{ifq}+\frac{1}{L_f}\right) & \frac{1}{L_f}k_p v_{dc0} & 0\\ \omega_0 k_{ifd} & 0 & \frac{1}{L_f}k_p v_{dc0}\\ 0 & -\frac{3}{2C_{dc}}k_p i_{fd0} & -\frac{3}{2C_{dc}}k_p i_{fq0}\end{bmatrix}\begin{bmatrix}\Delta v_{td}\\ \Delta u_d\\ \Delta u_q\end{bmatrix} \tag{5.20}$$

The characteristic equation of the D-STATCOM described by (5.20) is

$$s^3+\left(\frac{2}{T_f}+\frac{1}{T_{dc}}+\frac{k_{ifd}}{C_f}\right)s^2+\left[\frac{1}{T_f^2}+\frac{2}{T_f T_{dc}}+K\left(u_{d0}^2+u_{q0}^2\right)+\omega_0^2+\frac{k_{ifd}}{C_f}\left(\frac{1}{T_f}+\frac{1}{T_{dc}}\right)+\frac{k_{ifq}}{C_f}\omega_0\right]s+$$
$$\left[\frac{1}{T_f^2 T_{dc}}+\frac{K}{T_f}\left(u_{d0}^2+u_{q0}^2\right)+\frac{\omega_0^2}{T_{dc}}+K.u_{d0}^2\frac{k_{ifd}}{C_f}+K.u_{d0}u_{q0}\frac{k_{ifq}}{C_f}+\frac{k_{ifd}}{C_f}\frac{1}{T_f T_{dc}}+\frac{k_{ifq}}{C_f}\frac{\omega_0}{T_{dc}}\right] \tag{5.21}$$

where $K=\frac{3}{2}\frac{k_p^2}{L_f C_{dc}}$

$$k_{ifq}=\frac{i_{fq0}}{v_{td0}}$$

$$k_{ifd}=\frac{i_{fd0}}{v_{td0}}$$

$$\omega_0 = \frac{-i_{lq0} + i_{sq0} + i_{fq0}}{C_f v_{td0}}$$

However, the ω in (5.15) is a function of the load reactive current (i_{lq}), source reactive current (i_{sq}), D-STATCOM reactive current (i_{fq}) and the terminal voltage (v_{td}) as described by (3.16) in the Chapter 3. The varying of D-STATCOM's reactive current (i_{fq}) causes the load reactive current (i_{lq}), source reactive current (i_{sq}) and the terminal voltage (v_{td}) in the distribution system vary. These result in the variation of ω which will be constant in steady state at ω_s. If it is assumed that the ω in (5.15) is ω_s, the linearization of the systems around the operating point gives a set of linear equations as shown in (5.22) and then the characteristic equation of the D-STATCOM can be rewritten as (5.23).

$$\frac{d}{dt}\begin{bmatrix}\Delta i_{fd}\\ \Delta i_{fq}\\ \Delta v_{dc}\end{bmatrix} = \begin{bmatrix} -\frac{1}{T_f} & \omega_s & \frac{1}{L_f}k_p u_{d0} \\ -\omega_s & -\frac{1}{T_f} & \frac{1}{L_f}k_p u_{q0} \\ -\frac{3}{2}\frac{1}{C_{dc}}k_p u_{d0} & -\frac{3}{2}\frac{1}{C_{dc}}k_p u_{q0} & -\frac{1}{T_{dc}} \end{bmatrix}\begin{bmatrix}\Delta i_{fd}\\ \Delta i_{fq}\\ \Delta v_{dc}\end{bmatrix} + \begin{bmatrix} -\frac{1}{L_f} & \frac{1}{L_f}k_p v_{dc0} & 0 \\ 0 & 0 & \frac{1}{L_f}k_p v_{dc0} \\ 0 & -\frac{3}{2C_{dc}}k_p i_{fd0} & -\frac{3}{2C_{dc}}k_p i_{fq0} \end{bmatrix}\begin{bmatrix}\Delta v_{td}\\ \Delta u_d\\ \Delta u_q\end{bmatrix} \tag{5.22}$$

$$s^3 + \left(\frac{2}{T_f} + \frac{1}{T_{dc}}\right)s^2 + \left[\frac{1}{T_f^2} + \frac{2}{T_f T_{dc}} + K\left(u_{d0}^2 + u_{q0}^2\right) + \omega_s^2\right]s + \left[\frac{1}{T_f^2 T_{dc}} + \frac{K}{T_f}\left(u_{d0}^2 + u_{q0}^2\right) + \frac{\omega_s^2}{T_{dc}}\right] \tag{5.23}$$

As can be seen in (5.23), the characteristic is a function of the AC voltage command on *dq*-axis (u_{d0} and u_{q0}). The stability of D-STATCOM can be tested by Routh-Hurwitz criterion. By assigning *p*, *q* and *r* to represent the coefficients of s^2, s^1 and s^0, respectively, the (5.23) become $s^3 + ps^2 + qs + r = 0$, and the Routh's array is

$$\begin{array}{c|cc} s^3 & 1 & q \\ s^2 & p & r \\ s^1 & q - \dfrac{r}{p} & 0 \\ s^0 & r & 0 \end{array}$$

Substitute *p*, *q* and *r* to determine the element in the s^1 row

$$q - \frac{r}{p} = \frac{4}{T_f} + \frac{2}{T_{dc}} + \frac{2T_{dc}}{T_f^2} + K\left(u_d^2 + u_q^2\right)T_{dc} + K\left(u_d^2 + u_q^2\right)T_f + 2\omega_s^2 T_{dc} \geq 0$$

Examination of all elements in the first column of Routh's array reveals that all elements are positive, and the D-STATCOM in this case is a stable system. Therefore, the values of resistors (R_f), inductors (L_f) and capacitors (C_{dc}) have no effect on stability. To investigate the effect of D-STATCOM parameters on dynamic behavior, the parameters of the D-STATCOM as shown in Table 5.5 with $u_d = 0.6$ and $u_q = 0.0$ are used. The D-STATCOM parameters in Table 5.5 with $u_d = 0.6$ and $u_q = 0.0$ produce three characteristic roots comprising of real root and a pair of complex conjugate roots, which are -1.31 and $-1.37 \pm j525.56$.

The Root Loci diagram in Figure 5.13 presents the effect of inductance L_f on the transient performance. In this case, the inductance L_f is varied from 20% to 200%

of the value in Table 5.5 with 10% steps while the ratio of inductance over the resistance T_f is kept constant. In this figure, it is seen that the increasing inductance causes the complex roots to move away from the imaginary axis with reducing imaginary values. Meanwhile, the single real root moves towards the origin when the inductance increases.

Figure 5.14 shows the effect of inductance over resistance T_f on the transient performance. In this case, the inductance L_f is kept constant while the time constant T_f is varied from 20% to 200% with 10% steps increment. As can be seen in this figure, the complex roots move towards the imaginary axis which constant imaginary values when the time constant T_f increases. While the real root moves towards the origin when the time constant T_f increases.

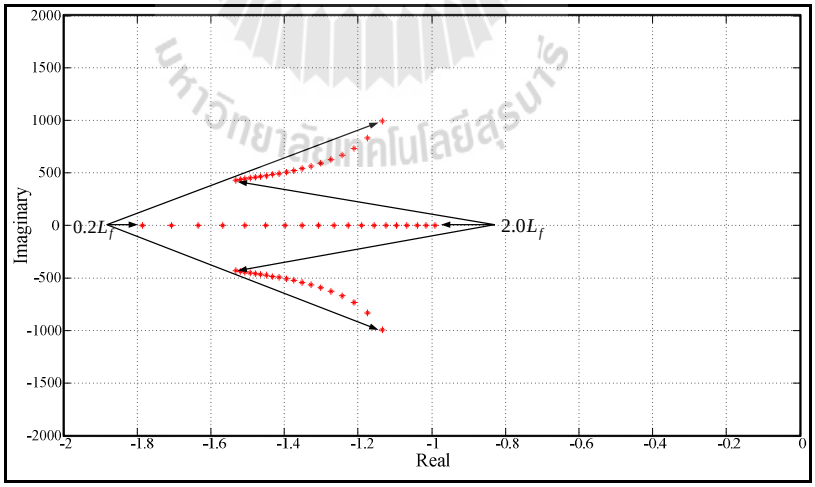

Figure 5.13 Effect of the inductance L_f

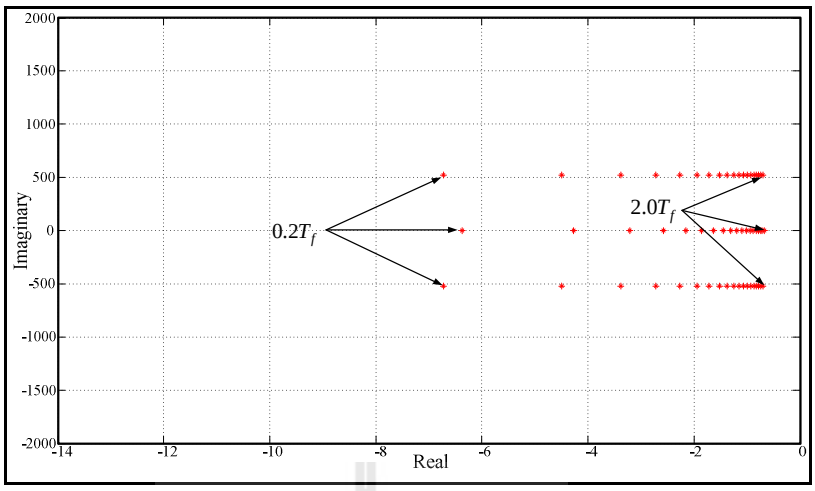

Figure 5.14 Effect of the time constant T_f

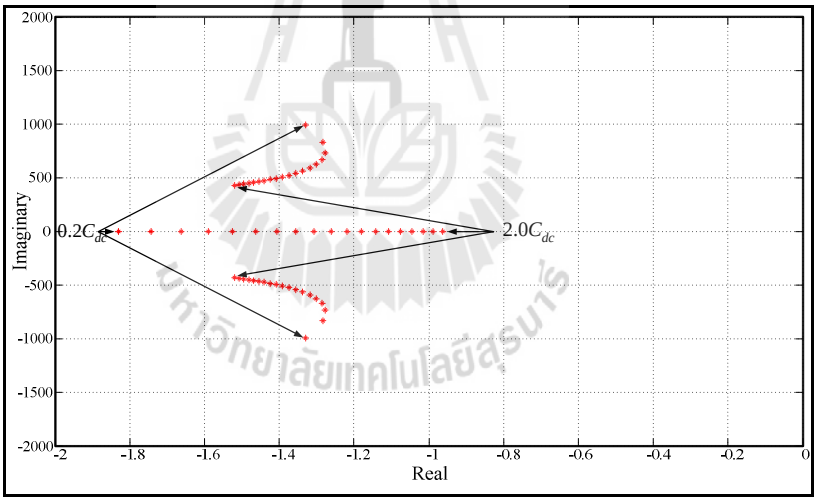

Figure 5.15 Effect of the DC capacitance C_{dc}

When the inductance L_f and time constant T_f are fixed, the DC capacitance C_{dc} is varied from 20% to 200% with 10% steps. The root locus is shown in Figure 5.15. It is seen that all roots move towards the imaginary axis when the DC

capacitance C_{dc} increases from 20% to 40%. However, when the DC capacitance C_{dc} further increases, the complex roots move away from the imaginary axis with reducing imaginary values while the real root moves towards the origin.

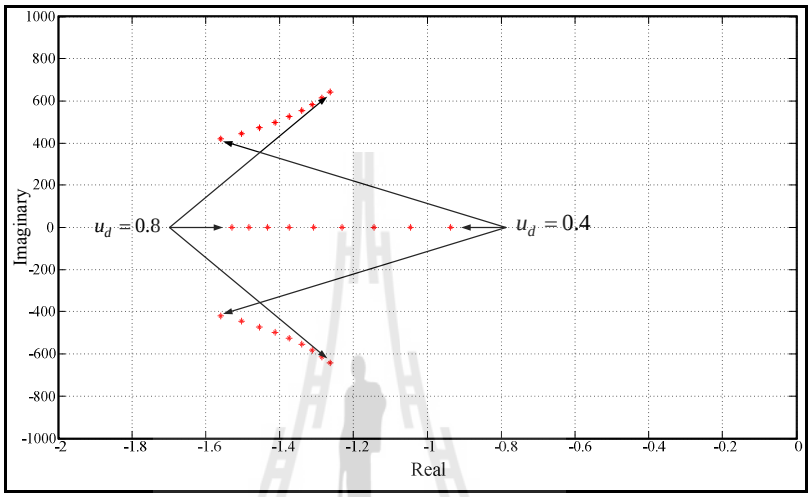

Figure 5.16 Effect of the AC voltage command on the *d*-axis u_d

The effect of the AC voltage command on *d*-axis u_d on characteristic roots is shown in Figure 5.16. The AC voltage command on *d*-axis u_d is varied from 0.4 to 0.8 with 0.05 increments. The complex roots move towards the imaginary axis and imaginary values increase while the real root moves away from the origin when AC voltage command on *d*-axis u_d increases.

As described in above, small change of the AC voltage command on *q*-axis u_q causes high change of the active current (I_{fd}), reactive current (I_{fq}) and DC voltage (V_{dc}) in steady state as can be seen in Figure 5.3. However, small changes of the AC

voltage command on *q*-axis u_q does not affect characteristic roots. Although, the small change of the AC voltage command on *q*-axis u_q does not affect characteristic roots, it affects the Zeros of the system. The effect of the AC voltage command on *q*-axis u_q is represented by bode diagram. The bode plot in Figure 5.17 to Figure 5.19 present frequency responses of the AC voltage command on *dq*-axis (u_d and u_q) on the magnitude and phase of active current (i_{fd}), reactive current (i_{fq}) and DC voltage (v_{dc}), respectively. In this case, the AC voltage command on *q*-axis u_q is varied from -0.002 to +0.002 with 0.001 per step. The Zeros in each step are calculated and shown in Table 5.6 to Table 5.8.

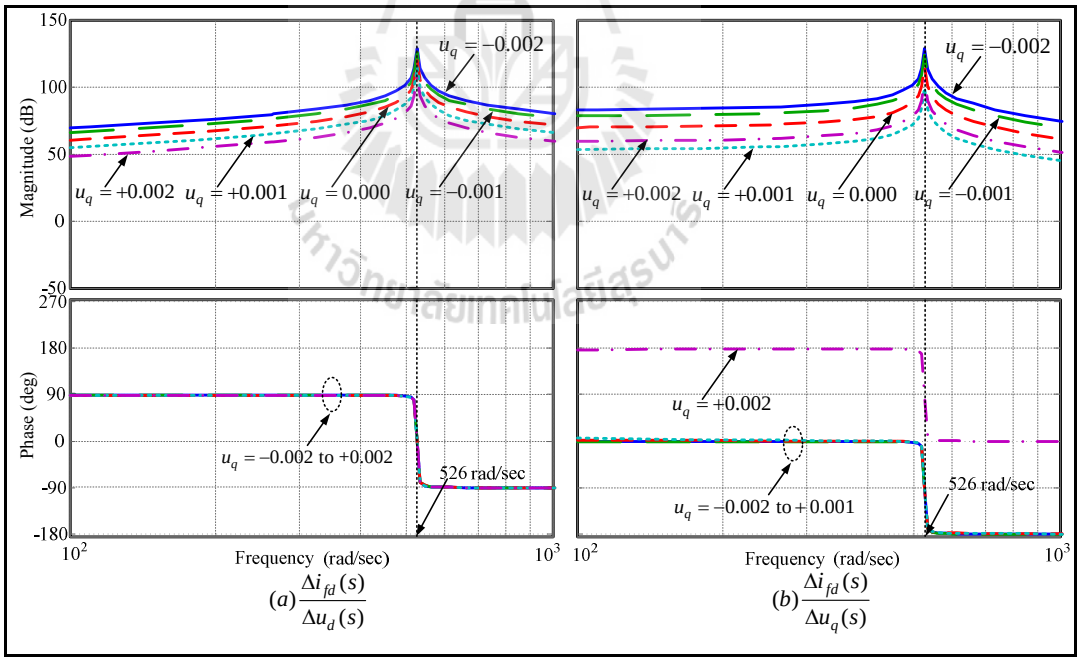

Figure 5.17 Bode plots of transfer function of the active current with respect to the AC voltage command on the *d* and *q*-axis

Table 5.6 Zeros of transfer functions of the active current with respect to the AC voltage command on the *d* and *q*-axis

u_q	**Zeros of** $\frac{\Delta i_{fd}(s)}{\Delta u_d(s)}$	**Zeros of** $\frac{\Delta i_{fd}(s)}{\Delta u_q(s)}$
- 0.002	$-1.40 \pm j0.94$	–1.60
- 0.001	–1.71, –0.65	–1.15
0.000	–1.97, –0.22	0.00
+0.001	$-1.28 \pm j0.53$	+9.62
+0.002	$-2.22 \pm j2.09$	+7.18

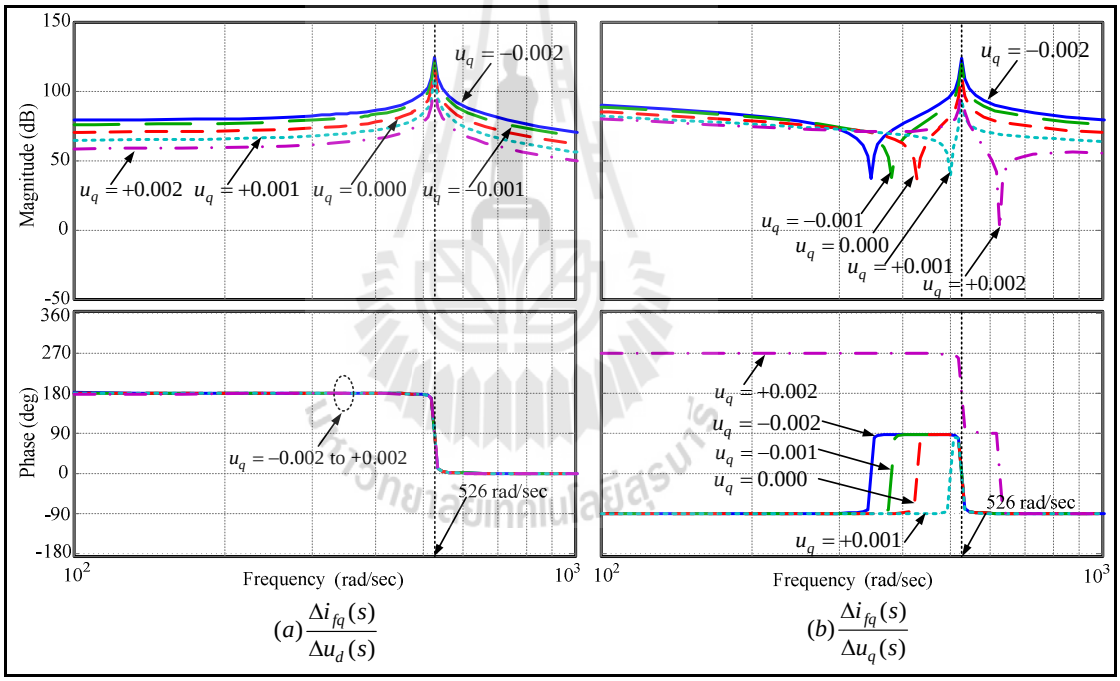

Figure 5.18 Bode plots of transfer function of the reactive current with respect to the AC voltage command on the *d* and *q*-axis

Table 5.7 Zeros of transfer functions of the reactive current with respect to the AC voltage command on the *d* and *q*-axis

u_q	**Zero of** $\frac{\Delta i_{fq}(s)}{\Delta u_d(s)}$	**Zero of** $\frac{\Delta i_{fq}(s)}{\Delta u_q(s)}$
- 0.002	+1.05	$-0.73 \pm j345.70$
- 0.001	+0.55	$-0.95 \pm j380.23$
0.000	–0.22	$-1.04 \pm j427.74$
+0.001	–1.54	$-0.85 \pm j499.08$
+0.002	–4.36	$-0.09 \pm j624.54$

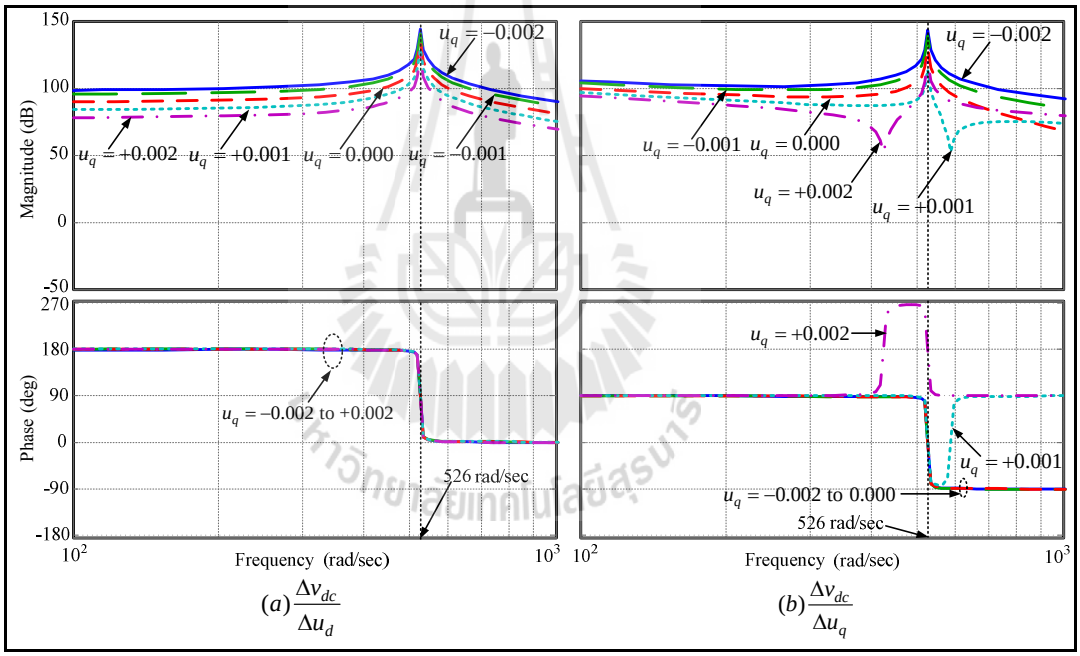

Figure 5.19 Bode plots of transfer function of the DC voltage with respect to the AC voltage command on the *d* and *q*-axis

Table 5.8 Zeros of transfer functions of the DC voltage with respect to the AC voltage command on the *d* and *q*-axis

u_q	**Zeros of** $\frac{\Delta v_{dc}(s)}{\Delta u_d(s)}$	**Zeros of** $\frac{\Delta v_{dc}(s)}{\Delta u_q(s)}$
- 0.002	–2.62, +245080.15	–454.52, +447.37
- 0.001	–2.33, +625966.17	–661.63, +654.86
0.000	–1.91, +1630575.46	$-1.97 \pm j1820.67$
+0.001	–1.18, +363338.50	$-2.62 \pm j586.08$
+0.002	+0.39, +75087.69	$-2.41 \pm j425.59$

It is seen from the bode plots in Figure 5.17 to Figure 5.19 that the resonant frequency in all figures occurs at 526 rad/sec. The resonant frequency is constant because the AC voltage command on *q*-axis u_q plays no role on the characteristic roots of the system. The transfer function of the active current (i_{fd}) with respect to the AC voltage command on *d*-axis u_d is shown in Figure 5.17(a). This transfer function consists of two zeros and locates on the Left Half Plane (LHP). They are complex conjugate zeros when u_q are -0.002, +0.001 and +0.002 whereas they are two real zeros when u_q are -0.001 and 0.000.

The transfer function of the active current (i_{fd}) with respect to the AC voltage command on *q*-axis u_q is shown in Figure 5.17(b). This transfer function has one real zero which locates on the Left Half Plane (LHP) when u_q are -0.002 and -0.001 while locates on the Right Half Plane (RHP) when u_q are +0.002 and +0.001. In addition, this transfer function has one zero that locates at the origin when the u_q is 0.000.

The transfer function of the reactive current i_{fq} with respect to the AC voltage command on *d*-axis u_d to is shown in Figure 5.18(a). This transfer function has one

real zero located on the Right Half Plane (RHP) and moves to the origin when u_q is in range of -0.002 to -0.001. However, the zero locates on the Right Half Plane (RHP) and moves away from the origin when u_q is varied from 0.000 to +0.002. Meanwhile, zeros of the transfer function of the reactive current i_{fq} with respect to the AC voltage command on *q*-axis u_q is a pair of complex conjugate zeros located on the LHP. Imaginary parts of the zeros increase when u_q varies from -0.002 to +0.002 while real part moves farther away from the origin when the u_q varies from -0.002 to 0.000 and it turn back to the origin when the u_q vary from +0.001 to +0.002. The bode plot of this transfer function is shown in Figure 5.18(b).

The bode plots of the transfer function of the DC voltage (v_{dc}) with respect to the AC voltage command on *d*-axis u_d and the AC voltage command on *q*-axis u_q are shown in Figure 5.19(a) and 5.19(b), respectively. The transfer function of the DC voltage (v_{dc}) with respect to the AC voltage command on *d*-axis u_d consists of two real zeros which one of those locates far from the origin on the Right Half Plane (RHP). The other zero locates on the Left Half Plane (LHP) and moves forward to the origin when u_q varies from -0.002 and +0.001. However, this zero locates on the Right Half Plane (RHP) when u_q is +0.002. It is seen that this transfer function is always a non-minimum phase system. Meanwhile, the zeros of the transfer function of the DC voltage (v_{dc}) with respect to the AC voltage command on *q*-axis u_q are two real zeros which one of those locates on the Right Half Plane (RHP) whereas the other zero locates on the Left Half Plane (LHP) when u_q varies from -0.002 and -0.001.

When the u_q varies from 0.000 to +0.002, the zeros of this transfer function are complex conjugates located on the Left Half Plane (LHP). The imaginary parts of the zeros decrease when the u_q increases from 0.000 to +0.002 while real part move away from the origin when the u_q increases from 0.000 to +0.002. It can also be seen that this transfer function is non-minimum phase system when the u_q is in the range of -0.002 to -0.001.

5.5 Summary

This chapter proposes the design of component rating and the D-STATCOM parameters for the load voltage regulation. In addition, the dynamic equations of D-STATCOM based on synchronously rotating reference frame are presented. And the steady state characteristic of the D-STATCOM is derived. To analyze the steady state performance, the effect of the control signal (u_d , u_q) and parameters of the AC inductor (L_f , R_f) on the active current, reactive current and DC voltage of the D-STATCOM are investigated. To investigate the dynamic performance of the D-STATCOM, linear approximation is applied.

For the steady state performance, the result shows that the DC capacitor dose not have any relation with the active and reactive current of the D-STATCOM. The reactive current (I_{fq}) is a linear function of the AC voltage command on *q*-axis (u_q). The DC voltage (V_{dc}) decreases linearly with the AC voltage command on *q*-axis (u_q) when the AC voltage command on *q*-axis varies from negative to positive. The active current (I_{fd}) is very small and is a quadratic function of the AC voltage

command on *q*-axis (u_q). This is because it only furnishes the power losses in the converter. Meanwhile, the increasing of the AC voltage command on *d*-axis u_d results in decreasing of the active current (I_{fd}) and increasing of the slop of reactive current (I_{fq}). The AC voltage command on *d*-axis u_d has significantly changed with the of DC voltage. The DC voltage decreases when the AC voltage commands on *d*-axis u_d increase and vise versa.

In addition, the active current (I_{fd}) and reactive current (I_{fq}) are very small changed at high inductance (L_f) while very high changed when the inductance (L_f) is lower, with respect to the AC voltage command on *q*-axis u_q varies from negative to positive. However, the DC voltage (V_{dc}) is changed very closely for each inductance (L_f). Meanwhile, the active current (I_{fd}), reactive current (I_{fq}) and DC voltage (V_{dc}) are very small changed at low time constant (T_f) while they are highly changed when the time constant (T_f) is higher, with respect to the AC voltage command on *q*-axis (u_q) varies from negative to positive.

For the dynamic performance, the result shows the values of resistors (R_f), inductors (L_f) and capacitors (C_{dc}) have no effect on stability. Although, the small change of the AC voltage command on *q*-axis (u_q) causes high change of the active current (I_{fd}), reactive current (I_{fq}) and DC voltage (V_{dc}) in steady state, it does not affect characteristic roots. However, the small change of the AC voltage command on *q*-axis (u_q) affects the Zeros of the system.

CHAPTER VI

DESIGN OF D-STATCOM CURRENT AND DC VOLTAGE CONTROL

The control system is the heart of state-of-the-art D-STATCOM controller for dynamic control of reactive power in the electrical system. Based on the operational requirements, type of applications, system configuration and its parameters, essential control parameters are controlled to obtain the desired performance. In this thesis, the control system for the D-STATCOM operated with PWM mode employs control of phase angle, α, and modulation index, *m*, (that correspond to control of the AC voltage command on *dq*-axis ,u_q and u_q) to change the converter AC voltages keeping V_{dc} constant. For voltage regulation, two control loop circuits namely inner current control loop and external / outer voltage control loop are employed in the D-STATCOM power circuit. The current control loops (reactive and active current controls) produce the desired magnitude and phase angle difference of the converter voltage relative to the system voltage and in turn, generates the gating pulses, whereas the voltage control loops (AC and DC voltage control) generate the reference reactive and active currents for the current controllers of the inner control loops. This control philosophy is implemented with proportional integral and derivative control (PID control) algorithm or with a combination of proportional (P), integral (I) and derivative (D) control algorithm in the *dq* synchronous rotating frame.

This chapter presents the current and DC voltage control design of the D-STATCOM. The decoupling current control based on the *dq* reference frame is presented. Although, the DC voltage can be controlled by active current of the D-STATCOM, reactive current still affects the DC voltage. To eliminate this effect, the control strategy with the elimination effect of the reactive current is proposed. For obtaining the proportional and integral gains of the PI controllers, the symmetrical optimum and genetic algorithms are applied. The stability margins of these methods are obtained and discussed in detail. In addition, the performances of the DC voltage control based on symmetrical optimum and genetic algorithms are compared. Effectiveness of the controllers designed was verified through computer simulation performed by using SIMULINK/MATLAB.

6.1 Current Control Strategy

It is seen from the Section 5.2 in Chapter 5, the D-STATCOM dynamic equations are expressed in (5.12) to (5.14). The equations in (5.12) and (5.13) are used for designing the D-STATCOM current controller. These equations clearly show that the D-STATCOM output currents are induced by its output voltage modulation. However, the current control of the converter on the synchronously rotating reference frame (*dq*-axis) is a two-input two-output system with cross coupling between the active and reactive currents. To obtain a decouple control for the i_{fd} and i_{fq}, (5.12) and (5.13) can be modified as:

$$\frac{di_{fd}}{dt} = -\frac{i_{fd}}{T_f} + x_d \tag{6.1}$$

$$\frac{di_{fq}}{dt} = -\frac{i_{fq}}{T_f} + x_q \tag{6.2}$$

Where the cross coupling terms ωi_{fq} and ωi_{fd} are collected by the actions x_d and x_q, respectively.

$$x_d = \omega i_{fq} - \frac{1}{L_f} v_{td} + \frac{1}{L_f} k_p u_d v_{dc} \tag{6.3}$$

$$x_q = -\omega i_{fd} + \frac{1}{L_f} k_p u_q v_{dc} \tag{6.4}$$

Equation (6.1) shows that the active current is increasingly induced following the transient in x_d. This is also true for the reactive current in (6.2). Based on these principles, a proportional-integral-derivative controller (PID controller) is considered to adjust the control signal x_d and x_q. The PID controller is a generic control loop feedback controller widely used in industrial control systems. The PID controller calculates an error value as the difference between a measured process variable and a desired setpoint. The controller attempts to minimize the error by adjusting the process control inputs. The control signal is thus a sum of three terms: a proportional term (P) that is proportional to the error, an integral term (I) that is proportional to the integral of the error, and a derivative term (D) that is proportional to the derivative of the error. However, the D controller is the derivative action that causes high overshoots in the control signal. This may causes damage to electrical devices,

especially in high power system. Therefore, the PI controller are used to control the D-STATCOM currents in the present work. The control actions x_d and x_q can be expressed as:

$$x_d = K_{Pid}\left(\frac{1+sT_{Iid}}{sT_{Iid}}\right)\left(i_{fd}^{*} - i_{fd}\right) \tag{6.5}$$

$$x_q = K_{Piq}\left(\frac{1+sT_{Iiq}}{sT_{Iiq}}\right)\left(i_{fq}^{*} - i_{fq}\right) \tag{6.6}$$

Once the control actions x_d and x_q are determined by (6.5) and (6.6), the D-STATCOM output voltage commands u_d^{*} and u_q^{*} in (6.3) and (6.4) can be rearranged as:

$$u_d^{*} = \frac{-\omega L_f i_{fq} + v_{td} + L_f x_d}{k_p v_{dc}} = \frac{v_{st,d}^{*}}{k_p v_{dc}} \tag{6.7}$$

$$u_q^{*} = \frac{\omega L_f i_{fd} + L_f x_q}{k_p v_{dc}} = \frac{v_{st,q}^{*}}{k_p v_{dc}} \tag{6.8}$$

Here, $v_{st,d}^{*}$ and $v_{st,q}^{*}$ represent the D-STATCOM output AC voltage on *d*-axis and *q*-axis , respectively. The current control structure for the D-STATCOM and the D-STATCOM output current are detailed in Figure 6.1. Since the D-STATCOM control is based on the VSC scheme, the D-STATCOM output voltage commands can be adjusted by using (6.7) and (6.8). In addition, the D-STATCOM output AC voltage

v_{st} is generated by the VSC with pulse width modulation (PWM) and the u_d^* and u_q^* are the inputs. The VSC with PWM can be modeled as $\frac{k_p v_{dc}}{sT_d + 1}$, where T_d represents a dead time.

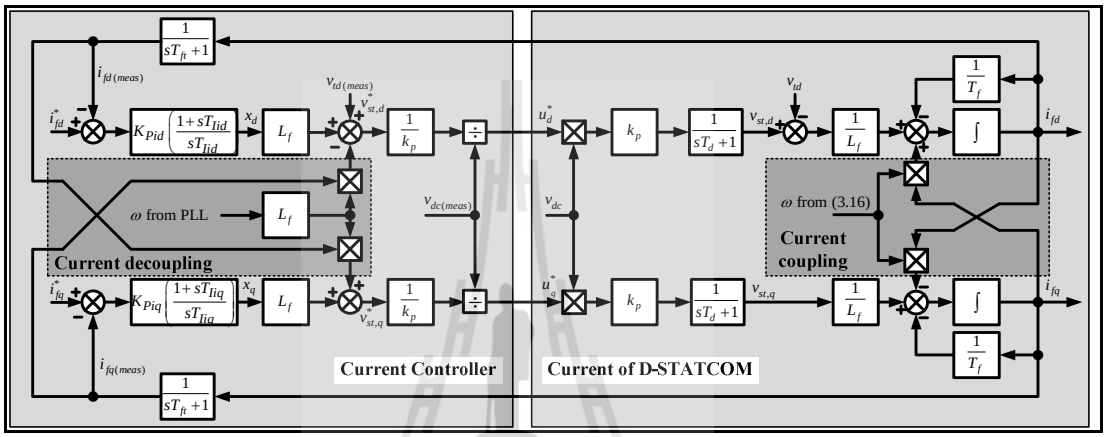

Figure 6.1 Control structure for the D-STATCOM and the D-STATCOM output current

As can be seen from Figure 6.1, the D-STATCOM currents with considering the dead time, T_d, can be written as

$$\frac{di_{fd}}{dt} = -\frac{1}{T_f} i_{fd} + \omega i_{fq} - \frac{1}{L_f} v_{td} + \frac{1}{L_f} v_{std} \tag{6.9}$$

$$\frac{di_{fq}}{dt} = -\frac{1}{T_f} i_{fq} - \omega i_{fd} + \frac{1}{L_f} v_{stq} \tag{6.10}$$

$$\frac{dv_{std}}{dt} = -\frac{1}{T_d} v_{std} + \frac{1}{T_d} k_p v_{dc} u_d \tag{6.11}$$

$$\frac{dv_{stq}}{dt} = -\frac{1}{T_d} v_{stq} + \frac{1}{T_d} k_p v_{dc} u_q \tag{6.12}$$

Where u_d and u_q are the outputs of current control with decoupling that can be derived from the current controller as

$$u_d = \frac{1}{k_p v_{dc(meas)}} \left[vtd_{(meas)} - \omega_{PLL} L_f i_{fq(meas)} + x_d L_f \right] \tag{6.13}$$

$$u_q = \frac{1}{k_p v_{dc(meas)}} \left[+\omega_{PLL} L_f i_{fd(meas)} + x_q L_f \right] \tag{6.14}$$

When

$i_{fd(meas)}$ and $i_{fq(meas)}$ are the measured D-STATCOM currents

$v_{td(meas)}$ is the measured load voltage

$v_{dc(meas)}$ is the measured DC voltage

ω_{PLL} is the speed angular velocity from the PLL

All inputs of the decoupling current control (i.e. $i_{fd(meas)}$, $i_{fq(meas)}$, $v_{td(meas)}$, $v_{dc(meas)}$ and ω_{PLL}) can be measured at the point of common coupling (PCC). It is assumed that the inputs measure at behind filter. Thus, the inputs can be derived as follows

$$\frac{di_{fd(meas)}}{dt} = \frac{i_{fd}}{T_{fi}} - \frac{i_{fd(meas)}}{T_{fi}} \tag{6.15}$$

$$\frac{di_{fq(meas)}}{dt} = \frac{i_{fq}}{T_{fi}} - \frac{i_{fq(meas)}}{T_{fi}} \tag{6.16}$$

$$\frac{dv_{dc(meas)}}{dt} = \frac{v_{dc}}{T_{fdc}} - \frac{v_{dc(meas)}}{T_{fdc}} \tag{6.17}$$

$$\frac{dv_{td(meas)}}{dt} = \frac{v_{td}}{T_{fac}} - \frac{v_{td(meas)}}{T_{fac}} \tag{6.18}$$

Therefore, equation (6.9) to (6.18) form a state equation of the D-STATCOM currents with the decoupling current control as shown in (6.19)

$$\frac{d}{dt}\begin{bmatrix} \Delta i_{fd} \\ \Delta i_{fq} \\ \Delta v_{std} \\ \Delta v_{stq} \\ \Delta i_{fd(meas)} \\ \Delta i_{fq(meas)} \\ \Delta v_{dc(meas)} \\ \Delta v_{td(meas)} \end{bmatrix} = \begin{bmatrix} -\frac{1}{T_f} & \omega_s & \frac{1}{L_f} & 0 & 0 & 0 & 0 & 0 \\ -\omega_s & -\frac{1}{T_f} & 0 & \frac{1}{L_f} & 0 & 0 & 0 & 0 \\ 0 & 0 & -\frac{1}{T_d} & 0 & 0 & -\frac{v_{dc0}\omega_{PLL}L_f}{V_{dc0(meas)}T_d} & K_1 & \frac{v_{dc0}}{v_{dc0(meas)}T_d} \\ 0 & 0 & 0 & -\frac{1}{T_d} & \frac{v_{dc0}\omega_{PLL}L_f}{V_{dc0(meas)}T_d} & 0 & K_2 & 0 \\ \frac{1}{T_{fi}} & 0 & 0 & 0 & -\frac{1}{T_{fi}} & 0 & 0 & 0 \\ 0 & \frac{1}{T_{fi}} & 0 & 0 & 0 & -\frac{1}{T_{fi}} & 0 & 0 \\ 0 & 0 & -1 & 0 & 0 & 0 & -\frac{1}{T_{fdc}} & 0 \\ 0 & 0 & 0 & -1 & 0 & 0 & 0 & -\frac{1}{T_{fac}} \end{bmatrix} \begin{bmatrix} \Delta i_{fd} \\ \Delta i_{fq} \\ \Delta v_{std} \\ \Delta v_{stq} \\ \Delta i_{fd(meas)} \\ \Delta i_{fq(meas)} \\ \Delta v_{dc(meas)} \\ \Delta v_{td(meas)} \end{bmatrix}$$

$$+\begin{bmatrix} 0 & 0 & 0 & -\frac{1}{L_f} \\ 0 & 0 & 0 & 0 \\ \frac{v_{dc0}L_f}{V_{dc0(meas)}T_d} & 0 & K_3 & 0 \\ 0 & \frac{v_{dc0}L_f}{V_{dc0(meas)}T_d} & K_4 & 0 \\ 0 & 0 & 0 & 0 \\ 0 & 0 & 0 & 0 \\ 0 & 0 & \frac{1}{T_{fdc}} & 0 \\ 0 & 0 & 0 & \frac{1}{T_{fac}} \end{bmatrix} \begin{bmatrix} \Delta x_d \\ \Delta x_q \\ \Delta v_{dc} \\ \Delta v_{td} \end{bmatrix} \quad (6.19)$$

Where $K_1 = -\frac{v_{dc0}}{T_d v_{dc0(meas)}^2}\left(v_{td\,0(meas)} - \omega_{PLL}L_f i_{fq0(meas)} + x_{d0}L_f\right)$

$$K_2 = -\frac{v_{dc0}}{T_d v_{dc0(meas)}^2}\left(\omega_{PLL}L_f i_{fd\,0(meas)} + x_q L_f\right)$$

$$K_3 = \frac{1}{T_d v_{dc0(meas)}}\left(v_{td\,0(meas)} - \omega_{PLL}L_f i_{fq0(meas)} + x_d L_f\right)$$

$$K_3 = \frac{1}{T_d v_{dc0(meas)}}\left(\omega_{PLL}L_f i_{fd\,0(meas)} + x_q L_f\right)$$

Where T_{fi}, T_{fdc} and T_{fac} are filter time delay of the measured current, DC voltage and load voltage, respectively. To simplify the design, the effect of the filter

time delays can be replaced by an equivalent time delay of the feedback filter (T_{ft}). Consequently, the measured values i.e. $i_{fd(meas)}$, $i_{fq(meas)}$, $v_{td(meas)}$, $v_{dc(meas)}$ and ω_{PLL} can be replaced by i_{fd}, i_{fq}, v_{td}, v_{dc} and ω, respectively. Then it is assumed that the power converter dead time (T_d), the equivalent time delay of the feedback filter (T_{ft}), and the digital signal processing delay ($T_{\mu p}$) are combined as

$$T_e = T_d + T_{ft} + T_{\mu p} \tag{6.20}$$

However, with the switching frequency, f_{sw}, the statistical delay of the PWM converter is $\frac{0.5}{2f_{sw}}$, the feedback delay (average) is $\frac{0.5}{2f_{sw}}$ and the delay of the discrete-time signal processing is $\frac{1}{2f_{sw}}$. The sum of the small time constant, T_e, is in the range of $\frac{1.5}{2f_{sw}}$ to $\frac{1}{f_{sw}}$ (Mariancet al., 2002). Since the current control with decoupling is applied, the D-STATCOM currents with cross coupling between the active and reactive currents can be separately represented on *d*-axis and *q*-axis as

$$\frac{di_{fd}}{dt} = -\frac{1}{T_f} i_{fd} + x_d \tag{6.21}$$

$$\frac{di_{fq}}{dt} = -\frac{1}{T_f} i_{fq} + x_q \tag{6.22}$$

Therefore, the simplified open-loop transfer function of the current control with decoupling as shown in Figure 6.1 is given as

$$G_{iopen}(s) = \left(\frac{T_f}{sT_f + 1}\right)\left(\frac{1}{sT_e + 1}\right) \tag{6.23}$$

where T_e is the sum of the small time constant.

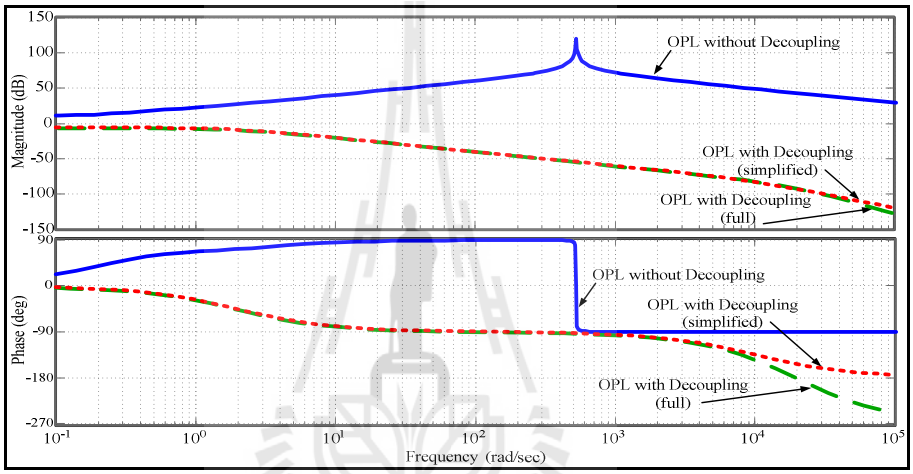

Figure 6.2 Bode plot of the open loop transfer function of the active current

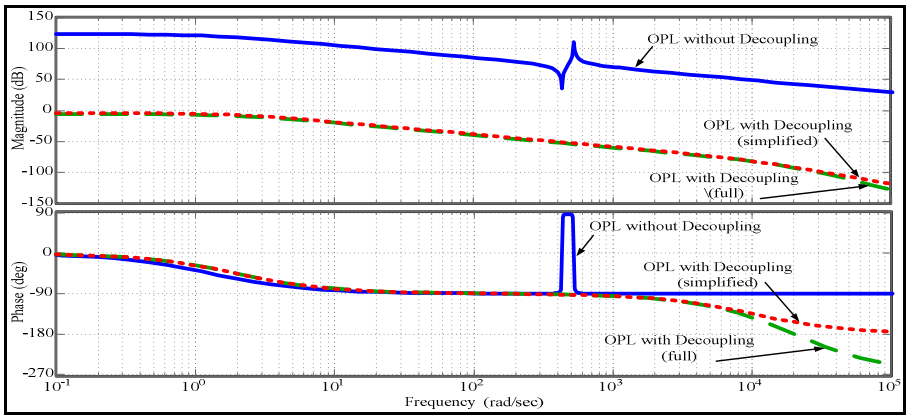

Figure 6.3 Bode plot of the open loop transfer function of the reactive current

Figure 6.2 and 6.3 show bode plots of an open loop transfer function (OPL) of active and reactive current, respectively. In these figures, the bode plots of the open loop transfer function with and without decoupling control are demonstrated. In addition, the bode plots of full and simplified open loop transfer functions are compared. The full open loop transfer function can be derived from (6.19) whereas the equivalent open loop transfer function is shown in (6.23). The D-STATCOM parameters as shown in Table 5.5 in Chapter 5 and $T_e = 0.0001$ are applied to these calculations bode plots. As can be seen in these figures, the bode plots of both full and simplified open loop transfer functions are very close to each other at lower frequency than 10^4 rad/sec. However, at higher frequency, the bode plots of those are apart.

6.2 PI Controller of the Current Control Based on Symmetrical Optimum Method

The PI controllers' parameters depend on the parameters of the open loop transfer function (i.e., natural frequency (ω_0), damping coefficient (ζ), and pole value (p)). In general, ω_0 and ζ characterize the desired system behavior and they are arbitrarily constant, while the location of poles can be chosen. The specific pole locations can be imposed by using supplementary conditions. The conditions for choosing the pole locations refer to the symmetrical optimum method (SO), which simplifies the expressions of the PI parameters. The goal of this scheme is to find the pole locations of the closed-loop transfer function, which satisfy the assumptions given by the SO design around ω_0, for the transfer function of the open - loop system.

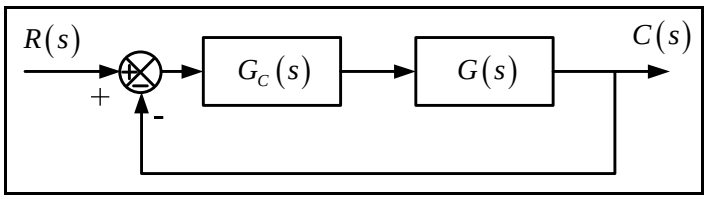

Figure 6.4 Classical control system

The SO method is suitable for an open-loop transfer function of a third-order polynomial in the denominator. Consider the classical control loop, as shown in Figure 6.4. The controller is of PI type as described in (6.24). If the plant includes a delay whose time constant is more than four time as large as the sum of the time constants of the remaining delays ($T_1 > 4T_e$) as described in (6.25), then the large delay acts, as a first approximation, like an integrator.

$$G_c(s) = K_p\left(\frac{1+sT_I}{sT_I}\right) \tag{6.24}$$

$$G(s) = \frac{k_1}{(sT_1+1)(sT_e+1)} \tag{6.25}$$

The proportional gain and integral time constant of the PI controller can be calculated in the following forms (Frohr and Orttenburger, 1992):

$$K_p = \frac{T_1}{2k_1T_e} \tag{6.26}$$

$$T_I = 4T_e \tag{6.27}$$

Since the open-loop transfer function of the current control is described in (6.23), the proportional gain, $K_{Pid} = K_{Piq}$, and integral time constant, $T_{Iid} = T_{Iiq}$, of PI controllers can be obtained by the SO method in (6.26) and (6.27), respectively. For example, the parameters of the D-STATCOM in Table 5.5 are used. Given that sum of the small time constant $T_e = 0.0001$, the PI controller's parameters of the current control can be obtained as

$$K_{pid} = K_{piq} = \frac{T_f}{2T_f T_e} = \frac{1}{0.0002} = 5000$$

$$T_{Iid} = T_{Iiq} = 4T_e = 0.0004$$

It is to clarify the concept of SO. Figure 6.5 shows the frequency characteristics (bode plot) of the individual system elements in the compensating current control loop. Solid line trace for the modulus of the open-loop transfer function of the current control which shows symmetry of the corner points $\frac{1}{4T_e}$ and $\frac{1}{T_e}$ with respect to the gain crossover frequency $\frac{1}{2T_e}$ on the 0 dB line. If the control loop is adjusted in accordance with the SO, the behavior is dependent on the sum of the time constants of the small delays in the control loop.

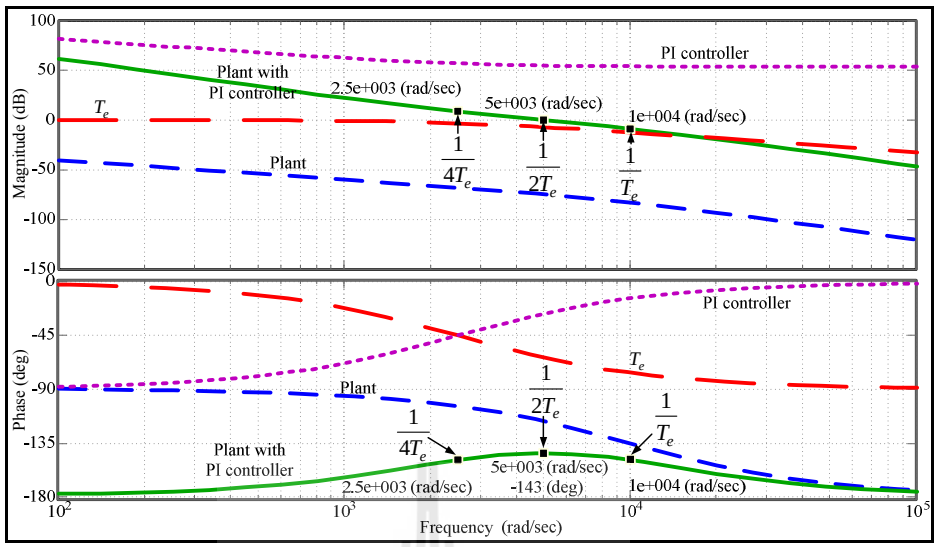

Figure 6.5 Bode plot of the open loop transfer function with the PI controller

6.3 PI Controller of the Current Control Based on Genetic Algorithms

There exist many different approaches to tune PI controller's parameters. The genetic algorithms (GAs) is well-known and there exist a hundred of works employing the GAs technique to design the controller in various forms. The GAs is a stochastic search technique that leads a set of population in solution space evolved using the principles of genetic evolution and natural selection, called genetic operators e.g. crossover, mutation, etc. With successive updating new generation, a set of updated solutions gradually converges to the real solution. Because the GAs is very popular and widely used in most research areas (Rashidi et al., 2003; Kulworawanichpong et al., 2005; Wang et al., 2000) where an intelligent search technique is applied, it can be summarized briefly as shown in the flowchart of Figure 6.6 (Kulworawanichpong et al., 2005).

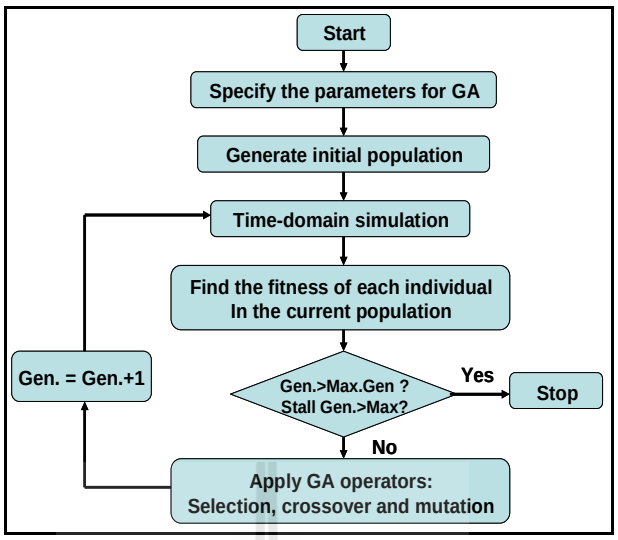

Figure 6.6 Flowchart of the GAs procedures

In this section, the GAs is selected to build up an algorithm to tune K_P and K_I parameters of the current control. The procedure to perform the proposed parameter tuning is described as follows. First, time-domain results of magnitude and frequency swing obtained by simulating the current control system in SIMULINK are obtained. Second, the Genetic Algorithms (GADS TOOLBOX) is employed to generate a set of initial random parameters. With the searching process, the parameters are adjusted to give response of best fitting close to the desired response. To perform the searching properly, its objective function is the key. In this section, the objective function is defined in (6.28).

$$\int_0^{t_{sim}} \left|\Delta i_{fd}(t) + \Delta i_{fq}(t)\right| dt \tag{6.28}$$

where $\Delta i_{fd} = y_{desired(d-axis)} - y_{simulated(d-axis)}$

$\Delta i_{fq} = y_{desired(q-axis)} - y_{simulated(q-axis)}$

$y_{desired(d-axis)}$ and $y_{desired(q-axis)}$ are the desired response on *d* and *q* axis, respectively.

$y_{simulated(d-axis)}$ and $y_{simulated(q-axis)}$ are the simulated response on *d* and *q* axis, respectively.

By using MATLAB/SIMULINK, the control block diagram of each test case can be formed graphically. In this section, a control model is presented in Figure 6.1 for the current control with the decoupling. Parameter tuning of its PI control was performed by using the GAs. For K_P and K_I parameters of the current control tuning based on the GAs, the reference D-STATCOM currents are step changed, i.e. i_{fd}^* and i_{fq}^* from 0 *A* to -200 *A*, -200 *A* to 0 *A* and 0 *A* to 200 *A*. With 30 computational trials in each test case of the parameter tuning based on the GAs, the best parameters obtained for each test case are put in Table 6.1.

Table 6.1 Best PI parameters for each test case

Case	K_{Pid}	T_{Iid}	K_{Piq}	T_{Iiq}	Fitness
1. *d*-axis current is step changed	20,972.62	1.99	5,000 (Fixed)	0.0004 (Fixed)	16,669.60
2. *q*-axis current is step changed	5,000 (Fixed)	0.0004 (Fixed)	20,970.36	1.85	16,675.11
3. *d* and *q*-axis current are step changed	20,950.12	2.01	20,878.70	1.77	16,022.40
4. *d* and *q*-axis current are step changed (SO method)	5,000 (Fixed)	0.0004 (Fixed)	5,000 (Fixed)	0.0004 (Fixed)	52,635.62

6.4 Result and Comparison of the Current Control

Effectiveness of the D-STATCOM model and the current controllers designed above were verified through computer simulation performed by using SIMULINK/MATLAB. The current controllers with the decoupling based on the symmetrical optimum method (CC-SO) and based on the genetic algorithms (CC-GAs) are compared. To study the current control, it is noted that the DC voltage and the AC voltage are kept constant. Figure 6.7 compares the response of the CC-SO and CC-GAs to step changes in the reference *d*-axis current, i_{fd}^{*}, from 0 *A* to -200 *A*, -200 *A* to 0 *A*, 0 *A* to 200 *A* and 200 *A* to 0 *A*. As can be seen in this figure, the CC-GAs gives the best dynamic response. It also gives the smaller settling time with the same overshoot in the *d* and *q* axis currents (i_{fd} and i_{fq}) as shown in Figure 6.7(a) – 6.7(d).

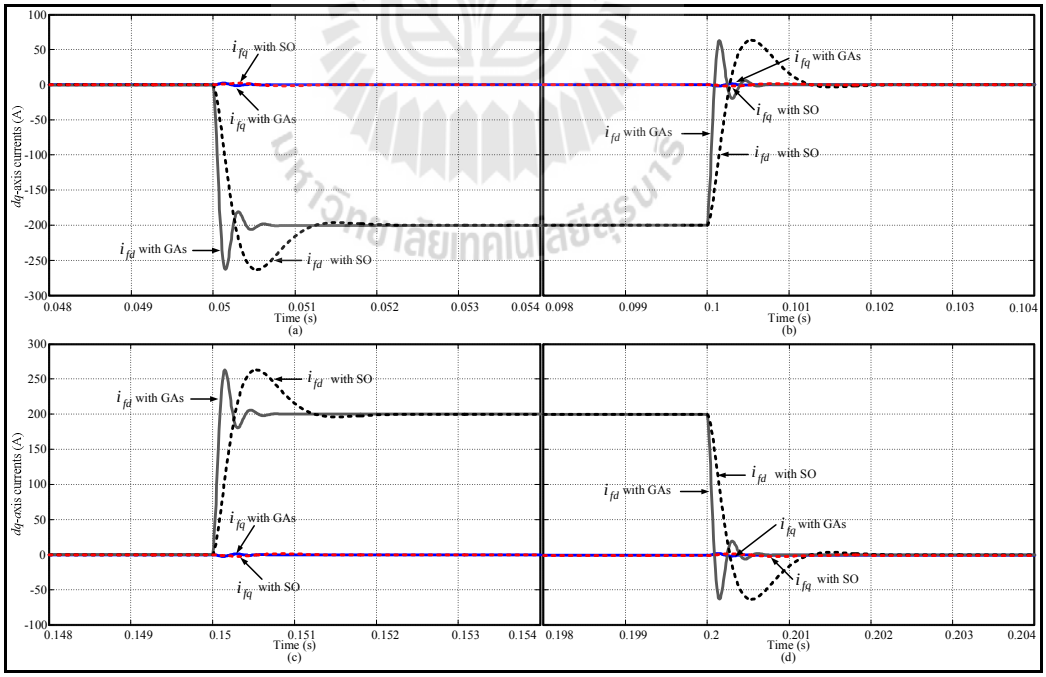

Figure 6.7 Respond of the *dq*-axis currents when the *d*-axis current is step changed

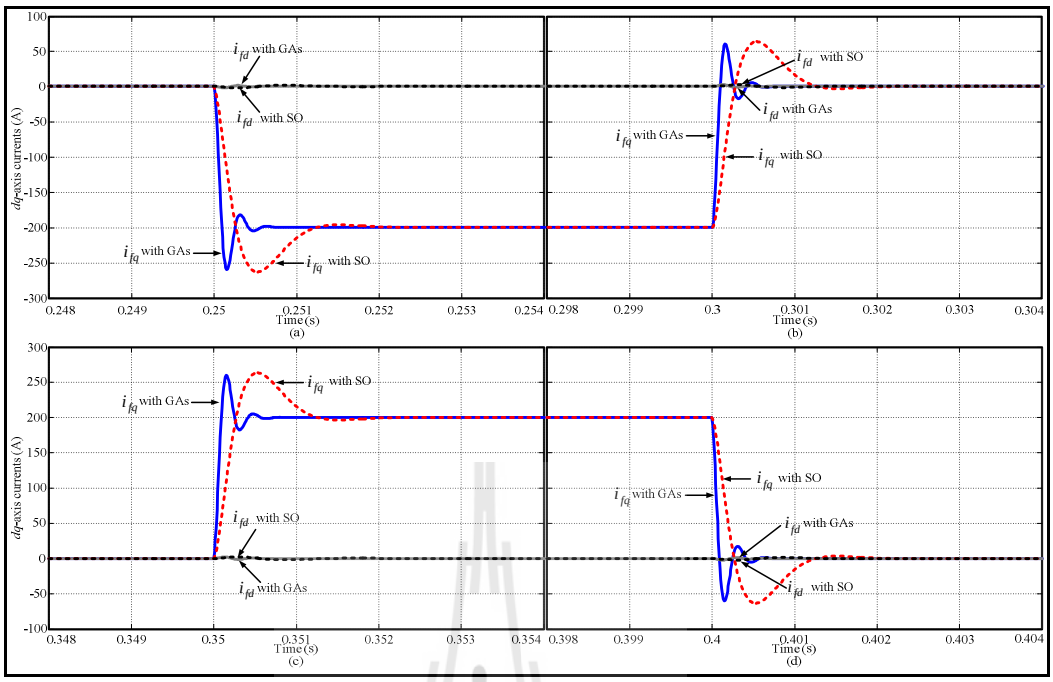

Figure 6.8 Respond of the *dq*-axis currents when the *q*-axis current is step changed

Althouth, the CC-GAs gives the best dynamic response, it gives high overshoot of control signal as shown in Figure 6.9(a). This signal is higher than the limited reference signal (± 1) in transient. This may results in the instability of the current control. However, this problem can be solved by adding the limiter in the current control system. The control signal and response of the CC-GAs with the limiter are shown in Figure 6.9(a) and 6.9(b), respectively. As can be seen in this figure, this control signal is not higher than the limited reference signal and it has a good performance.

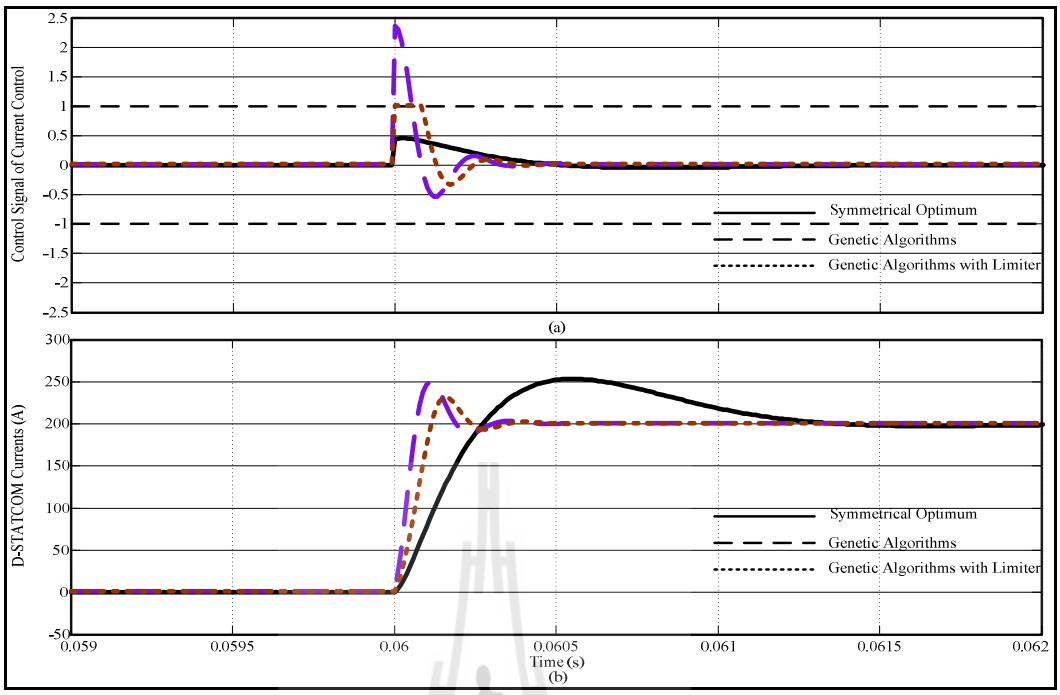

Figure 6.9 Control signal and response of the current control system

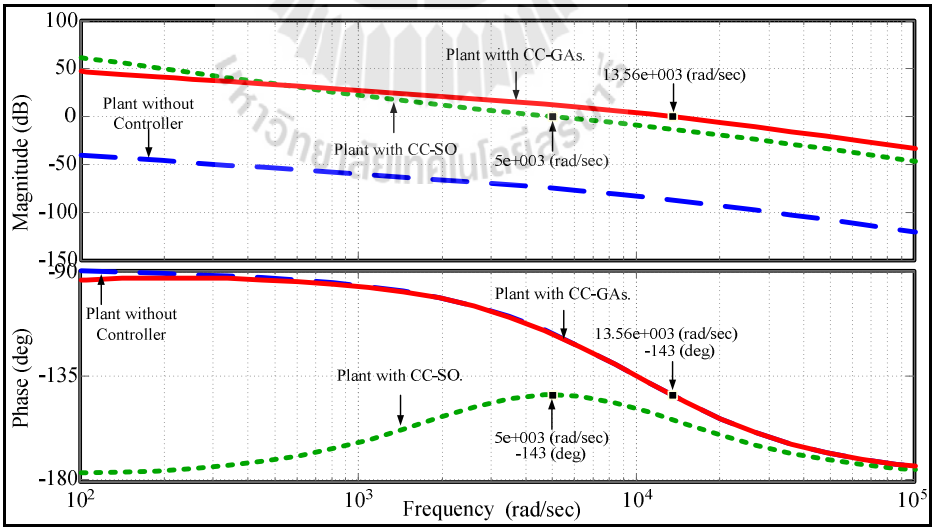

Figure 6.10 Comparison the bode plots of the current control based on symmetrical optimum (CC-SO) and based on genetic algorithms (CC-GAs)

In addition, the bode plots of the CC-SO and CC-GAs are compared as shown in Figure 6.10. From this figure, gain and phase stability margin of the CC-SO and CC-GAs can be obtained and compared. It is seen that gain crossover frequency of the CC-SO is 5,000 rad/sec while that of the CC-GAs is 13,560 rad/sec. However, both the CC-SO and CC-GAs have the same gain and phase stability margin which are ∞ (dB) and 37 (deg), respectively.

6.5 DC Voltage Control Strategy

The secondary control objective is to keep the DC voltage around its reference. This objective cannot be achieved directly by u_d through (5.14) as there might be possibility of i_{fd} going to zero during a transient. However, the DC voltage can be regulated indirectly by controlling i_{fd}. For designing the DC voltage controller, (5.14) is used. Although, the DC voltage can be controlled by i_{fd}, i_{fq} still affects the DC voltage as there exists the term of $u_q i_{fq}$ in (5.14). To eliminate this effect, the strategy like those of the current control is also applied. To obtain the DC voltage control, (5.14) can be modified as:

$$\frac{dv_{dc}}{dt} + v_{dc} = -x_{dc} \tag{6.26}$$

where the term $u_q i_{fq}$ is included in x_{dc} as

$$x_{dc} = \frac{3}{2}\frac{1}{C_{dc}} k_p \left(u_d i_{fd} + u_q i_{fq} \right) \tag{6.27}$$

Equation (6.26) shows that the DC voltage is increased following the transient with negative x_{dc}. Based on this principle, the control action x_{dc} can be expressed as:

$$x_{dc} = -K_{pvdc} \left(\frac{1 + sT_{Ivdc}}{sT_{Ivdc}} \right) \left(v_{dc}^{*} - v_{dc} \right) \tag{6.28}$$

Similar to the current control, the proportional-plus-integral regulators are used to control the DC voltage in the present work. Since the control action x_{dc} is determined by (6.28), the D-STATCOM active current command i_{fd}^{*} in (6.27) can be rearranged as:

$$-\left(\frac{x_{dc}}{\frac{3}{2}\frac{1}{C_{dc}} k_p} + u_q i_{fq} \right) \left(\frac{1}{u_d} \right) = i_{fd}^{*} \tag{6.29}$$

The DC voltage control structure and the D-STATCOM's DC voltage are demonstrated in Figure 6.11. The active current command i_{fd}^{*}, accounting for the DC voltage regulation, can be generated by the DC voltage controller with the DC voltage deviation as the input. The active current command i_{fd}^{*} is used as the input of the

current control loop, $G_{cl,i}(s)$, then, the controlled active current results in the DC voltage which enables the DC voltage control.

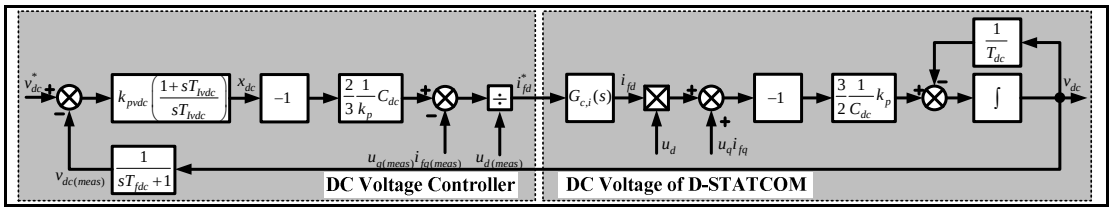

Figure 6.11 DC voltage control structure and the D-STATCOM DC voltage

As seen from Figure 6.11, the control loop is a cascade control in which the DC voltage control is a main control loop and the current control is an auxiliary control loop. The main control loop is superimposed on the auxiliary control loop. This means that the current control is substantially faster than the DC voltage control. From the decoupling current control loop shown in Figure 6.1, the control actions x_d and x_q can be derived by the PI controller. For this closed loop current control with PI controller, the control actions x_d and x_q in (6.5) and (6.6) can be modified as

$$x_d = \frac{K_{Pid}}{T_{Iid}} f_d + K_{Pid}\left(i_{fd}^{*} - i_{fd(meas)}\right) \tag{6.30}$$

$$x_q = \frac{K_{Piq}}{T_{Iiq}} f_q + K_{Piq}\left(i_{fq}^{*} - i_{fq(meas)}\right) \tag{6.31}$$

where the control actions of the I controller f_d and f_q can be expressed as

$$\frac{df_d}{dt} = i_{fd}^* - i_{fd(meas)} \tag{6.32}$$

$$\frac{df_q}{dt} = i_{fq}^* - i_{fq(meas)} \tag{6.33}$$

Meanwhile, i_{fd}^* and i_{fq}^* are the d and q axis current commands that they are generated by the DC voltage and AC voltage controller, respectively. It is seen in Figure 6.11, the d-axis current command i_{fd}^* can be written as

$$i_{fd}^* = -\left(\frac{2}{3}\frac{1}{k_p}C_{dc}x_{dc} + u_{q(meas)}i_{fq(meas)}\right)\frac{1}{u_{d(meas)}} \tag{6.34}$$

When $u_{d(meas)}$ and $u_{q(meas)}$ are the measured outputs of the current control that can be measured at the PCC. It is assumed that they are measured at behind filter, these can be expressed as

$$\frac{du_{d(meas)}}{dt} = \frac{u_d}{T_{ud}} - \frac{u_{d(meas)}}{T_{ud}} \tag{6.35}$$

$$\frac{du_{q(meas)}}{dt} = \frac{u_q}{T_{uq}} - \frac{u_{q(meas)}}{T_{uq}} \tag{6.36}$$

Where T_{ud} and T_{uq} are filter time delay of the measured output of the current control. Thus, full open loop transfer function of the DC voltage with including the decoupling current control loop can be obtained by using (6.9) – (6.18), (6.26) – (6.27) and (6.30) – (6.36). By linearization of these equations around the operating point, i.e. output of the PI controller of DC control (x_{dc0}), the *q*-axis current command (i^*_{fq0}) and terminal voltage (v_{td0}), the transfer function of the DC voltage v_{dc} with respect to the output of the PI controller of DC control x_{dc} can be obtained. However, if the current control is adjusted in conformity with the SO method, then its action is a third-order delay. To simplify the overall behavior of the controlled system relevant to the superimposed loop, the current control loop can be replaced by a first-order delay (Frohr and Orttenburger, 1992). Therefore, the transfer function of the current control loop can be simplified as:

$$G_{cl,i}(s) = \frac{1}{sT_{ei} + 1} \tag{6.37}$$

Where T_{ei} is an equivalent time constant of the current control loop. However, the equivalent time constant for the symmetrical optimum control loop can be defined by $T_{ei} = 4T_e$ (Frohr and Orttenburger, 1992) where T_e is defined in (6.20). To simplify this design, the effect of the filter time delays can be neglected. Consequently, the measured values i.e. $u_{d(meas)}$, $u_{q(meas)}$ and $i_{fq(meas)}$ in (6.34) can be replaced by u_d, u_q and i_{fq}, respectively. Then it is assumed that the time delay of the feedback filter and the equivalent time constant of the current control loop (T_{ei}) are combined as

$$T_v = T_{fdc} + T_{ei} \tag{6.38}$$

Hence, the simplified open loop transfer function of the DC voltage v_{dc} with respect to the output of PI controller of DC control x_{dc} is given as

$$G_{vdcopen}(s) = \left(\frac{T_{dc}}{sT_{dc}+1}\right)\left(\frac{1}{sT_v+1}\right) \tag{6.39}$$

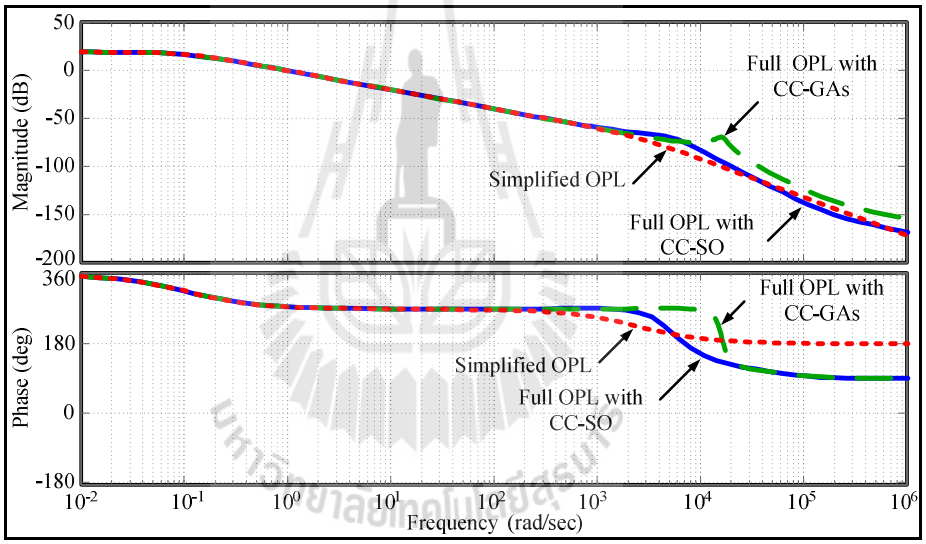

Figure 6.12 Bode plots of the full open loop transfer function with the CC-SO and CC-GAs

To confirm the proposed simplified open loop transfer function of the DC voltage, the frequency responds of the simplified and full open loop transfer function are obtained and compared as shown in Figure 6.12. In addition, bode plots of the full open loop transfer function with the CC-SO and CC-GAs are demonstrated. The full

open loop transfer function can be obtained by linearization of (6.9) – (6.18), (6.26) – (6.27) and (6.30) – (6.36), whereas the simplified open loop transfer function is shown in (6.39). For these calculation bode plots, the parameters of the D-STATCOM as shown in Table 5.5 and $T_v = 0.0004$ are applied. As can be seen in these figure, the bode plots of both full and simplified open loop transfer functions are very close to each other at lower frequency than 10^3 rad/sec. However, at higher frequency, the bode plots of those are apart.

6.6 DC Voltage PI Controller Design

Similar to the current control, the PI controllers design based on SO and GAs methods are applied in this case. Since the open-loop transfer function of the DC voltage is described in (6.39) and $T_{dc} \approx 4T_v$, the proportional gain, K_{Pvdc}, and integral time constant, T_{Ivdc}, of PI controllers can be obtained by the SO method in (6.26) and (6.27), respectively. For example, the parameters of the D-STATCOM in Table 5.5 are used. Given that sum of the small time constant $T_v = 0.0004$, the PI controller's parameters of the DC voltage control can be obtained as

$$K_{pvdc} = \frac{T_{dc}}{2T_{dc}T_v} = \frac{1}{0.0008} = 1250$$

$$T_{Ivdc} = 4T_v = 0.0016$$

In case of tuning PI controller's parameters of the DC voltage control based on GAs, the objective function is defined in (6.40).

$$\int_{0}^{t_{sim}} \left|\Delta v_{dc}(t)\right| dt \tag{6.40}$$

where $\Delta v_{dc} = y_{desired(v_{dc})} - y_{simulated(v_{dc})}$

$y_{desired(v_{dc})}$ is the desired response of the DC voltage.

$y_{simulated(v_{dc})}$ is the simulated response of the DC voltage.

By using MATLAB/SIMULINK, the DC voltage control block diagram of this section can be formed graphically as presented in Figure 6.11. Meanwhile, the current control is an auxiliary control loop that the block diagram is shown in Figure 6.1. In this section, two cases of the DC voltage controller i.e. the DC voltage controller with non-elimination and elimination term of $u_q i_{fq}$ are used. Furthermore, the CC-SO and CC-GAs are applied in each case. PI controller's parameter tuning of the DC voltage control was performed by using the GAs. For K_P and K_I parameters of the DC voltage control tuning based on the GAs, the reference D-STATCOM reactive current is step changed, i.e. i_{fq}^* from 0 *A* to -400 *A*, -400 *A* to 0 *A* and 0 *A* to 400 *A*. With 30 computational trials in each test case of the parameter tuning based on the GAs, the best parameters obtained for each test case are put in Table 6.2.

Table 6.2 Best PI parameters of the DC voltage control for each test case

DC voltage control : non-elimination term of $u_q i_{fq}$			
Current controller :	K_{Pvdc}	T_{Iiq}	**Fitness**
1. CC-SO	4138.382	0.00160	15,533.29
2. CC-GAs	8412.702	0.000169	2,394.04
DC voltage control : elimination term of $u_q i_{fq}$			
Current controller :	K_{Pvdc}	T_{Iiq}	**Fitness**
1. CC-SO	4341.241	0.01003	14,017.91
2. CC-GAs	8264.893	0.000167	2,436.14

6.7 Result and Comparison of the DC Voltage Control

The performance of the DC voltage control designed above is verified through computer simulation performed by using SIMULINK/MATLAB and it is studied in step changes the reference *q*-axis current, i_{fq}^{*}, from 0 *A* to -400 *A* and -400 *A* to 0 *A*. At t = 0.05 sec, the reference *q*-axis current is changed from 0 *A* to -400 *A* and at t = 0.1 sec it is changed from -400 *A* to 0 *A*. In this section, the responses of the DC voltage control with and without the elimination term of $u_q i_{fq}$ based on the symmetrical optimum method (DCVC-SO) and based on the genetic algorithm method (DCVC-GAs) are compared. The performances of the DCVC-SO with and without elimination term of $u_q i_{fq}$ are shown in Figure 6.13. In this figure, the responses of the DCVC-SO with the CC-SO and CC-GAs are also compared.

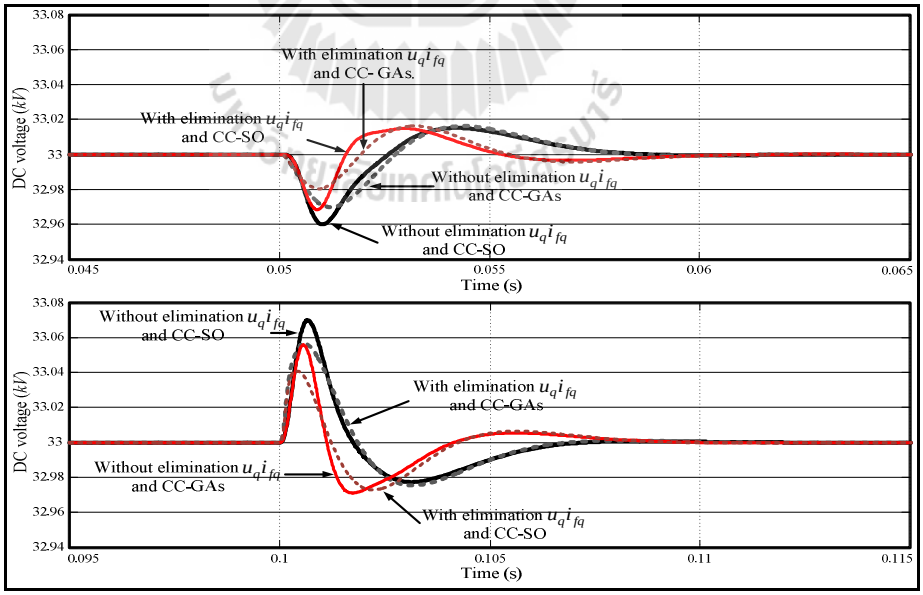

Figure 6.13 Performance of the DC voltage control based on the symmetrical optimum method (DCVC-SO)

As can be seen in this figure, the DC voltage control with the elimination term of $u_q i_{fq}$ gives the best dynamic response. This control gives smaller settling time and smaller overshoot. Furthermore, the DC voltage control including with the CC-GAs also gives smaller settling time and also smaller overshoot than with the CC-SO. However, it is not significant.

Meanwhile, the performances of the DCVC-GAs with and without elimination term of $u_q i_{fq}$ are illustrated in Figure 6.14. In this figure, the responses of the DCVC-GAs with the CC-SO and CC-GAs are also compared.

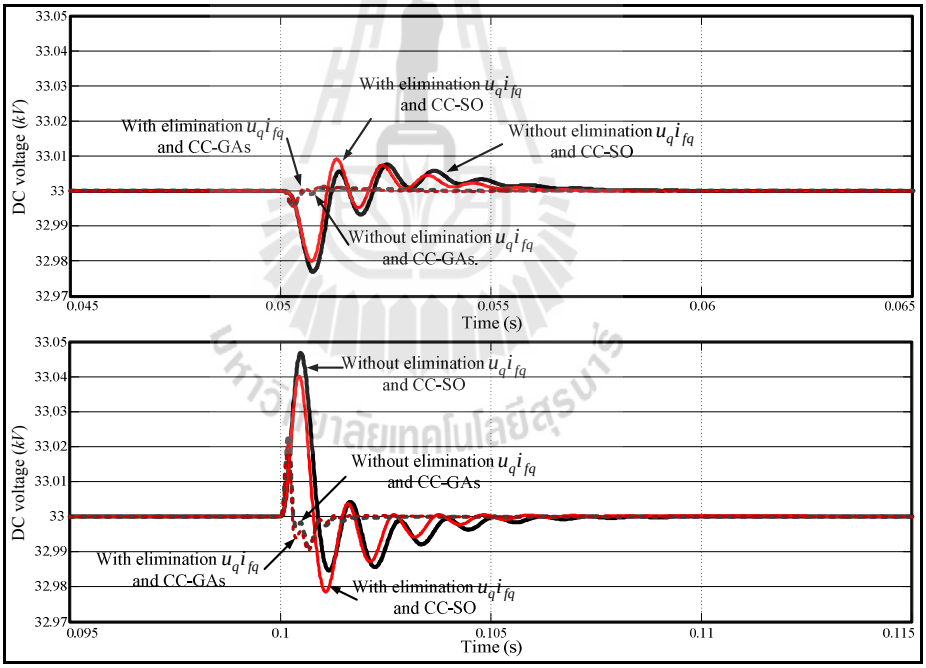

Figure 6.14 Performance of the DC voltage control based on genetic algorithms (DCVC-GAs)

In this figure, it is seen that the responses of the DCVC-GAs with and without the elimination term of $u_q i_{fq}$ are almost the same. Meanwhile, the DCVC-GAs including with the CC-GAs gives the best dynamic response. This control also gives smaller settling time and also smaller overshoot than the DCVC-GAs including with the CC-SO.

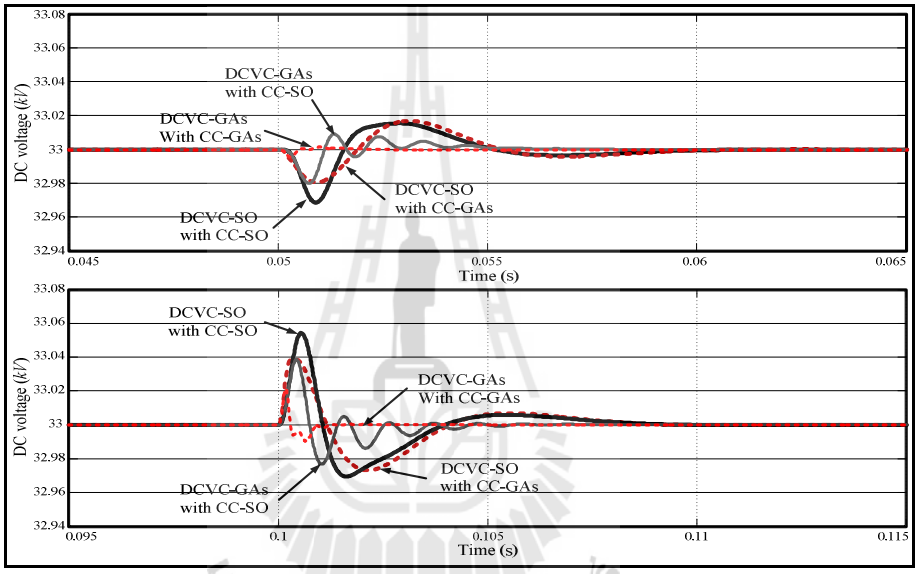

Figure 6.15 Comparison performance of DCVC-SO and DCVC-GAs

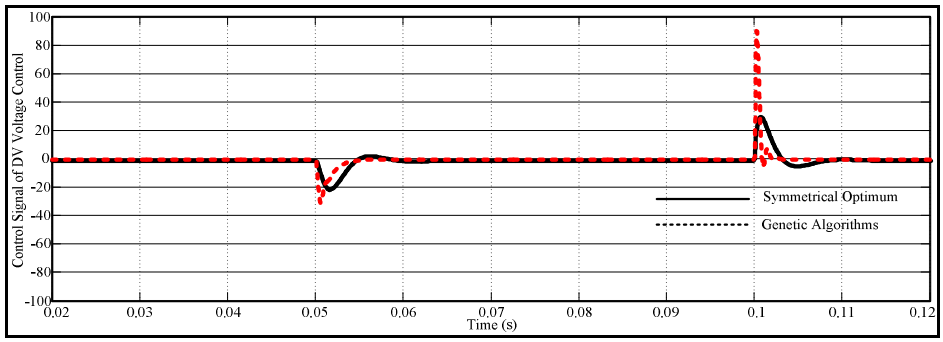

Figure 6.16 Comparison of the control signal of the DCVC-GAs and DCVC-SO

In addition, the response of the DC voltage when the DCVC-SO and DCVC-GAs are presented and compared as shown in Figure 6.15. It is seen that the DCVC-GAs with the CC-GAs gives the best dynamic response. This control also gives smaller settling time and also smaller overshoot. Although this control gives the best dynamic response, the gain and phase stability margin are not as so. Additionally, this control has higher overshoot of control signal than the DCVC-SO as can be seen in Figure 6.16.

The bode plots of the DCVC-SO and DCVC-GAs with the CC-SO and CC-GAs are compared as shown in Figure 6.17. From this figure, gain and phase stability margin can be obtained and compared. The gain crossover frequency, phase crossover frequency, gain stability margin and phase stability margin are shown in Table 6.3. It is seen that the DCVC-SO with the CC-GAs gives the best gain stability margin at 21.3 dB and the DCVC-SO with the CC-SO gives the best phase stability margin at 64 deg. Meanwhile, the DCVC-GAs with the CC-GAs gives the worst gain stability margin at 2.93 dB and the DCVC-GAs with the CC-SO gives the worst phase stability margin at 24.2 deg.

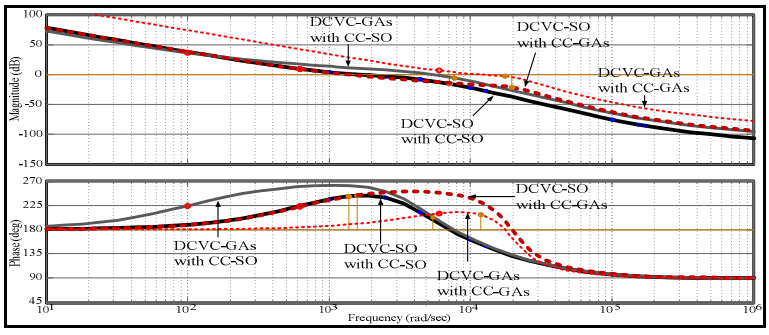

Figure 6.17 Bode plots of the DC voltage control based on symmetrical optimum (DCVC-SO) and based on genetic algorithms (DCVC-GAs)

Table 6.3 Stability margin of the DC voltage control

Control	Gain cross over frequency (red/sec)	Phase cross over frequency (red/sec)	Gain margin (dB)	Phase margin (deg)
1. DCVC-SO with CC-SO	1,580	7,140	15.5	64
2. DCVC-SO with CC-GAs	1,380	19,700	21.3	62.6
3. DCVC-GAs with CC-SO	5,410	7,610	5.9	24.2
4. DCVC-GAs with CC-GAs	11,800	17,500	2.93	28.5

6.8 Summary

This chapter presents the current and DC voltage control design of the D-STATCOM. The decoupling current control based on the *dq* reference frame is presented. Although, the DC voltage can be controlled by active current of the D-STATCOM, reactive current still affects the DC voltage. To eliminate this effect, the control strategy with the elimination effect of the reactive current is proposed. For obtaining the proportional and integral gains of the PI controllers, the symmetrical optimum and genetic algorithms are applied. The stability margins of these methods are obtained and discussed in detail. In addition, the performance of the DC voltage control based on symmetrical optimum and genetic algorithms are compared. Effectiveness of the controllers designed was verified through computer simulation performed by using SIMULINK/MATLAB.

For the current control design, the decoupling current control based on the genetic algorithm (CC-GAs) gives the best dynamic response. However, both the current control based on symmetrical optimum and genetic algorithms (CC-SO and CC-GAs) have the same gain and phase stability margin.

For the DC voltage control design, the DC voltage control based on the genetic algorithm (DCVC-GAs) with the CC-GAs gives the best dynamic response.

Although this control gives the best dynamic response, the gain and phase stability margin are not. It is seen that the DC voltage control based on the symmetrical optimum method (DCVC-SO) with the CC-GAs gives the best gain stability margin and the DCVC-SO with the CC-SO gives the best phase stability margin. Meanwhile, the DCVC-GAs with the CC-GAs gives the worst gain stability margin and the DCVC-GAs with the CC-SO gives the worst phase stability margin.

CHAPTER VII

DESIGN OF AC VOLTAGE CONTROL

This chapter presents the AC voltage control design for the load voltage regulation by using the D-STATCOM. The modeling strategy similar to that used for the field oriented control of three phase AC machines is employed. The D-STATCOM model and its control were integrated with the power distribution systems that are used for the load voltage controller design. This derived model is exact and can be used for the load voltage controller design using linear techniques. The classical loop shaping method is applied to the load voltage controller design. By using the software in MATLAB for adjusting the open loop transfer function to satisfy the loop shaping specifications, the controller parameters and the stability margins for the R and RL load with various operating conditions can be obtained. The performance of the proposed model and the controller design were verified using computer simulation performed in SIMULINK/MATLAB.

7.1 The Distribution System with Detailed D-STATCOM

Based on the distribution system model described in the Section 3.1, this section proceeds to design the load voltage controller. The D-STATCOM model and its control were integrated with the power distribution system for designing the load voltage controller. From the current control with decoupling shown in Figure 6.1, the

control inputs, u_d and u_q of the D-STATCOM current control can be expressed in (6.13) and (6.14), respectively. While the signals x_d and x_q can be derived from the PI current controller and expressed in (6.30) and (6.31), respectively. Meanwhile, the DC voltage control of the D-STATCOM is shown in Figure 6.11. The active current command i_{fd}^{*} can be derived from the DC voltage control and expressed in (6.34). Where the signal x_{dc} is derived from the PI DC voltage controller as

$$x_{dc} = \frac{K_{Pvdc}}{T_{Ivdc}} f_{dc} + K_{Pvdc}\left(v_{dc}^{*} - v_{dc(meas)}\right) \tag{7.1}$$

Where the control actions of the I controller f_{dc} can be expressed as

$$\frac{df_{dc}}{dt} = v_{dc}^{*} - v_{dc(meas)} \tag{7.2}$$

Therefore, the equations of the D-STATCOM and its control were integrated with the power distribution system can be formed by using the distribution system model described in Chapter 3, the D-STATCOM dynamics described in Chapter 5 and the dynamic equations of current and DC voltage control of the D-STATCOM described in Chapter 6 that can be written as follows

$$\frac{di_{sd}}{dt} = -\frac{1}{T_s} i_{sd} + \omega i_{sq} - \frac{1}{L_s} v_{td} + \frac{V_s}{L_s}\cos\alpha \tag{7.3}$$

$$\frac{di_{sq}}{dt} = -\frac{1}{T_s} i_{sq} - \omega i_{sd} - \frac{V_s}{L_s} \sin\alpha \tag{7.4}$$

$$\frac{dv_{td}}{dt} = -\frac{1}{C_f} i_{ld} + \frac{1}{C_f} i_{sd} + \frac{1}{C_f} i_{fd} \tag{7.5}$$

$$\frac{di_{ld}}{dt} = -\frac{1}{T_l} i_{ld} + \omega i_{lq} + \frac{1}{L_l} v_{td} \tag{7.6}$$

$$\frac{di_{lq}}{dt} = -\frac{1}{T_l} i_{lq} - \omega i_{ld} \tag{7.7}$$

$$\frac{d\alpha}{dt} = \omega - \omega_s \tag{7.8}$$

$$\frac{di_{fd}}{dt} = -\frac{1}{T_f} i_{fd} + \omega i_{fq} - \frac{1}{L_f} v_{td} + \frac{1}{L_f} v_{std} \tag{7.9}$$

$$\frac{di_{fq}}{dt} = -\frac{1}{T_f} i_{fq} - \omega i_{fd} + \frac{1}{L_f} v_{stq} \tag{7.10}$$

$$\frac{dv_{std}}{dt} = -\frac{1}{T_d} v_{std} + \frac{1}{T_d} k_p v_{dc} u_d \tag{7.11}$$

$$\frac{dv_{stq}}{dt} = -\frac{1}{T_d} v_{stq} + \frac{1}{T_d} k_p v_{dc} u_q \tag{7.12}$$

$$\frac{dv_{dc}}{dt} = -\frac{v_{dc}}{T_{dc}} - \frac{3}{2}\frac{1}{C_{dc}} k_p u_d i_{fd} - \frac{3}{2}\frac{1}{C_{dc}} k_p u_q i_{fq} \tag{7.13}$$

$$\frac{df_d}{dt} = i_{fd}^{*} - i_{fd(meas)} \tag{7.14}$$

$$\frac{df_q}{dt} = i_{fq}^{*} - i_{fq(meas)} \tag{7.15}$$

$$\frac{di_{fd(meas)}}{dt} = \frac{i_{fd}}{T_{fi}} - \frac{i_{fd(meas)}}{T_{fi}} \tag{7.16}$$

$$\frac{di_{fq(meas)}}{dt} = \frac{i_{fq}}{T_{fi}} - \frac{i_{fq(meas)}}{T_{fi}} \tag{7.17}$$

$$\frac{dv_{dc(meas)}}{dt} = \frac{v_{dc}}{T_{fdc}} - \frac{v_{dc(meas)}}{T_{fdc}} \tag{7.18}$$

$$\frac{dv_{td(meas)}}{dt} = \frac{v_{td}}{T_{fac}} - \frac{v_{td(meas)}}{T_{fac}} \tag{7.19}$$

$$\frac{du_{d(meas)}}{dt} = \frac{u_d}{T_{ud}} - \frac{u_{d(meas)}}{T_{ud}} \tag{7.20}$$

$$\frac{du_{q(meas)}}{dt} = \frac{u_q}{T_{uq}} - \frac{u_{q(meas)}}{T_{uq}} \tag{7.21}$$

$$\frac{df_{dc}}{dt} = v_{dc}^{*} - v_{dc(meas)} \tag{7.22}$$

Where

$$x_{dc} = \frac{K_{Pvdc}}{T_{Ivdc}} f_{dc} + K_{Pvdc}\left(v_{dc}^{*} - v_{dc(meas)}\right) \tag{7.23}$$

$$i_{fd}^{*} = -\left(\frac{2}{3}\frac{1}{k_p} C_{dc} x_{dc} + u_{q(meas)} i_{fq(meas)}\right)\frac{1}{u_{d(meas)}} \tag{7.24}$$

$$x_d = \frac{K_{Pid}}{T_{Iid}} f_d + K_{Pid}\left(i_{fd}^{*} - i_{fd(meas)}\right) \tag{7.25}$$

$$x_q = \frac{K_{Piq}}{T_{Iiq}} f_q + K_{Piq}\left(i_{fq}^{*} - i_{fq(meas)}\right) \tag{7.26}$$

$$u_d = \frac{1}{k_p v_{dc(meas)}}\left[vtd_{(meas)} - \omega_{PLL} L_f i_{fq(meas)} + x_d L_f\right] \tag{7.27}$$

$$u_q = \frac{1}{k_p v_{dc(meas)}}\left[+\omega_{PLL} L_f i_{fd(meas)} + x_q L_f\right] \tag{7.28}$$

However, these equations are a set of nonlinear differential equations. To investigate the dynamic performance of these systems, linear approximation is

applied. Linearization of the systems around the operating that described in (D'Azzo and Houpis, 1995), gives a set of linear equations as shown in (7.29).

$$\Delta\dot{x}(t) = \left\{\frac{\partial f}{\partial x}(x_0, u_0)\right\}\Delta x(t) + \left\{\frac{\partial f}{\partial u}(x_0, u_0)\right\}\Delta u(t) \tag{7.29}$$

The partial derivatives in the linearization are evaluated at the initial points. The coefficients A_0 and B_0 can be solved and expressed as (7.30) – (7.31). Therefore the linearized system of the dynamic system can be represented as (7.32).

$$A_0 = \frac{\partial f}{\partial x}(x_0, u_0) \tag{7.30}$$

$$B_0 = \frac{\partial f}{\partial u}(x_0, u_0) \tag{7.31}$$

$$\Delta\dot{x}(t) = A_0\Delta x(t) + B_0\Delta u(t) \tag{7.32}$$

For designing the load voltage control, the load voltage v_{td} is chosen as the output of the system with the reactive current command i_{fq}^{*} as the control input. To illustrate the control technique, the parameters of the distribution power system and the D-STATCOM as shown in Table 3.1 and Table 5.5 are used. The current control parameters based on genetic algorithm and DC voltage control parameters based on

symmetrical optimum are applied. The bode plots of the transfer function $\frac{\Delta v_{td}(s)}{\Delta i_{fq}^{*}(s)}$ of the linearization systems with the R and RL load are shown in Figure 7.1 and 7.2, respectively.

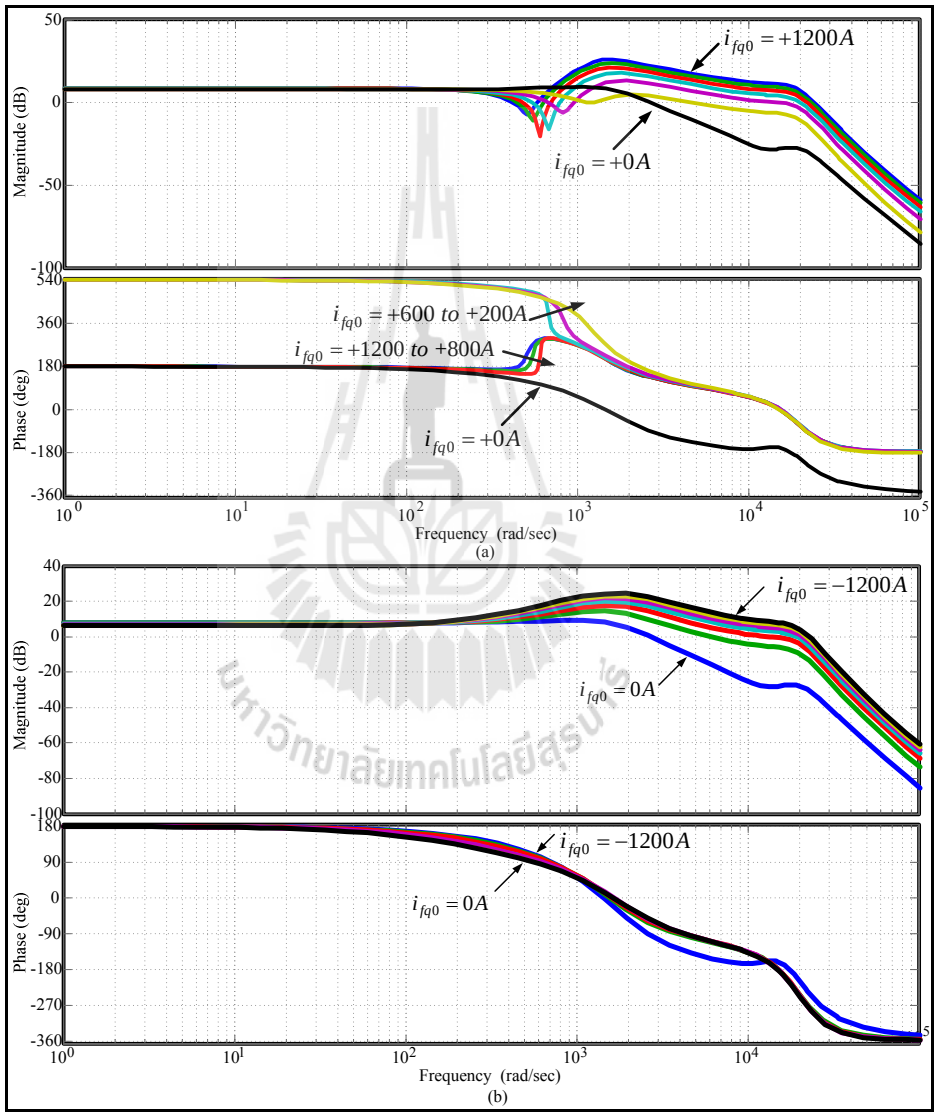

Figure 7.1 Bode plots of the transfer function $\frac{\Delta v_{td}(s)}{\Delta i_{fq}^{*}(s)}$ of the systems with the Rload

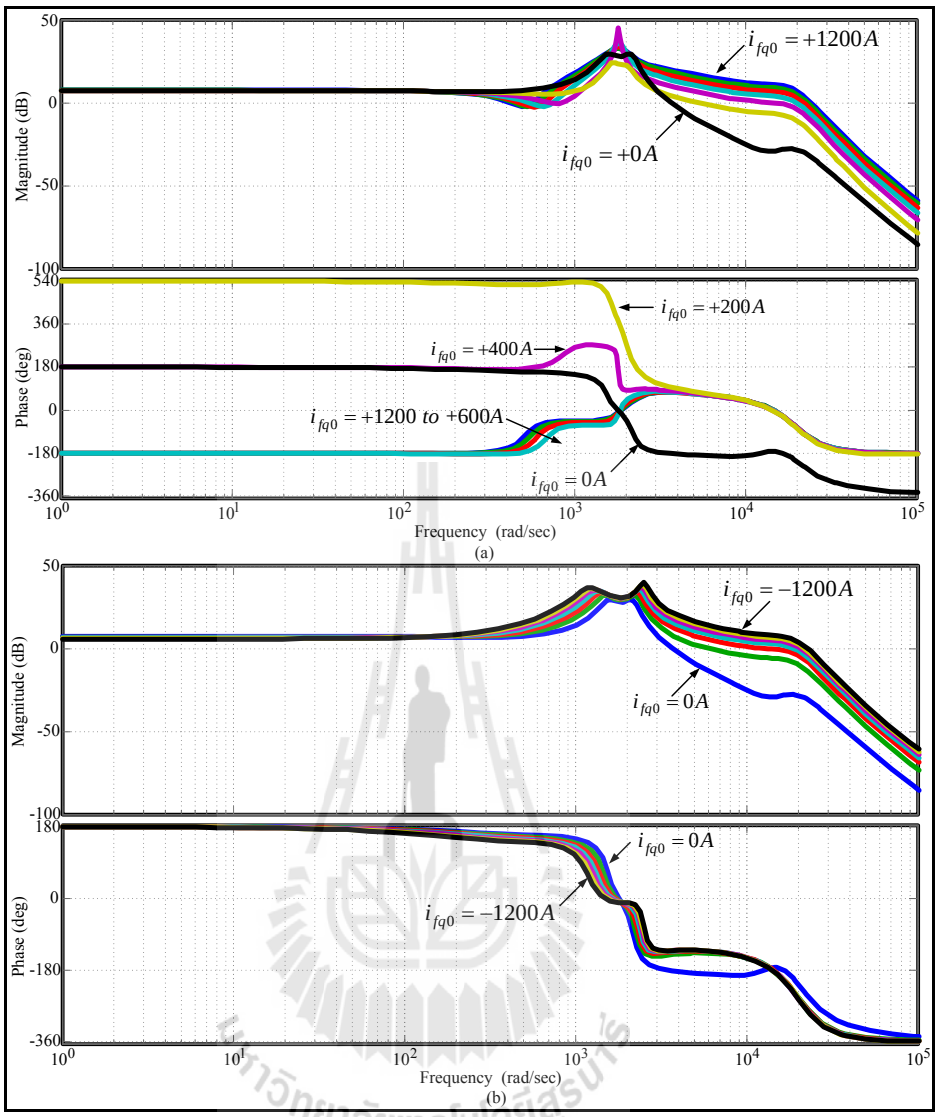

Figure 7.2 Bode plots of the transfer function $\frac{\Delta v_{td}(s)}{\Delta i_{fq}^{*}(s)}$ of the systems with the RL load

In these figures, the bode plots of the transfer function for various operating conditions, each corresponding to a different value of i_{fq}, are presented. i_{fq} is varied from +1200*A* to -1200*A* with 200*A* step in these cases. For the R load, the frequency

responses for i_{fq} varied from +1200*A* to 0*A* are shown in Figure 7.1(a) and for i_{fq} varied from 0*A* to -1200*A* are shown in Figure 7.1(b). Meanwhile, the frequency responses for the RL load when i_{fq} varied from +1200*A* to 0*A* and i_{fq} varied from 0*A* to -1200*A* are shown in Figure 7.2(a) and Figure 7.2(b), respectively. In addition, the frequency responses of the distribution system with ideal and detailed D-STATCOM are compared as shown in Figure 7.3.

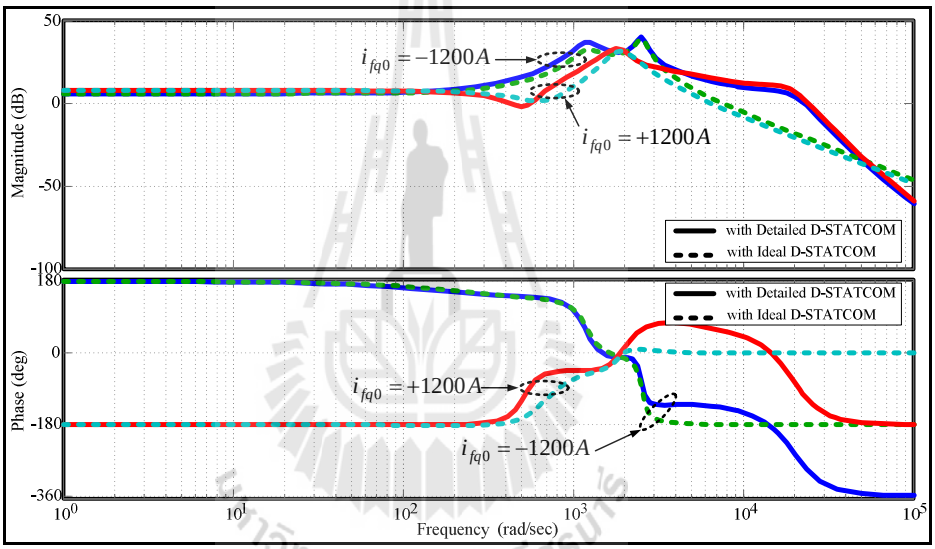

Figure 7.3 Comparing the frequency responses of the distribution system with ideal and detailed D-STATCOM for The RL load

As can be seen in these figures, this system is complicated, especially for RL load. Thus, this system cannot be approximated as a low order system. Moreover, this transfer function is non-minimum phase system when i_{fq} are varied between +200*A* and -1200*A*. Therefore, the simple method particularly symmetrical optimum method (SO) is not suitable to apply to this system.

7.2 The Controller Design with the Classical Loop Shaping Method

The load voltage control is the Single Input Single Output (SISO) control system with the load voltage v_{td} chosen as the output of the system and the reactive current command i_{fq}^{*} as the control input. For SISO systems, the classical loop shaping concepts are the basis for designing the load voltage controller. The unity feedback SISO system depicted in Figure 7.4 where $P(s)$ represents the plant transfer function and $C(s)$ represents the controller transfer function. The signals $r(t)$, $d_i(t)$, $d_o(t)$, and $n(t)$ represent the reference input, input disturbance, output disturbance, and sensor noise, respectively. The signal $y(t)$ is the output, $e(t)$ is the tracking error, and $u(t)$ is the control input. The definitions of the open loop transfer function $L(s)$, the sensitivity function $S(s)$ and the complementary sensitivity function $T(s)$ are

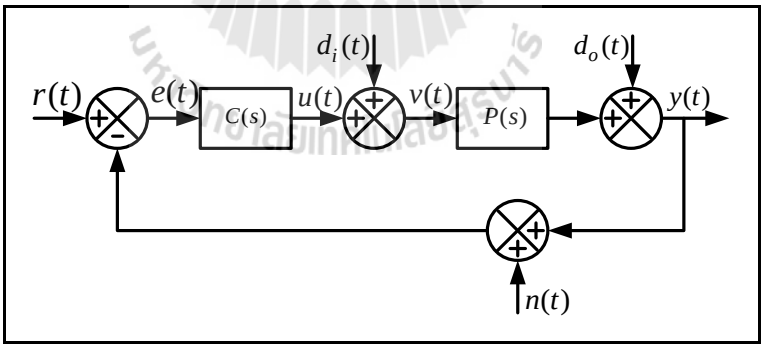

Figure 7.4 Block diagram of unity feedback SISO system

$$L(s) = P(s)C(s) \tag{7.33}$$

$$S(s) = \left[1 + L(s)\right]^{-1} \tag{7.34}$$

$$T(s) = L(s)\left[1 + L(s)\right]^{-1} \tag{7.35}$$

The classical loop shaping is a graphical procedure to design a proper controller $C(s)$ satisfying the requirements on stability and performance. The basic idea of the method is to construct the open loop transfer function $L(s)$ to satisfy the requirements performance and stability criterion approximately, and then to obtain the controller. The classical loop shaping design is based on two important observations (Barratt and Boyd, 1992):

1. The open loop transfer function $L(s)$ has a very simple dependence on the controller transfer function $C(s)$, especially in a logarithmic (gain and phase) representation.

2. Many important requirements for the closed loop system can be approximately reflected as requirements on the loop gain $L(s)$.

Loop shaping specifications constrain the magnitude and possibly the phase of the loop transfer function at each frequency. If the given ω_r and ω_n are frequencies separating three frequency range i.e. Low frequency (0, ω_r), Medium or Crossover frequency (ω_r, ω_n) and High frequency (ω_n, ∞), there are three basic types of loop shaping specifications, which are imposed in different frequency.

Figure 7.5 illustrates the requirement magnitudes of the sensitivity and the complementary sensitivity function, $\left|S(j\omega)\right|$ and $\left|T(j\omega)\right|$, in each frequency that corresponds to the bode plot of the open loop transfer function as shown in Figure 7.6.

As can be seen in these figures, the loop shaping specifications can be described as follows:

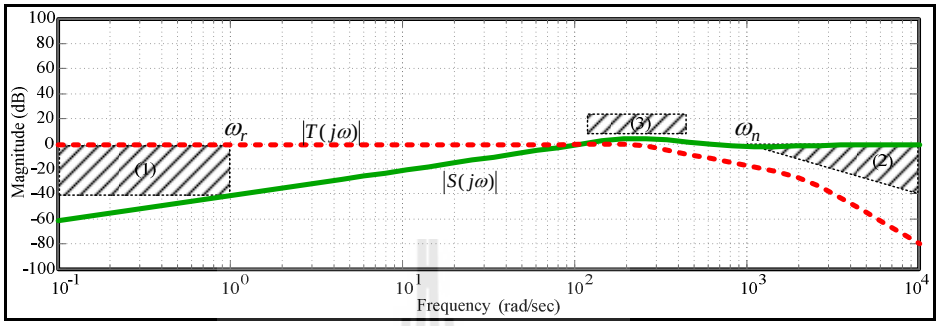

Figure 7.5 Requirement magnitudes of the sensitivity and the complementary sensitivity function

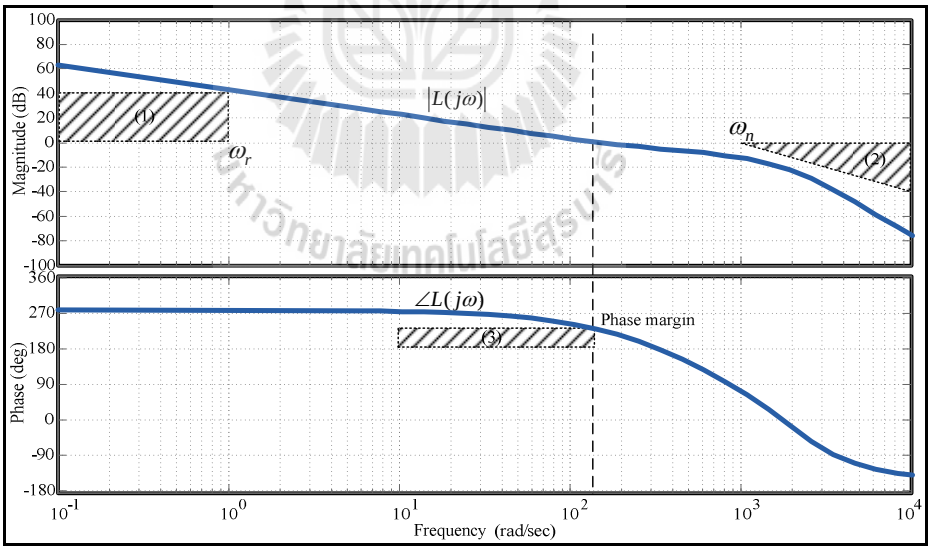

Figure 7.6 Bode plot of the open loop transfer function

1. Low frequency specifications. At these frequencies we require $|L(j\omega)|$ to be large, so that $|S(j\omega)|$ is small and $T(j\omega) \approx 1$. This ensures good command tracking, and low sensitivity to plant variations, two of the most important benefits of feedback.

2. High frequency specifications. At these frequencies we require $|L(j\omega)|$ to be small, so that $|T(j\omega)|$ is small. This ensures that the output $y(t)$ will be relatively insensitive to the sensor noise $n(t)$, and that the system will remain closed loop stable in the face of plant variations at these frequencies.

3. Crossover frequency (margin) specifications. Crossover or transition frequency specifications are imposed between the control frequency (where $|L(j\omega)|$ is large) and high frequency (where $|L(j\omega)|$ is small). At these frequencies, the slope of $|L(j\omega)|$ should be close to -20 dB/decade. If $|L(j\omega)|$ drops off too quickly through crossover, internal instability will result, so a gentle slope is crucial. In addition, since $|S(j\omega)|$ is inverted with the distance between the Nyquist plot of $L(j\omega)$ and critical point $-1+j0$, so the peak of $|S(j\omega)|$ should not be more than 6 dB in these frequencies.

Based on the distribution system with detailed D-STATCOM model described in Section 7.1, the specifications for the load voltage control performance are as follows:

1. Zero steady-state tracking error.

2. At least 40 dB of disturbance rejection at low frequency.

3. The output $y(t)$ must be relatively insensitive to the sensor noise $n(t)$ at high frequency.

4. The gain margin should be greater than 5 dB and the phase margin should be greater than 50°.

Satisfying the specifications 1 and 2 requires the proportional-plus-integral regulators in the controller. To adjust the frequency response of the system to satisfy the specifications 3 and 4, lead or lag compensators may be used. The designed controller for the load voltage control is shown in Figure 5.7. By using the software in MATLAB for adjusting the open loop transfer function $L(j\omega)$ to satisfy the loop shaping specifications described above, the controller parameters and the stability margins for R and RL load with various operating conditions, each corresponding to a different value of i_{fq} are obtained and presented in Tables 7.1 and 7.2, respectively. As can be seen in these Tables, the controller parameters are selected when the gain and phase margin more than 5 dB and 50 deg, respectively.

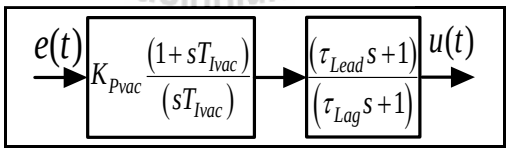

Figure 7.7 Designed controller for the load voltage control

Table 7.1 Controller parameters and the stability margins for the R load

Operating conditions		Controller parameters				Stability margins	
$v_s(kV)$	$i_{fq}(A)$	K_{Pvac}	T_{Ivac}	τ_{Lead}	τ_{Lag}	$GM(dB)$	$PM(deg)$
15.50	+1200	-0.2700	0.001	0.0000	0.00001	5.17	67.97
14.92	+1000	-0.3400	0.001	0.0000	0.00001	5.10	66.59
14.34	+800	-0.4400	0.001	0.0000	0.00001	5.14	66.05
13.76	+600	-0.6200	0.001	0.0000	0.00001	5.01	65.24
13.20	+400	-0.0220	0.0001	0.0000	0.00001	20.57	50.71
12.64	+200	-0.0160	0.0001	0.0000	0.00001	9.61	50.98
12.10	0	-0.0130	0.0001	0.0000	0.00001	6.11	50.85
11.56	-200	-0.0102	0.0001	0.0000	0.00001	5.04	54.38
11.04	-400	-0.0079	0.0001	0.0000	0.00001	5.03	59.31
10.54	-600	-0.0065	0.0001	0.0000	0.00001	5.02	62.08
10.05	-800	-0.0055	0.0001	0.0000	0.00001	5.11	63.95
9.58	-1000	-0.0049	0.0001	0.0000	0.00001	5.03	64.35
9.14	-1200	-0.0044	0.0001	0.0000	0.00001	5.02	64.60

Table 7.2 Controller parameters and the stability margins for the RL load

Operating conditions		Controller parameters				Stability margins	
$v_s(kV)$	$i_{fq}(A)$	K_{Pvac}	T_{Ivac}	τ_{Lead}	τ_{Lag}	$GM(dB)$	$PM(deg)$
17.08	+1200	-0.20000	0.00100	0.0000	0.00001	7.52	51.14
16.48	+1000	-0.30000	0.00100	0.0000	0.00001	5.92	50.01
15.88	+800	-0.35000	0.00100	0.0000	0.00001	6.85	50.13
15.29	+600	-0.40000	0.00100	0.0000	0.00001	8.52	50.87
14.71	+400	-0.50000	0.00100	0.0000	0.00001	10.48	54.42
14.13	+200	-0.01000	0.00010	0.0000	0.00300	18.25	52.17
13.56	0	-0.00950	0.00010	0.0000	0.00300	16.57	51.01
13.00	-200	-0.00900	0.00010	0.0000	0.00300	12.84	50.03
12.44	-400	-0.00800	0.00010	0.0000	0.00300	11.12	50.93
11.90	-600	-0.00750	0.00010	0.0000	0.00300	9.61	50.44
11.37	-800	-0.00700	0.00010	0.0000	0.00300	8.52	50.16
10.86	-1000	-0.00650	0.00010	0.0000	0.00300	7.71	50.13
10.36	-1200	-0.00600	0.00010	0.0000	0.00300	7.12	50.40

To illustrate the classical loop shaping technique, the bode plots of the open loop transfer function $L(s)$, the sensitivity function $S(s)$ and the complementary sensitivity function $T(s)$ of the system with RL load when the reactive currents are +1200*A* and -1200*A* are demonstrated in Figure 7.8 and 7.9, respectively. As seen in

these figures, the Low frequency, Medium or Crossover frequency and High frequency are selected between 0 – 1 red/sec, 1 - 2×10^4 red/sec, and 2×10^4 - ∞ red/sec, respectively. At Low frequency, $|S(j\omega)|$ is less than -40 dB while $|T(j\omega)|\approx1$ dB, so that $|L(j\omega)|$ is more than +40 dB in this frequency. For the High frequency, $|S(j\omega)|$ is about 1dB while $|T(j\omega)|$ is attenuated rapidly, so that $|L(j\omega)|$ is attenuated rapidly in this frequency as well. At the Medium or Crossover frequency, the slope of $|L(j\omega)|$ near the gain crossover frequency is about -20 dB/decade that corresponds to the phase margin is about 50 deg whereas the peak of $|S(j\omega)|$ and $|T(j\omega)|$ in this frequency are about +5 dB and 0 dB, respectively. Meanwhile, the Nyquits plots of the open loop transfer function are demonstrated in Figure 7.10. As can be seen in this figure, the dash line presents the Nyquits plot of the open loop transfer function when the reactive current is +1200*A*. Since this transfer function has two poles in the right-half *s* plane, in this case, the system is stable because the number of counterclockwise encirclements of the $-1+j0$ point is the same as the number of poles of the open loop transfer function in the right-half *s* plane. Whilst, the solid line in this figure presents the Nyquits plot of the open loop transfer function when the reactive current is -1200*A*. This is no pole of the open loop transfer function in the right-half *s* plane and no encirclement of the $-1+j0$ point. This implies that the system is stable.

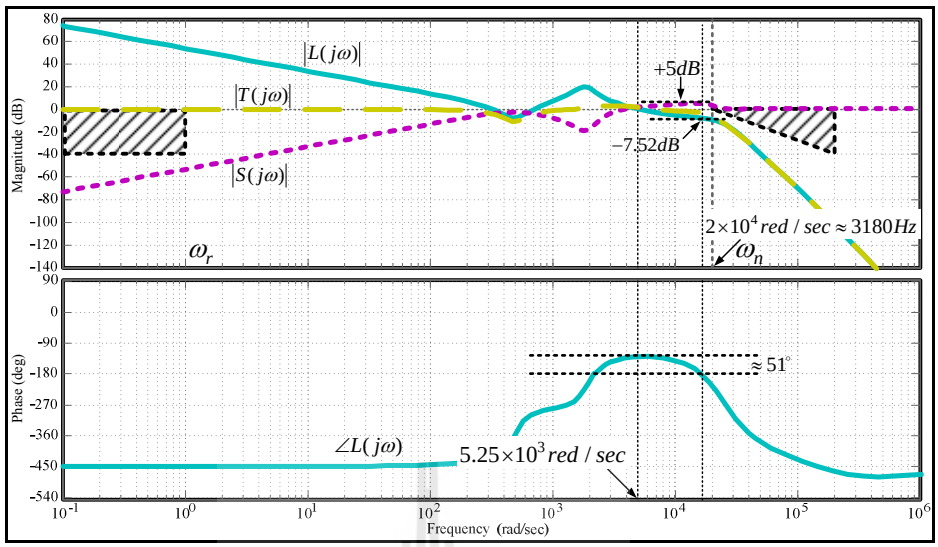

Figure 7.8 Bode plots of $L(s)$, $S(s)$ and $T(s)$ of the system with the RL load when the reactive current is +1200*A*

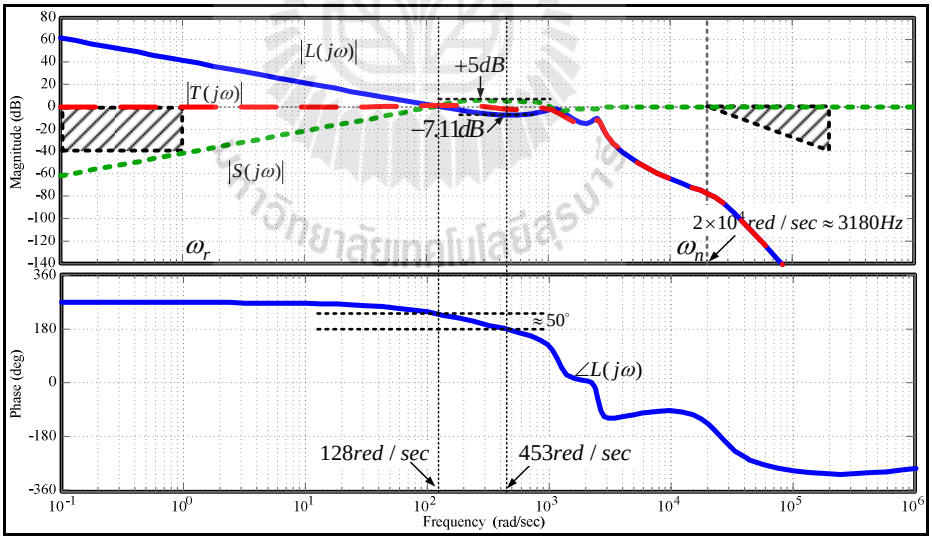

Figure 7.9 Bode plots of $L(s)$, $S(s)$ and $T(s)$ of the system with the RL load when the reactive current is -1200*A*

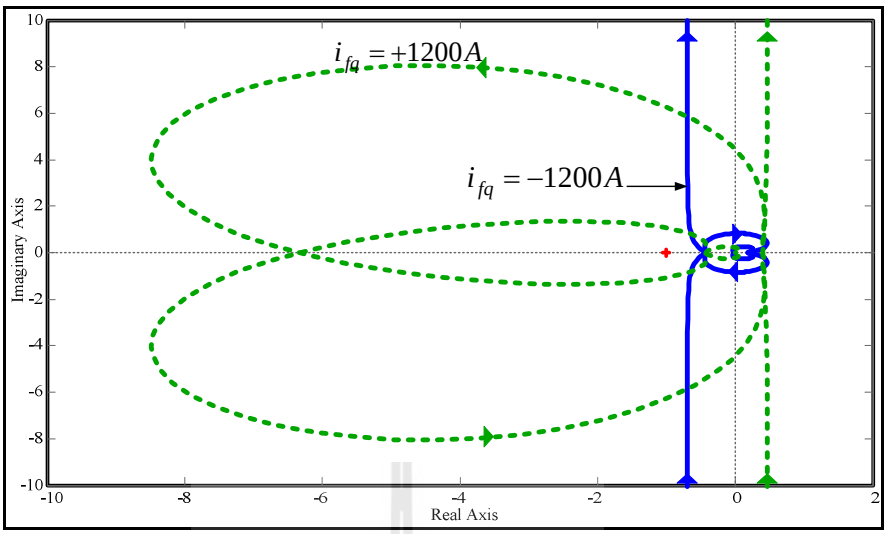

Figure 7.10 Nyquits plots of the open loop transfer function

In addition, the designed controller applied to the load voltage regulation when the load varied is investigated. The stability margins for the R and RL load with various operating conditions, each corresponding to a different value of i_{fq} are obtained and presented in Tables 7.3 and 7.4, respectively. For the R load, the load resistance is varied from 31.258 to 5.0386Ω that correspond to the reactive current i_{fq} for regulation the load voltage at a desired value (11.00*kV*) that are varied from +400 to -1200*A* as shown in Table 7.3. As can be seen in this table, the desired controller in the case of source voltage variations can be used in that of load variations. All gain margins in this case are more than 5 dB while most phase margins are more than 50 deg accepted when the load resistance is 31.2580Ω. However, all of operating conditions with each designed controller are stable. Meanwhile, for the RL load, the load resistance and inductance are varied from 57.9890 to 5.5743Ω and from 89.3990 to 8.5936 *mH*, respectively. These correspond to the reactive current i_{fq}

for regulation the load voltage at the desired value (11.00*kV*) that are varied from +400 to -1200*A* as shown in Table 7.4. Similar to the R load, all gain margins in this case are more than 5 dB while most phase margins are more than 50 deg accepted when the load resistance and inductance are 14.8649 Ω and 22.9163 *mH* and they are 11.1486 Ω and 17.1872 *mH*. However, all of operating conditions with each designed controller are stable.

The step responses of both cases of source voltage and the load variation with the designed controller for R and RL load are compared as shown in Figure 7.11 and 7.12, respectively. In these figures, the responses when the reactive currents are +400*A* and -1200*A* are compared. It can be seen in Figure 7.11, the response in case of load variations when the reactive current is +400*A* has a high frequency oscillation than the source voltage variations. Whilst, when the reactive current is -1200*A*, the response in case of source voltage variations reach the steady state faster than a case of load variations. Meanwhile, for RL load, the responses of both cases are close as shown in Figure 7.12.

Table 7.3 Stability margins in case of the R load when load variations

Operating conditions			**Controller parameters**				**Stability margins**	
$R_L(\Omega)$	$L_L(mH)$	$i_{fq}(A)$	K_{Pvac}	T_{Ivac}	τ_{Lead}	τ_{Lag}	$GM(dB)$	$PM(deg)$
31.2580	0.0000	+400	-0.0220	0.0001	0.0000	0.00001	33.10	39.80
14.2170	0.0000	+200	-0.0160	0.0001	0.0000	0.00001	8.57	54.34
10.0833	0.0000	0	-0.0130	0.0001	0.0000	0.00001	6.11	50.85
8.1272	0.0000	-200	-0.0102	0.0001	0.0000	0.00001	6.62	54.59
6.9978	0.0000	-400	-0.0079	0.0001	0.0000	0.00001	7.87	60.17
6.2517	0.0000	-600	-0.0065	0.0001	0.0000	0.00001	8.87	64.01
5.7273	0.0000	-800	-0.0055	0.0001	0.0000	0.00001	9.77	67.09
5.3381	0.0000	-1000	-0.0049	0.0001	0.0000	0.00001	10.31	68.93
5.0386	0.0000	-1200	-0.0044	0.0001	0.0000	0.00001	10.83	70.59

Table 7.4 Stability margins in case of the RL load when load variations

Operating conditions			Controller parameters				Stability margins	
$R_L(\Omega)$	$L_L(mH)$	$i_{fq}(A)$	K_{Pvac}	T_{Ivac}	τ_{Lead}	τ_{Lag}	$GM\,(dB)$	$PM\,(deg)$
57.9890	89.3990	+400	-0.5000	0.00100	0.0000	0.00001	10.53	53.85
23.1140	35.6336	+200	-0.0100	0.00010	0.0000	0.00300	11.08	50.22
14.8649	22.9163	0	-0.0095	0.00010	0.0000	0.00300	12.41	48.69
11.1486	17.1872	-200	-0.0090	0.00010	0.0000	0.00300	10.99	48.06
9.0823	14.0016	-400	-0.0080	0.00010	0.0000	0.00300	10.50	50.07
7.7346	11.9240	-600	-0.0075	0.00010	0.0000	0.00300	9.94	51.00
6.7954	10.4760	-800	-0.0070	0.00010	0.0000	0.00300	9.64	52.41
6.1028	9.4083	-1000	-0.0065	0.00010	0.0000	0.00300	9.53	54.21
5.5743	8.5936	-1200	-0.0060	0.00010	0.0000	0.00300	9.39	56.56

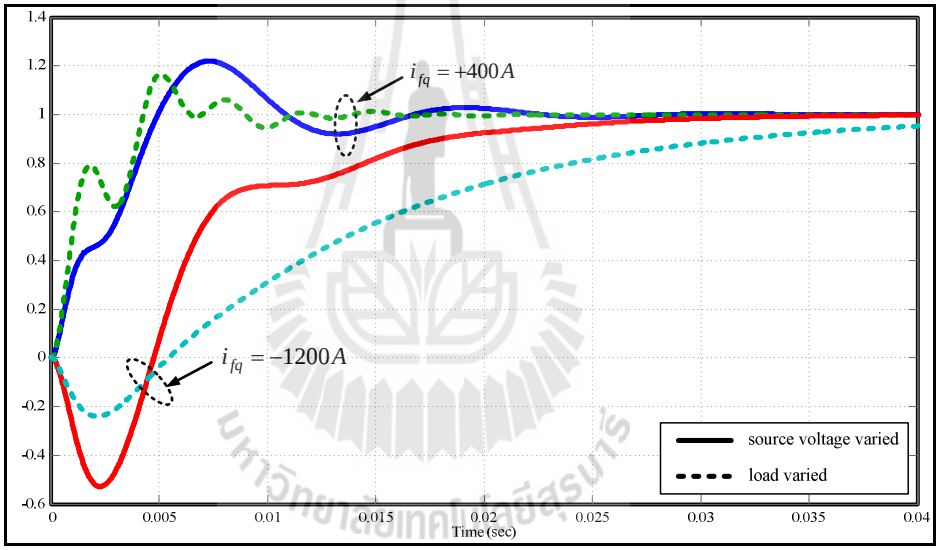

Figure 7.11 Comparison step responses in cases of source voltage and the load variations for the R load

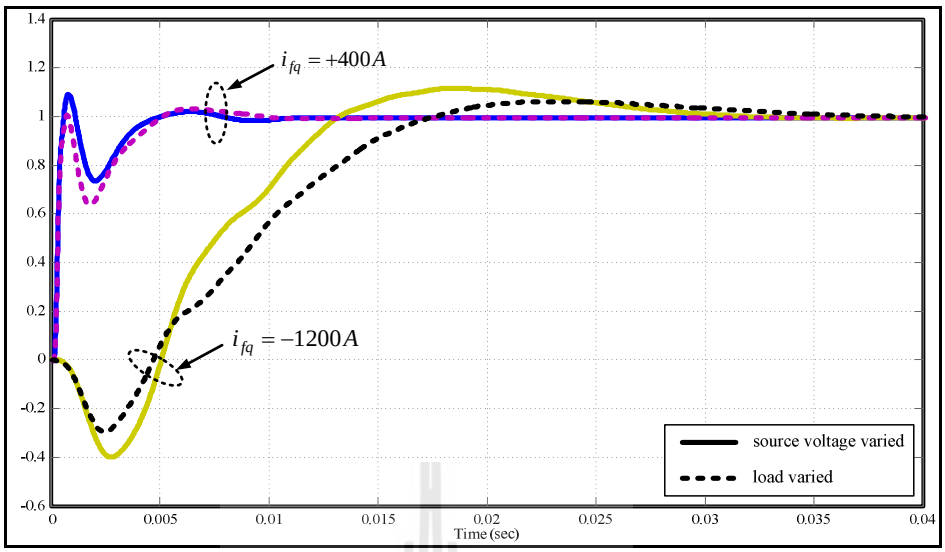

Figure 7.12 Comparison step responses in cases of source voltage and the load variations for the RL load

7.3 Tuning Controller Parameters

In previous Section, the controller parameters in each operating conditions are selected when the gain and phase margin of open loop transfer function are considered. However, the response of the load voltage control is unconsidered for obtaining the controller parameters. In this Section, the controller parameters are obtained by considering the gain margin, phase margin and the load voltage control response. There exist many different approaches to tune controller's parameters. However, in this section, the GAs is selected to build up an algorithm to tune parameters (i.e. K_{Pvac}, T_{Ivac}, τ_{Lead} and τ_{Lag}) of the load voltage control. Let $P(s)$ in Figure 7.13 represents the transfer function of $\frac{\Delta v_{td}(s)}{\Delta i^{*}_{fd}(s)}$ each operating condition that correspond to a different value of i_{fq} and $C(s)$ be the controllers with each operating

condition. For each of the controllers we assume a control structure with the dynamic model consisting of the PI controller and lead-lag stage as can be seen in Figure 7.7. The main consideration is that the set of the four parameters K_{Pvac}, T_{Ivac}, τ_{Lead} and τ_{Lag} each operating condition to be searched by the GAs. In this load voltage control of the distribution system with D-STATCOM, the procedure to perform the proposed parameter tuning is described as follows. First, time-domain step response results of magnitude and frequency swing obtained by using the step response of the load voltage control in MATLAB. Second, the Genetic Algorithms (GADS TOOLBOX) is employed to generate a set of initial random parameters. With the searching process, the parameters are adjusted to give response of best fitting close to the desired step response. Furthermore, the gain and phase margins are considered as operating constraints on this proposed parameter tuning. To perform the searching properly, its objective function with the operating constraint is the key. The objective function is defined to be the sum of square error between the desired step response and the step response of the load voltage control. The constraint set comprises the gain and phase margin requirement for the control system has enough stability margins.

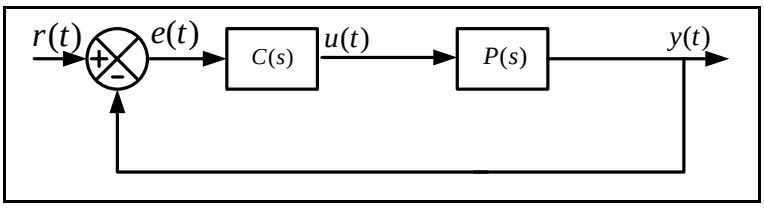

Figure 7.13 Closed loop of unity feedback SISO system setup

Therefore, the tuning problem each operating condition can be formulated as the following optimization problem:

$$\text{Minimize} \qquad \sum_{k=1}^{N}\left(\Delta v_{ac}(k)\right)^2 \tag{7.36}$$

Subject to

$Gm \geq 5dB$ and $Pm \geq 50^{\circ}$

Where $\Delta v_{ac} = v_{ac,desired} - v_{ac,step}$

$v_{ac,desired}$ is the desired step response.

$v_{ac,step}$ is the step response of the load voltage control.

Gm and Pm are gain and phase margin requirement, respectively.

Table 7.5 Controller parameters, stability margins and fitness for the R load

Operating conditions		Controller parameters				Stability margins		Fitness
$v_s(kV$	$i_{fq}(A)$	K_{Pvac}	T_{Ivac}	τ_{Lead}	τ_{Lag}	$GM(dB)$	$PM(deg)$	
15.50	+1200	-0.22413	0.00145	0.00006	0.00000	5.62	98.84	28.83
14.92	+1000	-0.15162	0.00097	0.00088	0.00037	5.09	81.88	26.16
14.34	+800	-0.20890	0.00135	0.00016	0.00000	5.06	95.01	24.09
13.76	+600	-0.22183	0.00132	0.00021	0.00000	5.34	90.45	20.89
13.20	+400	-0.19587	0.00107	0.00060	0.00010	5.58	85.37	16.25
12.64	+200	-0.19603	0.00095	0.00068	0.00001	6.39	76.53	11.49
12.10	0	-0.11694	0.00078	0.00044	0.00000	5.66	66.92	16.17
11.56	-200	-0.24673	0.00226	0.00070	0.00273	5.26	57.88	26.83
11.04	-400	-0.00790	0.00010	0.00196	0.00222	5.68	57.55	44.43
10.54	-600	-0.00650	0.00009	0.00140	0.00180	5.10	55.24	56.37
10.05	-800	-0.00573	0.00009	0.00178	0.00238	5.30	55.24	70.19
9.58	-1000	-0.00490	0.00009	0.00006	0.00087	5.05	55.23	113.58
9.14	-1200	-0.28493	0.00560	0.00001	0.00651	5.01	57.09	158.97

Table 7.6 Controller parameters, stability margins and fitness for the RL load

Operating conditions		Controller parameters				Stability margins		Fitness
$v_s(kV)$	$i_{fq}(A)$	K_{Pvac}	T_{Ivac}	τ_{Lead}	τ_{Lag}	$GM(dB)$	$PM(deg)$	
17.08	+1200	-0.27819	0.00131	0.00470	0.00481	5.11	55.18	23.17
16.48	+1000	-0.32224	0.00034	0.00003	0.00000	5.28	50.27	19.95
15.88	+800	-0.44963	0.00043	0.00002	0.00000	5.03	50.05	15.98
15.29	+600	-0.61318	0.00036	0.00003	0.00000	5.02	50.06	9.38
14.71	+400	-0.88247	0.00029	0.00004	0.00000	5.28	50.51	3.15
14.13	+200	-0.00592	0.00006	-0.00020	0.00112	10.03	63.49	53.63
13.56	0	-0.02354	0.00019	-0.00040	0.00124	7.62	53.54	53.12
13.00	-200	-0.03836	0.00036	-0.00022	0.00180	7.42	53.51	67.43
12.44	-400	-0.00836	0.00010	-0.00030	0.00137	6.14	57.21	61.88
11.90	-600	-0.00750	0.00010	-0.00050	0.00141	5.39	55.68	72.27
11.37	-800	-0.00700	0.00010	-0.00003	0.00183	5.60	56.99	84.55
10.86	-1000	-0.00650	0.00010	-0.00008	0.00190	5.11	55.72	96.70
10.36	-1200	-0.00600	0.00010	0.00000	0.00209	5.01	55.21	114.85

With 30 computational trials in each test case of the parameter tuning based on the GAs, the best parameters are obtained. The best controller parameters, fitness value and the stability margins in each operating condition for R and RL load are shown in Table 7.5 and Table 7.6, respectively. As can be seen in these Tables, gain margins and phase margins in these operating conditions are more than 5 dB and 50 deg, respectively.

The step responds of the parameter tuning based on the classical loop shaping and GAs methods are compared as shown in Figure 7.15 and Figure 7.16. In Figure 7.15, the step responds of the system with the R load are presented whereas the step responds of the system with the RL load are indicated in Figure 7.16. In these figures, the D-STATCOM reactive currents as +1,200 and -1,200 *A* are presented. The comparisons show that the responds of both the classical loop shaping and the genetic algorithms methods are close. However, the genetic algorithms methods tuning gives smaller settling time and also smaller overshoot but it is not significant.

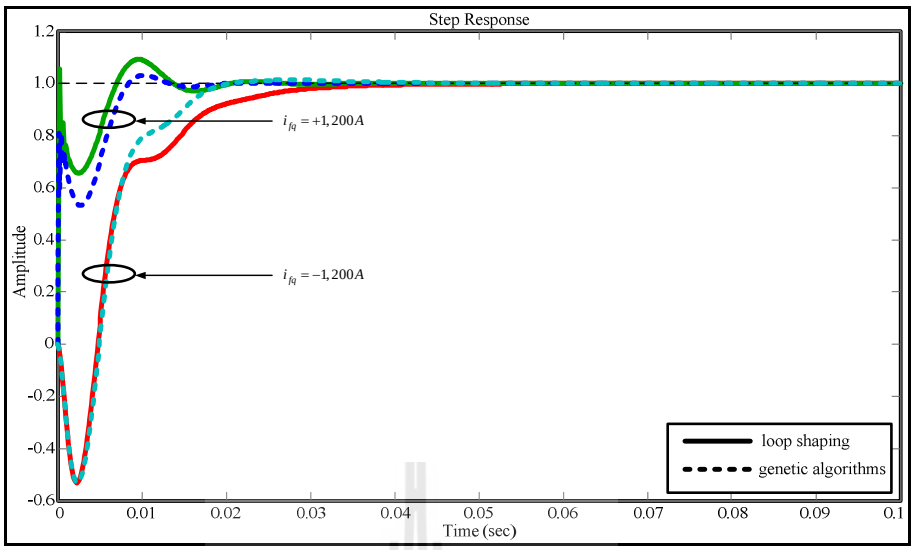

Figure 7.14 Comparison step responses in cases of loop shaping and genetic algorithms tuning for the system with the R load

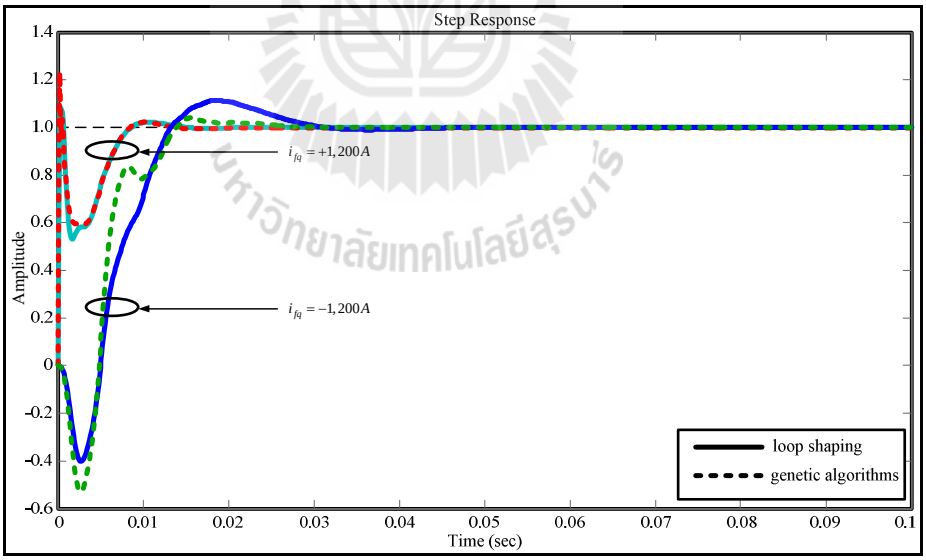

Figure 7.15 Comparison step responses in cases of loop shaping and genetic algorithms tuning for the system with the RL load

7.4 Summary

This chapter presents the AC voltage control design for the load voltage regulation by using the D-STATCOM. The D-STATCOM model and its control were integrated with the power distribution systems that are used for the load voltage controller design. This derived model is exact and can be used for the load voltage controller design using linear techniques. The classical loop shaping method is applied to the load voltage controller design. The classical loop shaping is a graphical procedure to design a proper controller satisfying the requirements on stability and performance. The basic idea of the method is to construct the open loop transfer function to satisfy the requirements performance and stability criterion approximately, and then to obtain the controller.

In this chapter, the specifications for the load voltage control performance are 1) zero steady-state tracking error, 2) at least 40 dB of disturbance rejection at low frequency, 3) the output must be relatively insensitive to the sensor noise at high frequency and 4) the gain margin should be greater than 5 dB and the phase margin should be greater than 50°. To satisfy the specifications the proportional-plus-integral regulators with the lag compensator is used. By using the software in MATLAB for adjusting the open loop transfer function to satisfy the loop shaping specifications, the controller parameters with various operating conditions, each corresponding to a different value of i_{fq} are obtained. In addition, the tuning controller parameters based on the genetic algorithms is proposed in this chapter. The step responds of the parameter tuning based on the classical loop shaping and GAs methods are compared. From the comparison, the responds of both the classical loop shaping and the genetic algorithms methods are close.

CHAPTER VIII

APPLICATION OF D-STATCOM FOR LOAD VOLTAGE REGULATION

This chapter presents the application of the D-STATCOM with the proposed design control technique for load voltage regulation. The D-STATCOM systems usually consists of a voltage source converter (VSC) which dynamically injects a current of desired amplitude, frequency and phase into the grid line in order to mitigate sags at the point of common coupling (PCC). The decoupling current control of the D-STATCOM with the parameters tuning based on the genetic algorithm (CC-GA) and the DC voltage control with an elimination term of $u_q i_{fq}$ based on the symmetrical optimum method (DCVC-SO) are used. Meanwhile, the AC voltage control based on the classical loop shaping is applied to many cases in this chapter. In this chapter a simplified 22-*kV*, 2-bus test power system is employed for the simulation. The remainder of this chapter is organized as follows. The next section presents a brief review of the D-STATCOM system. The applications of D-STATCOM for load voltage regulation of the distribution system with the R and RL loads are discussed in Section 8.2. In Section 8.3, the applications of the D-STATCOM in the distribution system with the distributed generators are presented. A summary of this chapter is presented in Section 8.4.

8.1 Brief Review of the D-STATCOM for Voltage Regulation

Recently, the distribution static synchronous compensator (D-STATCOM) has been introduced to distribution systems to manage the system reactive power and regulate the voltage at the point of common coupling. A D-STATCOM usually consists of a shunt connected voltage source converter (VSC). The benefits of using a VSC are sinusoidal currents, high current bandwidth, and controllable reactive power to regulate the bus voltage level. A system with these characteristics can be used to inject a controllable current into the system. By injecting a popper current into the system, a shunt connected VSC can boost the voltages at that point during a voltage sags. The configuration of the D-STATCOM with the proposed control that connected to the distribution system for regulating the load voltage is illustrated in Figure 8.1. The D-STATCOM consists of a three-phase voltage source converter (VSC), a DC-side capacitor C_{dc} with parallel resistance R_{dc}. The resistance R_{dc} represents losses in the converter. Two kinds of losses are of interest in such the converter configurations which are conduction losses and switching losses. The losses are both in the diodes and in the switches such as IGBT and MOSFET (Blaabjerg et al., 1996). An inductance L_f and the resistance R_f represent the inductance and resistance of the AC-side of the converter. A shunt filter capacitor with capacitance C_f is added to the AC-side of the voltage source converter that forms a LC filter. This filter helps in effectively filtering out the switching ripple in the output voltage waveform. The distribution system is represented by using an ideal voltage source and impedance. This impedance consists of an inductance L_s and a resistance R_s which characterizes the transformer and power line respectively. The analysis and design of the D-

STATCOM controller are conducted in the rotating reference frame which is synchronized to the voltage vector at the PCC. As explained earlier in previous, the D-STATCOM mitigates the voltage sags by dynamically injecting a current of desired amplitude and phase angle into the system. A schematic diagram of the D-STATCOM with the proposed control is presented in Figure 6.1. The current control in Figure 6.1 force the converter currents i_{fd} and i_{fq} to follow the command currents i_{fd}^{*} and i_{fq}^{*} respectively. The command i_{fd}^{*} to the *d*-axis current loop is obtained by the DC voltage controller while the command i_{fq}^{*} is obtained from the AC voltage controller. The purpose of the outer loop DC voltage controller is to regulate the DC voltage to a required level. The current controller and DC voltage controller design for this D-STATCOM are similar to the controller design presented in the Chapter 6, since they have the same structure and serve the same purpose. Meanwhile, the AC voltage controller design and parameters are explained in the Chapter 7.

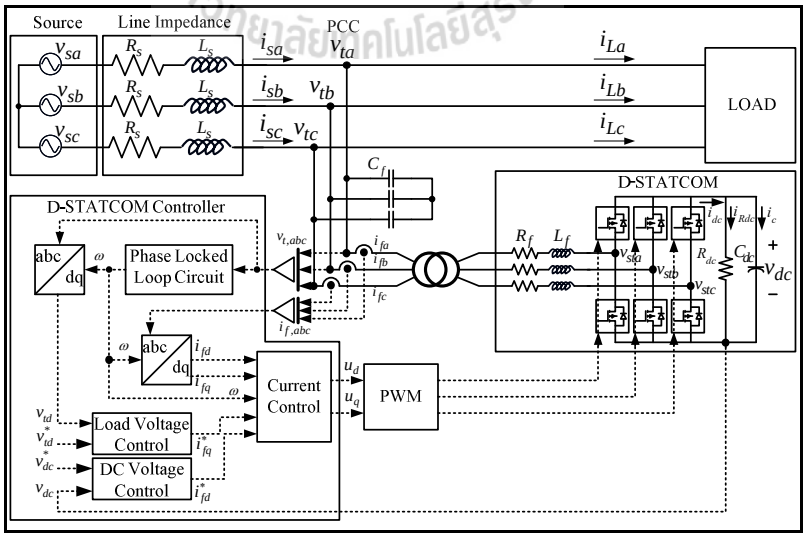

Figure 8.1 Overall schematic diagram of D-STATCOM for load voltage regulation

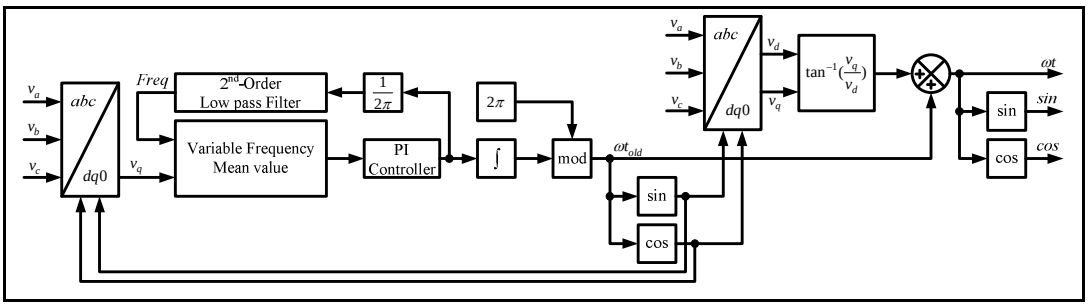

Figure 8.2 Modified PLL block diagram

In addition, the basic PLL block diagram in Figure 2.14 is modified in this chapter that can be seen in Figure 8.2. Since using the modified PLL, $v_{tq} \equiv 0$ for any times and v_{td} represents the instantaneous magnitude of the phase voltages, while i_{fq} denotes the instantaneous reactive current supplied by the D-STATCOM and is the control input to the system for the load voltage regulation.

8.2 Modeling and Simulation Results of the D-STATCOM for Load Voltage Regulation

In this section, the simulation results for the D-STATCOM with the proposed controller design will be presented. The configuration of the D-STATCOM system with the proposed controller designed for load voltage regulation that shown in Figure 8.1 is modeled using the MATLAB/SIMULINK software package. The model utilizes SIMULINK control and SimPower Blocks are illustrated in Figure 8.3 and Figure 8.4. In Figure 8.3, the D-STATCOM is connected with the system though the 22/2.2 *kV* (Y/Y) transformer. Figure 8.4 presents the model of the D-STATCOM controller. The

system data used are taken from the simplification network of a 166 buses Nakhonrachasima, Thailand at bus 99. The system parameters are

	V_s (L-L rms)	= 22 *kV*	L_s	= 38.666 *mH*
	R_s	= 1.4564 Ω	ω_s	= 100π $rad.s^{-1}$
	R_l	= 116.68 Ω	L_l	= 0.00 *mH* (for R load)
And	R_l	= 89.346 Ω	L_l	= 157.35 *mH* (for RL load)

According to the steady state analysis of the distribution system with D-STATCOM that discussed in the Chapter 3, the maximum load active power, $P_{l,desired}(\max)$, and minimum source voltage, $V_s(\min)$ of the system with the given parameters in the above are 34.85 *MW* and 4.93 *kV*, respectively. These correspond to the reactive power of regulating the load voltage as 22 *kV* is about 37.50 *MVar* for R load while 40.00 and 57.00 *MVar* for RL load with minimum source voltage and maximum load active power, respectively. However, a ± 15 *MVA* D-STATCOM is selected for load voltage regulation in this system. This D-STATCOM can regulate the load voltage as 22 *kV* when the source voltage is more than 15.40 *kV* (or 0.7 *pu*.). In addition, it can be used to regulate the load voltage as 22 *kV* when the load active power is less than 16.59 *MW* (or 4.0 *pu*.). The required reactive power for different source voltage is given in Table 8.1. Meanwhile, the required reactive power for different load power is given in Table 8.2. The parameters of the D-STATCOM that corresponding to source voltage sags and load power variations are shown in Table 8.3 and Table 8.4, respectively. However, the parameters of the D-STATCOM at the maximum required reactive power (13.82 *MVar*) are used in the section.

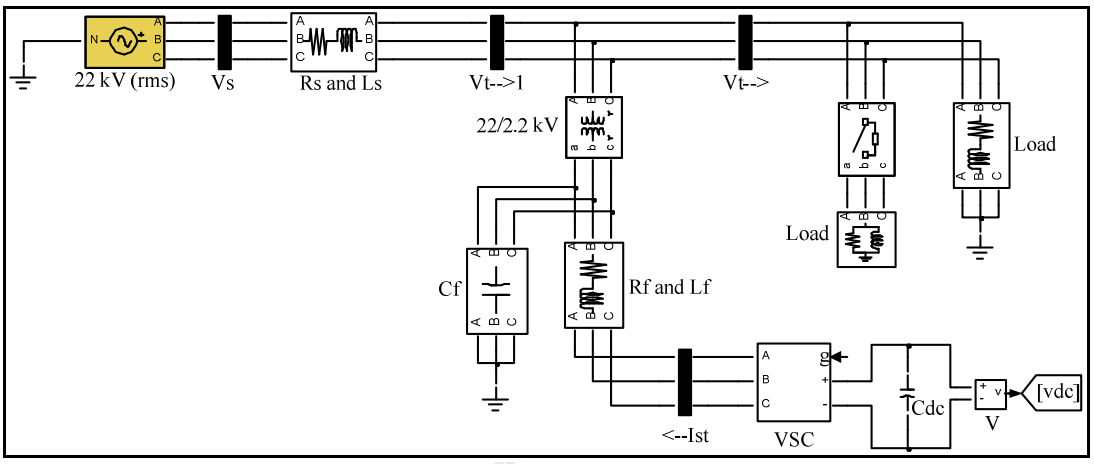

Figure 8.3 MATLAB/SIMULINK model of the distribution system with the D-STATCOM

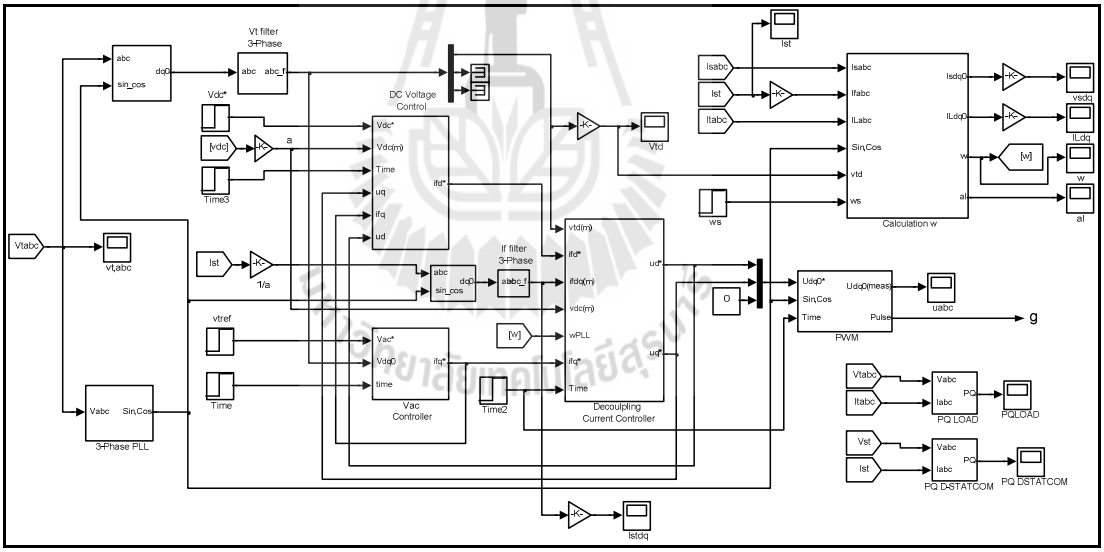

Figure 8.4 MATLAB/SIMULINK model of the D-STATCOM controller

Table 8.1 Required reactive power for different source voltage

Source voltage (*kV*)	Load as PF= 1.0	Load as PF= 0.875 lag
	Required reactive power (*MVar*)	Required reactive power (*MVar*)
28.60 (1.3 *pu*.)	12.90	10.61
26.40 (1.2 *pu*.)	8.88	6.59
24.20 (1.1 *pu*.)	4.85	2.55
22.00 (1.0 *pu*.)	0.80	-1.50
19.80 (0.9 *pu*.)	-3.27	-5.57
17.60 (0.8 *pu*.)	-7.37	-9.67
15.40 (0.7 *pu*.)	-11.52	-13.82

Table 8.2 Required reactive power for different load power

Load active power (*MW*)	Load as PF= 1.0	Load as PF= 0.875 lag
	Required reactive power (*MVar*)	Required reactive power (*MVar*)
0.415 (0.1 *pu*.)	1.47	1.24
2.074 (0.5 *pu*.)	1.22	0.07
4.148 (1.0 *pu*.)	0.80	-1.50
6.221 (1.5 *pu*.)	0.26	-3.18
8.295 (2.0 *pu*.)	-0.40	-4.99
10.369 (2.5 *pu*.)	-1.18	-6.92
12.442 (3.0 *pu*.)	-2.11	-9.00
14.520 (3.5 *pu*.)	-3.18	-11.22
16.590 (4.0 *pu*.)	-4.42	-13.60

Table 8.3 D-STATCOM parameters for different source voltage

Source voltage (*kv*)	Load as PF= 1.0				Load as PF= 0.875 lag			
	DC bus Voltage (*kV*)	Current Rating (*kA*)	AC Inductance (*mH*)	DC bus Capacitance (μF)	DC bus Voltage (*kV*)	Current Rating (*kA*)	AC Inductance (*mH*)	DC bus Capacitance (μF)
28.60	6.532	+58.644	0.1474	2984	6.532	+48.214	0.1793	2453
26.40	6.532	+40.366	0.2141	2054	6.532	+29.935	0.2887	1523
24.20	6.532	+22.032	0.3923	1121	6.532	+11.602	0.7450	590
22.00	6.532	+3.6260	2.3837	184	6.532	-6.805	1.2700	346
19.80	6.532	-14.879	0.5808	757	6.532	-25.310	0.3415	1288
17.60	6.532	-33.522	0.2578	1706	6.532	-43.953	0.1966	2236
15.40	6.532	-52.368	0.1650	2664	6.532	-62.799	0.1376	3195

Table 8.4 D-STATCOM parameters for different load power

Load active power (*MW*)	Load as *pf* = 1.0				Load as *pf* = 0.875 lag			
	DC bus Voltage (*kV*)	Current Rating (*kA*)	AC Inductance (*mH*)	DC bus Capacitance (μF)	DC bus Voltage (*kV*)	Current Rating (*A*)	AC Inductance (*mH*)	DC bus Capacitance (μF)
0.415	6.532	+6.674	1.2950	340	6.532	+5.632	1.5346	287
2.074	6.532	+5.527	1.5636	281	6.532	+0.312	27.7170	16
4.148	6.532	+3.626	2.3837	184	6.532	-6.805	1.2700	346
6.221	6.532	+1.190	7.2634	061	6.532	-14.456	0.5978	735
8.295	6.532	-1.803	4.7931	092	6.532	-22.664	0.3813	1153
10.369	6.532	-5.383	1.6054	274	6.532	-31.460	0.2747	1600
12.442	6.532	-9.590	0.9012	488	6.532	-40.882	0.2114	2080
14.520	6.532	-14.473	0.5972	736	6.532	-50.980	0.1695	2594
16.590	6.532	-20.098	0.4300	1023	6.532	-61.820	0.1398	3145

In this section, the simulation results of the D-STATCOM with the proposed controller design were presented in two cases: (i) voltage regulation when the distribution system with the R loads and (ii) voltage regulation when the distribution system with the RL loads.

8.2.1 Voltage Regulation when the Distribution System with the R Load

According to the current control and DC voltage control strategy described in Chapter 6, the decoupling current control based on GAs and the DC voltage control based on SO are used in this section. The parameters of the current and DC voltage control are shown in Table 8.5. Meanwhile, the AC voltage control with the classical loop shaping method that described in Chapter 7 is used for the R load. The AC voltage controller parameters and the stability margins for the R load with various operating conditions, each corresponding to a different value of source voltage (that means corresponding to a different i_{fq}) are presented in Table 8.6.

Table 8.5 Current and DC voltage controller parameters

Controller	Parameter
K_{Pid} and K_{Piq}	26,709.6
T_{Iid} and T_{Iiq}	3.7
K_{pvdc}	1,250
T_{Ivdc}	0.0016

Table 8.6 AC voltage controller for the distribution system with the R load

Source Voltage (*kV*)	PI Parameters	Compensator 1 Parameters	Compensator 2 Parameters	Gain Margin (*dB*)	Phase Margin (*deg*)
28.82	$0.042\left(\frac{0.0014s+1}{0.0014s}\right)$	$\frac{1}{0.00001s+1}$	1	10.92	51.10
27.59	$0.049\left(\frac{0.0014s+1}{0.0014s}\right)$	$\frac{1}{0.00001s+1}$	1	11.46	51.18
26.40	$0.056\left(\frac{0.0014s+1}{0.0014s}\right)$	$\frac{1}{0.00001s+1}$	1	12.35	51.78
25.19	$0.063\left(\frac{0.0014s+1}{0.0014s}\right)$	$\frac{1}{0.00001s+1}$	1	14.17	53.94
23.98	$0.070\left(\frac{0.0014s+1}{0.0014s}\right)$	$\frac{1}{0.00001s+1}$	1	17.00	61.57
22.77	$0.002\left(\frac{0.0001s+1}{0.0001s}\right)$	$\frac{1}{0.0013s+1}$	1	13.16	64.19
21.56	$0.0002\left(\frac{0.00001s+1}{0.00001s}\right)$	$\frac{1}{0.0013s+1}$	1	7.56	60.41
20.35	$0.00018\left(\frac{0.00001s+1}{0.00001s}\right)$	$\frac{1}{0.0016s+1}$	1	6.16	57.90
19.14	$0.00016\left(\frac{0.00001s+1}{0.00001s}\right)$	$\frac{1}{0.0020s+1}$	1	5.84	55.76
17.93	$0.00014\left(\frac{0.00001s+1}{0.00001s}\right)$	$\frac{1}{0.0024s+1}$	1	6.13	55.24
16.81	$0.00012\left(\frac{0.00001s+1}{0.00001s}\right)$	$\frac{1}{0.0027s+1}$	1	6.44	56.44
15.62	$0.00012\left(\frac{0.00001s+1}{0.00001s}\right)$	$\frac{1}{0.0027s+1}$	1	5.02	54.00
14.41	$0.00010\left(\frac{0.00001s+1}{0.00001s}\right)$	$\frac{1}{0.0027s+1}$	1	5.16	58.04

The controllers that are designed in each source voltage operation points i.e. 28.82, 26.40 and 23.93 *kV* (i_{fq} = +600, +400 and +200A) for the load voltage regulation in case of the source voltage variations between 28.82 and 23.98

kV are demonstrated and compared as shown in Figure 8.5. As can be seen in this Figure, the controller that is designed in case of the source voltage as 23.93 *kV* (i_{fq} = +200*A*) cannot be used for the source voltage as 28.82 *kV* (i_{fq} = +600*A*) and the controller that is designed in case of the source voltage as 26.40 *kV* (i_{fq} = +400*A*) gives the high overshoot and oscillation response in some case. Whilst, the controller that is designed in case of the source voltage as 28.82 *kV* (i_{fq} = +600*A*) can be used for all cases and gives a good dynamic response.

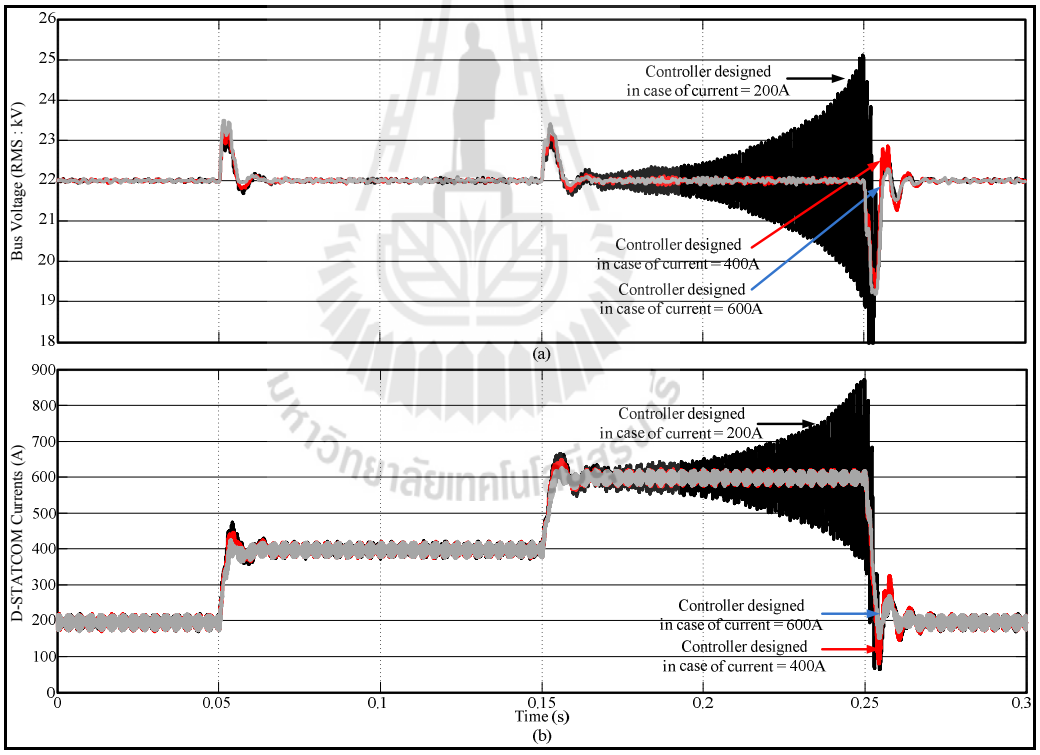

Figure 8.5 Comparison the controller in case of the source voltage variations between 28.82 and 23.98 *kV*

Similarly, the controllers that are designed in each source voltage operation points i.e. 21.56, 19.14, 16.18 and 14.41 kV (i_{fq} = 0, -200, -400 and -600A) for the load voltage regulation in case of the source voltage variations between 21.56 and 14.41 kV are demonstrated and compared as shown in Figure 8.6. As can be seen in this Figure, the controller that is designed in case of the source voltage as 14.41 kV (i_{fq} = -600A) can be used for all cases and gives a good dynamic response.

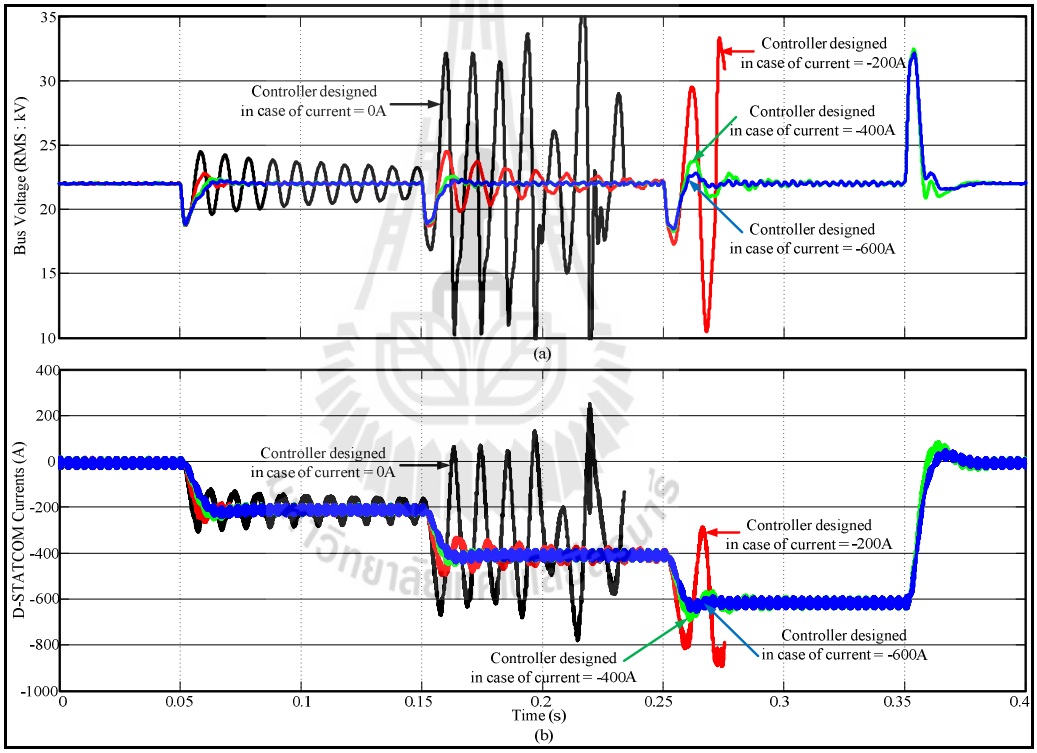

Figure 8.6 Comparison the controller in case of the source voltage variations between 21.56 and 14.41 kV

Therefore, the parameters of PI controller and the compensator when the source voltage of 28.82 kV are used in case of the source voltage variations

between 28.82 and 23.98 *kV* (i.e. i_{fq} varies between +600 and +200 *A*). Whilst, the parameters of PI controller and the compensator when the source voltage of 14.41 *kV* are used in case of the source voltage variations between 22.77 and 14.41 *kV* (i.e. i_{fq} varies between +100 and -600 *A*).

In this case, the system is simulated for time varying source voltage conditions. The dash lines of figure 8.7(a) shows the load voltage of the system without D-STATCOM when the source voltage is varied. As may be seen, the load voltage corresponds to five different source voltage conditions: source voltage of 23.98 *kV* from t = 0.00 to 0.05 second; source voltage of 27.59 *kV* from t = 0.05 to 0.15 second; source voltage at 25.19 *kV* from t = 0.15 to 0.25 second; source voltage of 28.82 *kV* from t = 0.25 to 0.35 second; and source voltage of 23.98 *kV* from t = 0.35 to 0.40 second. Meanwhile, the solid line of figure 8.7(a) shows the load voltage of the system with D-STATCOM when the source voltage is varied. It can be observed from this figure that the D-STATCOM with proposed control design can be regulated the load voltage at the desired value. The load voltage took approximately 0.01 seconds to settle in each source voltage. It can be seen in figure 8.7(b) that the load voltage waveform reaches the desired value within a haft cycle.

Figure 8.8 presents the currents, DC voltage and power of the D-STATCOM for the system with R load when the source voltage is varied between 28.82 and 23.98 *kV*. As may be seen in figure 8.8(a), that the reactive currents (i_{fq}) are +200, +500, +300, +600 and +200 *A* to compensate the load voltage swell when the source voltages are 23.98, 27.59, 25.19, 28.82 and 23.98 *kV*, respectively. Whilst, the active current (i_{fd}) very small change when the D-STATCOM compensate the

load voltage. These correspond to the reactive and active powers of the D-STATCOM as shown in Figure 8.8(b). The reactive powers are -4.4, -10.1, -6.6, -13.2 and -4.4 *MVar* to compensate the load voltage swell when the source voltages are 23.98, 27.59, 25.19, 28.82 and 23.98 *kV*, respectively. Meanwhile, the active power very small change in positive when the D-STATCOM compensation the load voltage. This means that the D-STATCOM consumes active power to regulate the DC voltage at the constant value as can be seen in figure 8.8(c). As seen in this figure, the DC voltage is always regulated at 6.6 *kV* for all of source voltages.

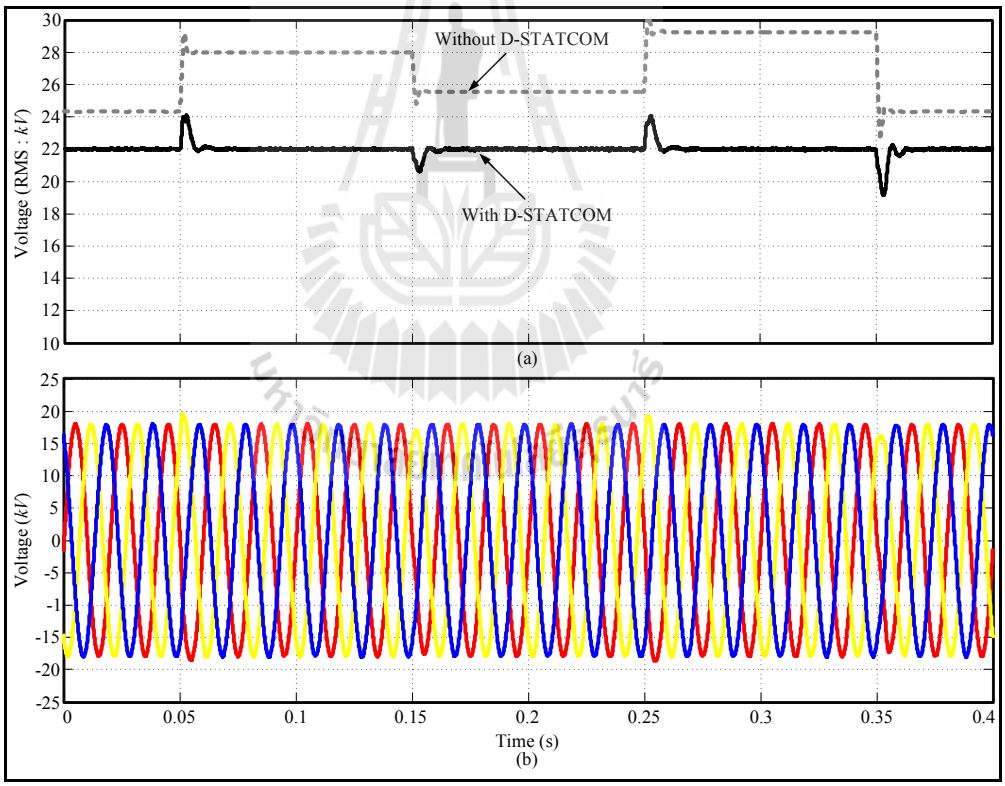

Figure 8.7 Load voltage of the system with the R load which the source voltage varying between 28.82 and 23.98 *kV*

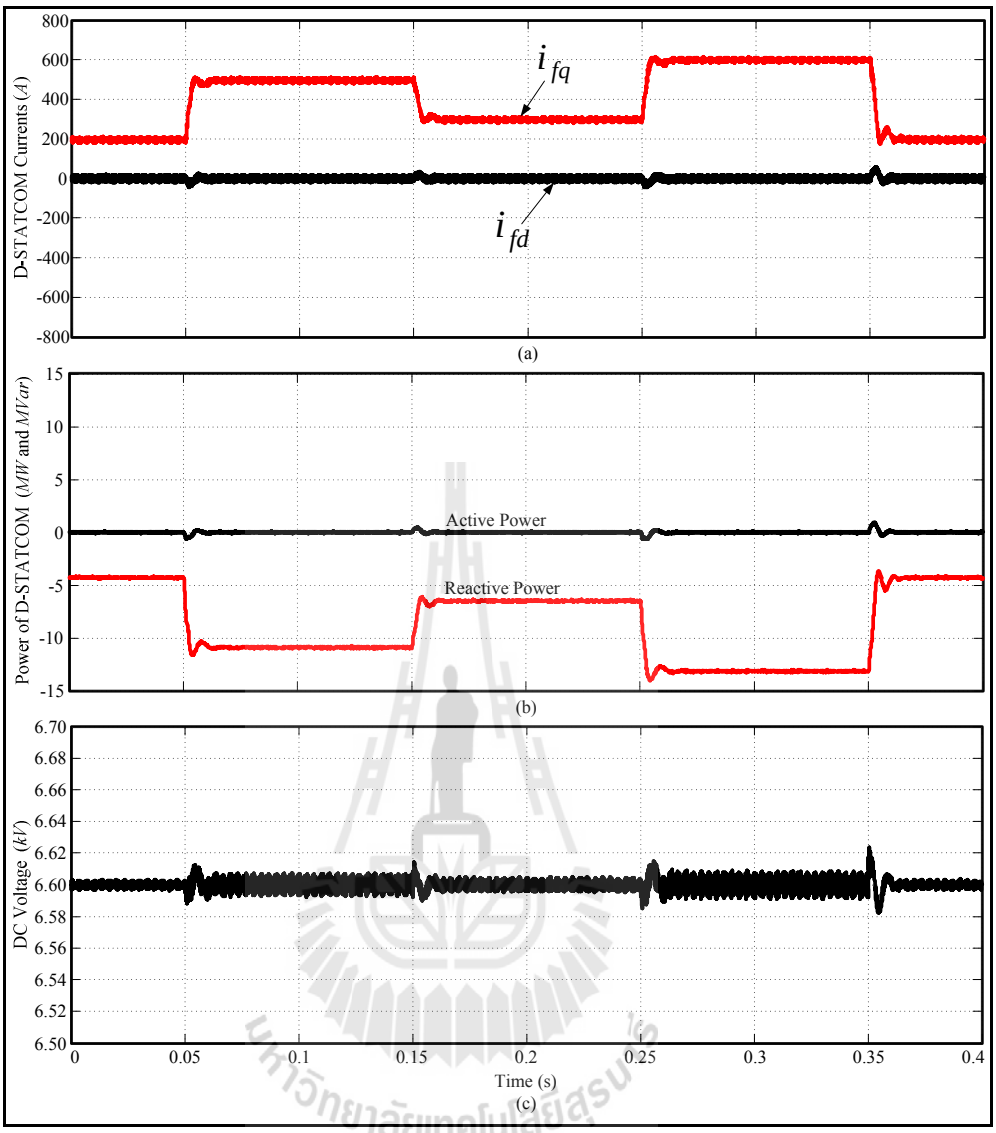

Figure 8.8 Currents, DC voltage and power of the D-STATCOM for the system with the R load which the source voltage varying between 28.82 and 23.98 *kV*

In case of the source voltage varying between 22.77 and 14.41 *kV*, the load voltage of the system with the R load is shown in Figure 8.9. The dashes line of Figure 8.9(a) shows the load voltage of the system without D-STATCOM when the source voltage is varied. As seen in this Figure, the load voltage corresponds to five

different source voltage conditions: source voltage of 21.56 *kV* from t = 0.00 to 0.05 second; source voltage of 17.93 *kV* from t = 0.05 to 0.15 second; source voltage at 22.77 *kV* from t = 0.15 to 0.25 second; source voltage of 14.41 *kV* from t = 0.25 to 0.35 second; and source voltage of 21.56 *kV* from t = 0.35 to 0.40 second. Whilst, the solid line of Figure 8.9(a) shows the load voltage of the system with D-STATCOM. As can be observed from this Figure that the D-STATCOM with proposed control design can be regulated the load voltage at the desired value. The load voltage took approximately 0.02 seconds to settle in each source voltage. As can be seen in Figure 8.9(b), the load voltage reaches the desired value within one cycle.

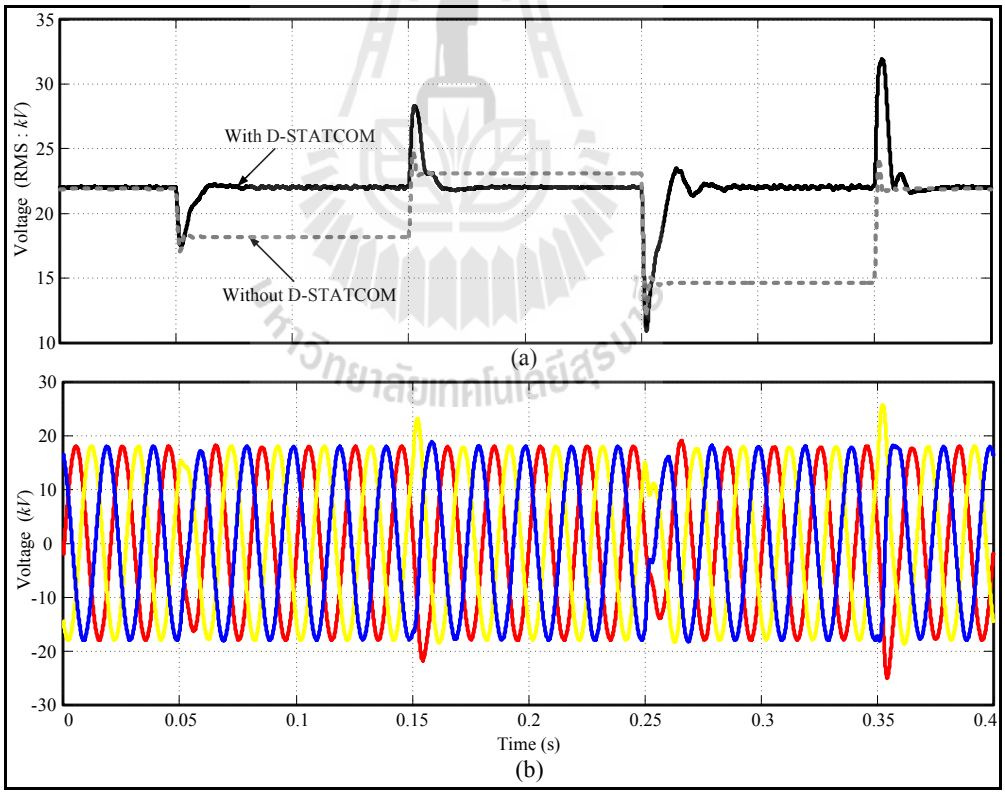

Figure 8.9 Load voltage of the system with the R load which the source voltage varying between 22.77 and 14.41 *kV*

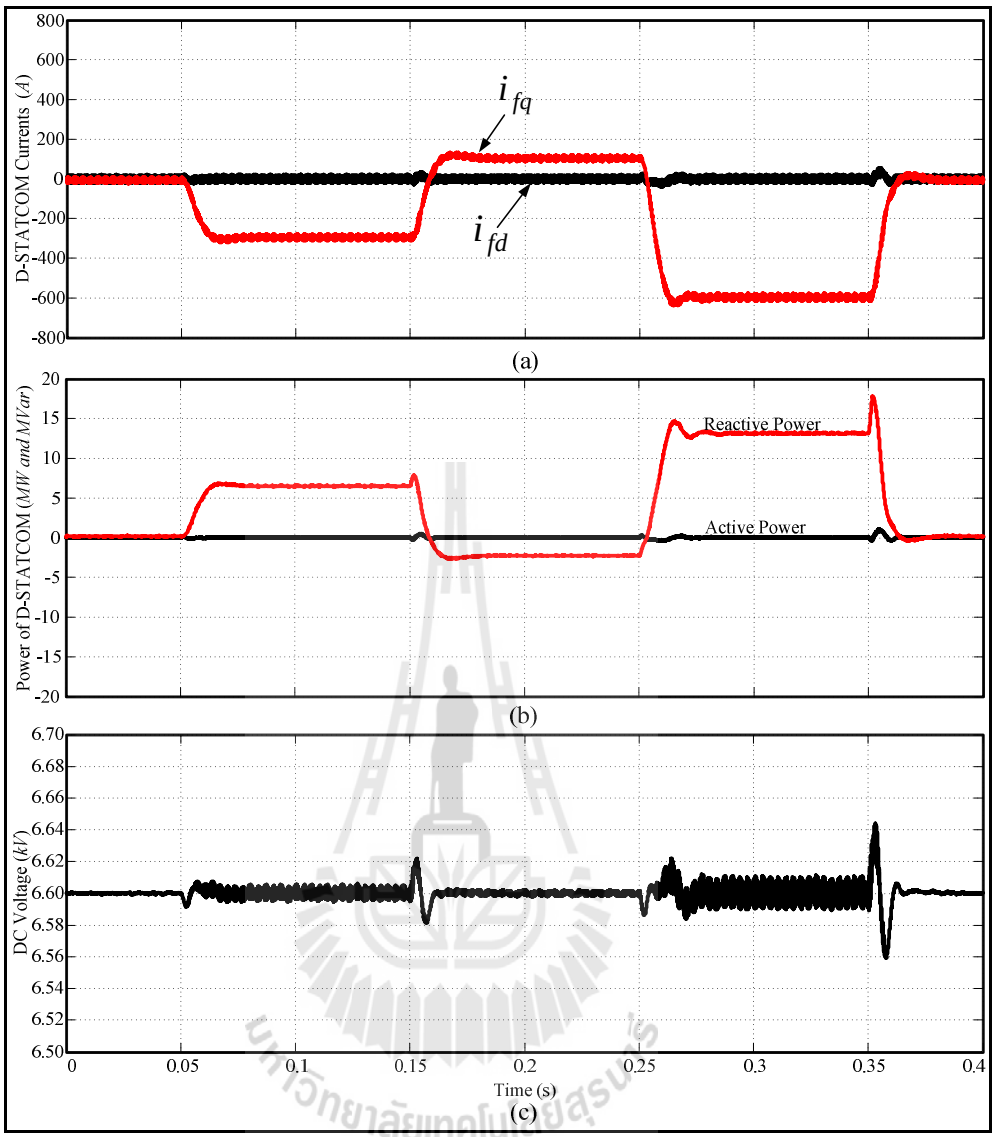

Figure 8.10 Currents, DC voltage and power of the D-STATCOM for the system with the R load which the source voltage varying between 22.77 and 14.41 *kV*

Figure 8.10 presents the currents, DC voltage and power of the D-STATCOM for the system with the R load when the source voltage is varied between 22.77 and 14.41 *kV*. As may be seen in Figure 8.10(a), that the reactive currents (i_{fq})

are about 0, -300, +100, -600 and 0 *A* to compensate the load voltage swell when the source voltages are 21.56, 17.93, 22.77, 14.41 and 21.56 *kV*, respectively. Whilst, the active current (i_{fd}) very small changes when the D-STATCOM compensate the load voltage. These correspond to the reactive and active powers of the D-STATCOM as shown in Figure 8.10(b). The reactive powers are of 0.0, +6.6, +2.2, +13.2 and 0.0 *MVar* to compensate the load voltage when the source voltages are 21.56, 17.93, 22.77, 14.41 and 21.56 *kV*, respectively. Meanwhile, the active power very small changes in positive when the D-STATCOM compensating the load voltage. So, the D-STATCOM consumes active power to regulate the DC voltage at the constant value. Furthermore, the D-STATCOM always consumes active power no matter how much it absorbs or generates reactive power. As can be seen in figure 8.10(c), the DC voltage is always regulated at 6.6 *kV* for all of source voltages.

In addition, the application of the D-STATCOM for load voltage regulation when varying the load is demonstrated in this section. The load powers are shown in Figure 8.11. As seen in this Figure, the active powers are 0. 415 *MW* (0.1 *pu.*) from t = 0.00 to 0.05 second, 4.15 *MW* (1.0 *pu.*) from t = 0.05 to 0.15 second, 8.30 *MW* (2.0 *pu.*) from t = 0.15 to 0.25 second, 12.45 *MW* (3.0 *pu.*) from t = 0.25 to 0.35 second, 16.60 *MW* (4.0 *pu.*) from t = 0.35 to 0.45 second and come back to 4.15 *MW* (1.0 *pu.*) from t = 0.45 to 0.50 second, while the reactive power is not changed in this case. The load voltage of the system without the D-STATCOM is shown as the dash line in Figure 8.12. Meanwhile, the solid line presents the load voltage of system with D-STATCOM. As seen in this Figure, the D-STATCOM with the proposed control in case of source voltage variations can be used in case of load varied as well. The powers of the D-STATCOM to compensate the load voltage are shown in Figure

8.13. In this Figure, the reactive powers are -1.47, -0.80, +0.40, +2.11, +4.42 and -0.80 *MVar* when the load powers are 0.415, 4.15, 8.30, 12.45, 16.60 and 4.15 *MW*, respectively, while the active power very small change in this case.

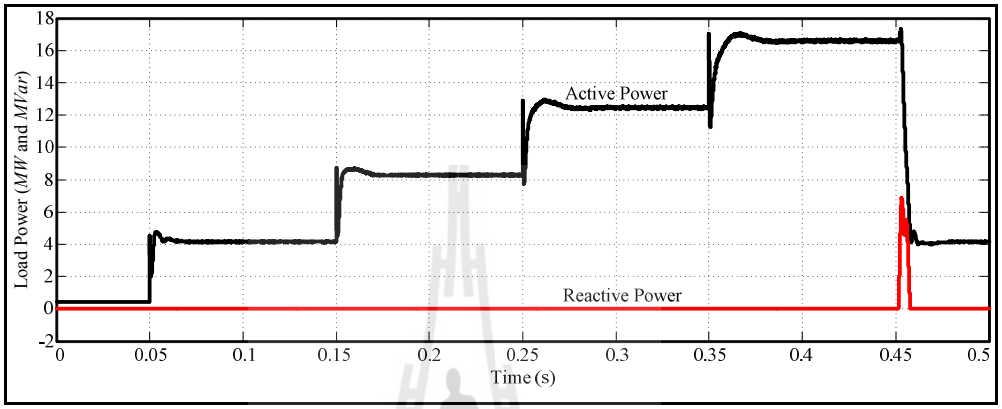

Figure 8.11 Load varying when the system with the R load

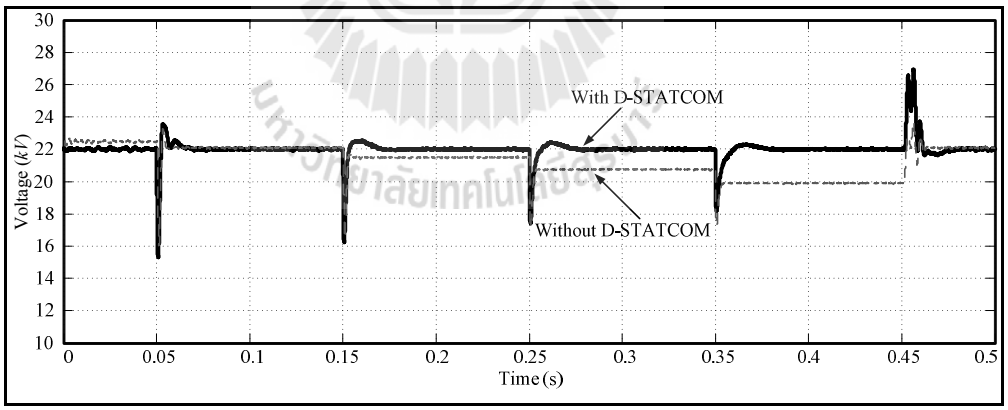

Figure 8.12 Load voltages in the system with the R load in case of the load variations

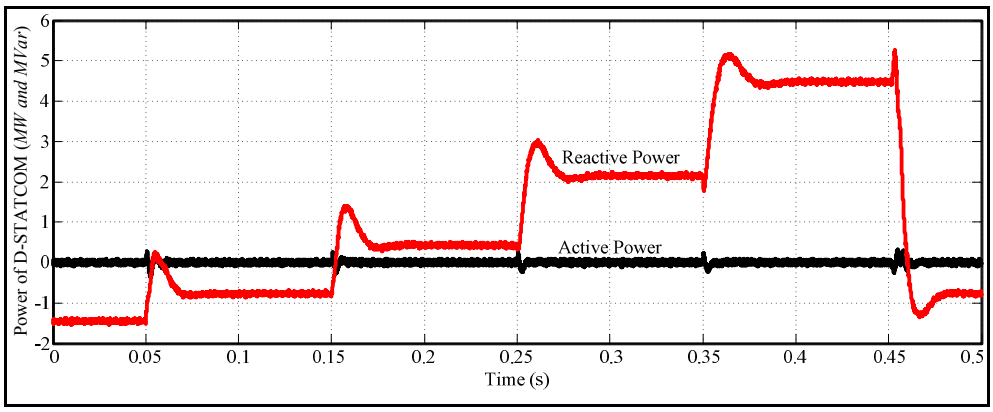

Figure 8.13 Powers of the D-STATCOM for the system with the R load in case of the load variations

8.2.2 Voltage Regulation when the Distribution System with the RL Load

In this case, the current control and DC voltage control with the parameters similar to case i as shown in Table 8.5 are used. Meanwhile, the AC voltage control with the classical loop shaping method that described in chapter 7 is used. The AC voltage controller parameters and the stability margins for RL load with various operating conditions, each corresponding to a different value of source voltage (that means corresponding to a different i_{fq}) are presented in Table 8.7.

In Figure 8.14, the controllers that are designed in each source voltage operation points i.e. 30.14, 27.72 and 25.30 kV ($i_{fq} = +600$, +400 and +200A) for the load voltage regulation in case of the source voltage variations between 30.14 and 25.30 kV are demonstrated and compared. As can be seen in this Figure, the controllers that are designed in case of the source voltage as 25.30 kV ($i_{fq} = +200A$) and 27.72 kV ($i_{fq} = +400A$) give the high overshoot and oscillation response in some

case. Whilst, the controller that is designed in case of the source voltage as 30.14 *kV* ($i_{fq} = +600A$) can be used for all cases and gives a good dynamic response.

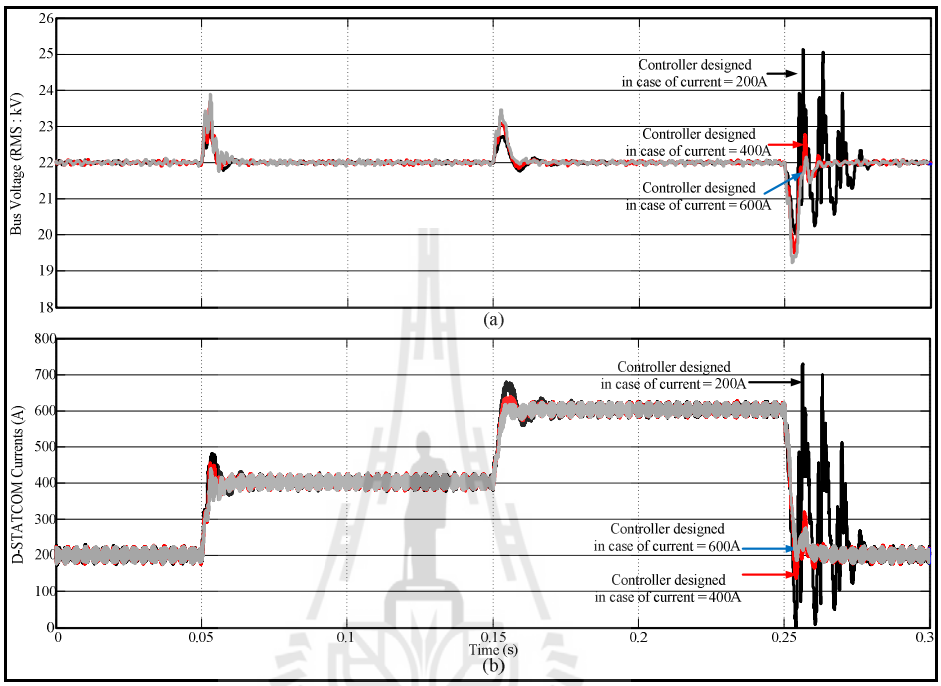

Figure 8.14 Comparison the controller in case of the source voltage variations between 30.14 and 25.30 *kV*

Similarly, the controllers that are designed in each source voltage operation points i.e. 22.77, 20.35, 18.04 and 15.71 *kV* ($i_{fq} = 0$, -200, -400 and -600A) for the load voltage regulation in case of the source voltage variations between 22.77 and 15.71 *kV* are demonstrated and compared as shown in Figure 8.15. As can be seen in this Figure, the controllers that are designed in case of the source voltage as 15.71 *kV* ($i_{fq} = -600A$) and 18.04 *kV* ($i_{fq} = -400A$) can be used for all cases and give a good dynamic response.

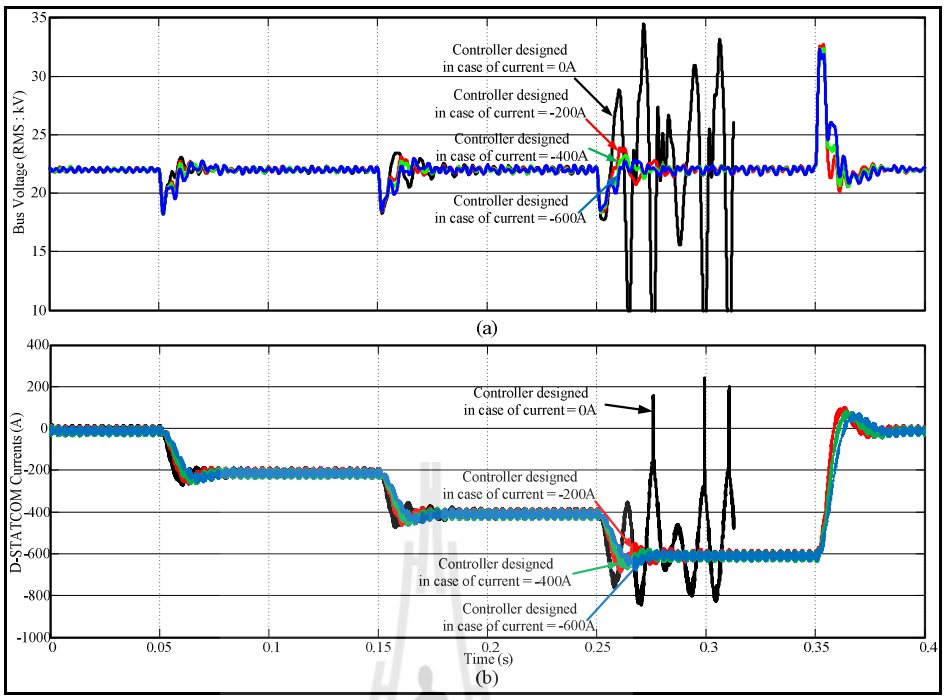

Figure 8.15 Comparison the controller in case of the source voltage variations between 22.77 and 15.71 *kV*

However, the parameters of PI controller and the compensator when the source voltage of 30.14 *kV* are selected in case of the source voltage variations between 30.14 and 25.30 *kV* (i.e. i_{fq} varies between +600 and +200 *A*). Whilst, the parameters of PI controller and the compensator when the source voltage of 15.71 *kV* are selected in case of the source voltage variations between 24.09 and 15.71 *kV* (i.e. i_{fq} varies between +100 and -600 *A*). In addition, the notch compensator (i.e. $\frac{0.00096^2 s^2 + 0.00014s + 1}{0.00096^2 s^2 + 0.00192s + 1}$) is used in the case of the source voltage variations between 24.09 and 15.71 *kV*. This compensator is applied in order to mitigate the effect of resonance of the system.

Table 8.7 AC voltage controller for the distribution system with the RL load

Source voltage (*kV*)	PI Parameters	Compensator 1 Parameters	Compensator 2 Parameters	Gain Margin (*dB*)	Phase Margin (*deg*)
30.14	$0.042\left(\frac{0.0014s+1}{0.0014s}\right)$	$\frac{0.0001s+1}{0.00001s+1}$	1	6.38	55.63
28.82	$0.049\left(\frac{0.0014s+1}{0.0014s}\right)$	$\frac{0.0001s+1}{0.00001s+1}$	1	6.80	54.51
27.72	$0.056\left(\frac{0.0014s+1}{0.0014s}\right)$	$\frac{0.0001s+1}{0.00001s+1}$	1	7.85	51.43
26.47	$0.070\left(\frac{0.0014s+1}{0.0014s}\right)$	$\frac{0.0001s+1}{0.00001s+1}$	1	8.64	50.39
25.30	$0.098\left(\frac{0.0014s+1}{0.0014s}\right)$	$\frac{0.0001s+1}{0.00001s+1}$	1	9.57	51.87
24.09	$0.020\left(\frac{0.0008s+1}{0.0008s}\right)$	$\frac{1}{0.0010s+1}$	$\frac{0.00062^2s^2+4.4e^{-5}s+1}{0.00062^2s^2+0.00124s+1}$	18.71	63.28
22.77	$0.0072\left(\frac{0.0004s+1}{0.0004s}\right)$	$\frac{1}{0.0012s+1}$	$\frac{0.00068^2s^2+6.0e^{-5}s+1}{0.00068^2s^2+0.00136s+1}$	14.24	60.88
21.56	$0.0032\left(\frac{0.0002s+1}{0.0002s}\right)$	$\frac{1}{0.0012s+1}$	$\frac{0.00073^2s^2+7.2e^{-5}s+1}{0.00073^2s^2+0.00146s+1}$	11.20	60.00
20.35	$0.00112\left(\frac{0.00008s+1}{0.00008s}\right)$	$\frac{1}{0.0014s+1}$	$\frac{0.00078^2s^2+8.4e^{-5}s+1}{0.00078^2s^2+0.00156s+1}$	9.94	58.45
19.14	$0.00072\left(\frac{0.00006s+1}{0.00006s}\right)$	$\frac{1}{0.0016s+1}$	$\frac{0.00082^2s^2+9.7e^{-5}s+1}{0.00082^2s^2+0.00164s+1}$	9.71	59.48
18.04	$0.00048\left(\frac{0.00004s+1}{0.00004s}\right)$	$\frac{1}{0.0016s+1}$	$\frac{0.00087^2s^2+0.00011s+1}{0.00087^2s^2+0.00174s+1}$	8.33	57.33
16.83	$0.00020\left(\frac{0.00002s+1}{0.00002s}\right)$	$\frac{1}{0.0018s+1}$	$\frac{0.00092^2s^2+0.00013s+1}{0.00092^2s^2+0.00184s+1}$	8.74	59.71
15.71	$0.00020\left(\frac{0.00002s+1}{0.00002s}\right)$	$\frac{1}{0.0020s+1}$	$\frac{0.00096^2s^2+0.00014s+1}{0.00096^2s^2+0.00192s+1}$	7.75	56.62

In this case, the system is simulated for time varying source voltage conditions. The dashes line of Figure 8.16(a) shows the load voltage of the system without D-STATCOM when the source voltage is varied. It can be seen that the load voltage corresponds to five different source voltage conditions: source voltage of 25.30 *kV* from t = 0.00 to 0.05 second; source voltage of 28.82 *kV* from t = 0.05 to 0.15 second; source voltage at 26.47 *kV* from t = 0.15 to 0.25 second; source voltage of 30.14 *kV* from t = 0.25 to 0.35 second; and source voltage of 25.30 *kV* from t = 0.35 to 0.40 second. Meanwhile, the solid line of Figure 8.16(a) presents the load

voltage of the system with D-STATCOM when the source voltage is varied. It can be observed from this Figure, the D-STATCOM with proposed control design can be regulated the load voltage at the desired value. The load voltage took approximately 0.01 seconds to settle in each source voltage. It can be seen in Figure 8.16(b) that the load voltage waveform reaches the desired value within a haft cycle.

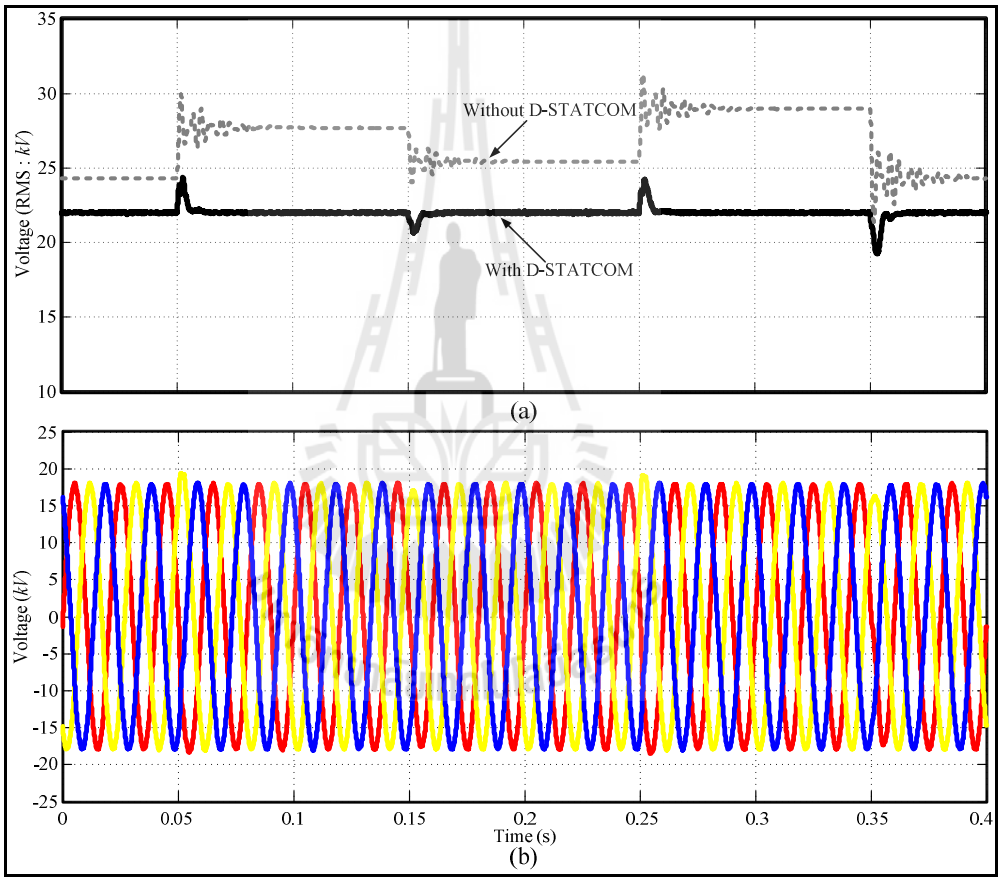

Figure 8.16 Load voltage of the system with the RL load which the source voltage varying between 28.82 and 23.98 *kV*

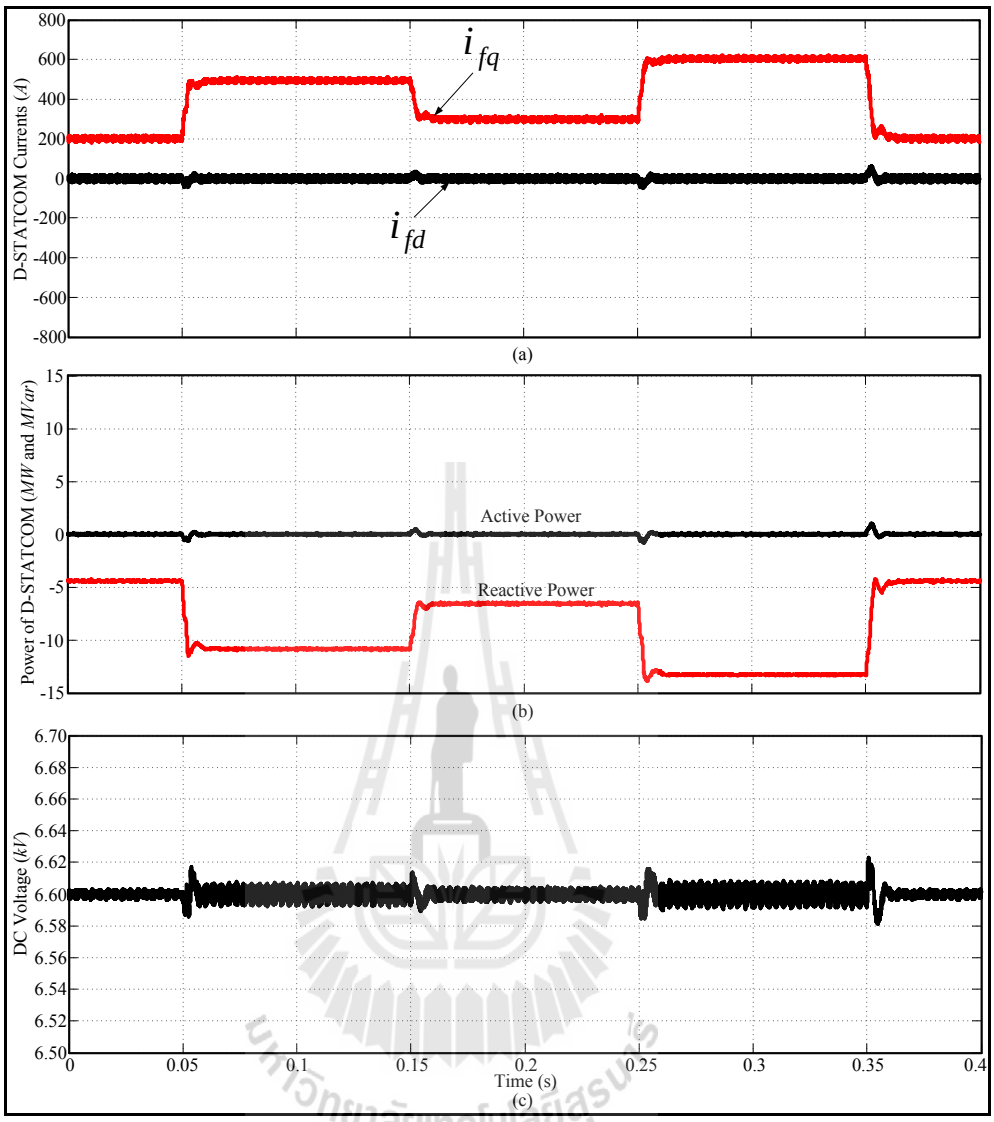

Figure 8.17 Currents, DC voltage and power of the D-STATCOM for the system with the RL load which the source voltage varying between 28.82 and 23.98 *kV*

Figure 8.17 presents the currents, DC voltage and power of the D-STATCOM for the system with the RL load when the source voltage is varied between 28.82 and 23.98 *kV*. As may be seen in Figure 8.17(a), that the reactive

currents (i_{fq}) are +200, +500, +300, +600 and +200 *A* to compensate the load voltage when the source voltages are 25.30, 28.82, 26.47, 30.14 and 25.30 *kV*, respectively. Whilst, the active current (i_{fd}) very small change when the D-STATCOM compensate the load voltage. These correspond to the reactive and active powers of the D-STATCOM as shown in Figure 8.17(b). The reactive powers are -4.4, -10.1, -6.6, -13.2 and -4.4 *MVar* to compensate the load voltage when the source voltages are 25.30, 28.82, 26.47, 30.14 and 25.30 *kV*, respectively. Meanwhile, the active power is very small changed in positive when the D-STATCOM compensates the load voltage. This means that the D-STATCOM consumes active power to regulate the DC voltage at the constant value as can be seen in Figure 8.17(c). As seen in this Figure, the DC voltage is always regulated at 6.6 *kV* for all of source voltages.

In case of the source voltage variations between 24.09 and 15.71 *kV*, the load voltage of the system with the RL load is shown in Figure 8.18. The dash line of Figure 8.18(a) presents the load voltage of the system without D-STATCOM when the source voltage is varied. As seen in this Figure, the load voltage corresponds to five different source voltage conditions: source voltage of 22.77 *kV* from t = 0.00 to 0.05 second; source voltage of 15.71 *kV* from t = 0.05 to 0.15 second; source voltage at 20.35 *kV* from t = 0.15 to 0.25 second; source voltage of 24.09 *kV* from t = 0.25 to 0.35 second; and source voltage of 22.77 *kV* from t = 0.35 to 0.40 second. Whilst, the solid line of Figure 8.18(a) shows the load voltage of the system with D-STATCOM. As can be observed from this Figure that the D-STATCOM with proposed control design can be regulated the load voltage at the desired value. The load voltage took approximately 0.02 seconds to settle in each source voltage. As can be seen in Figure 8.18(b), the load voltage reaches the desired value within one cycle.

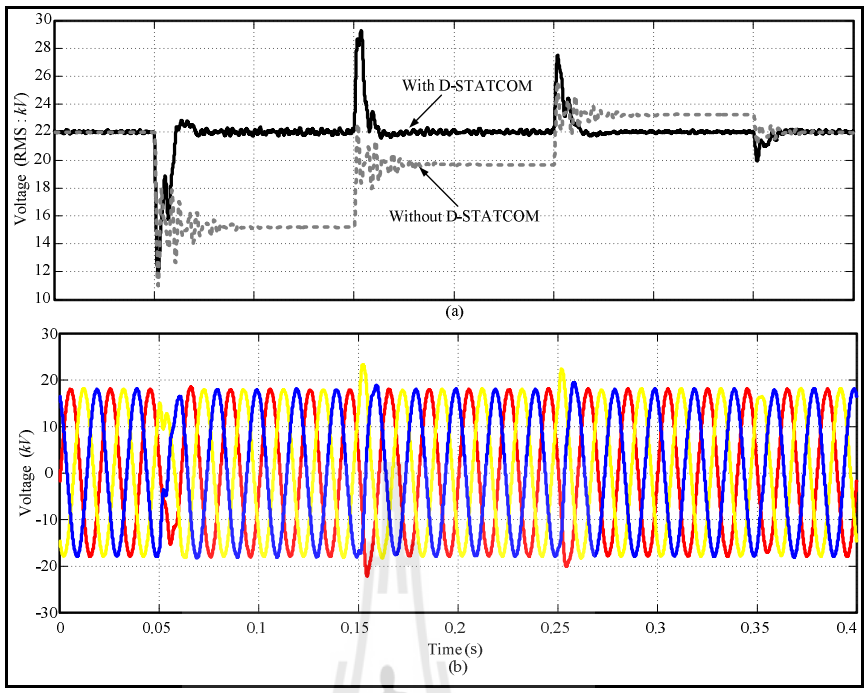

Figure 8.18 Load voltage of the system with the RL load which the source voltage varying between 22.77 and 14.41 *kV*

Figure 8.19 presents the currents, DC voltage and power of the D-STATCOM for the system with the RL load when the source voltage is varied between 24.09 and 15.71 *kV*. As may be seen in Figure 8.19(a), that the reactive currents (i_{fq}) are about 0, -600, -200, +100 and 0 *A* to compensate the load voltage swell when the source voltages are 22.77, 15.71, 20.35, 24.09 and 22.77 *kV*, respectively. Whilst, the active current (i_{fd}) very small changes when the D-STATCOM compensate the load voltage. These correspond to the reactive and active powers of the D-STATCOM as shown in Figure 8.19(b). The reactive powers are of 0.0, +13.2, +4.4, -2.2 and 0.0 *MVar* to compensate the load voltage when the source voltages are 22.77, 15.71, 20.35, 24.09 and 22.77 *kV*, respectively. Meanwhile, the

active power is very small changed in positive when the D-STATCOM compensates the load voltage. So, the D-STATCOM consumes active power to regulate the DC voltage at the constant value. Furthermore, the D-STATCOM always consumes active power no matter how much it absorbs or generates reactive power. As can be seen in Figure 8.19(c), the DC voltage is always regulated at 6.6 *kV* for all of source voltages.

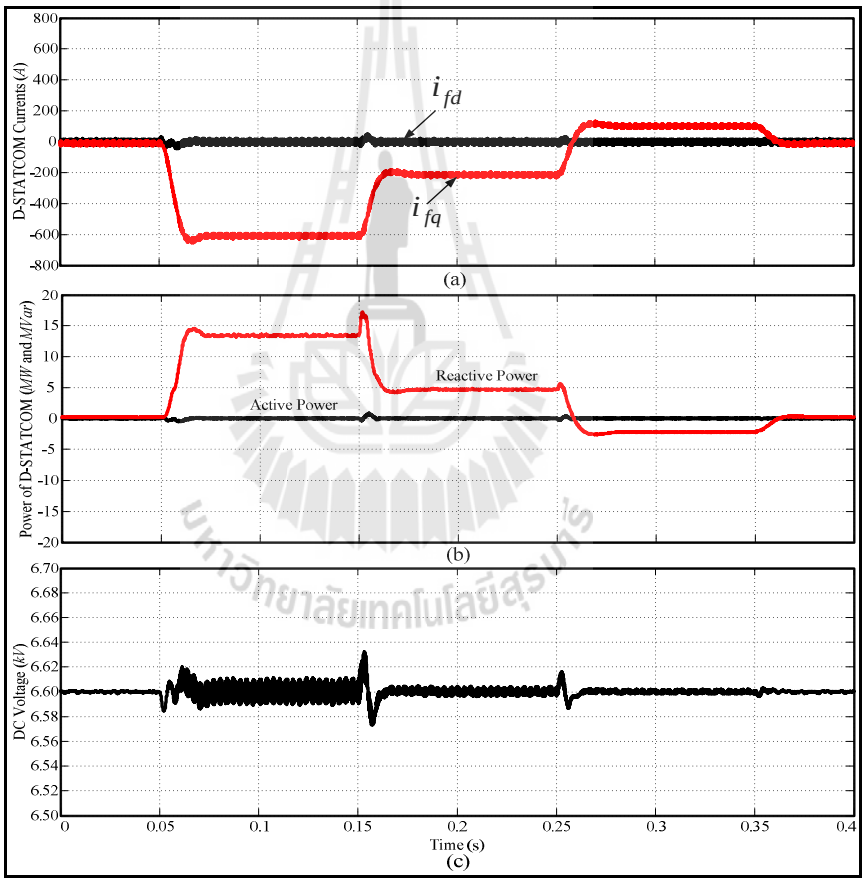

Figure 8.19 Currents, DC voltage and power of the D-STATCOM for the system with the RL load which the source voltage varying between 22.77 and 14.41 *kV*

In addition, the application of the D-STATCOM for load voltage regulation which loads varying is demonstrated in this section. The load powers are shown in Figure 8.20. As seen in this figure, the active powers are 0. 415 *MW* (0.1 *pu.*) from t = 0.00 to 0.05 second, 4.15 *MW* (1.0 *pu.*) from t = 0.05 to 0.15 second, 8.30 *MW* (2.0 *pu.*) from t = 0.15 to 0.25 second, 12.45 *MW* (3.0 *pu.*) from t = 0.25 to 0.35 second, 16.60 *MW* (4.0 *pu.*) from t = 0.35 to 0.45 second and come back to 4.15 *MW* (1.0 *pu.*) from t = 0.45 to 0.50 second which the constant load power factor at 0.875 in this case. The load voltage of the system without the D-STATCOM is shown as the dash line in Figure 8.21. Meanwhile, the solid line presents the load voltage of the system with D-STATCOM. As seen in this Figure, the D-STATCOM with the proposed control in case of source voltage variations can be used in case of load variations as well. The powers of the D-STATCOM to compensate the load voltage are shown in Figure 8.22. In this Figure, the reactive powers are -1.24, +1.50, +4.99, +9.00, +13.60 and +1.50 *MVar* when the load powers are 0.415, 4.15, 8.30, 12.45, 16.60 and 4.15 *MW*, respectively, while the active power very small change in this case.

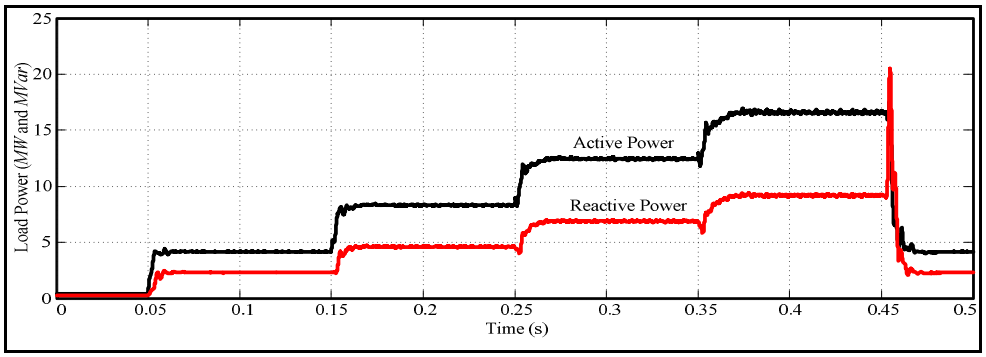

Figure 8.20 Load varying when the system with the RL load

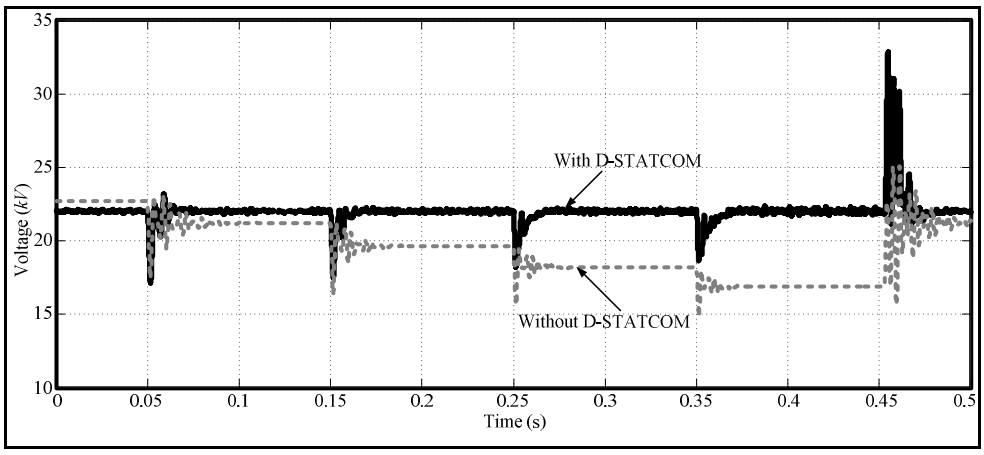

Figure 8.21 Load voltages of the system with the RL load in case of the load variations

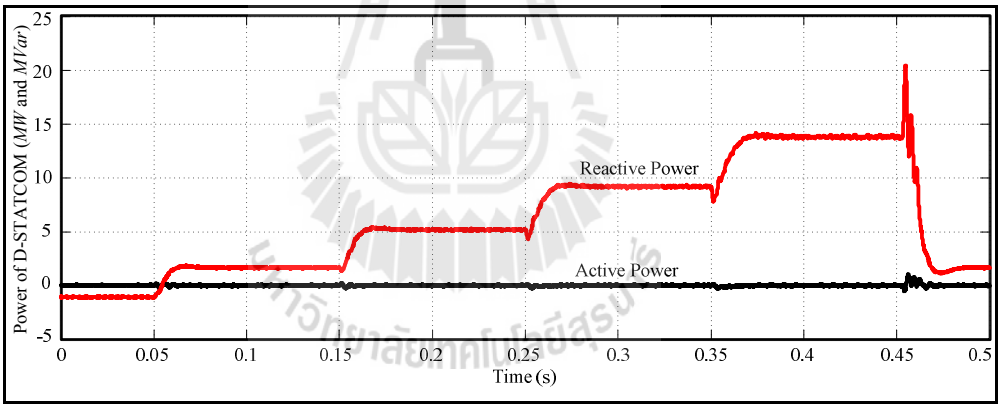

Figure 8.22 Powers of the D-STATCOM for the system with the RL load in case of the load variations

8.3 Application of the D-STATCOM for the System with the Distributed Generator

In this section, the D-STATCOM with the proposed control has been tested for the performance in regulating of the load voltage in case of the system including the distributed generator (DG). The configuration of the system including the DG and D-STATCOM is modeled using the MATLAB/SIMULINK software package as shown in Figure 8.23. The parameters of the system and D-STATCOM in section 8.2 are used in this section. The modeling and simulations of the D-STATCOM have been carried out in two different cases: the system with a synchronous generator (SG) and the system with an induction generator (IG).

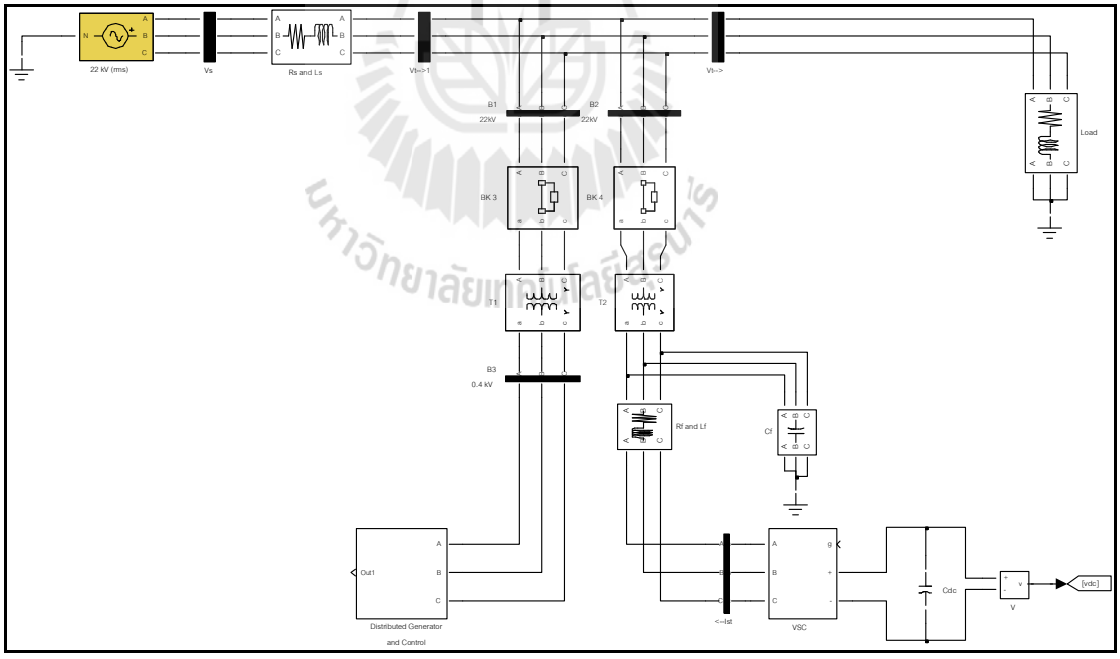

Figure 8.23 MATLAB/SIMULINK model for the system with the DG and D-STATCOM

8.3.1 Distribution System with the Synchronous Generator (SG)

In this section, the standard per unit salient-pole synchronous machine model 12 (400 V, 50 Hz, 2,000 *kVA* and 1500 *rpm*) with an excitation system in MATLAB/SIMULINK is used. The parameters of the synchronous generator are shown in Table 8.8. Meanwhile, an IEEE type 1 synchronous machine voltage regulator combined to an exciter is used as the excitation system in this case. The excitation system configuration modeled in MATLAB/SIMULINK is shown in Figure 8.24 while the parameters of excitation system are shown in Table 8.9.

Table 8.8 Parameters of the synchronous generator

Parameters	Value
d-axis synchronous reactance (x_d), transient reactance (x'_d) and subtransient reactance (x''_d)	2.11, 0.17 and 0.13 *pu*
q-axis synchronous reactance (x_q), subtransient reactance (x''_q) and leakage reactance (x_l)	1.56, 0.23 and 0.05 *pu*
d axis transient and subtransient short-circuit time constant (T'_d and T''_d) and q-axis subtransient short-circuit time constant (T''_q)	0.33, 0.03 and 0.03 *pu*
stator resistance (R_s)	0.03 *pu*
coefficient of inertia (H), friction factor (F) and pole pairs (p)	0.3072 (sec.), 0.00987 (*pu*) and 2 *pairs*

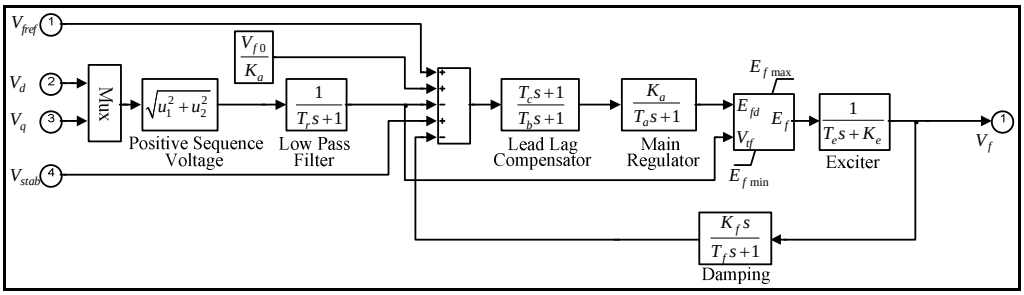

Figure 8.24 Excitation system configurations

Table 8.9 Parameters of the excitation system

Parameters	Value
Low-pass filter time constant (T_r)	20e-3 (sec.)
Regulator gain and time constant (K_a and T_a)	400 and 0.001 (sec.)
Exciter gain and time constant (K_e and T_e)	1 and 0.0 (sec.)
Transient gain reduction time constants (T_b and T_c)	1 and 1 (sec.)
Damping filter gain and time constant (K_f and T_f)	0.003 and 1 (sec.)
Regulator output gain Limits and gain ($E_{f\min}$, $E_{f\max}$ and K_p)	-6.0, 6.0 (*pu*) and 0

To investigate the performance of D-STATCOM with the proposed control in regulating of the load voltage in case of the system including the synchronous generator, the source voltage sag at 15.71 *kV* is applied to the system with the RL load at t = 0.05 second. The AC voltage controller and compensator for RL load in section 8.2 are used in this case. The load voltages when the system with and without D-STATCOM are presented in Figure 8.25. Without the D-STATCOM for dynamic reactive compensation, the source voltage sag results in the load voltage sag. Then the generator generates high reactive power to the system while the active power of the generator cannot reach the set value during the source voltage sag as can be seen in Figure 8.26. As a result, the synchronous generator may be disconnected from the power grid. However, when using the D-STATCOM with the proposed control, the load voltage can be regulated at the desired value. The load voltage took approximately 0.02 seconds to settle. In this case, the generator generates small increased reactive power to the system while the active power of the generator can reach the set value during the source voltage sag.

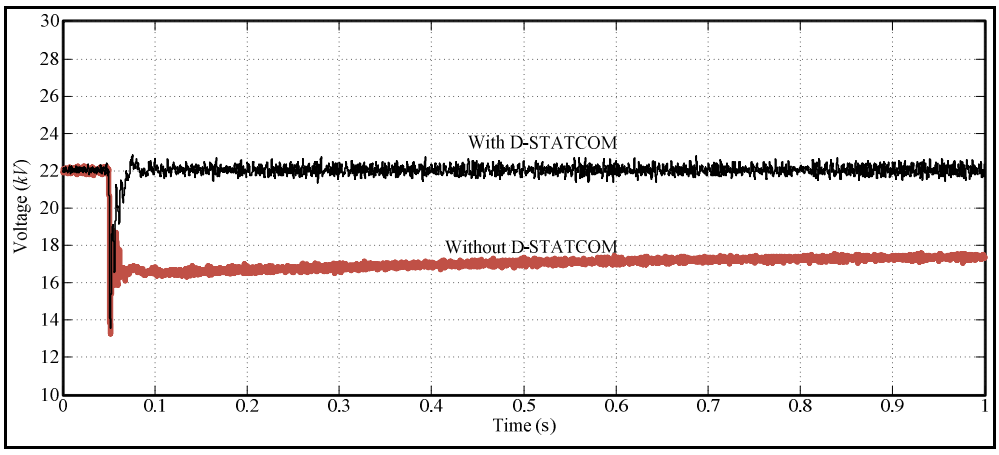

Figure 8.25 Load voltages of the system with the RL load and synchronous generator

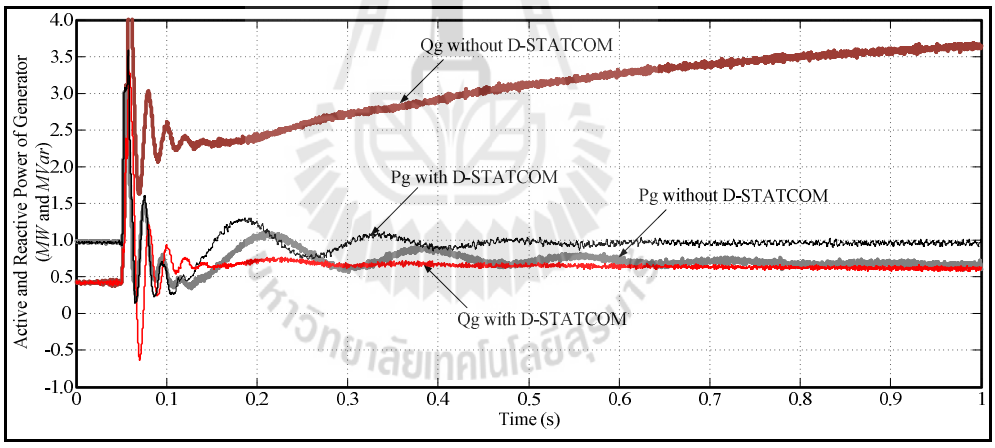

Figure 8.26 Powers of synchronous generator and D-STATCOM when source voltage sag

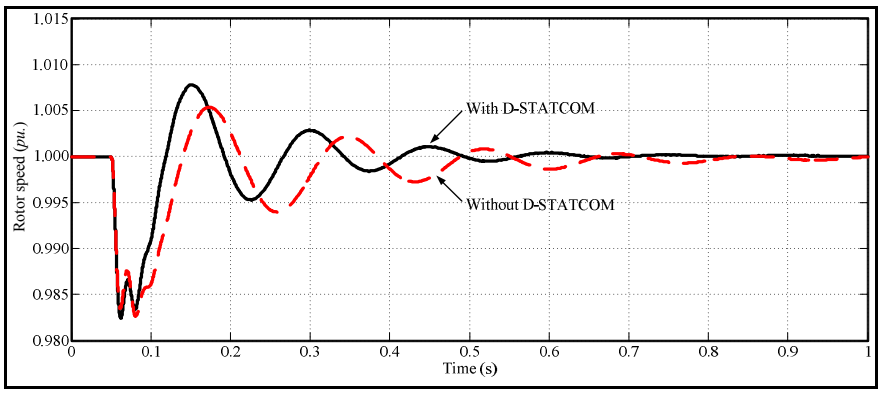

Figure 8.27 Rotor speed of the synchronous generator when source voltage sag

Figure 8.27 presents the rotor speed of synchronous generator when the source voltage sags. As can be seen in this figure, the rotor speed of the system with the D-STATCOM has a high frequency oscillation. However, the system with the D-STATCOM results faster settles in rotor speed variation. Meanwhile, Figure 8.28 shows the active and reactive powers of the D-STATCOM in order to compensate the load voltage in this case.

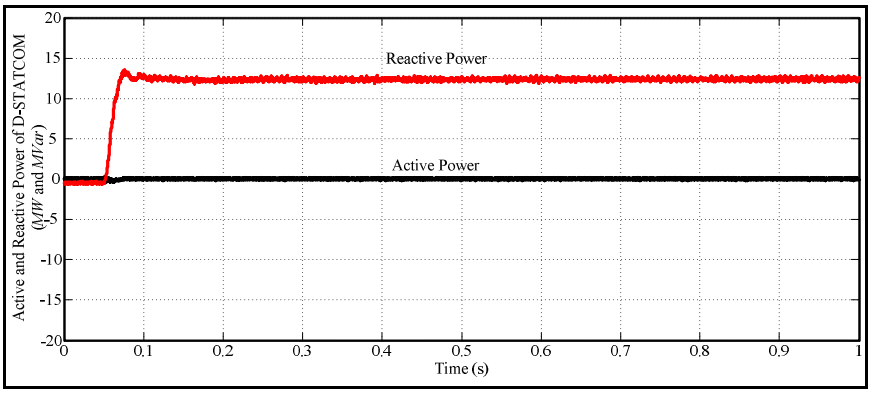

Figure 8.28 Active and reactive powers of the D-STATCOM for the load voltage regulation in case of the system with the synchronous generator

8.3.2 Distribution System with the Induction Generator (wind IG)

In this case, the D-STATCOM applies to the load voltage regulation of the system including the induction generator with fixed-speed wind turbines (FSWTs) is investigated. The squirrel-cage induction generator (SCIG) is used in this section and its parameters are shown in Table 8.10. Meanwhile, the characteristics of the fixed-speed wind turbines are shown in Figure 8.29. To investigate the performance of D-STATCOM with the proposed control in regulating of the load voltage in case of the system including the induction generator with fixed-speed wind turbines, the source voltage sag at 15.71 *kV* is applied to the system with the RL load at t = 0.05 second. Whilst, the wind speed assume to be constant at 10 m / second during the entire test. The AC voltage controller and compensator for RL load in section 8.2 are used in this case. The load voltages when the system with and without D-STATCOM are presented in Figure 8.30. Without the D-STATCOM for dynamic reactive compensation, the source voltage sag results in the load voltage sag. The active and reactive powers of the generator oscillate in a transient state as can be seen in Figure 8.31. However, they can be settled within 0.15 seconds. In addition, the generator can be generated the active power nearly the set value which absorbing the small decreased reactive power. As a result, the induction generator with fixed-speed wind turbines can be connected to the power grid during the source voltage sag when the system without the D-STATCOM. However, the rotor speed of the generator is increased in this case as can be seen in Figure 8.32.

When using the D-STATCOM with the proposed control, the load voltage can be regulated at the desired value. The load voltage took approximately 0.02 seconds to settle. The powers of the D-STATCOM in order to compensate the

load voltage are shown in Figure 8.33. Similar to the case of without the D-STATCOM, the active and reactive powers of the generator oscillate in a transient state and they can be settled within 0.15 seconds. However, in this case, the generator can be generated the active power at the set value which absorbing the same reactive power. Furthermore, the rotor speed of the generator can be regulated at the same value in this case. As a result, the induction generator with fixed-speed wind turbines can be connected to the power grid during the source voltage sag as well.

Table 8.10 Parameters of the induction generator

Parameters	Value
Stator resistance and leakage inductance (R_s and L_{ls})	0.016 and 0.06 (*pu*)
Rotor resistance and leakage inductance (R'_r and L'_{lr})	0.015 and 0.06 (*pu*)
Magnetizing inductance (L_m)	3.5 (*pu*)
Coefficient of inertia (H), friction factor (F) and pole pairs (p)	2 (*sec.*), 0 (*pu*) and 2 (*pairs*)

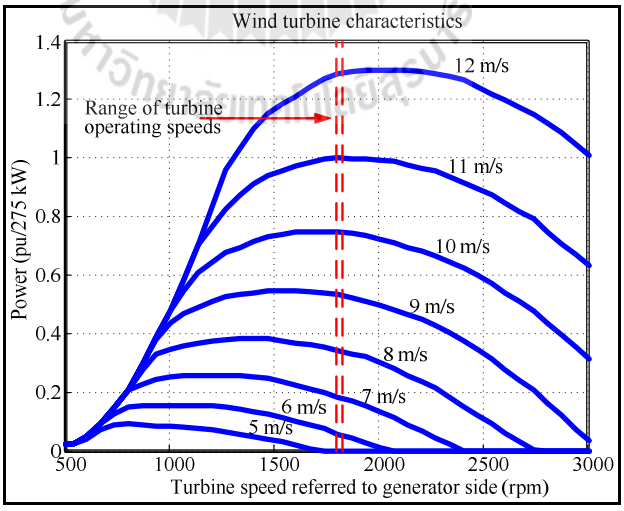

Figure 8.29 Characteristics of the fixed-speed wind turbines

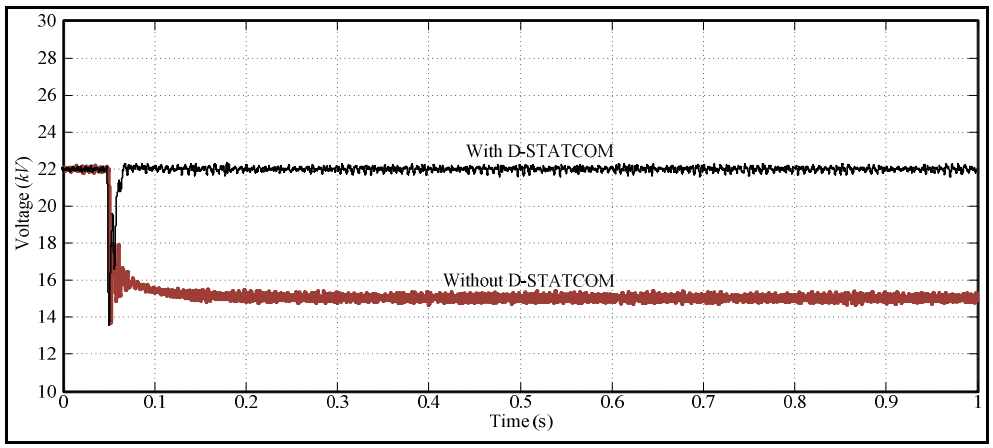

Figure 8.30 Load voltages of the system with the RL load and induction generator

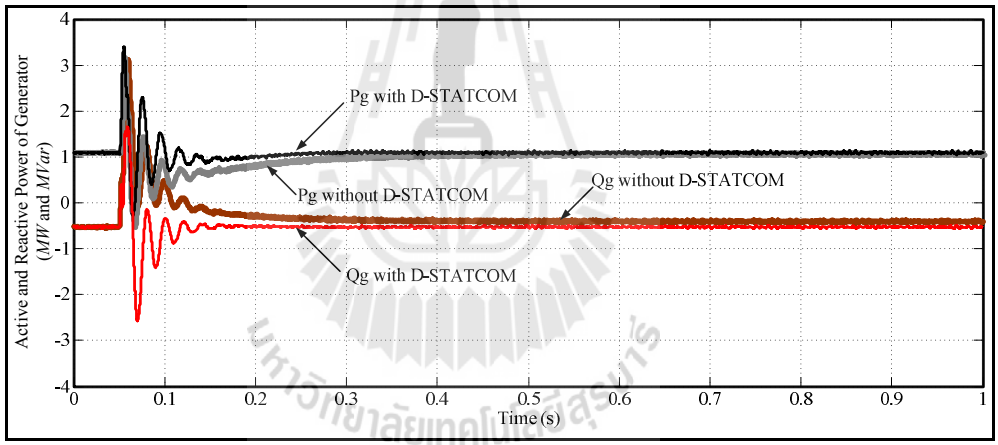

Figure 8.31 Powers of the induction generator and D-STATCOM when the source voltage sag

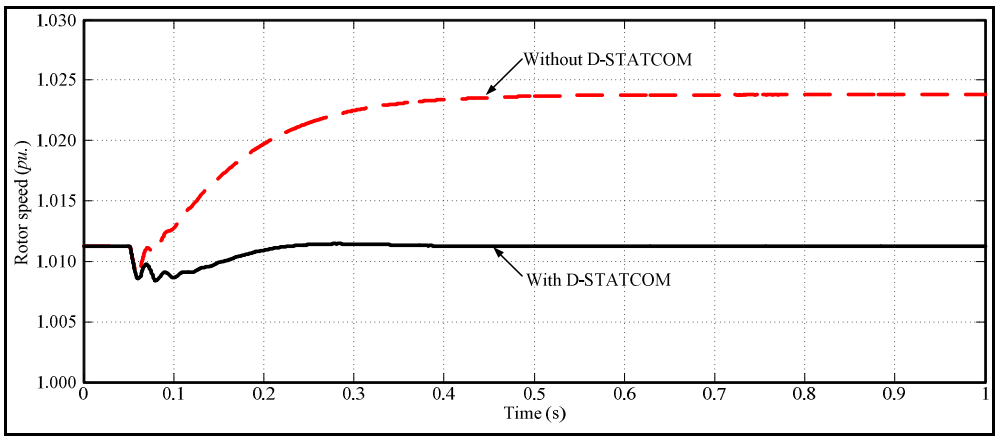

Figure 8.32 Rotor speed of the induction generator when the source voltage sag

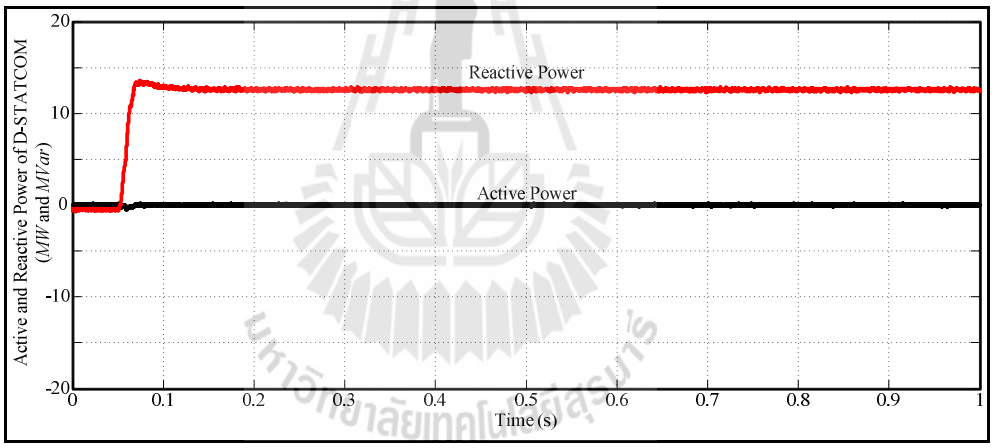

Figure 8.33 Active and reactive powers of the D-STATCOM for the load voltage regulation in case of the system with the induction generator

8.4 Summary

This chapter presents the application of the D-STATCOM with the proposed design control technique for load voltage regulation. The decoupling current control of the D-STATCOM with the parameters tuning based on the genetic algorithm

(CC-GA) and the DC voltage control with an elimination term of $u_q i_{fq}$ based on the symmetrical optimum method (DCVC-SO) are used. Meanwhile, the AC voltage control based on the classical loop shaping is applied to many cases. In this chapter a simplified 22 *kV*, 2 bus test power system is employed for the simulation. The application of D-STATCOM for load voltage regulation of the distribution system with the R and RL loads is discussed. In addition, the D-STATCOM is applied to the system including with the distribution generator are presented.

For the load voltage regulation when the distribution system with the R loads, the load voltage regulations in case of the source voltage variations between 28.82 and 23.98 *kV* (i_{fq} varies between +600 and +200 *A*) and the source voltage variations between 14.41 and 22.77 *kV* (i_{fq} varies between +100 and -600 *A*) are illustrated. In addition, the load voltage regulation when the loads vary is demonstrated. The load power is varied between 0.415 *MW* (0.1 *pu.*) to 16.60 *MW* (4.0 *pu.*) while the reactive power is not changed in this case.

For the load voltage regulation when the distribution system with the RL loads, the load voltage regulations in case of the source voltage variations between 30.14 and 25.30 *kV* (i_{fq} varies between +600 and +200 *A*) and the source voltage variations between 15.71 and 24.09 *kV* (i_{fq} varies between +100 and -600 *A*) are illustrated. In addition, the load voltage regulation when the loads vary is demonstrated. The load power is varied between 0.415 *MW* (0.1 *pu.*) to 16.60 *MW* (4.0 *pu.*) which the constant load power factor at 0.875.

As the results, the D-STATCOM with proposed control design can be regulated the load voltage at the desired value. Furthermore, the D-STATCOM with

the proposed control in case of source voltage variations can be used in case of load varied as well. However, the controller designed in case of i_{fq} varies between +600 and +200 *A* cannot use in case of i_{fq} varies between +100 and -600 *A*, and vice versa.

In the application of the D-STATCOM for the system including the distributed generator, the simulations of the D-STATCOM with two different cases: the system with a synchronous generator (SG) and the system with an induction generator (IG) are presented. From the results, the D-STATCOM with the proposed control can be regulated the load voltage at the desired value. The load voltage took approximately 0.02 seconds to settle. Furthermore, the generator can be connected to the power grid and the active power of the generator can reach the set value during the source voltage sag in both cases.

CHAPTER VIII

APPLICATION OF D-STATCOM FOR LOAD VOLTAGE REGULATION

This chapter presents the application of the D-STATCOM with the proposed design control technique for load voltage regulation. The D-STATCOM systems usually consists of a voltage source converter (VSC) which dynamically injects a current of desired amplitude, frequency and phase into the grid line in order to mitigate sags at the point of common coupling (PCC). The decoupling current control of the D-STATCOM with the parameters tuning based on the genetic algorithm (CC-GA) and the DC voltage control with an elimination term of $u_q i_{fq}$ based on the symmetrical optimum method (DCVC-SO) are used. Meanwhile, the AC voltage control based on the classical loop shaping is applied to many cases in this chapter. In this chapter a simplified 22-*kV*, 2-bus test power system is employed for the simulation. The remainder of this chapter is organized as follows. The next section presents a brief review of the D-STATCOM system. The applications of D-STATCOM for load voltage regulation of the distribution system with the R and RL loads are discussed in Section 8.2. In Section 8.3, the applications of the D-STATCOM in the distribution system with the distributed generators are presented. A summary of this chapter is presented in Section 8.4.

8.1 Brief Review of the D-STATCOM for Voltage Regulation

Recently, the distribution static synchronous compensator (D-STATCOM) has been introduced to distribution systems to manage the system reactive power and regulate the voltage at the point of common coupling. A D-STATCOM usually consists of a shunt connected voltage source converter (VSC). The benefits of using a VSC are sinusoidal currents, high current bandwidth, and controllable reactive power to regulate the bus voltage level. A system with these characteristics can be used to inject a controllable current into the system. By injecting a popper current into the system, a shunt connected VSC can boost the voltages at that point during a voltage sags. The configuration of the D-STATCOM with the proposed control that connected to the distribution system for regulating the load voltage is illustrated in Figure 8.1. The D-STATCOM consists of a three-phase voltage source converter (VSC), a DC-side capacitor C_{dc} with parallel resistance R_{dc}. The resistance R_{dc} represents losses in the converter. Two kinds of losses are of interest in such the converter configurations which are conduction losses and switching losses. The losses are both in the diodes and in the switches such as IGBT and MOSFET (Blaabjerg et al., 1996). An inductance L_f and the resistance R_f represent the inductance and resistance of the AC-side of the converter. A shunt filter capacitor with capacitance C_f is added to the AC-side of the voltage source converter that forms a LC filter. This filter helps in effectively filtering out the switching ripple in the output voltage waveform. The distribution system is represented by using an ideal voltage source and impedance. This impedance consists of an inductance L_s and a resistance R_s which characterizes the transformer and power line respectively. The analysis and design of the D-

STATCOM controller are conducted in the rotating reference frame which is synchronized to the voltage vector at the PCC. As explained earlier in previous, the D-STATCOM mitigates the voltage sags by dynamically injecting a current of desired amplitude and phase angle into the system. A schematic diagram of the D-STATCOM with the proposed control is presented in Figure 6.1. The current control in Figure 6.1 force the converter currents i_{fd} and i_{fq} to follow the command currents i_{fd}^{*} and i_{fq}^{*} respectively. The command i_{fd}^{*} to the *d*-axis current loop is obtained by the DC voltage controller while the command i_{fq}^{*} is obtained from the AC voltage controller. The purpose of the outer loop DC voltage controller is to regulate the DC voltage to a required level. The current controller and DC voltage controller design for this D-STATCOM are similar to the controller design presented in the Chapter 6, since they have the same structure and serve the same purpose. Meanwhile, the AC voltage controller design and parameters are explained in the Chapter 7.

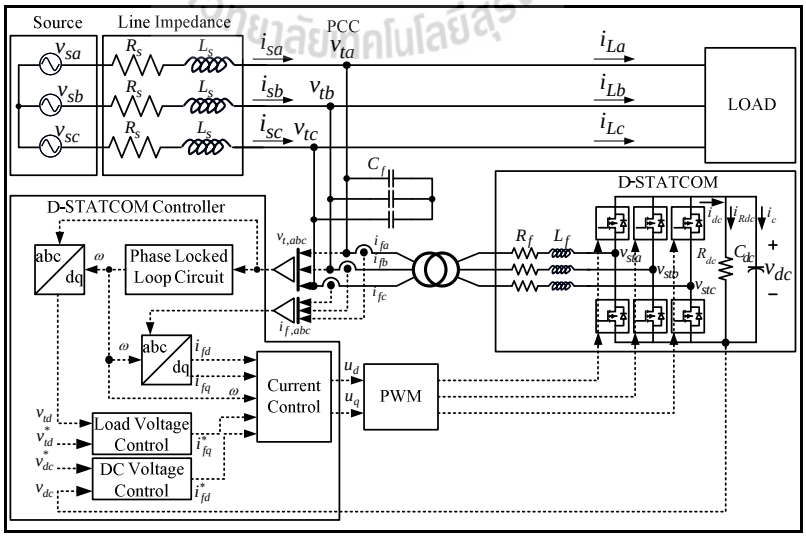

Figure 8.1 Overall schematic diagram of D-STATCOM for load voltage regulation

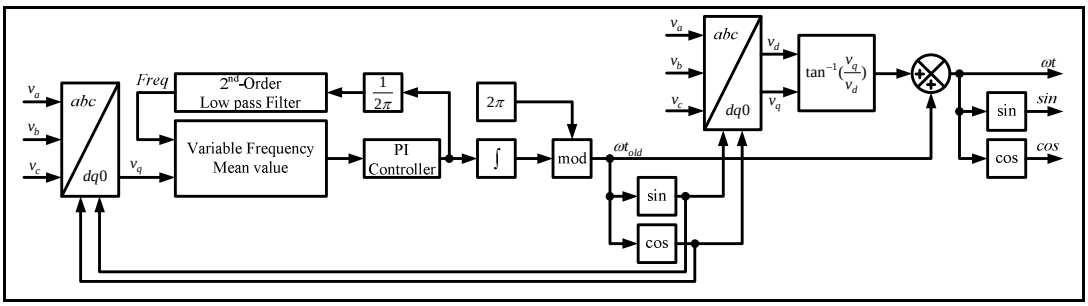

Figure 8.2 Modified PLL block diagram

In addition, the basic PLL block diagram in Figure 2.14 is modified in this chapter that can be seen in Figure 8.2. Since using the modified PLL, $v_{tq} \equiv 0$ for any times and v_{td} represents the instantaneous magnitude of the phase voltages, while i_{fq} denotes the instantaneous reactive current supplied by the D-STATCOM and is the control input to the system for the load voltage regulation.

8.2 Modeling and Simulation Results of the D-STATCOM for Load Voltage Regulation

In this section, the simulation results for the D-STATCOM with the proposed controller design will be presented. The configuration of the D-STATCOM system with the proposed controller designed for load voltage regulation that shown in Figure 8.1 is modeled using the MATLAB/SIMULINK software package. The model utilizes SIMULINK control and SimPower Blocks are illustrated in Figure 8.3 and Figure 8.4. In Figure 8.3, the D-STATCOM is connected with the system though the 22/2.2 *kV* (Y/Y) transformer. Figure 8.4 presents the model of the D-STATCOM controller. The

system data used are taken from the simplification network of a 166 buses Nakhonrachasima, Thailand at bus 99. The system parameters are

	V_s (L-L rms)	= 22 *kV*	L_s	= 38.666 *mH*
	R_s	= 1.4564 Ω	ω_s	= 100π $rad.s^{-1}$
	R_l	= 116.68 Ω	L_l	= 0.00 *mH* (for R load)
And	R_l	= 89.346 Ω	L_l	= 157.35 *mH* (for RL load)

According to the steady state analysis of the distribution system with D-STATCOM that discussed in the Chapter 3, the maximum load active power, $P_{l,desired}(\max)$, and minimum source voltage, $V_s(\min)$ of the system with the given parameters in the above are 34.85 *MW* and 4.93 *kV*, respectively. These correspond to the reactive power of regulating the load voltage as 22 *kV* is about 37.50 *MVar* for R load while 40.00 and 57.00 *MVar* for RL load with minimum source voltage and maximum load active power, respectively. However, a ± 15 *MVA* D-STATCOM is selected for load voltage regulation in this system. This D-STATCOM can regulate the load voltage as 22 *kV* when the source voltage is more than 15.40 *kV* (or 0.7 *pu*.). In addition, it can be used to regulate the load voltage as 22 *kV* when the load active power is less than 16.59 *MW* (or 4.0 *pu*.). The required reactive power for different source voltage is given in Table 8.1. Meanwhile, the required reactive power for different load power is given in Table 8.2. The parameters of the D-STATCOM that corresponding to source voltage sags and load power variations are shown in Table 8.3 and Table 8.4, respectively. However, the parameters of the D-STATCOM at the maximum required reactive power (13.82 *MVar*) are used in the section.

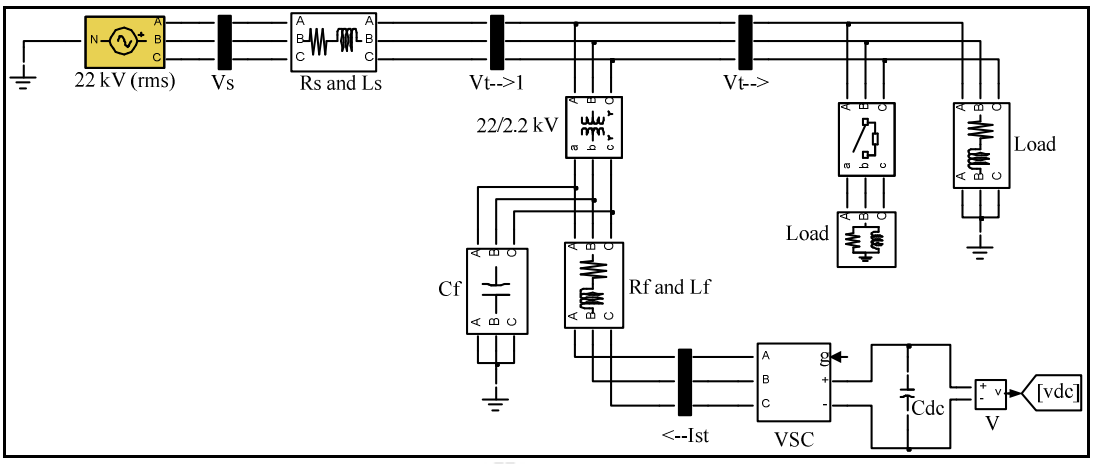

Figure 8.3 MATLAB/SIMULINK model of the distribution system with the D-STATCOM

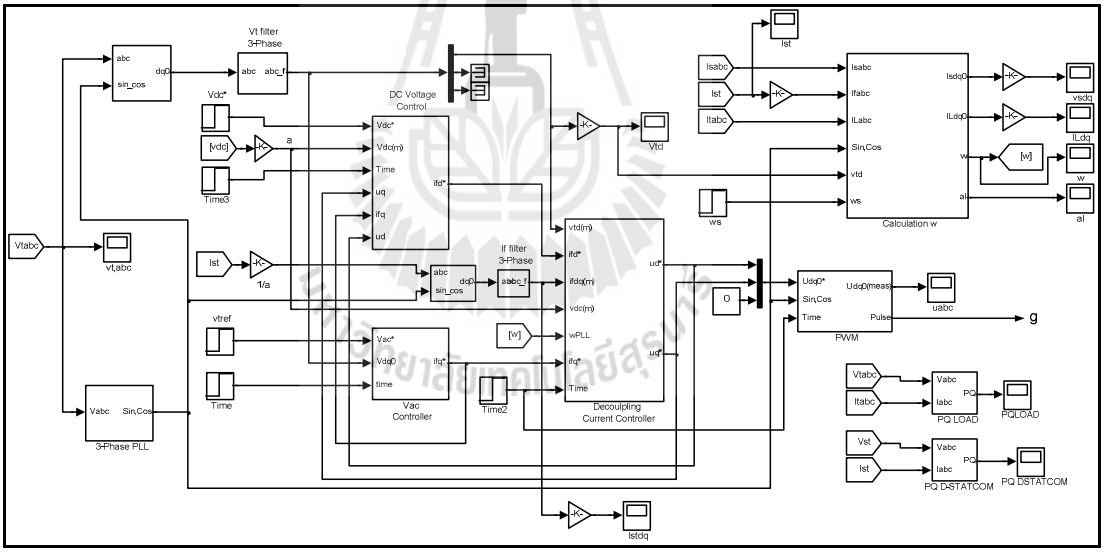

Figure 8.4 MATLAB/SIMULINK model of the D-STATCOM controller

Table 8.1 Required reactive power for different source voltage

Source voltage (*kV*)	Load as PF= 1.0	Load as PF= 0.875 lag
	Required reactive power (*MVar*)	Required reactive power (*MVar*)
28.60 (1.3 *pu*.)	12.90	10.61
26.40 (1.2 *pu*.)	8.88	6.59
24.20 (1.1 *pu*.)	4.85	2.55
22.00 (1.0 *pu*.)	0.80	-1.50
19.80 (0.9 *pu*.)	-3.27	-5.57
17.60 (0.8 *pu*.)	-7.37	-9.67
15.40 (0.7 *pu*.)	-11.52	-13.82

Table 8.2 Required reactive power for different load power

Load active power (*MW*)	Load as PF= 1.0	Load as PF= 0.875 lag
	Required reactive power (*MVar*)	Required reactive power (*MVar*)
0.415 (0.1 *pu*.)	1.47	1.24
2.074 (0.5 *pu*.)	1.22	0.07
4.148 (1.0 *pu*.)	0.80	-1.50
6.221 (1.5 *pu*.)	0.26	-3.18
8.295 (2.0 *pu*.)	-0.40	-4.99
10.369 (2.5 *pu*.)	-1.18	-6.92
12.442 (3.0 *pu*.)	-2.11	-9.00
14.520 (3.5 *pu*.)	-3.18	-11.22
16.590 (4.0 *pu*.)	-4.42	-13.60

Table 8.3 D-STATCOM parameters for different source voltage

Source voltage (*kv*)	Load as PF= 1.0				Load as PF= 0.875 lag			
	DC bus Voltage (*kV*)	Current Rating (*kA*)	AC Inductance (*mH*)	DC bus Capacitance (μF)	DC bus Voltage (*kV*)	Current Rating (*kA*)	AC Inductance (*mH*)	DC bus Capacitance (μF)
28.60	6.532	+58.644	0.1474	2984	6.532	+48.214	0.1793	2453
26.40	6.532	+40.366	0.2141	2054	6.532	+29.935	0.2887	1523
24.20	6.532	+22.032	0.3923	1121	6.532	+11.602	0.7450	590
22.00	6.532	+3.6260	2.3837	184	6.532	-6.805	1.2700	346
19.80	6.532	-14.879	0.5808	757	6.532	-25.310	0.3415	1288
17.60	6.532	-33.522	0.2578	1706	6.532	-43.953	0.1966	2236
15.40	6.532	-52.368	0.1650	2664	6.532	-62.799	0.1376	3195

Table 8.4 D-STATCOM parameters for different load power

Load active power (*MW*)	Load as *pf* = 1.0				Load as *pf* = 0.875 lag			
	DC bus Voltage (*kV*)	Current Rating (*kA*)	AC Inductance (*mH*)	DC bus Capacitance (μF)	DC bus Voltage (*kV*)	Current Rating (*A*)	AC Inductance (*mH*)	DC bus Capacitance (μF)
0.415	6.532	+6.674	1.2950	340	6.532	+5.632	1.5346	287
2.074	6.532	+5.527	1.5636	281	6.532	+0.312	27.7170	16
4.148	6.532	+3.626	2.3837	184	6.532	-6.805	1.2700	346
6.221	6.532	+1.190	7.2634	061	6.532	-14.456	0.5978	735
8.295	6.532	-1.803	4.7931	092	6.532	-22.664	0.3813	1153
10.369	6.532	-5.383	1.6054	274	6.532	-31.460	0.2747	1600
12.442	6.532	-9.590	0.9012	488	6.532	-40.882	0.2114	2080
14.520	6.532	-14.473	0.5972	736	6.532	-50.980	0.1695	2594
16.590	6.532	-20.098	0.4300	1023	6.532	-61.820	0.1398	3145

In this section, the simulation results of the D-STATCOM with the proposed controller design were presented in two cases: (i) voltage regulation when the distribution system with the R loads and (ii) voltage regulation when the distribution system with the RL loads.

8.2.1 Voltage Regulation when the Distribution System with the R Load

According to the current control and DC voltage control strategy described in Chapter 6, the decoupling current control based on GAs and the DC voltage control based on SO are used in this section. The parameters of the current and DC voltage control are shown in Table 8.5. Meanwhile, the AC voltage control with the classical loop shaping method that described in Chapter 7 is used for the R load. The AC voltage controller parameters and the stability margins for the R load with various operating conditions, each corresponding to a different value of source voltage (that means corresponding to a different i_{fq}) are presented in Table 8.6.

Table 8.5 Current and DC voltage controller parameters

Controller	Parameter
K_{Pid} and K_{Piq}	26,709.6
T_{Iid} and T_{Iiq}	3.7
K_{pvdc}	1,250
T_{Ivdc}	0.0016

Table 8.6 AC voltage controller for the distribution system with the R load

Source Voltage (*kV*)	PI Parameters	Compensator 1 Parameters	Compensator 2 Parameters	Gain Margin (*dB*)	Phase Margin (*deg*)
28.82	$0.042\left(\frac{0.0014s+1}{0.0014s}\right)$	$\frac{1}{0.00001s+1}$	1	10.92	51.10
27.59	$0.049\left(\frac{0.0014s+1}{0.0014s}\right)$	$\frac{1}{0.00001s+1}$	1	11.46	51.18
26.40	$0.056\left(\frac{0.0014s+1}{0.0014s}\right)$	$\frac{1}{0.00001s+1}$	1	12.35	51.78
25.19	$0.063\left(\frac{0.0014s+1}{0.0014s}\right)$	$\frac{1}{0.00001s+1}$	1	14.17	53.94
23.98	$0.070\left(\frac{0.0014s+1}{0.0014s}\right)$	$\frac{1}{0.00001s+1}$	1	17.00	61.57
22.77	$0.002\left(\frac{0.0001s+1}{0.0001s}\right)$	$\frac{1}{0.0013s+1}$	1	13.16	64.19
21.56	$0.0002\left(\frac{0.00001s+1}{0.00001s}\right)$	$\frac{1}{0.0013s+1}$	1	7.56	60.41
20.35	$0.00018\left(\frac{0.00001s+1}{0.00001s}\right)$	$\frac{1}{0.0016s+1}$	1	6.16	57.90
19.14	$0.00016\left(\frac{0.00001s+1}{0.00001s}\right)$	$\frac{1}{0.0020s+1}$	1	5.84	55.76
17.93	$0.00014\left(\frac{0.00001s+1}{0.00001s}\right)$	$\frac{1}{0.0024s+1}$	1	6.13	55.24
16.81	$0.00012\left(\frac{0.00001s+1}{0.00001s}\right)$	$\frac{1}{0.0027s+1}$	1	6.44	56.44
15.62	$0.00012\left(\frac{0.00001s+1}{0.00001s}\right)$	$\frac{1}{0.0027s+1}$	1	5.02	54.00
14.41	$0.00010\left(\frac{0.00001s+1}{0.00001s}\right)$	$\frac{1}{0.0027s+1}$	1	5.16	58.04

The controllers that are designed in each source voltage operation points i.e. 28.82, 26.40 and 23.93 *kV* (i_{fq} = +600, +400 and +200A) for the load voltage regulation in case of the source voltage variations between 28.82 and 23.98

kV are demonstrated and compared as shown in Figure 8.5. As can be seen in this Figure, the controller that is designed in case of the source voltage as 23.93 *kV* (i_{fq} = +200*A*) cannot be used for the source voltage as 28.82 *kV* (i_{fq} = +600*A*) and the controller that is designed in case of the source voltage as 26.40 *kV* (i_{fq} = +400*A*) gives the high overshoot and oscillation response in some case. Whilst, the controller that is designed in case of the source voltage as 28.82 *kV* (i_{fq} = +600*A*) can be used for all cases and gives a good dynamic response.

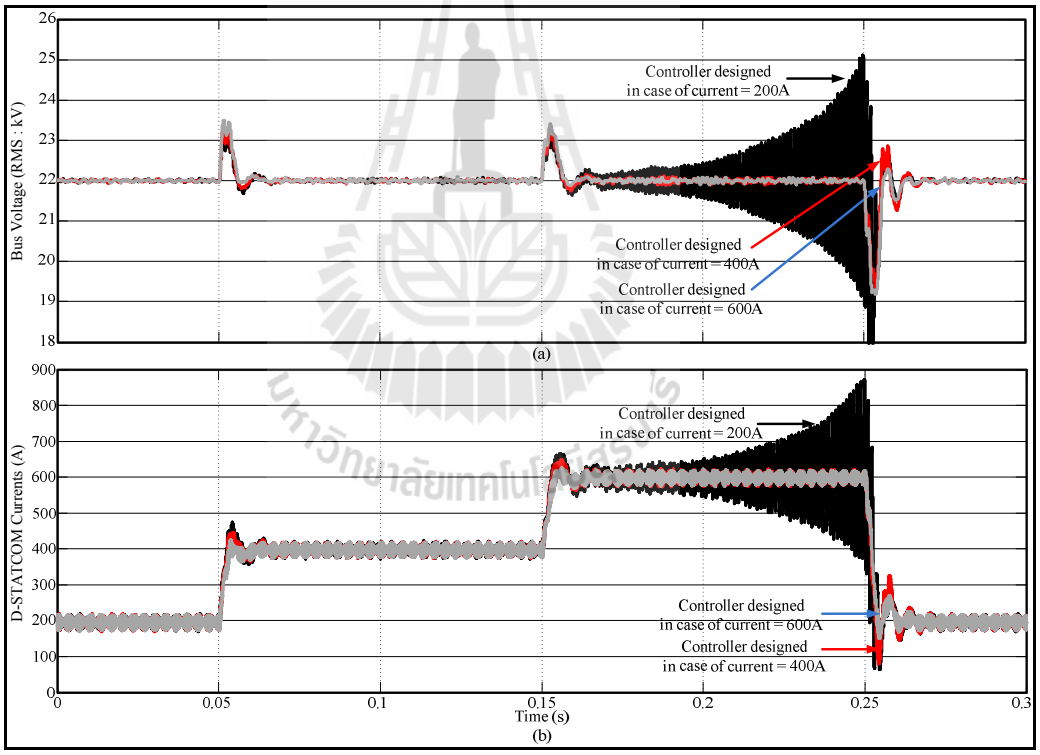

Figure 8.5 Comparison the controller in case of the source voltage variations between 28.82 and 23.98 *kV*

Similarly, the controllers that are designed in each source voltage operation points i.e. 21.56, 19.14, 16.18 and 14.41 kV (i_{fq} = 0, -200, -400 and -600A) for the load voltage regulation in case of the source voltage variations between 21.56 and 14.41 kV are demonstrated and compared as shown in Figure 8.6. As can be seen in this Figure, the controller that is designed in case of the source voltage as 14.41 kV (i_{fq} = -600A) can be used for all cases and gives a good dynamic response.

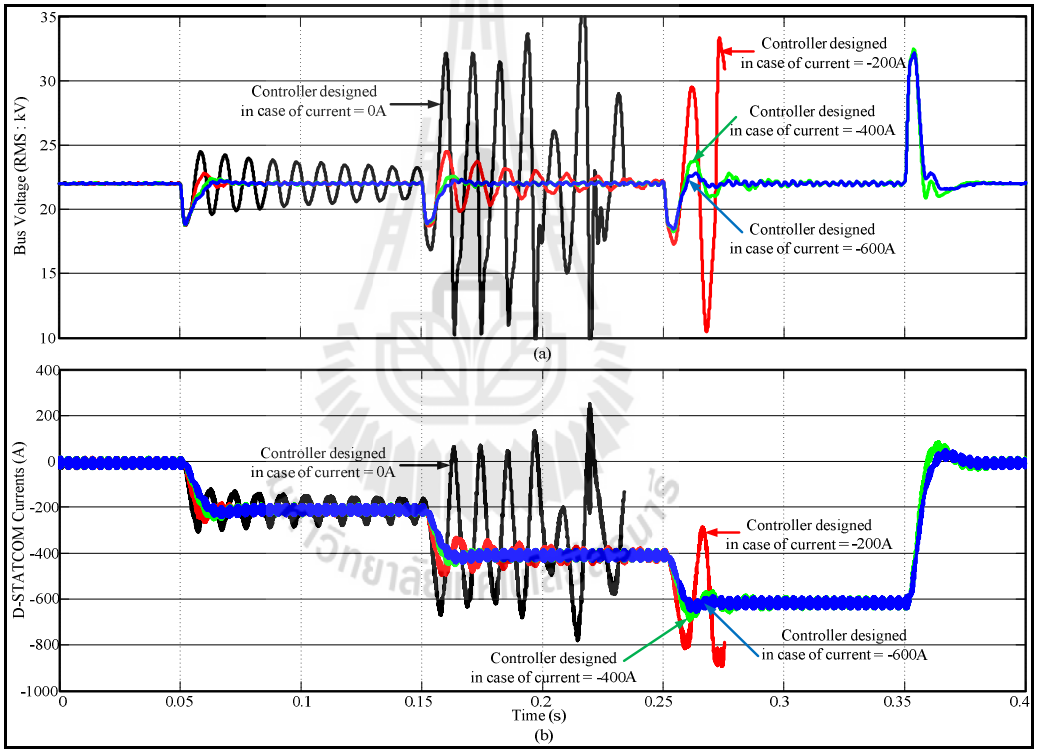

Figure 8.6 Comparison the controller in case of the source voltage variations between 21.56 and 14.41 kV

Therefore, the parameters of PI controller and the compensator when the source voltage of 28.82 kV are used in case of the source voltage variations

between 28.82 and 23.98 *kV* (i.e. i_{fq} varies between +600 and +200 *A*). Whilst, the parameters of PI controller and the compensator when the source voltage of 14.41 *kV* are used in case of the source voltage variations between 22.77 and 14.41 *kV* (i.e. i_{fq} varies between +100 and -600 *A*).

In this case, the system is simulated for time varying source voltage conditions. The dash lines of figure 8.7(a) shows the load voltage of the system without D-STATCOM when the source voltage is varied. As may be seen, the load voltage corresponds to five different source voltage conditions: source voltage of 23.98 *kV* from t = 0.00 to 0.05 second; source voltage of 27.59 *kV* from t = 0.05 to 0.15 second; source voltage at 25.19 *kV* from t = 0.15 to 0.25 second; source voltage of 28.82 *kV* from t = 0.25 to 0.35 second; and source voltage of 23.98 *kV* from t = 0.35 to 0.40 second. Meanwhile, the solid line of figure 8.7(a) shows the load voltage of the system with D-STATCOM when the source voltage is varied. It can be observed from this figure that the D-STATCOM with proposed control design can be regulated the load voltage at the desired value. The load voltage took approximately 0.01 seconds to settle in each source voltage. It can be seen in figure 8.7(b) that the load voltage waveform reaches the desired value within a haft cycle.

Figure 8.8 presents the currents, DC voltage and power of the D-STATCOM for the system with R load when the source voltage is varied between 28.82 and 23.98 *kV*. As may be seen in figure 8.8(a), that the reactive currents (i_{fq}) are +200, +500, +300, +600 and +200 *A* to compensate the load voltage swell when the source voltages are 23.98, 27.59, 25.19, 28.82 and 23.98 *kV*, respectively. Whilst, the active current (i_{fd}) very small change when the D-STATCOM compensate the

load voltage. These correspond to the reactive and active powers of the D-STATCOM as shown in Figure 8.8(b). The reactive powers are -4.4, -10.1, -6.6, -13.2 and -4.4 *MVar* to compensate the load voltage swell when the source voltages are 23.98, 27.59, 25.19, 28.82 and 23.98 *kV*, respectively. Meanwhile, the active power very small change in positive when the D-STATCOM compensation the load voltage. This means that the D-STATCOM consumes active power to regulate the DC voltage at the constant value as can be seen in figure 8.8(c). As seen in this figure, the DC voltage is always regulated at 6.6 *kV* for all of source voltages.

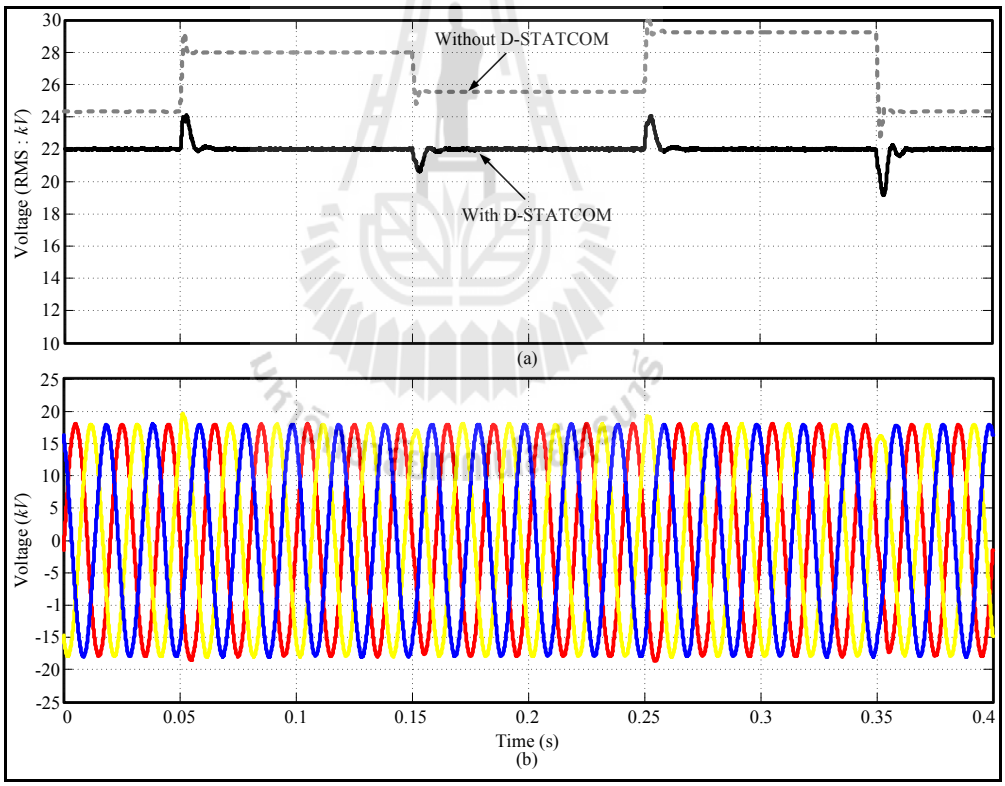

Figure 8.7 Load voltage of the system with the R load which the source voltage varying between 28.82 and 23.98 *kV*

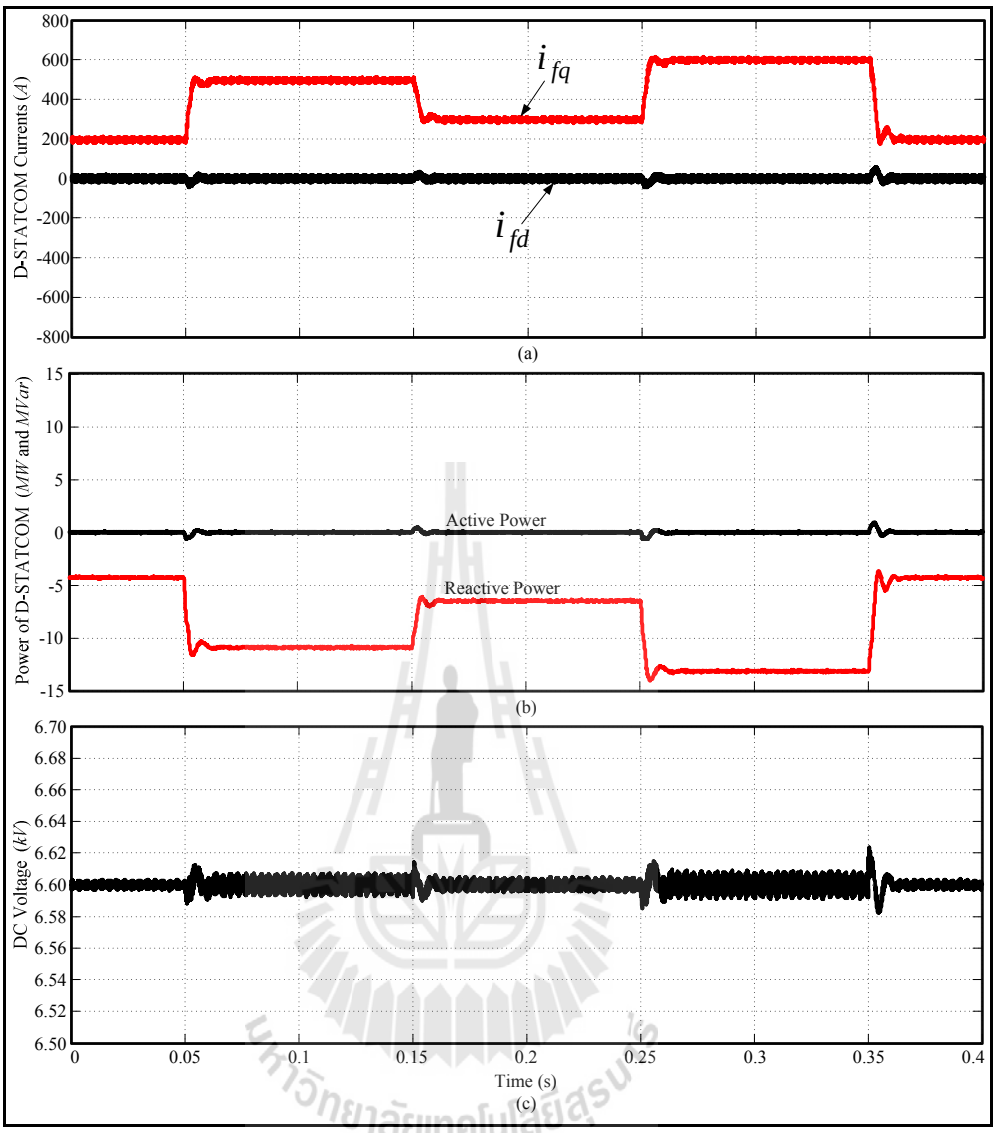

Figure 8.8 Currents, DC voltage and power of the D-STATCOM for the system with the R load which the source voltage varying between 28.82 and 23.98 *kV*

In case of the source voltage varying between 22.77 and 14.41 *kV*, the load voltage of the system with the R load is shown in Figure 8.9. The dashes line of Figure 8.9(a) shows the load voltage of the system without D-STATCOM when the source voltage is varied. As seen in this Figure, the load voltage corresponds to five

different source voltage conditions: source voltage of 21.56 *kV* from t = 0.00 to 0.05 second; source voltage of 17.93 *kV* from t = 0.05 to 0.15 second; source voltage at 22.77 *kV* from t = 0.15 to 0.25 second; source voltage of 14.41 *kV* from t = 0.25 to 0.35 second; and source voltage of 21.56 *kV* from t = 0.35 to 0.40 second. Whilst, the solid line of Figure 8.9(a) shows the load voltage of the system with D-STATCOM. As can be observed from this Figure that the D-STATCOM with proposed control design can be regulated the load voltage at the desired value. The load voltage took approximately 0.02 seconds to settle in each source voltage. As can be seen in Figure 8.9(b), the load voltage reaches the desired value within one cycle.

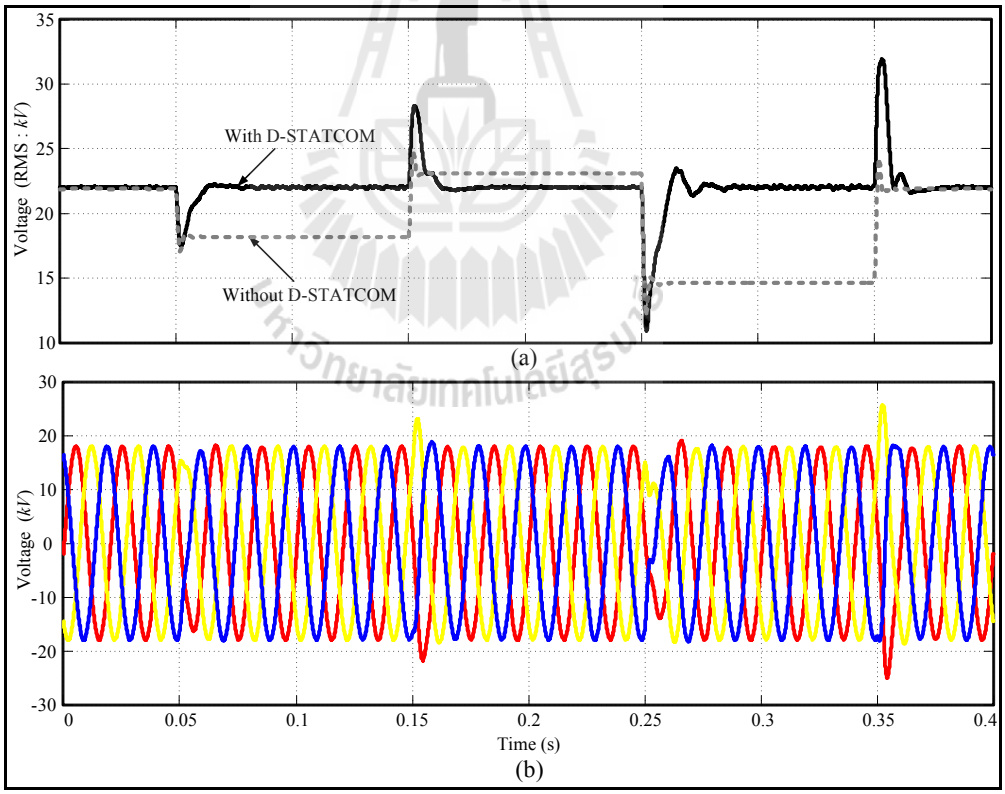

Figure 8.9 Load voltage of the system with the R load which the source voltage varying between 22.77 and 14.41 *kV*

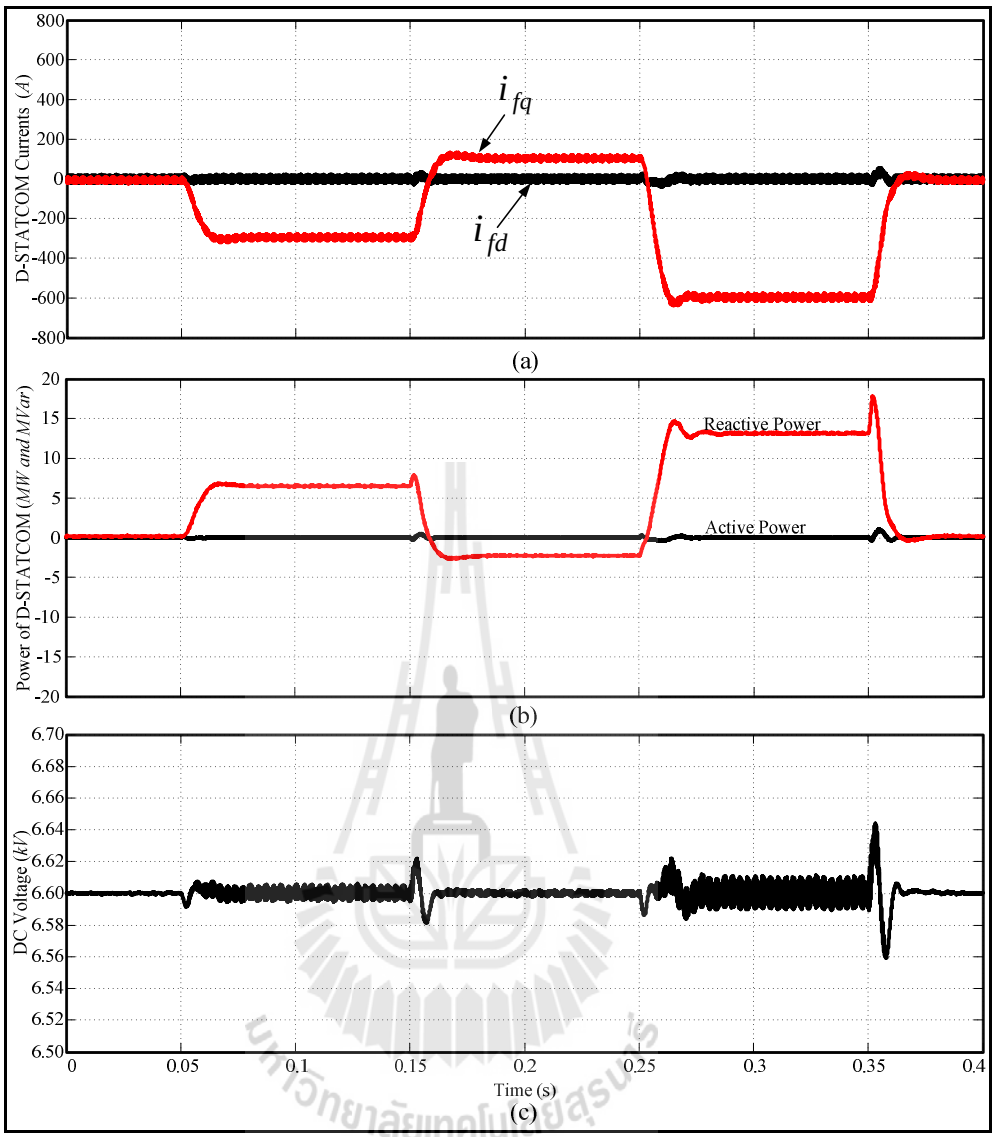

Figure 8.10 Currents, DC voltage and power of the D-STATCOM for the system with the R load which the source voltage varying between 22.77 and 14.41 *kV*

Figure 8.10 presents the currents, DC voltage and power of the D-STATCOM for the system with the R load when the source voltage is varied between 22.77 and 14.41 *kV*. As may be seen in Figure 8.10(a), that the reactive currents (i_{fq})

are about 0, -300, +100, -600 and 0 *A* to compensate the load voltage swell when the source voltages are 21.56, 17.93, 22.77, 14.41 and 21.56 *kV*, respectively. Whilst, the active current (i_{fd}) very small changes when the D-STATCOM compensate the load voltage. These correspond to the reactive and active powers of the D-STATCOM as shown in Figure 8.10(b). The reactive powers are of 0.0, +6.6, +2.2, +13.2 and 0.0 *MVar* to compensate the load voltage when the source voltages are 21.56, 17.93, 22.77, 14.41 and 21.56 *kV*, respectively. Meanwhile, the active power very small changes in positive when the D-STATCOM compensating the load voltage. So, the D-STATCOM consumes active power to regulate the DC voltage at the constant value. Furthermore, the D-STATCOM always consumes active power no matter how much it absorbs or generates reactive power. As can be seen in figure 8.10(c), the DC voltage is always regulated at 6.6 *kV* for all of source voltages.

In addition, the application of the D-STATCOM for load voltage regulation when varying the load is demonstrated in this section. The load powers are shown in Figure 8.11. As seen in this Figure, the active powers are 0. 415 *MW* (0.1 *pu.*) from t = 0.00 to 0.05 second, 4.15 *MW* (1.0 *pu.*) from t = 0.05 to 0.15 second, 8.30 *MW* (2.0 *pu.*) from t = 0.15 to 0.25 second, 12.45 *MW* (3.0 *pu.*) from t = 0.25 to 0.35 second, 16.60 *MW* (4.0 *pu.*) from t = 0.35 to 0.45 second and come back to 4.15 *MW* (1.0 *pu.*) from t = 0.45 to 0.50 second, while the reactive power is not changed in this case. The load voltage of the system without the D-STATCOM is shown as the dash line in Figure 8.12. Meanwhile, the solid line presents the load voltage of system with D-STATCOM. As seen in this Figure, the D-STATCOM with the proposed control in case of source voltage variations can be used in case of load varied as well. The powers of the D-STATCOM to compensate the load voltage are shown in Figure

8.13. In this Figure, the reactive powers are -1.47, -0.80, +0.40, +2.11, +4.42 and -0.80 *MVar* when the load powers are 0.415, 4.15, 8.30, 12.45, 16.60 and 4.15 *MW*, respectively, while the active power very small change in this case.

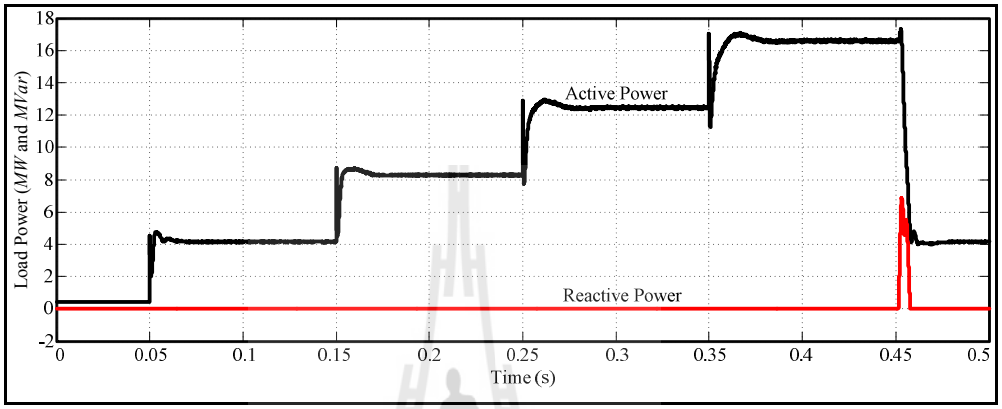

Figure 8.11 Load varying when the system with the R load

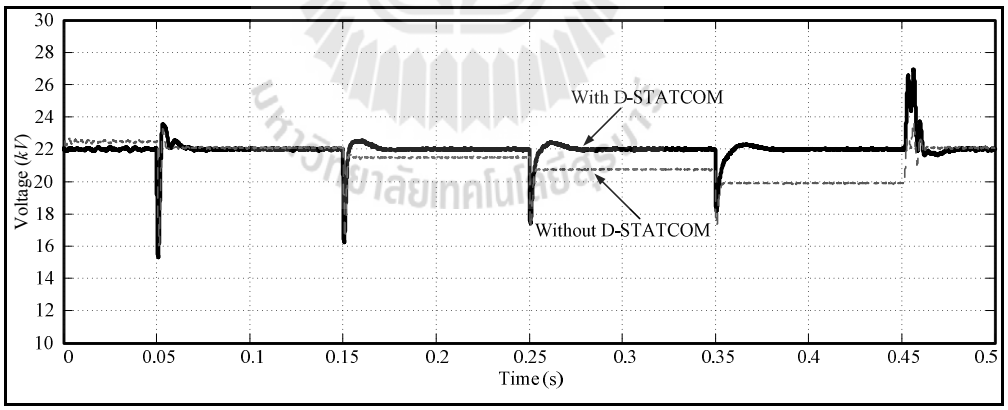

Figure 8.12 Load voltages in the system with the R load in case of the load variations

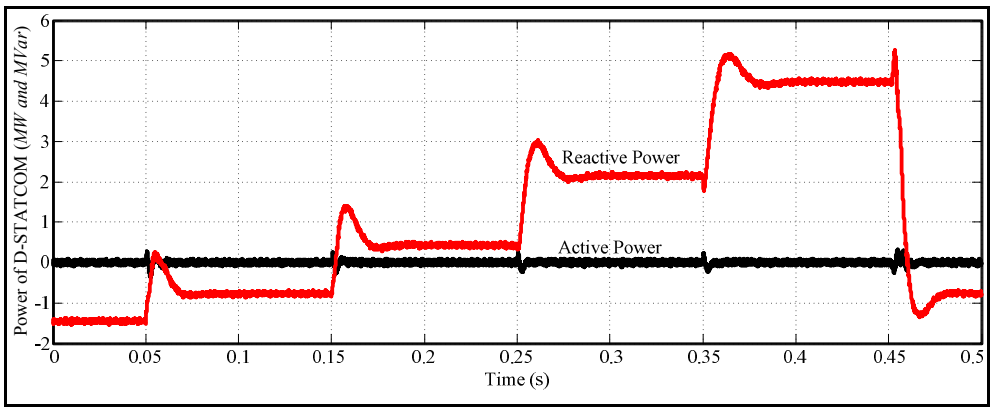

Figure 8.13 Powers of the D-STATCOM for the system with the R load in case of the load variations

8.2.2 Voltage Regulation when the Distribution System with the RL Load

In this case, the current control and DC voltage control with the parameters similar to case i as shown in Table 8.5 are used. Meanwhile, the AC voltage control with the classical loop shaping method that described in chapter 7 is used. The AC voltage controller parameters and the stability margins for RL load with various operating conditions, each corresponding to a different value of source voltage (that means corresponding to a different i_{fq}) are presented in Table 8.7.

In Figure 8.14, the controllers that are designed in each source voltage operation points i.e. 30.14, 27.72 and 25.30 kV ($i_{fq} = +600$, +400 and +200A) for the load voltage regulation in case of the source voltage variations between 30.14 and 25.30 kV are demonstrated and compared. As can be seen in this Figure, the controllers that are designed in case of the source voltage as 25.30 kV ($i_{fq} = +200A$) and 27.72 kV ($i_{fq} = +400A$) give the high overshoot and oscillation response in some

case. Whilst, the controller that is designed in case of the source voltage as 30.14 *kV* ($i_{fq} = +600A$) can be used for all cases and gives a good dynamic response.

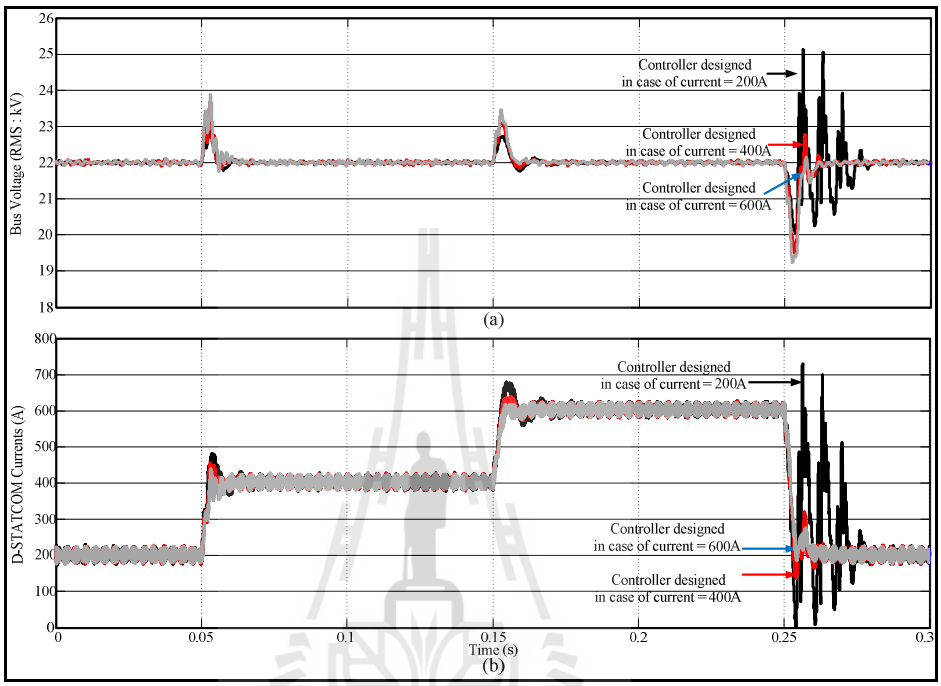

Figure 8.14 Comparison the controller in case of the source voltage variations between 30.14 and 25.30 *kV*

Similarly, the controllers that are designed in each source voltage operation points i.e. 22.77, 20.35, 18.04 and 15.71 *kV* ($i_{fq} = 0$, -200, -400 and -600A) for the load voltage regulation in case of the source voltage variations between 22.77 and 15.71 *kV* are demonstrated and compared as shown in Figure 8.15. As can be seen in this Figure, the controllers that are designed in case of the source voltage as 15.71 *kV* ($i_{fq} = -600A$) and 18.04 *kV* ($i_{fq} = -400A$) can be used for all cases and give a good dynamic response.

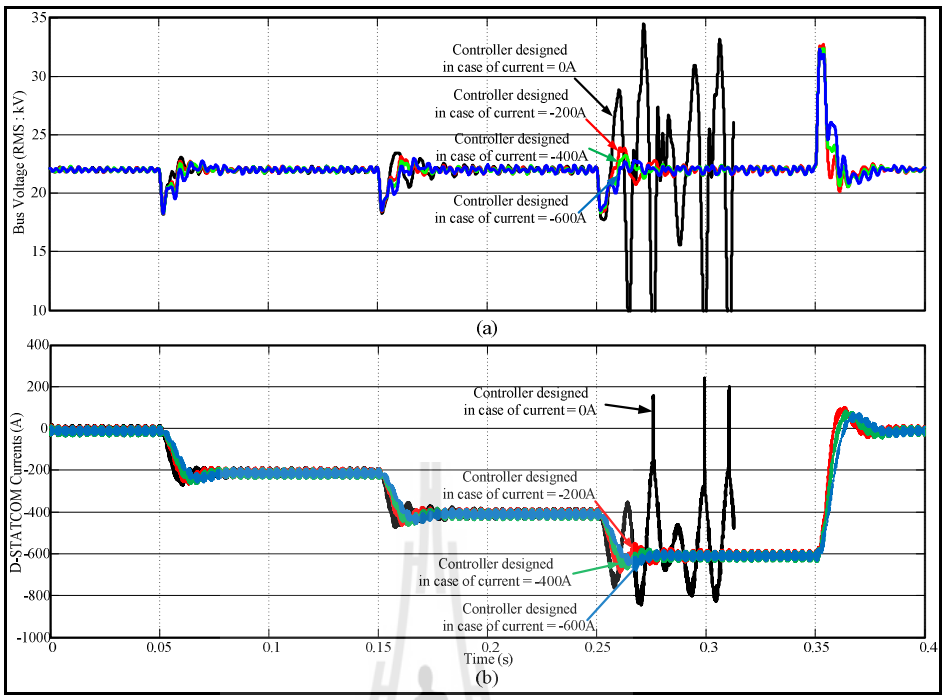

Figure 8.15 Comparison the controller in case of the source voltage variations between 22.77 and 15.71 *kV*

However, the parameters of PI controller and the compensator when the source voltage of 30.14 *kV* are selected in case of the source voltage variations between 30.14 and 25.30 *kV* (i.e. i_{fq} varies between +600 and +200 *A*). Whilst, the parameters of PI controller and the compensator when the source voltage of 15.71 *kV* are selected in case of the source voltage variations between 24.09 and 15.71 *kV* (i.e. i_{fq} varies between +100 and -600 *A*). In addition, the notch compensator (i.e. $\frac{0.00096^2 s^2 + 0.00014s + 1}{0.00096^2 s^2 + 0.00192s + 1}$) is used in the case of the source voltage variations between 24.09 and 15.71 *kV*. This compensator is applied in order to mitigate the effect of resonance of the system.

Table 8.7 AC voltage controller for the distribution system with the RL load

Source voltage (*kV*)	PI Parameters	Compensator 1 Parameters	Compensator 2 Parameters	Gain Margin (*dB*)	Phase Margin (*deg*)
30.14	$0.042\left(\frac{0.0014s+1}{0.0014s}\right)$	$\frac{0.0001s+1}{0.00001s+1}$	1	6.38	55.63
28.82	$0.049\left(\frac{0.0014s+1}{0.0014s}\right)$	$\frac{0.0001s+1}{0.00001s+1}$	1	6.80	54.51
27.72	$0.056\left(\frac{0.0014s+1}{0.0014s}\right)$	$\frac{0.0001s+1}{0.00001s+1}$	1	7.85	51.43
26.47	$0.070\left(\frac{0.0014s+1}{0.0014s}\right)$	$\frac{0.0001s+1}{0.00001s+1}$	1	8.64	50.39
25.30	$0.098\left(\frac{0.0014s+1}{0.0014s}\right)$	$\frac{0.0001s+1}{0.00001s+1}$	1	9.57	51.87
24.09	$0.020\left(\frac{0.0008s+1}{0.0008s}\right)$	$\frac{1}{0.0010s+1}$	$\frac{0.00062^2s^2+4.4e^{-5}s+1}{0.00062^2s^2+0.00124s+1}$	18.71	63.28
22.77	$0.0072\left(\frac{0.0004s+1}{0.0004s}\right)$	$\frac{1}{0.0012s+1}$	$\frac{0.00068^2s^2+6.0e^{-5}s+1}{0.00068^2s^2+0.00136s+1}$	14.24	60.88
21.56	$0.0032\left(\frac{0.0002s+1}{0.0002s}\right)$	$\frac{1}{0.0012s+1}$	$\frac{0.00073^2s^2+7.2e^{-5}s+1}{0.00073^2s^2+0.00146s+1}$	11.20	60.00
20.35	$0.00112\left(\frac{0.00008s+1}{0.00008s}\right)$	$\frac{1}{0.0014s+1}$	$\frac{0.00078^2s^2+8.4e^{-5}s+1}{0.00078^2s^2+0.00156s+1}$	9.94	58.45
19.14	$0.00072\left(\frac{0.00006s+1}{0.00006s}\right)$	$\frac{1}{0.0016s+1}$	$\frac{0.00082^2s^2+9.7e^{-5}s+1}{0.00082^2s^2+0.00164s+1}$	9.71	59.48
18.04	$0.00048\left(\frac{0.00004s+1}{0.00004s}\right)$	$\frac{1}{0.0016s+1}$	$\frac{0.00087^2s^2+0.00011s+1}{0.00087^2s^2+0.00174s+1}$	8.33	57.33
16.83	$0.00020\left(\frac{0.00002s+1}{0.00002s}\right)$	$\frac{1}{0.0018s+1}$	$\frac{0.00092^2s^2+0.00013s+1}{0.00092^2s^2+0.00184s+1}$	8.74	59.71
15.71	$0.00020\left(\frac{0.00002s+1}{0.00002s}\right)$	$\frac{1}{0.0020s+1}$	$\frac{0.00096^2s^2+0.00014s+1}{0.00096^2s^2+0.00192s+1}$	7.75	56.62

In this case, the system is simulated for time varying source voltage conditions. The dashes line of Figure 8.16(a) shows the load voltage of the system without D-STATCOM when the source voltage is varied. It can be seen that the load voltage corresponds to five different source voltage conditions: source voltage of 25.30 *kV* from t = 0.00 to 0.05 second; source voltage of 28.82 *kV* from t = 0.05 to 0.15 second; source voltage at 26.47 *kV* from t = 0.15 to 0.25 second; source voltage of 30.14 *kV* from t = 0.25 to 0.35 second; and source voltage of 25.30 *kV* from t = 0.35 to 0.40 second. Meanwhile, the solid line of Figure 8.16(a) presents the load

voltage of the system with D-STATCOM when the source voltage is varied. It can be observed from this Figure, the D-STATCOM with proposed control design can be regulated the load voltage at the desired value. The load voltage took approximately 0.01 seconds to settle in each source voltage. It can be seen in Figure 8.16(b) that the load voltage waveform reaches the desired value within a haft cycle.

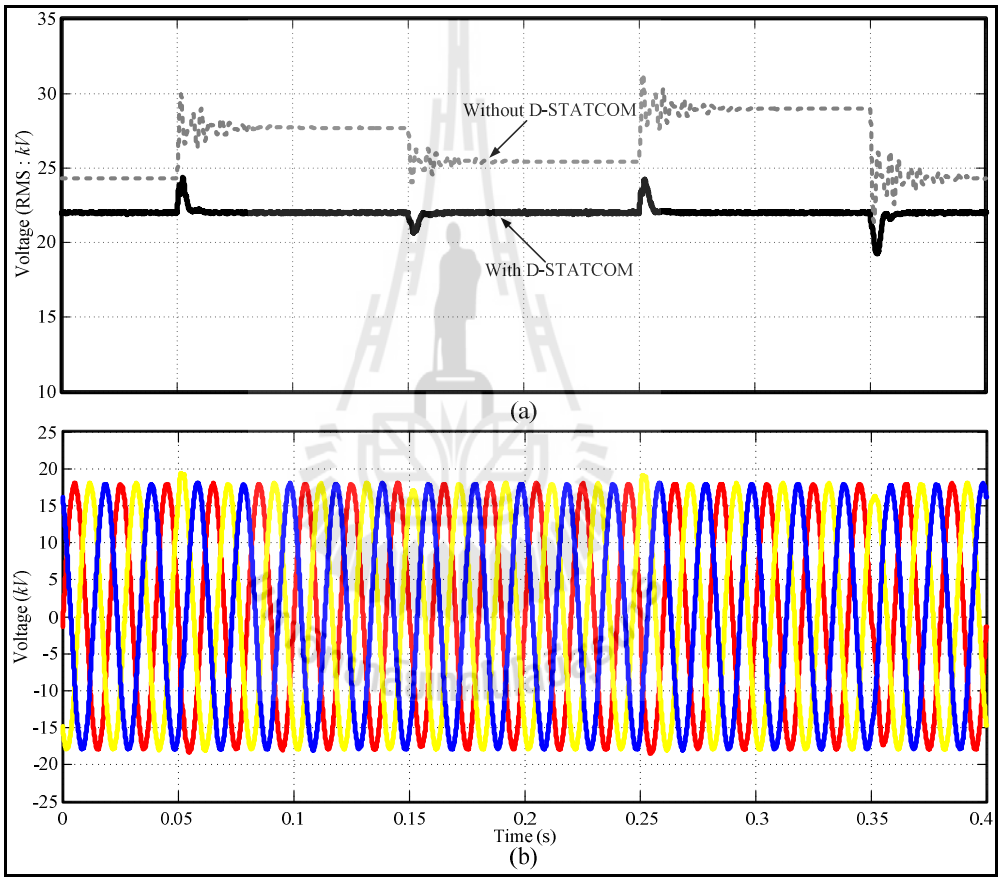

Figure 8.16 Load voltage of the system with the RL load which the source voltage varying between 28.82 and 23.98 *kV*

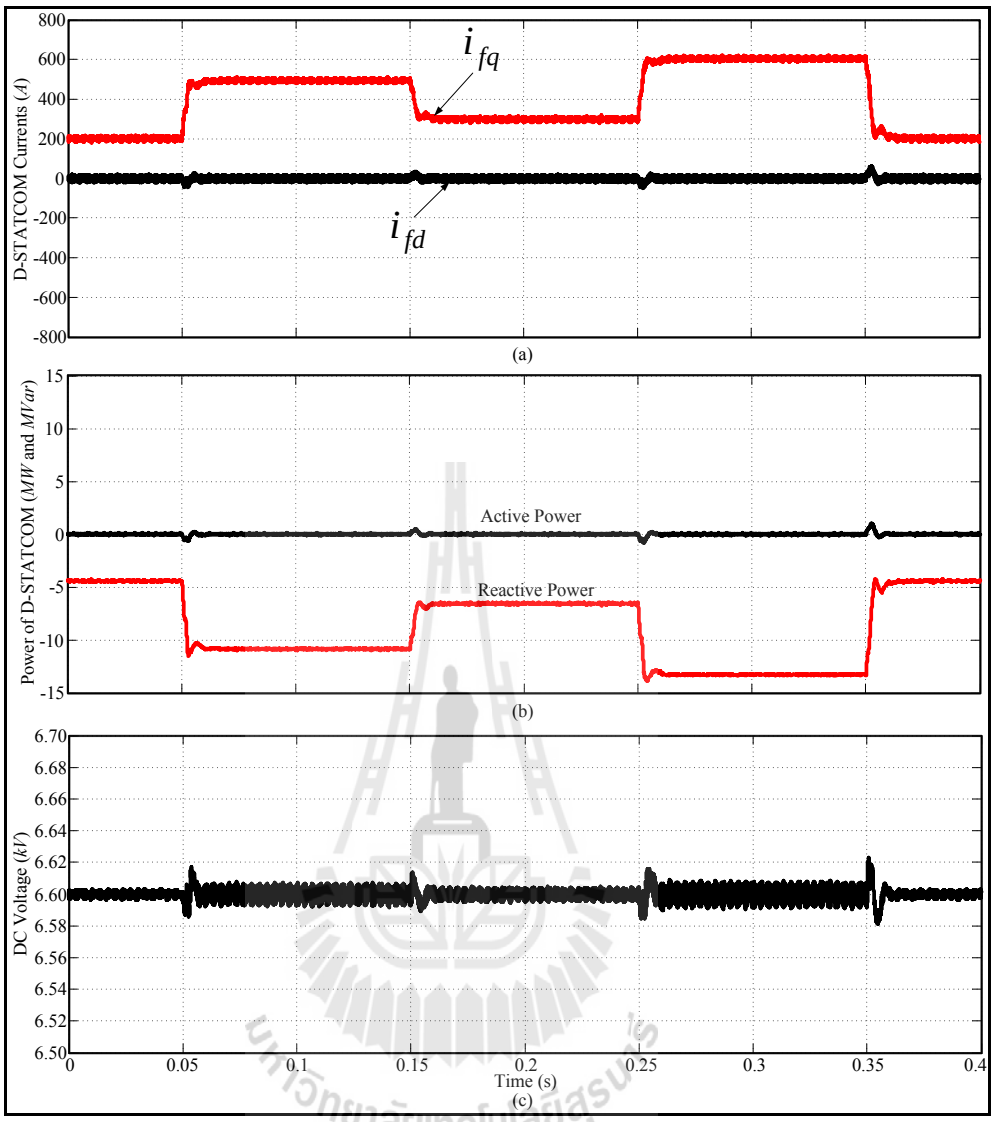

Figure 8.17 Currents, DC voltage and power of the D-STATCOM for the system with the RL load which the source voltage varying between 28.82 and 23.98 *kV*

Figure 8.17 presents the currents, DC voltage and power of the D-STATCOM for the system with the RL load when the source voltage is varied between 28.82 and 23.98 *kV*. As may be seen in Figure 8.17(a), that the reactive

currents (i_{fq}) are +200, +500, +300, +600 and +200 *A* to compensate the load voltage when the source voltages are 25.30, 28.82, 26.47, 30.14 and 25.30 *kV*, respectively. Whilst, the active current (i_{fd}) very small change when the D-STATCOM compensate the load voltage. These correspond to the reactive and active powers of the D-STATCOM as shown in Figure 8.17(b). The reactive powers are -4.4, -10.1, -6.6, -13.2 and -4.4 *MVar* to compensate the load voltage when the source voltages are 25.30, 28.82, 26.47, 30.14 and 25.30 *kV*, respectively. Meanwhile, the active power is very small changed in positive when the D-STATCOM compensates the load voltage. This means that the D-STATCOM consumes active power to regulate the DC voltage at the constant value as can be seen in Figure 8.17(c). As seen in this Figure, the DC voltage is always regulated at 6.6 *kV* for all of source voltages.

In case of the source voltage variations between 24.09 and 15.71 *kV*, the load voltage of the system with the RL load is shown in Figure 8.18. The dash line of Figure 8.18(a) presents the load voltage of the system without D-STATCOM when the source voltage is varied. As seen in this Figure, the load voltage corresponds to five different source voltage conditions: source voltage of 22.77 *kV* from t = 0.00 to 0.05 second; source voltage of 15.71 *kV* from t = 0.05 to 0.15 second; source voltage at 20.35 *kV* from t = 0.15 to 0.25 second; source voltage of 24.09 *kV* from t = 0.25 to 0.35 second; and source voltage of 22.77 *kV* from t = 0.35 to 0.40 second. Whilst, the solid line of Figure 8.18(a) shows the load voltage of the system with D-STATCOM. As can be observed from this Figure that the D-STATCOM with proposed control design can be regulated the load voltage at the desired value. The load voltage took approximately 0.02 seconds to settle in each source voltage. As can be seen in Figure 8.18(b), the load voltage reaches the desired value within one cycle.

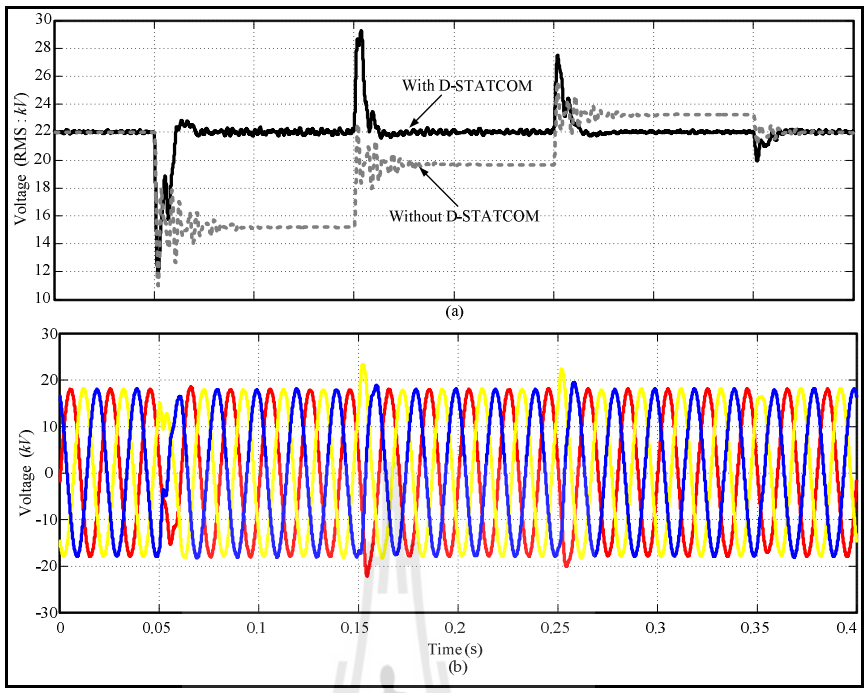

Figure 8.18 Load voltage of the system with the RL load which the source voltage varying between 22.77 and 14.41 *kV*

Figure 8.19 presents the currents, DC voltage and power of the D-STATCOM for the system with the RL load when the source voltage is varied between 24.09 and 15.71 *kV*. As may be seen in Figure 8.19(a), that the reactive currents (i_{fq}) are about 0, -600, -200, +100 and 0 *A* to compensate the load voltage swell when the source voltages are 22.77, 15.71, 20.35, 24.09 and 22.77 *kV*, respectively. Whilst, the active current (i_{fd}) very small changes when the D-STATCOM compensate the load voltage. These correspond to the reactive and active powers of the D-STATCOM as shown in Figure 8.19(b). The reactive powers are of 0.0, +13.2, +4.4, -2.2 and 0.0 *MVar* to compensate the load voltage when the source voltages are 22.77, 15.71, 20.35, 24.09 and 22.77 *kV*, respectively. Meanwhile, the

active power is very small changed in positive when the D-STATCOM compensates the load voltage. So, the D-STATCOM consumes active power to regulate the DC voltage at the constant value. Furthermore, the D-STATCOM always consumes active power no matter how much it absorbs or generates reactive power. As can be seen in Figure 8.19(c), the DC voltage is always regulated at 6.6 *kV* for all of source voltages.

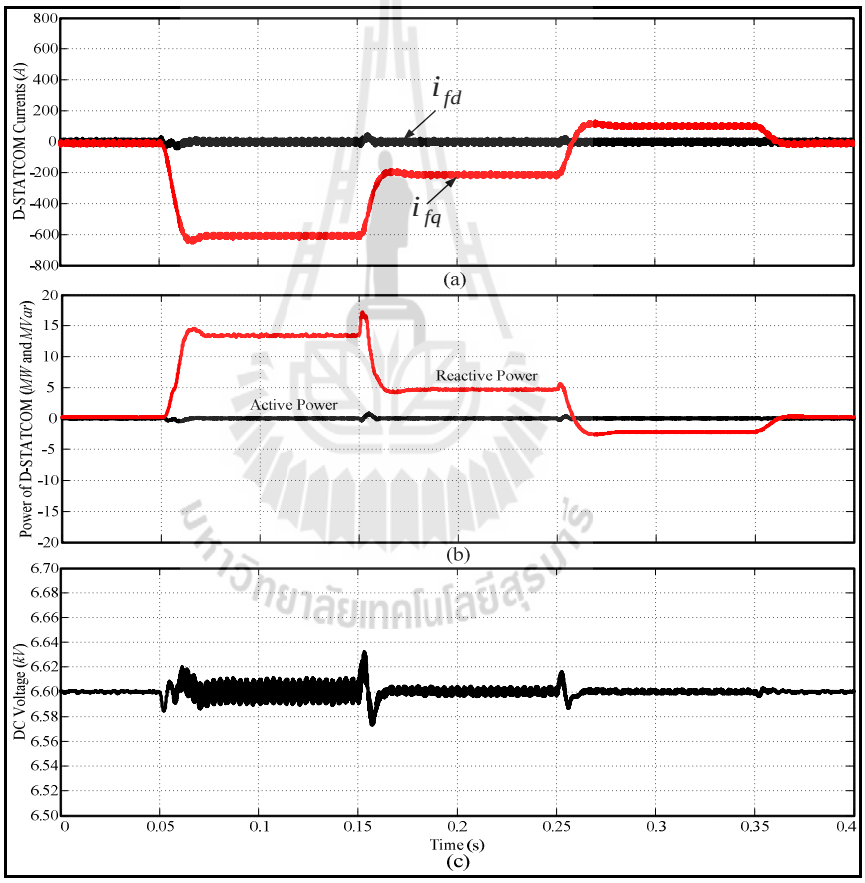

Figure 8.19 Currents, DC voltage and power of the D-STATCOM for the system with the RL load which the source voltage varying between 22.77 and 14.41 *kV*

In addition, the application of the D-STATCOM for load voltage regulation which loads varying is demonstrated in this section. The load powers are shown in Figure 8.20. As seen in this figure, the active powers are 0. 415 *MW* (0.1 *pu.*) from t = 0.00 to 0.05 second, 4.15 *MW* (1.0 *pu.*) from t = 0.05 to 0.15 second, 8.30 *MW* (2.0 *pu.*) from t = 0.15 to 0.25 second, 12.45 *MW* (3.0 *pu.*) from t = 0.25 to 0.35 second, 16.60 *MW* (4.0 *pu.*) from t = 0.35 to 0.45 second and come back to 4.15 *MW* (1.0 *pu.*) from t = 0.45 to 0.50 second which the constant load power factor at 0.875 in this case. The load voltage of the system without the D-STATCOM is shown as the dash line in Figure 8.21. Meanwhile, the solid line presents the load voltage of the system with D-STATCOM. As seen in this Figure, the D-STATCOM with the proposed control in case of source voltage variations can be used in case of load variations as well. The powers of the D-STATCOM to compensate the load voltage are shown in Figure 8.22. In this Figure, the reactive powers are -1.24, +1.50, +4.99, +9.00, +13.60 and +1.50 *MVar* when the load powers are 0.415, 4.15, 8.30, 12.45, 16.60 and 4.15 *MW*, respectively, while the active power very small change in this case.

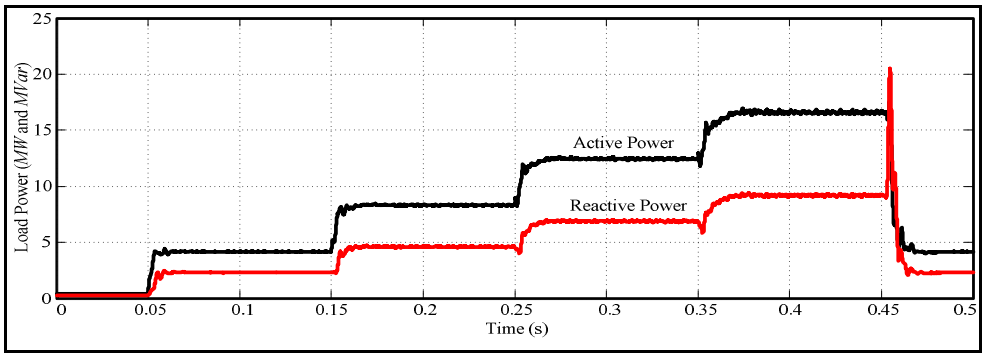

Figure 8.20 Load varying when the system with the RL load

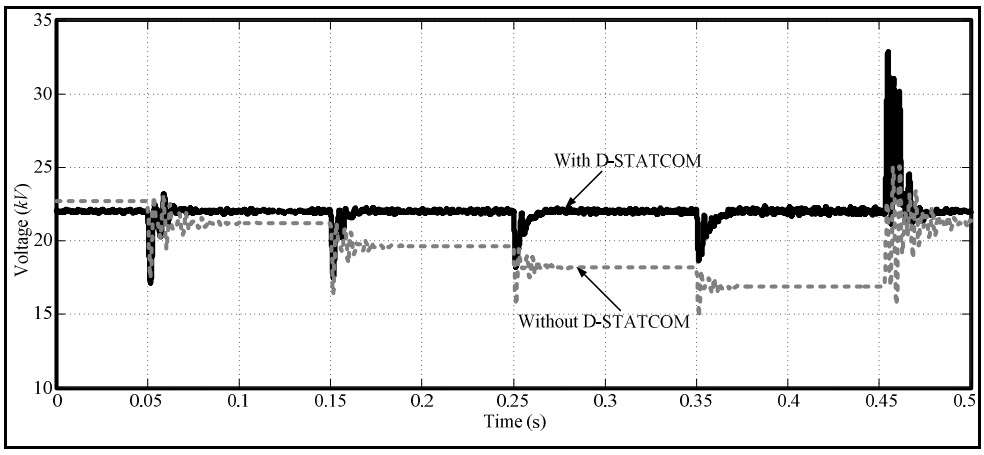

Figure 8.21 Load voltages of the system with the RL load in case of the load variations

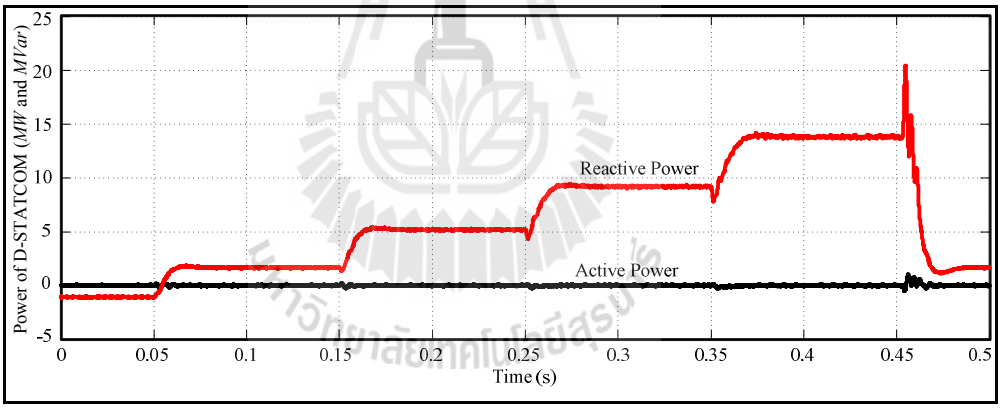

Figure 8.22 Powers of the D-STATCOM for the system with the RL load in case of the load variations

8.3 Application of the D-STATCOM for the System with the Distributed Generator

In this section, the D-STATCOM with the proposed control has been tested for the performance in regulating of the load voltage in case of the system including the distributed generator (DG). The configuration of the system including the DG and D-STATCOM is modeled using the MATLAB/SIMULINK software package as shown in Figure 8.23. The parameters of the system and D-STATCOM in section 8.2 are used in this section. The modeling and simulations of the D-STATCOM have been carried out in two different cases: the system with a synchronous generator (SG) and the system with an induction generator (IG).

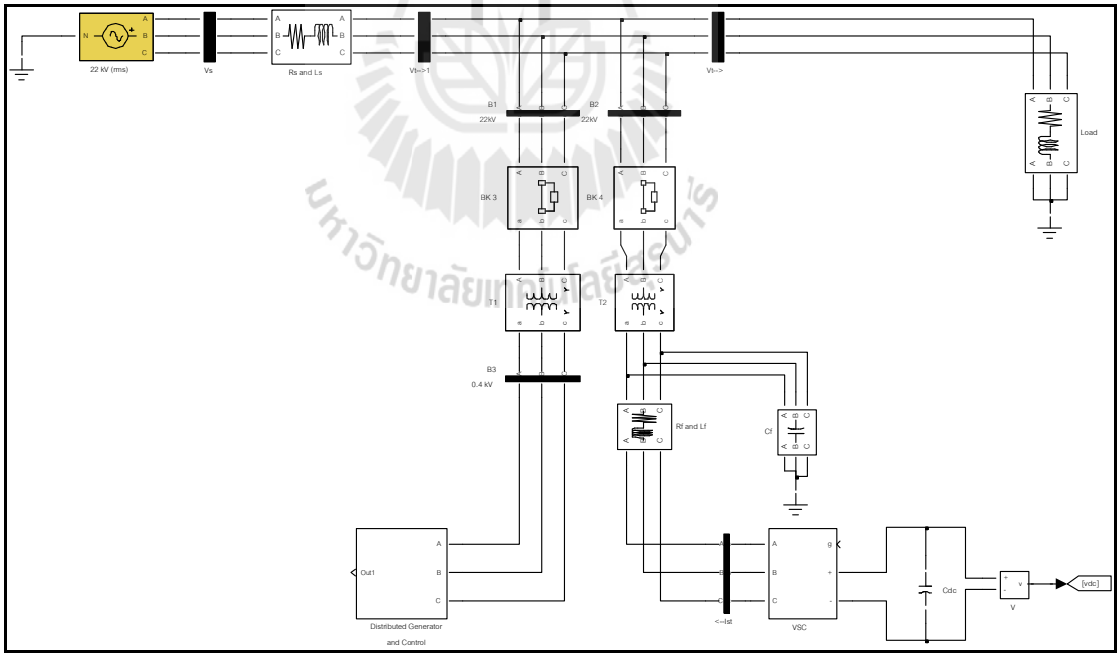

Figure 8.23 MATLAB/SIMULINK model for the system with the DG and D-STATCOM

8.3.1 Distribution System with the Synchronous Generator (SG)

In this section, the standard per unit salient-pole synchronous machine model 12 (400 V, 50 Hz, 2,000 *kVA* and 1500 *rpm*) with an excitation system in MATLAB/SIMULINK is used. The parameters of the synchronous generator are shown in Table 8.8. Meanwhile, an IEEE type 1 synchronous machine voltage regulator combined to an exciter is used as the excitation system in this case. The excitation system configuration modeled in MATLAB/SIMULINK is shown in Figure 8.24 while the parameters of excitation system are shown in Table 8.9.

Table 8.8 Parameters of the synchronous generator

Parameters	Value
d-axis synchronous reactance (x_d), transient reactance (x'_d) and subtransient reactance (x''_d)	2.11, 0.17 and 0.13 *pu*
q-axis synchronous reactance (x_q), subtransient reactance (x''_q) and leakage reactance (x_l)	1.56, 0.23 and 0.05 *pu*
d axis transient and subtransient short-circuit time constant (T'_d and T''_d) and q-axis subtransient short-circuit time constant (T''_q)	0.33, 0.03 and 0.03 *pu*
stator resistance (R_s)	0.03 *pu*
coefficient of inertia (H), friction factor (F) and pole pairs (p)	0.3072 (sec.), 0.00987 (*pu*) and 2 *pairs*

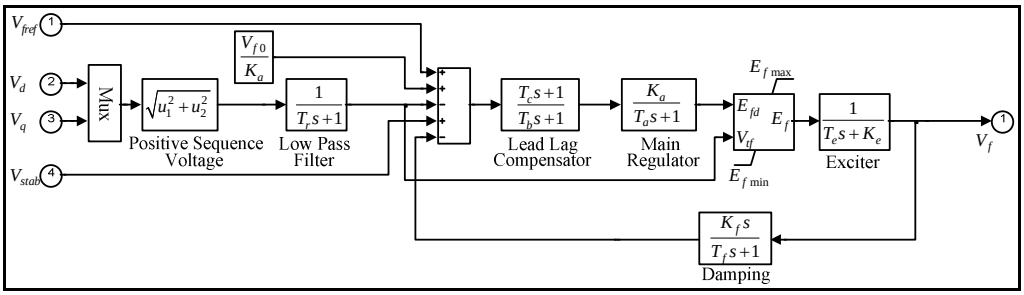

Figure 8.24 Excitation system configurations

Table 8.9 Parameters of the excitation system

Parameters	Value
Low-pass filter time constant (T_r)	20e-3 (sec.)
Regulator gain and time constant (K_a and T_a)	400 and 0.001 (sec.)
Exciter gain and time constant (K_e and T_e)	1 and 0.0 (sec.)
Transient gain reduction time constants (T_b and T_c)	1 and 1 (sec.)
Damping filter gain and time constant (K_f and T_f)	0.003 and 1 (sec.)
Regulator output gain Limits and gain ($E_{f\min}$, $E_{f\max}$ and K_p)	-6.0, 6.0 (*pu*) and 0

To investigate the performance of D-STATCOM with the proposed control in regulating of the load voltage in case of the system including the synchronous generator, the source voltage sag at 15.71 *kV* is applied to the system with the RL load at t = 0.05 second. The AC voltage controller and compensator for RL load in section 8.2 are used in this case. The load voltages when the system with and without D-STATCOM are presented in Figure 8.25. Without the D-STATCOM for dynamic reactive compensation, the source voltage sag results in the load voltage sag. Then the generator generates high reactive power to the system while the active power of the generator cannot reach the set value during the source voltage sag as can be seen in Figure 8.26. As a result, the synchronous generator may be disconnected from the power grid. However, when using the D-STATCOM with the proposed control, the load voltage can be regulated at the desired value. The load voltage took approximately 0.02 seconds to settle. In this case, the generator generates small increased reactive power to the system while the active power of the generator can reach the set value during the source voltage sag.

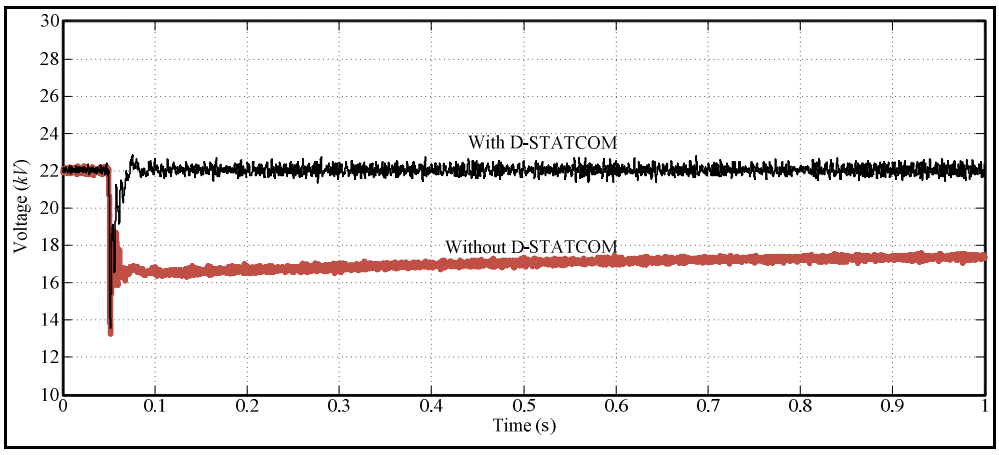

Figure 8.25 Load voltages of the system with the RL load and synchronous generator

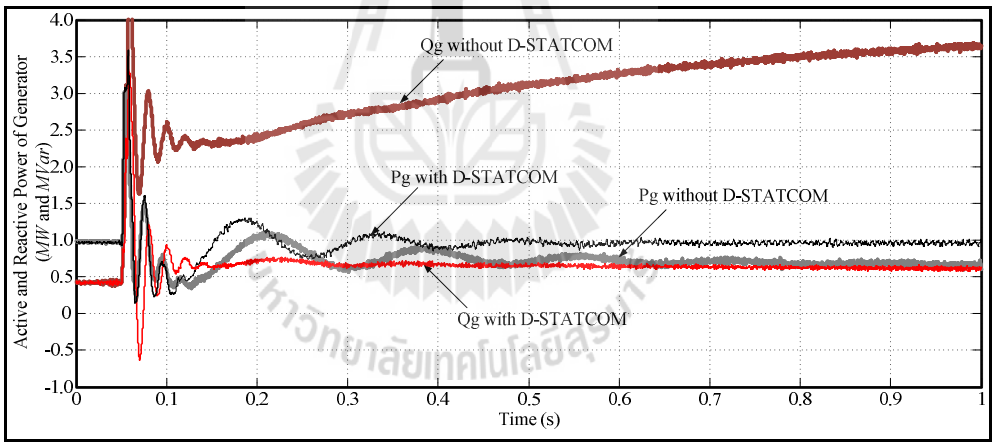

Figure 8.26 Powers of synchronous generator and D-STATCOM when source voltage sag

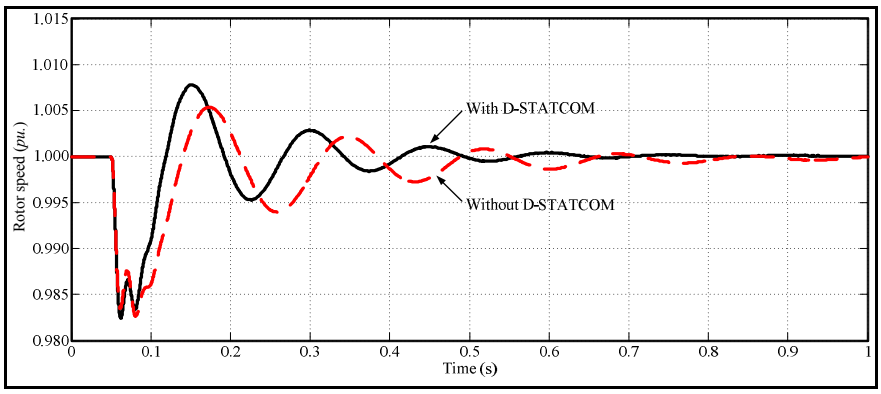

Figure 8.27 Rotor speed of the synchronous generator when source voltage sag

Figure 8.27 presents the rotor speed of synchronous generator when the source voltage sags. As can be seen in this figure, the rotor speed of the system with the D-STATCOM has a high frequency oscillation. However, the system with the D-STATCOM results faster settles in rotor speed variation. Meanwhile, Figure 8.28 shows the active and reactive powers of the D-STATCOM in order to compensate the load voltage in this case.

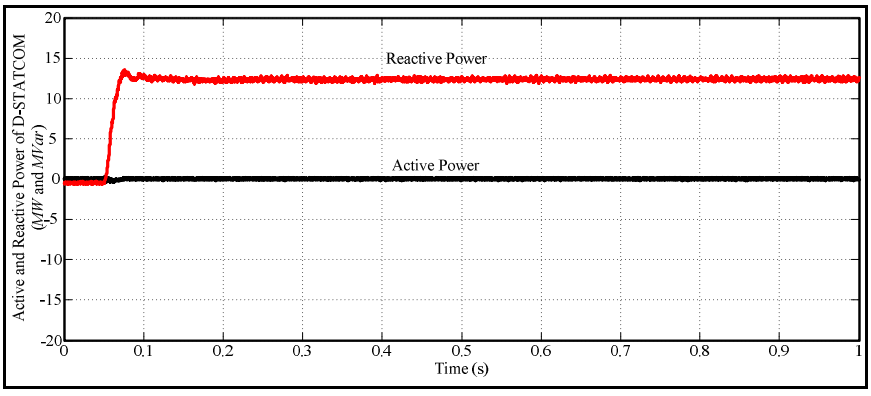

Figure 8.28 Active and reactive powers of the D-STATCOM for the load voltage regulation in case of the system with the synchronous generator

8.3.2 Distribution System with the Induction Generator (wind IG)

In this case, the D-STATCOM applies to the load voltage regulation of the system including the induction generator with fixed-speed wind turbines (FSWTs) is investigated. The squirrel-cage induction generator (SCIG) is used in this section and its parameters are shown in Table 8.10. Meanwhile, the characteristics of the fixed-speed wind turbines are shown in Figure 8.29. To investigate the performance of D-STATCOM with the proposed control in regulating of the load voltage in case of the system including the induction generator with fixed-speed wind turbines, the source voltage sag at 15.71 *kV* is applied to the system with the RL load at t = 0.05 second. Whilst, the wind speed assume to be constant at 10 m / second during the entire test. The AC voltage controller and compensator for RL load in section 8.2 are used in this case. The load voltages when the system with and without D-STATCOM are presented in Figure 8.30. Without the D-STATCOM for dynamic reactive compensation, the source voltage sag results in the load voltage sag. The active and reactive powers of the generator oscillate in a transient state as can be seen in Figure 8.31. However, they can be settled within 0.15 seconds. In addition, the generator can be generated the active power nearly the set value which absorbing the small decreased reactive power. As a result, the induction generator with fixed-speed wind turbines can be connected to the power grid during the source voltage sag when the system without the D-STATCOM. However, the rotor speed of the generator is increased in this case as can be seen in Figure 8.32.

When using the D-STATCOM with the proposed control, the load voltage can be regulated at the desired value. The load voltage took approximately 0.02 seconds to settle. The powers of the D-STATCOM in order to compensate the

load voltage are shown in Figure 8.33. Similar to the case of without the D-STATCOM, the active and reactive powers of the generator oscillate in a transient state and they can be settled within 0.15 seconds. However, in this case, the generator can be generated the active power at the set value which absorbing the same reactive power. Furthermore, the rotor speed of the generator can be regulated at the same value in this case. As a result, the induction generator with fixed-speed wind turbines can be connected to the power grid during the source voltage sag as well.

Table 8.10 Parameters of the induction generator

Parameters	Value
Stator resistance and leakage inductance (R_s and L_{ls})	0.016 and 0.06 (*pu*)
Rotor resistance and leakage inductance (R'_r and L'_{lr})	0.015 and 0.06 (*pu*)
Magnetizing inductance (L_m)	3.5 (*pu*)
Coefficient of inertia (H), friction factor (F) and pole pairs (p)	2 (*sec.*), 0 (*pu*) and 2 (*pairs*)

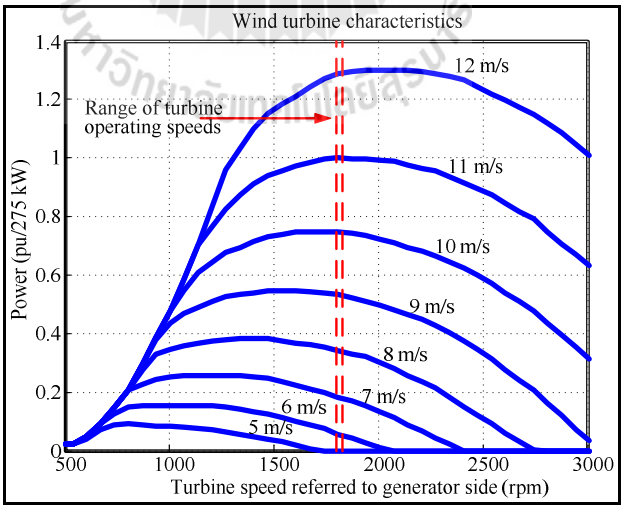

Figure 8.29 Characteristics of the fixed-speed wind turbines

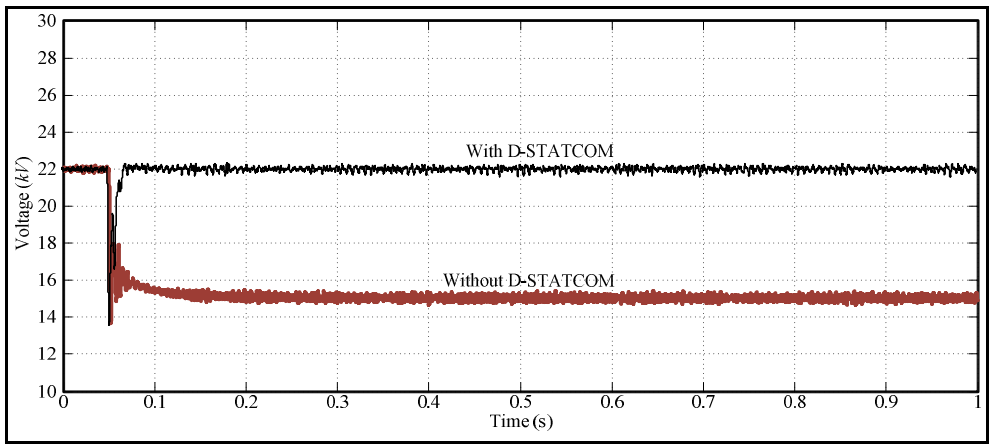

Figure 8.30 Load voltages of the system with the RL load and induction generator

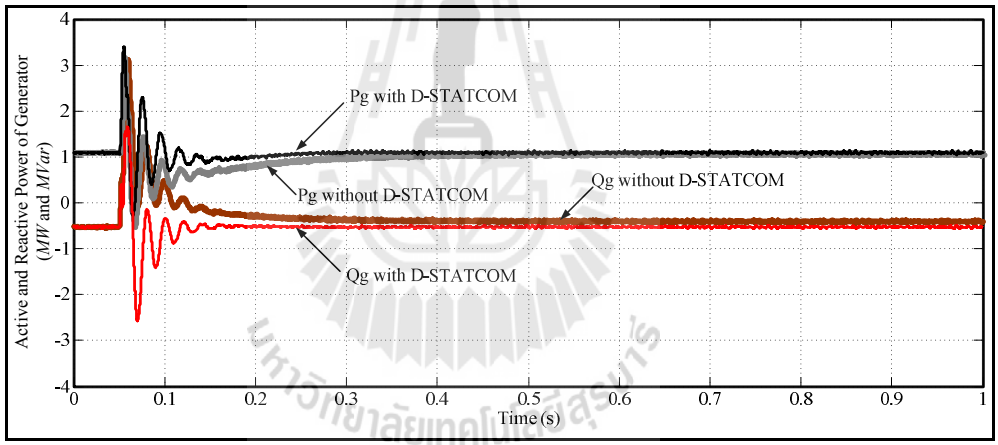

Figure 8.31 Powers of the induction generator and D-STATCOM when the source voltage sag

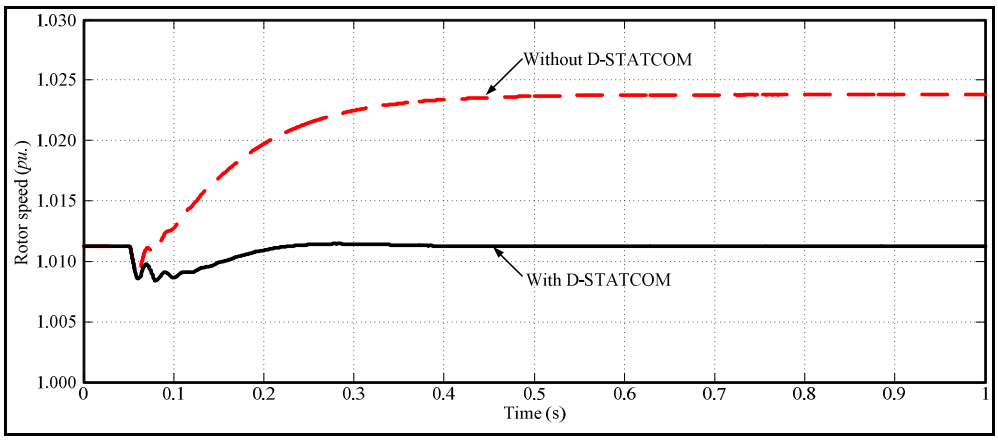

Figure 8.32 Rotor speed of the induction generator when the source voltage sag

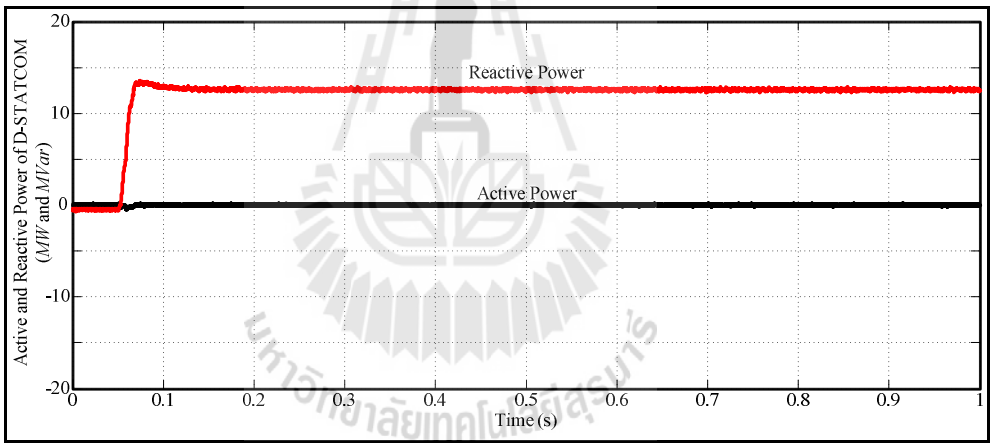

Figure 8.33 Active and reactive powers of the D-STATCOM for the load voltage regulation in case of the system with the induction generator

8.4 Summary

This chapter presents the application of the D-STATCOM with the proposed design control technique for load voltage regulation. The decoupling current control of the D-STATCOM with the parameters tuning based on the genetic algorithm

(CC-GA) and the DC voltage control with an elimination term of $u_q i_{fq}$ based on the symmetrical optimum method (DCVC-SO) are used. Meanwhile, the AC voltage control based on the classical loop shaping is applied to many cases. In this chapter a simplified 22 *kV*, 2 bus test power system is employed for the simulation. The application of D-STATCOM for load voltage regulation of the distribution system with the R and RL loads is discussed. In addition, the D-STATCOM is applied to the system including with the distribution generator are presented.

For the load voltage regulation when the distribution system with the R loads, the load voltage regulations in case of the source voltage variations between 28.82 and 23.98 *kV* (i_{fq} varies between +600 and +200 *A*) and the source voltage variations between 14.41 and 22.77 *kV* (i_{fq} varies between +100 and -600 *A*) are illustrated. In addition, the load voltage regulation when the loads vary is demonstrated. The load power is varied between 0.415 *MW* (0.1 *pu.*) to 16.60 *MW* (4.0 *pu.*) while the reactive power is not changed in this case.

For the load voltage regulation when the distribution system with the RL loads, the load voltage regulations in case of the source voltage variations between 30.14 and 25.30 *kV* (i_{fq} varies between +600 and +200 *A*) and the source voltage variations between 15.71 and 24.09 *kV* (i_{fq} varies between +100 and -600 *A*) are illustrated. In addition, the load voltage regulation when the loads vary is demonstrated. The load power is varied between 0.415 *MW* (0.1 *pu.*) to 16.60 *MW* (4.0 *pu.*) which the constant load power factor at 0.875.

As the results, the D-STATCOM with proposed control design can be regulated the load voltage at the desired value. Furthermore, the D-STATCOM with

the proposed control in case of source voltage variations can be used in case of load varied as well. However, the controller designed in case of i_{fq} varies between +600 and +200 *A* cannot use in case of i_{fq} varies between +100 and -600 *A*, and vice versa.

In the application of the D-STATCOM for the system including the distributed generator, the simulations of the D-STATCOM with two different cases: the system with a synchronous generator (SG) and the system with an induction generator (IG) are presented. From the results, the D-STATCOM with the proposed control can be regulated the load voltage at the desired value. The load voltage took approximately 0.02 seconds to settle. Furthermore, the generator can be connected to the power grid and the active power of the generator can reach the set value during the source voltage sag in both cases.

CHAPTER IX

COST ESTIMATION FOR REACTIVE POWER COMPENSATION USING D-STATCOM

Although in the past most electricity-consuming devices could “ride through” voltage sags (e.g., a light bulb might dim momentarily), many of the electricity-consuming devices associated with today’s digital economy (e.g., equipment controlled by programmable logic chips) cannot tolerate a partial drop in voltage for even a fraction of a second. Voltage sags may cause this equipment to shutdown and remain off even after service is restored to normal levels. Voltage sags are rapid and not easily detectable by an untrained observer, and so consumers may not realize that a power quality ‘event’ caused their equipment to fail or stop operating. The D-STATCOM is most widely used for power factor correction, to eliminate current based distortion and load balancing, when connected at the load terminals. It can also perform voltage regulation when connected to a distribution bus. Although significant improvements in the overall power quality can be achieved, the high cost of the D-STATCOM can limit the benefits resulting from its application. However, in this chapter, the voltage regulation and power factor correction have been chosen as the main targets for the customer side investigation while the energy loss reduction has been chosen as the main target for the utility side investigation. The investigation

involves cost estimation for voltage regulation, power factor correction and energy loss reduction by the use of the D-STATCOM.

9.1 Benefits and Costs of Reactive Power Compensation

9.1.1 Losses due to Sag and Interruption

Power quality problems can lead to a number of costs to industrial and commercial facilities. These costs can include the value of lost production, increased labor costs, damage to work-in-process with resulting reduced value or costs of reworking, value of lost materials, equipment damage, revenue (opportunity) loss due to failure to perform contracts, transaction processing losses and the need to ration services to customers. About two million business establishments in three critical sectors were evaluated by EPRI in terms of the costs of power quality disturbances. This evaluation grouped the power quality sensitive businesses into three areas as follows (Darrow and Hedman, 2005):

1) Digital Economy: Firms that rely heavily on data storage and retrieval, data processing, or research and development. Table 9.1 shows examples of the high costs of power outages in these sectors.

2) Continuous Process Manufacturing: Manufacturing facilities that continuously feed raw materials, often at high temperatures, though an industrial process. Table 9.2 shows average costs by industry per disruption (both voltage sags and outages).

3) Fabrication and Essential Services: This sector includes other manufacturing industries plus utilities and transportation facilities.

Table 9.1 Example outage costs for sensitive customers

Business Activity	Outage costs *Baht / hour*
Cellular Communications	1,365,850
Telephone ticket sales	2,398,560
Airline Reservations	2,998,200
Credit card operations	85,948,300
Brokerage operations	215,870,000

Table 9.2 Average costs per PQ event for sensitive process industries

Industry	*Baht / kVA* per event
Semiconductors	2665.06 – 3997.60
Glass	333.13 – 499.70
Automotive	199.88 – 333.13
Plastics	133.25 – 233.19
Textile	99.94 – 266.51

In addition, to evaluate the costs and benefits of mitigating power quality problems on must look at the costs for PQ problems within industry groups or even at individual facilities. The costs incurred by a site as a function of its capacity (*kW*) and unserved energy used (*kWh*) provide a benchmark for evaluating control strategies. Table 9.3 and Table 9.4 show some average costs for industrial facilities and commercial buildings (IEEE Standaed 493-497, 1997).

Table 9.3 Average costs of a single power interruption for industrial plants

Plants	Costs
All plants	214.21(*Baht*) / *kW* + 303.48(*Baht*) / *kWh*
Plants > 1,000 *kW* max. demand	118.93(*Baht*) / *kW* + 106.60(*Baht*) / *kWh*
Plants < 1,000 *kW* max. demand	519.69(*Baht*) / *kW* + 918.45(*Baht*) / *kWh*

Table 9.4 Average costs of a single power interruption for commercial buildings

Buildings	Costs
All commercial buildings	725.23(*Baht*) / *kWh* (not delivered)
Office building only	891.46(*Baht*) / *kWh* (not delivered)
Office building with computer centers	835.16(*Baht*) / *kWh* (not delivered)

9.1.2 Benefit due to Voltage Sag Mitigation

Costs will typically vary with the severity (both magnitude and duration) of the power quality disturbance. This relationship can often be defined by a matrix of weighting factors. The weighting factors are developed using the cost of a momentary interruption as base. Usually, a momentary interruption will cause a disruption to any load or process that is not specifically protected with some type of energy storage technology. Voltage sags and other power quality variations will always have an impact that is some portion of this total shutdown. If a voltage sags to 40% causes 80% of the economic impact that a momentary interruption causes, then the weighting factor for 40% sag would be 0.8. Similarly, if sag to 75% only results in 10% of the costs that an interruption causes, then the weighting factor is 0.1. After the weighting factors are applied to an event, the costs of the event are expressed in per unit of the cost of a momentary interruption. The weighted events can then be summed, and the total is the total cost of all the events expressed in the number of equivalent momentary interruptions. Table 9.5 provides an example of weighting factors that were used for one investigation. The weighting factors can be further expanded to differentiate between sags that affect all three phases and sags that only affect one or two phases.

Furthermore, Table 9.6 provides a hypothetical example of the power quality disturbances seen by a large commercial or industrial customer on a distribution system (Darrow and Hedman, 2005). As can be seen in this table, the sags trip sensitive equipment off-line resulting in a 50 minutes loss of productivity for the facility for each occurrence whereas the momentary interruptions disrupt the facility for 1.4 hours each time. Recovery from such a long duration outage requires 4 hours.

Table 9.5 Example of weighting factors for different voltage sag magnitudes

Event Category	Weighting for Economic Analysis (W_{int})
Interruption	1.0
Sag with min. voltage below 50%	0.8
Sag with min. voltage between 50 and 70%	0.4
Sag with min. voltage between 70 and 90%	0.1

Table 9.6 Power quality disruption and facility disruption per occurrence

Power quality disruption	Duration per occurrence	Facility disruption per occurrence (*F*)
Voltage sags	0 - 2 seconds	50 minutes
Momentary interruptions	0 - 2 seconds	1.4 hours
Long duration interruptions	2 - 60 minutes	4.0 hours

Note that the D-STATCOM cannot completely mitigate for all of sags and interruptions. For example, the D-STATCOM designed for 100% mitigation of sags with minimum voltage over 65% can mitigate about 20 – 30% for sag with minimum voltage below 50%. Thus, benefit due to voltage sag mitigation can be calculated as follows.

$$\Phi_{sag} = k_{sag} \times F_{int} \times \left(W_{bef} - W_{aft}\right) \times Cap \tag{9.1}$$

where

Φ_{sag} is benefit due to voltage sag mitigation (*Baht*)

k_{sag} is the cost of per unit losses (*Baht / kWh*)

F_{int} is the facility of momentary interruption (*h*)

W_{bef} , W_{aft} are weighting factors before and after mitigation for different voltage sag magnitudes

Cap is the capacity of customer (kW)

9.1.3 Benefit due to Power Factor Correction

In general, installing a reactive power source such as the D-STATCOM can correct the load power factor as well as reducing the electricity charge when the loads have low power factor. The corrected power factor may be interpreted as a reduction of the electricity charge from the utility. Thus, the reduction of the low power factor charge can be expressed as follows.

$$\Phi_{PF} = k_{PF} \times Q_{com} \tag{9.2}$$

where

$$Q_{com} = P_L \left(\sqrt{\frac{1 - PF_{old}^2}{PF_{old}^2}} - \sqrt{\frac{1 - PF_{\min}^2}{PF_{\min}^2}} \right) (kVar)$$

$PF_{\min}$ is the acceptable minimum power factor

PF_{old} is the power factor before installation

Φ_{PF} is benefit due to power factor correction ($Baht$)

k_{PF} is the cost of low power factor charge ($Baht$ / $kVar$)

9.1.4 Benefit due to Energy Loss Reduction for the Utility

The power losses of the power distribution system can be reduced by the installing of the reactive power source such as the D-STATCOM. The saved power losses may be interpreted as a reduction of the cost of the electric power

supplying. Thus, the reduction of the electric energy charge can be expressed (Zhu and MOmoh, 1998; Baran and Wu, 1989) as follows.

$$\Phi_E = k_E \times \Delta E_{loss} \tag{9.3}$$

where

$\Delta E_{loss} = \Delta E_{loss}^{old} - \Delta E_{loss}^{new}$ (kWh)

ΔE_{loss}^{old}, ΔE_{loss}^{new} are the energy losses before and after installation, $E_{loss} = \int P_{loss} dt$

Φ_E is benefit due to energy loss reduction (*Baht*)

k_E is the cost of per unit energy charge (*Baht / kWh*)

9.1.5 D-STATCOM Costs

The costs of the reactive power source such as D-STATCOM can be divided into two parts: 1) fixed cost, and 2) operating costs. The fixed costs mainly consist of the D-STATCOM device cost and the cost to install it including labor hours, footprint of the device, time and so forth. The operating or variable costs are those which allow the D-STATCOM device to work. These operating costs consist of heating losses and maintenance costs etc. In principle, however, the operating costs may differ from year to year. The investment cost for the used D-STATCOM is given in Table 9.7 (Purewave, 2008).

Table 9.7 Example cost for the D-STATCOM device

Device	Initial cost (*Baht / kVar*)	Annual cost (%)
D-STATCOM	5330 – 6662	5

For simplification, the fixed costs can be considered as shown in (9.4).

$$C_{fixed} = k_q \times Q_c \tag{9.4}$$

where

C_{fixed} is the fixed cost (*Baht*)

Q_c is the size of the reactive power of D-STATCOM to be installed (*kVar*)

k_q is the per unit cost of the reactive power (*Baht / kVar*)

In addition, the operating cost can be described as follows (Chung and Shaoyun, 1997).

$$C_{op} = \sum_{y=1}^{y_{life}} C_{ann} \times \left(\frac{100 + \lambda}{100} \right)^{y-1} \tag{9.5}$$

where

C_{op} is the total operating cost (*Baht*)

C_{ann} is the annual maintenance cost (*Baht*)

λ is the annual percentage increment of the maintenance cost (%)

y_{life} is the lifetime of the D-STATCOM to be installed (*years*)

Therefore, the cost function of the reactive power compensation for the customer, utility and both of customer and utility are summarized as (9.6), (9.7) and (9.8), respectively.

$$C_{func,CUS} = -C_{fixed} + \left(\Phi_{sag} + \Phi_{PF} - C_{op}\right) \tag{9.6}$$

$$C_{func,EA} = -C_{fixed} + \left(\Phi_{E} - C_{op}\right) \tag{9.7}$$

$$C_{func,CUS\&EA} = -C_{fixed} + \left(\Phi_{sag} + \Phi_{PF} + \Phi_{E} - C_{op}\right) \tag{9.8}$$

where

$C_{func,CUS}$ is cost function for the customer

$C_{func,EA}$ is cost function for the utility

$C_{func,CUS\&EA}$ is cost function for the both of customer and utility

9.2 Cost Analysis and Methodology

Several evaluation methods can be used to cost analysis. It is important to include account of the different economic values of investments made at different times during the analysis period. When money is invested, compound interest is paid on the capital sum. The interest rate comprises inflation, risk and real costs of postponing consumption. Thus, money used to invest in this situation could be invest elsewhere and earn a dividend. To consider this effect, all future costs and benefits are

discounted to convert them to the net present values (NPV) of costs as shown in (9.9). NPV is a measure of the economic worth of an investment (Robinson et al., 1998). A positive NPV indicates that the investment is justified economically at a given discount rate.

$$NPV = -C_{fixed} + \sum_{i=1}^{n} \frac{B_i - C_i}{\left(1 + \frac{r}{100}\right)^i} \tag{9.9}$$

where

n is the analysis period in years

B_i is the sum of all benefits in year i

C_i is the sum of all costs in year i

r is the discount rate in percentage

The methodology for cost analysis can be described as follows:

1. Investigate and design the size of the D-STATCOM.

2. Estimate the number and severity of events the plant is subject to per year.

3. According to Table 9.5, convert the different events to a per unit interruption base value and determine the weighting factors before and after mitigation.

4. Calculate benefit due to voltage sag mitigation per year (for the customer side considerations) by using (9.1).

5. Calculate benefit due to power factor correction per year (for the customer side considerations) by using (9.2).

6. Calculate benefit due to energy loss reduction per year (for the utility side considerations) by using (9.3).

7. Determine the cost of installation such as the fixed costs and operation costs for the D-STATCOM by using (9.4) and (9.5).

8. Determine the cost function for the customer, utility and both of customer and utility side considerations by using (9.6), (9.7) and (9.8), respectively.

9. Estimate the future costs and benefits by converting them to the net present values (NPV) of costs as shown in (9.9).

10. Discuss and comment on the results.

9.3 Case Study and Results

The process of costs estimation and comparing the different sizes for improving performance involves determining the net present values (NPV) for each size, including the sum of all benefits and costs of implementing the D-STATCOM. For example, the industrial plant supplied by the Nakhonrachasima electricity authority, Thailand with the system parameters as presented in Section 8.2 is investigated. The facility has a total load of 5 *MW* with power factor = 0.80 must be protected to avoid production disruptions and corrected the power factor as more than 0.875. The cost of per unit low power factor charge is 15(*Baht*) / *kVar* / *month*. The voltage sag performance was given in Table 9.8. According to the average costs of a single power interruption for industrial plants in Table 9.3, the costs for an interruption are 118.93(*Baht*) / *kW* + 106.60(*Baht*) / *kWh*. The costs for voltage sags are based on the weighting factors in Table 9.5 whereas the momentary interruptions disrupt the facility for 1.4 hours each time. The three options given in Table 9.9 are

analyzed. The net present values (NPV) for each size can be summarized in Table 9.10 – Table 9.12 and can be plotted as shown in Figure 9.1. The NPV are calculated based on a 30-year life and an interest rate of 10%.

Table 9.8 Voltage sag performance

Event Category	Weighting for Economic Analysis	No. Events per Year	Total Equivalent Interruptions
Interruption	1.0	4	4
Sag with min. voltage below 50%	0.8	4	3.2
Sag with min. voltage between 50 and 70%	0.4	11	4.4
Sag with min. voltage between 70 and 90%	0.1	31	3.1
Total	-	**50**	**14.7**

Table 9.9 Costs and effectiveness of the power quality improvement options

	Costs		Effectiveness for a particular example case			
Sizes (*MVar*)	**Fixed (*Baht*)**	**Operating (% of fixed costs)**	**Interruption (%)**	**Sag with min. voltage < 50% (%)**	**Sag with min. voltage 50-70% (%)**	**Sag with min. voltage 70-90% (%)**
5	33,313,300	5	0	40	70	85
10	66,626,600	5	0	55	80	95
15	99,939,900	5	0	65	90	100

Table 9.10 NPV for 5 *MVar* of D-STATCOM

Year	Customer side consideration (4+5) (*Baht*)	Utility side consideration (6) (*Baht*)	Customer &Utility consideration (4+5+6) (*Baht*)
5	15,585,900	-46,875,844	20,923,117
10	95,946,200	-74,306,681	110,493,953
15	172,616,000	-107,415,138	196,543,739
20	233,459,000	-141,340,769	265,484,647
25	276,773,825	-173,389,563	315,239,260
30	304,980,130	-202,235,716	348,320,566

Table 9.11 NPV for 10 *MVar* of D-STATCOM

Year	Customer side consideration (4+5) (*Baht*)	Utility side consideration (6) (*Baht*)	Customer &Utility consideration (4+5+6) (*Baht*)
5	6,223,723	-99,088,911	11,560,947
10	123,891,096	-163,161,081	138,438,848
15	233,383,252	-238,758,286	257,311,262
20	317,217,570	-314,707,313	349,243,378
25	373,746,176	-385,244,562	412,211,645
30	407,371,222	-447,811,903	450,711,692

Table 9.12 NPV for 15 *MVar* of D-STATCOM

Year	Customer side consideration (4+5) (*Baht*)	Utility side consideration (6) (*Baht*)	Customer &Utility consideration (4+5+6) (*Baht*)
5	-21,707,112	-151,301,979	-16,369,889
10	101,222,961	-252,015,514	115,770,679
15	210,902,837	-370,101,435	234,830,848
20	289,555,339	-488,073,891	321,581,146
25	336,893,338	-597,099,594	375,358,773
30	358,976,525	-693,388,089	402,316,995

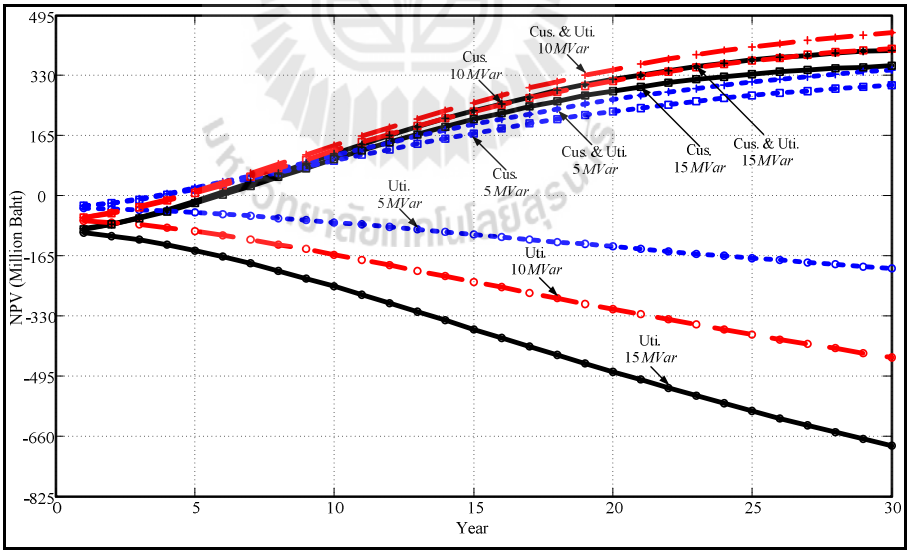

Figure 9.1 Net present values (NPV) for 50 events per year

These calculations include the effect of discounting cash flow to convert all costs and benefits of each size to present values for comparison. As a result, it is interesting to note that all of the options would have a positive net benefit to the facility with the assumed interest rate and life-time for the customer and both of customer and utility side considerations whereas only the utility side consideration have a negative net benefit. It is also interesting that the 10-*MVar* D-STATCOM is the best option in this account.

In addition, the voltage sag performances in Table 9.13 are used to demonstrate the effect of amount of sag event on the benefits and costs of implementing the D-STATCOM. The magnitude of the voltage sag in each category can be obtained by random. Three different sizes e.g. 5, 10 and 15 *MVar* of the D-STATCOM for improving the performance are also presented. The net present values in each event range (10-20, 20-30 and 30-40 events per year) are calculated based on average of 10 iterations and can be plotted as shown in Figure 9.2 to Figure 9.4. As can be seen in these figures, all of the sizes have a negative net benefit for the amount of sag event between 10 and 20 events per year. For the amount of sag event between 20 and 30 events per year, the 10-*MVar* rating of the D-STATCOM has a positive net benefit for the customer and both of customer and utility side considerations. And the 10 and 15-*MVar* ratings give the positive net benefits for the customer and both of customer and utility side considerations when the sags occur between 30 and 40 events per year.

Table 9.13 Number of the voltage sag event per year

Event Category	10-20 Events per Year	20-30 Events per Year	30-40 Events per Year
Interruption	1-2	2-2	2-3
Sag with min. voltage below 50%	1-2	2-2	2-3
Sag with min. voltage between 50 and 70%	2-4	4-7	7-9
Sag with min. voltage between 70 and 90%	6-12	12-19	19-25
Total	**10-20**	**20-30**	**30-40**

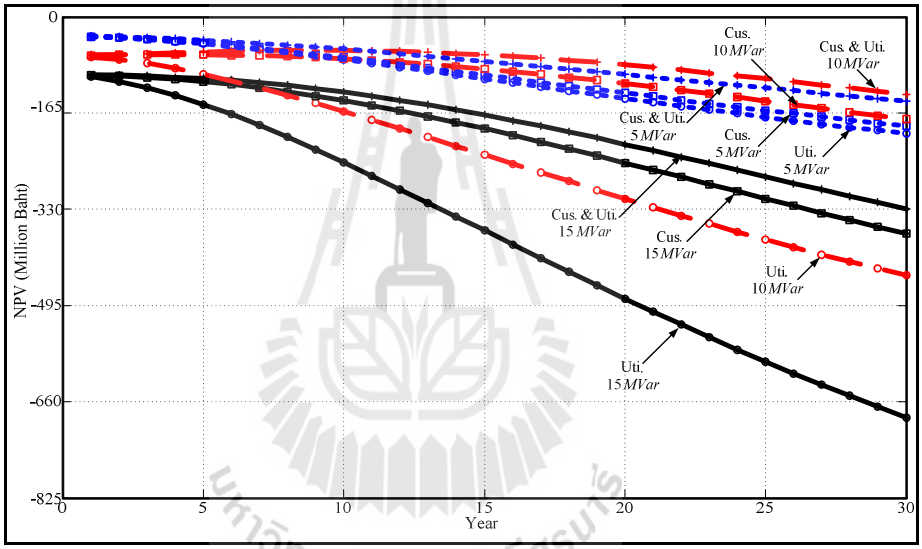

Figure 9.2 Net present values (NPV) for 10-20 events per year

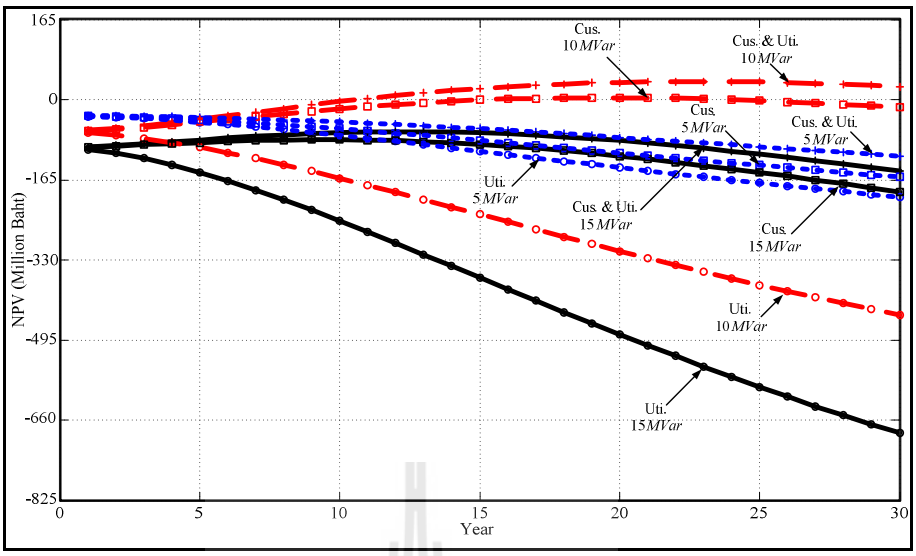

Figure 9.3 Net present values (NPV) for 20-30 events per year

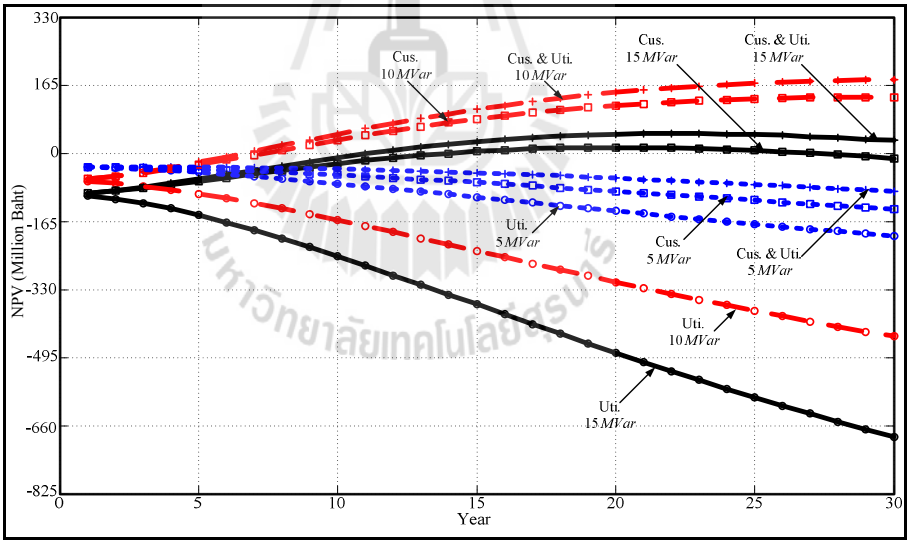

Figure 9.4 Net present values (NPV) for 30-40 events per year

9.4 Summary

This chapter demonstrates the cost estimation of reactive power compensation by using the D-STATCOM in distribution power systems. The process of costs

estimation and the comparison of three different sizes of the D-STATCOM (5, 10 and 15 *MVar*) for improving power quality are presented. The effects of the amount of sag event on the cost estimation are proposed. The voltage regulation, power factor correction and energy loss reduction has been chosen as the target for the cost estimation. The net present values (NPV) is applied to the cost estimation. The cost analysis procedure and the comparison among the results obtained from each option are proposed. With the assumed cost estimation parameters, the 10-*MVar* rating of the D-STATCOM gives the most benefit. In addition, the amount of sag event below 20 events per year gives the negative net benefit.

CHAPTER X

CONCLUSIONS

10.1 Summary of the Thesis

In this thesis, a brief description of the characteristics of category power quality problems and the importance of the power quality problems in the distribution system especially the voltage dips or sag were introduced and discussed in Chapter 1. The custom power devices (CPDs) for improving the power quality were introduced. The CPDs are basically of two types as network reconfiguring type and compensating type. The distribution STATCOM (D-STATCOM) is one of the compensating devices. It can be used for harmonics filtering, load balancing, power factor correction and voltage regulation. The answer to the most of power quality problems was found in the D-STATCOM.

In Chapter 2, the review of D-STATCOM and its application were proposed. The principle of D-STATCOM based on ideal current source and voltage source converter were discussed in detail. Several configurations of VSC-based D-STATCOM such as single-phase H-bridge, three-phase three-wire, three-phase four-wire and multilevel VSC were presented. The briefly review of the D-STATCOM control strategies were presented in this chapter. In addition, the examples of three categories of applications such as load compensation, voltage regulation and application with distributed generator were also presented. Regarding the applications of the D-STATCOM, the performances depend on the control algorithm. Of all the

mentioned applications, the most common type of controllers employs the PI controller. However, the details of the strategy to design the PI controller parameters have not been widely presented and discussed by various researchers, especially in terms of the applications for voltage regulation which is significant and interesting.

In Chapter 3, the modeling and the steady state characteristic of the distribution system with an ideal D-STATCOM were investigated. The *dq* synchronous rotating reference frame similar to that used for the field oriented control of three phase AC machines was applied to model the distribution system. Following this, the steady state characteristic has been obtained from the state equations. The steady state analysis results show that the maximum load power increases as the source inductance decreases while the increasing of the source time constant results in increasing of the maximum load power. The increasing of the source inductance results in linearly increases the minimum source voltage while the increasing of the source time constant results in decreasing the minimum source voltage. In addition, the comparison between the maximum load active power and PV curve was demonstrated in this chapter. From the comparison, the maximum load active power point is not the same as exactly the collapsing point in the PV curve. However, it is around the collapsing point. Furthermore, the effects of system parameters on size of D-STATCOM for voltage regulation when a source voltage sag or load power variation occur were investigated. It was seen that the size of D-STATCOM is a function of the system parameters e.g. source resistance, source inductance.

The small signal model and dynamic analysis of the distribution system with an ideal D-STATCOM were proposed in Chapter 4. The proposed non-linear model

in Chapter 3 can be linearized around some initial state conditions. Following this, the state-transition matrix representing the linearized model was obtained. A simplified model of D-STATCOM in power distribution systems on the *dq* synchronous rotating reference frame was used to investigate the system performance. Dynamic system stability of the linearized systems can be evaluated by means of eigenvalues. The variation of the location of an installed D-STATCOM, time constant of feeder section, initial state conditions, etc., was investigated to exhibit the dynamic system stability. The result shows that all variations have affected to the dynamic performance especially in the system with the RL load. In addition, all variations not to involve the instability of the system with the R load. However, some initial state conditions such as high positive active and reactive currents of the D-STATCOM caused the instability of the system with the RL load. Furthermore, the frequency responses of the transfer function of the load voltage with respect to the reactive current have indicated that the negative reactive currents cause some of Zeros locating on the RHP. In this consideration, the transfer function is a non-minimum phase system.

In Chapter 5, the design of component rating and parameters of the D-STATCOM for the load voltage regulation was presented. In addition, the dynamic equations and the steady state characteristic of D-STATCOM based on *dq* synchronously rotating reference frame were derived and investigated. The steady state performance results show that the DC capacitor does not have any relation with the active and reactive current of the D-STATCOM. The reactive current and DC voltage are a linear function of the AC voltage command on the *q*-axis whereas the active current is a quadratic function. The active current, reactive current and DC voltage are sensitive at the low AC voltage command on the *d*-axis. In addition, the

active and reactive currents are sensitive at low inductance whereas the DC voltage is slightly changed in each inductance. Meanwhile, the active current, reactive current and DC voltage are more sensitive when the time constant is increased.

The results of dynamic performances show that the values of resistors, inductors and capacitors have not affected to stability. Although, the small change of the AC voltage command on the *q*-axis causes high change of the active current, reactive current and DC voltage in steady state, it does not affect to characteristic roots whereas, the small change of the AC voltage command on the *q*-axis affects to the Zeros of the system.

In Chapter 6, the current and DC voltage control strategies for the D-STATCOM were described. The decoupling control based on the *dq* synchronously rotating reference frame was adapted in the current and DC voltage control schemes. The symmetrical optimum and genetic algorithms were applied to obtain the gains of the PI controllers. The stability margins of these methods were obtained and discussed. The proposed control schemes were simulated by using SIMULINK/MATLAB. The simulation results indicate that the decoupling current control based on the genetic algorithms gives the best dynamic response with the same gain and phase stability margins. Similar to the current controller parameter tuning, the symmetrical optimum and GA-based tuning methods were applied to the DC voltage control. Four strategies tuning that are i) DC voltage control and inner current control loop based on the symmetrical optimum method, ii) DC voltage control based on symmetrical optimum method with the inner current control loop based on genetic algorithms, iii) DC voltage control based on the genetic algorithms with the inner current control loop based on the symmetrical optimum method and iv)

DC voltage control and inner current control loop based on genetic algorithms were proposed. The DC voltage control based on the genetic algorithms with the inner current control loop based on genetic algorithms gives the best dynamic response. Meanwhile, the DC voltage control based on the symmetrical optimum method with the inner current control loop based on genetic algorithms gives the best gain stability margin and the inner current control loop based on the symmetrical optimum method gives the best phase stability margin.

The AC voltage control design of the D-STATCOM for the load voltage regulation was presented in Chapter 7. The D-STATCOM model and its control were integrated with the power distribution systems that used for the load voltage controller design. The classical loop shaping method was adapted for the load voltage controller design. The controller parameters were obtained by using MATLAB for adjusting the open loop transfer function to satisfy the loop shaping specifications. In addition, the tuning controller parameters based on the genetic algorithms was proposed and the step responses were compared with those of the classical loop shaping method. The comparison results indicate that the responses from both classical loop shaping and GA-based tuning method are similar. However, the classical loop shaping is easier that was appropriate for practical use.

In Chapter 8, four applications of the D-STATCOM, including the load voltage regulation for R load, RL load, RL load with a synchronous generator and RL load with an induction generator were simulated based on the proposed control strategy as described in Chapter 6 and Chapter 7. The simplified 22-*kV*, 2-bus test power system was employed for verifying of these applications. These applications were verified by SIMULINK/MATLAB. The simulation results indicate that the D-

STATCOM with the proposed control design can regulate the load voltage at the desired value by injecting reactive current within one cycle. The D-STATCOM with the proposed control can be used in case of the source voltage variations and load changes. However, the controller that is designed by using an unstable open loop transfer function cannot be use for a stable one, and vice versa. In the application of the D-STATCOM for the system including a distributed generator, the generator is remained stable and its active power can reach the set value during the source voltage sag in both cases.

In Chapter 9, the cost estimation of reactive power compensation by using the D-STATCOM in distribution power system was demonstrated. The process of costs estimation and the comparison of the different sizes of the D-STATCOM for improving power quality were presented. In addition, the effect of amount of sag event on the cost estimation was proposed. The cost estimation for voltage sag mitigation, power factor correction and energy loss reduction were conducted. The results show that the benefit of implementing of the D-STATCOM depends on the size of the D-STATCOM and amount of sag event. The proper size of the D-STATCOM for improving the high amount of sag event gives higher positive net benefit.

The procedure of D-STATCOM and its control system design for the load voltage regulation can be summarized in the flow diagram shown in Figure 10.1. In this procedure, the first step determines the equivalent parameters of the system such as the source voltage, source impedance and load. These parameters are involved the steady state analysis in the second step. The maximum load power, minimum source voltage and size of the D-STATCOM for the load voltage regulation by injecting only

the reactive power into the system are obtained. In the next step, the stable and unstable open loop transfer functions of the compensating current are determined. The size of D-STATCOM in the second step is used to design the component rating of the D-STATCOM in the fourth step. Then, the current and DC voltage control system are designed in the fifth step. In this step, the dynamic response and stability margins of the current and DC voltage control are checked. Subsequently, the stable and unstable open loop transfer functions in the third step are used to design the AC voltage control in the sixth step and then the dynamic response and stability margins of the control loop are checked in this step. In the finally step, the cost estimation of reactive power compensation by using the D-STATCOM in distribution power system is demonstrated.

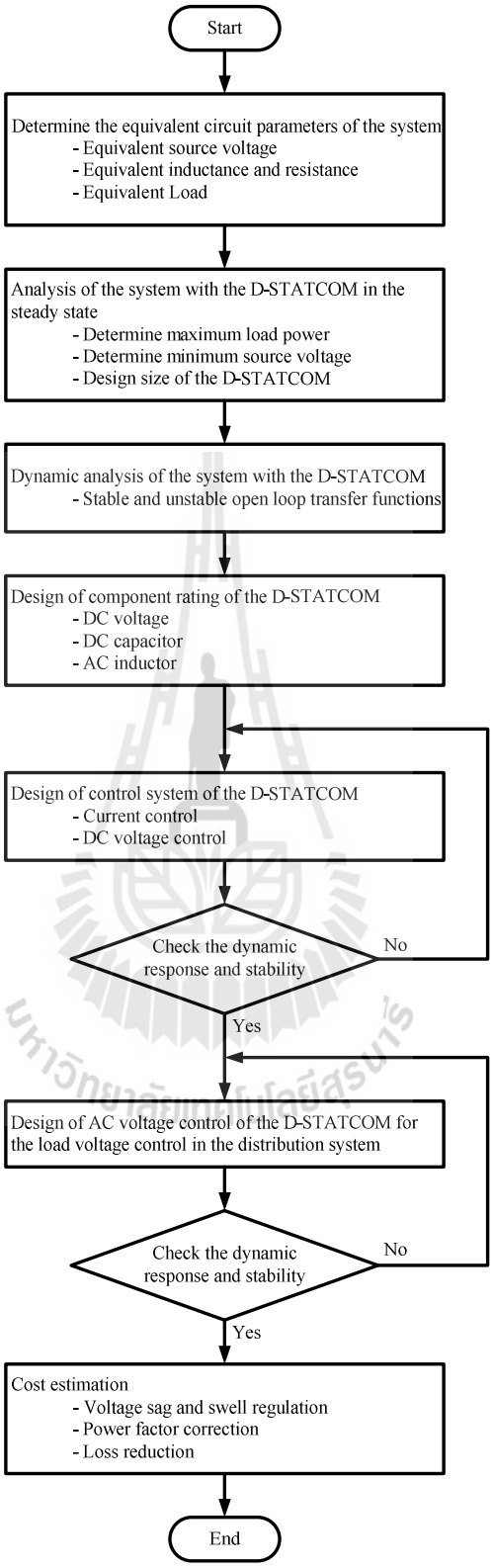

Figure 10.1 Flowchart of the design of D-STATCOM and its control system

10.2 Contributions

The contributions of this research are as follows:

1. The state equation of the distribution system with the D-STATCOM was obtained by modeling based on *dq* synchronous rotating reference frame. Following this, the steady state characteristics of this system were studied. From the steady state characteristics of the distribution system, the conditions of the maximum load active power and the minimum source voltage for the voltage regulation by injecting only the reactive power into the system were found. These steady state conditions can guarantee their dynamic transition behaviors because they are directly derived from the dynamic equations. The relation between the maximum load active power and the PV curve was also demonstrated. It indicates that the maximum load active power point is not the collapsing point in the PV curve.

2. The small signal model and dynamic analysis of the distribution system with the D-STATCOM were proposed in this thesis. Analysis result shows that some initial state conditions such as high positive active and reactive currents of the D-STATCOM leads to the instability of the system with RL loads. The frequency responses of the transfer function of the load voltage with respect to the reactive current indicated that the negative reactive currents cause a non-minimum phase system.

3. The decoupling control based on the *dq* synchronously rotating reference frame was adapted in the current and DC voltage control schemes. Two methods of the current controller parameter tuning that are the symmetrical optimum and genetic algorithms were proposed. The symmetrical optimum method is a classical method that requires very little knowledge of system parameters, which makes it very

appropriate for practical use. However, tuning with genetic algorithms gives the best dynamic response of the same stability margins with the symmetrical optimum tuning method. For the DC voltage control, the change of the reactive current affects to the DC voltage. The control with the elimination of reactive current effect was proposed in this thesis. The proposed control results in the reduction of the overshoot of the DC voltage response. In addition, the DC voltage control based on the symmetrical optimum method with the inner current control loop based on genetic algorithms was proposed. This control strategy gives a good dynamic response with the best gain stability margin.

4. The D-STATCOM model and its control were integrated with the power distribution system. The classical loop shaping method was proposed for the load voltage controller design. The step responses were compared with those obtained by using the controller parameters tuning based on genetic algorithms. The comparisons results indicate that the responses of the both classical loop shaping and genetic algorithms tuning methods are close. However, the classical loop shaping is easily tuning method that was appropriate for practical use.

10.3 Suggestions for Future Work

1. In this thesis, it assumes that the source and load voltages are balanced. However, the unbalanced voltage is one of serious power quality problems in distribution systems. Although, the unbalanced voltage mitigation by using D-STATCOM and other custom power devices have been proposed in many literatures, the control design algorithm especially the controller parameter tuning method of

unbalanced compensator is less reported. Therefore, the control design algorithm with proper parameter tuning can be extended to those unbalance conditions.

2. The small signal model is applied to design the controllers in this thesis. The controllers are tuned for the D-STATCOM at some particular operating point. However, the D-STATCOM must be applicable over a wide range of operating conditions. A nonlinear control strategy, adaptive control or robust control can be applied to this work.

3. Distributed generation has been increasingly installed in the distribution system to support customer's power quality and reliability. The integration of the distributed generation and custom power devices such as D-STATCOM for enhancing the power quality and reliability could be further investigated. However, it is noted that this system is very expensive, so its costs and benefits could be carefully assessed.

4. In this thesis, the D-STATCOM model and the proposed control are implemented on the SIMULINK/MATLAB to verify steady state and dynamic performance. The effect of resolution of digital signal processor on the dynamic performance is not investigated. The experimental of D-STATCOM and the proposed control with the digital signal processor could be further investigated.

REFERENCE

Akagi, H., Kanazawa, Y. and Nabae, A. (1984). Instantaneous Reactive Power Compensators Comprising Switching Devices without Energy Storage Components. In **Industry Applications, IEEE Transactions on**. IA-20(3): 625-630.

Akagi, H., Nabae, A. and Atoh, S. (1986). Control Strategy of. Active Power Filters Using Multiple Voltage-Source PWM Converters. **In IEEE Trans. Industry Application**. IA-22(3): 460-465.

Akagi, H., Watanabe, E.H. and Aredes, M. (2007). **Instantaneous power theory and applications to power conditioning**. New York: IEEE Press.

Anaya-Lara, O. and Acha, E. (2002). Modeling and analysis of custom power systems by PSCAD/EMTDC. In **Power Delivery, IEEE Transactions on**. 17(1): 266-272.

Baran, M.E. and Wu, F.F. (1989). Optimal capacitor placement on radial distribution systems. In **IEEE Trans. on Power Delivery**. 4(1): (725–734).

Barratt, C. and Boyd, S. (1992). Interactive Loop-Shaping Design of MIMO Controllers. In **IEEE Symposium on Computer Aided Control System Design**. (pp. 76 – 81). New York : IEEE Press.

Bhatia, R. S., Jain, D. K., Singh, B. and Jain, S. P. (2004). Battery energy storage system for power conditioning. In **Proc. of National Power Sys. Conf. NPSC-2004**. (pp. 86-91).

Bhattacharya, S., Po-Tai Cheng and Divan, D. M., (1997). Hybrid Solution for Improving Passive filter performance in High Power Applications. In **IEEE Trans. on Indus. App**. 33(3): 1302- 1309.

Blaabjerg, F., Pedersen, J.K., Sigurjonsson, S. and Elkjaer, A. (1996). An extendedmodel of power losses in hard-switched IGBT-inverters. In **Industry Applications Conference**. (pp. 1454-1463). New York : IEEE Press.

Blazic, B. and Papic, I. (2006). Improved D-StatCom Control for Operation With Unbalanced Currents and Voltages. In **IEEE Trans. Power Delivery**. 21(1): 225-233.

Chong, H., Zhanoning, Y., Bin, C., Huang, A. Q., Bin, Z., Ingram, M. R. and Edris, A. (2007). Evaluation of cascademultilevel converter based STATCOM for arc furnace flicker mitigation. In **IEEE Trans. Ind. Appl**. 43(2): 378-385.

Chung, T.S. and Shaoyun, G. (1997). A recursive LP-based approach for optimal capacitor allocation with cost-benefit consideration. In **Electric Power Systems Research, Elsevier Science**. 39(2): (129–136).

Correa, J. M., Farret, F. A. and Simoes, M. G. (2005). Application of a Modified single –phase PQ Theory in the control of Shunt and Series Active Filters in a 400Hz Microgrid. In **Proc. IEEE Conf. on Power Electron Specialists Conf**. (pp. 2585-2591). New York : IEEE Press.

D'Azzo, J. and Houpis, H. (1995). **Linear control system analysis and design: conventional and modern**. New York: McGraw-Hill.

Darrow. K. and Hedman, B. (2005). **The Role of Distributed Generation in Power Quality and Reliability**. New York: Energy and Environmental Analysis Inc.

Dugan, R. C., McGranaghan, M. F. and Wayne Beaty, H., (1996). **Electrical Power System Quality**. McGraw-Hill.

Ferrero, A. and Superti-Furga, G. (1991). A new approach to the definition of power components in three-phasesystems under nonsinusoidal conditions. In **Instrumentation and Measurement, IEEE Transactions on**. 40(3): 568-577.

Freitas, W., Asada, E., Morelato, A. and Wilsun Xu. (2002). Dynamic improvement of induction generators connected to distribution systems using a DSTATCOM. In **Power System Technology, 2002. Proceedings. PowerCon 2002. International Conference on**. (pp. 173 - 177). New York : IEEE Press.

Freitas, W., Asada, E., Morelato, A. and Xu, W. (2002). Dynamic Improvement of Induction Generators Connected to Distribution Systems Using a DSTATCOM. In **Proc. of IEEE int. Con. on Power System Technology, PowerCon**. (pp. 173-177). New York : IEEE Press.

Freitas, W., Morelato, A., Wilsun Xu. and Sato, F. (2005). Impacts of AC Generators and DSTATCOM devices on the dynamic performance of distribution systems. In **Power Delivery, IEEE Transactions on**. 20(2): 1493- 1501.

Frohr, F. and Orttenburger, F. (1992). **Introduction to electronic control engineering**. New Delhi: Second Wiley Eastern Reprint.

Furuhashi, T., Okuma, S. and Uchikawa, Y. (1990). A study on the theory of instantaneous reactive power. In **Industrial Electronics, IEEE Transactions on**. 37(1): 86-90.

Ghosh, A. and Joshi, A. (2000). A new approach to load balancing and power factor correction inpower distribution system. In **Power Delivery, IEEE Transactions on**. 15(1): 417-422.

Ghosh, A and Ledwich, G. (2002). **Power Quality Enhancement Using Custom Power Devices**. America: Kluwer Academic Publishers.

Ghosh, A. and Ledwich, G. (2003). Load compensating DSTATCOM in weak AC systems. In **Power Delivery, IEEE Transactions on**. 18(4): 1302- 1309.

Gonzalez, P. and Cerrada, A., (2000). Control System for a PWM-based STATCOM. **In IEEE Trans. Power Delivery**. 15(0): 1252-1257.

Gupta, R. Ghosh, A. and Joshi, A. (2011). Performance Comparison of VSC-Based Shunt and Series Compensators Used for Load Voltage Control in Distribution Systems. In **Power Delivery, IEEE Transactions on**. 26(1): 268-278.

Haque, M.H. (2001). Compensation of distribution system voltage sag by DVR and D-STATCOM. In **Power Tech Proceedings, 2001 IEEE Porto**. (pp. 1-5). New York : IEEE Press.

Hasanzadeh, A., Parniani, M. and Sadriyeh, S.M.R. (2005). A comparative study on current control methods for load balancing and power factor correction using STATCOM. In **Power Tech, 2005 IEEE Russia**. (pp. 1-7). New York : IEEE Press.

Hingorani, N.G. and Gyugyi, L. (1995). Introducing custom power. In **IEEE spectrum**. 32(6): 41-48.

Hingorani, N.G. and Gyugyi, L. (2000). **Understanding FACTS**. New York: IEEE Press.

Hoffman, K. and Ledwich, G. (1994). Improved power system performance using inverter based resonant switched compensators. In **IEEE Power Electronics Specialists Conf. (PESC)**. (pp. 205-210). New York : IEEE Press.

IEEE 519: 1992. **IEEE Recommended Practices and Requirements for Harmonic Control in Electric Power Systems (ANSI)**: New York : IEEE Press.

IEEE P1409. (1999). **Distribution Custom Power Task Force 2, Custom Power Technology Development**.

IEEE Standaed 493-497. (1997). **IEEE Recommended Practices for Design of Reliable Industrial and Commercial Power Systems**. New York : IEEE Press.

Jain, A., Joshi, K., Behal, A. and Mohan, N. (2006). Voltage regulation with STATCOMs: modeling, control and results. In **IEEE Trans. Power Del**. 21(2): 726 – 735.

Jazayeri, M. and Fendereski, M. (2007). Stabilization of Grid Connected Wind Generator during Power Network Disturbances by STATCOM. In **Proc. of IEEE 42nd Inter. Conf. Uni. Power Engg., UPEC 2007**. (pp. 1182-1186). New York : IEEE Press.

Kansal, G. K. and Singh, B. (2008). Decoupled Voltage and Frequency Controller for Isolated Asynchronous Generators Feeding Three-Phase Four-wire Loads. In **IEEE Trans. on Power Delivery**. 23(2): 966-973.

Kulworawanichpong, T., Areerak, K-L., Areerak, K-N., Pao-la-or, P., Puangdownreong, P. and Sujitjorn, S. (2005). Dynamic parameter identification of induction motors using intelligent search techniques. In **The**

24th IASTED Int. Conf. Modelling, Identification, and Control (MIC 2005). (pp. 328-332).

Ledwich, G. and Ghosh, A. (2002). A Flexible DSTATCOM operating in Voltage or Current Control Mode. In **IEE Proc. Gener, Transm, Distrib**. 149(2): 724 – 738.

Marian P. K., Krishnan, R. and Blaabjerg, F. (2002). **Control in power electronics selected problems**. California: Elsevier Science.

Miller, T. J. E., (1982). **Reactive Power Control in Electric Systems**: John Wiley & Sons Press.

Mishra, M. K., Ghosh, A. and Joshi, A. (2002). Operation of a DSTATCOM in Voltage Control Mode. In **Power Engineering Review, IEEE**. 22(4): 258-264.

Mishra, M. K., Ghosh, A. and Joshi, A. (2006). A new STATCOM topology to compensate loads containing ac and dc components. In **IEEE Power Engineering Society Winter Meeting**. New York : IEEE Press.

Mishra, M.K. and Karthikeyan, K. (2008). A three phase DSTATCOM compensating AC and DC loads with fast dynamic response. In **Electrical and Computer Engineering, 2008. CCECE 2008. Canadian Conference on**. (pp. 1199-1202). New York : IEEE Press.

Mohamed, Y. A. R. I. and Saadany, E. F. E., (2009). Grid interface of photovoltaic-micro turbine hybrid based power for voltage support and control using VSI in rural applications. In **IEEE Trans. Power Syst**. 24(1): 489-491.

Purewave, (2008). **dstatcom** (On-line). Avaliable: http://www.sandc.com/products/power-quality/purewave-dstatcom.asp

Quinn, C. A., Mohan, N. and Mehta, H. (1992). Active filtering of harmonic currents in three-phase, four-wire systems with three-phase and single-phase nonlinear loads. In **Proc. IEEE Applied Power Electronics Conf. (APEC)**. (pp. 829-836). York : IEEE Press.

Quinn, C. A., Mohan, N. and Mehta, H. (1993). A Four-wire current-controlled converter provides harmonic neutralization in three-phase, four-wire systems. In **Proc. Applied Power Electronics Conf. (APEC'93)**. (pp. 841-846).

Rashidi, M., Rashidi, F. and Monavar, H. (2003). Tuning of power system stabilizers via genetic algorithm for stabilization of power system. In **IEEE Int. Conf. Systems, Man and Cybernetics**. (pp. 4649-4654). New York: IEEE Press.

Ravi Kumar, S.V. and Siva Nagaraju, S. (2007). Simulation of D-STATCOM and DVR in Power Systems. In **ARPN Journal of Engineering and Applied Sciences**. 2(3): (7-13).

Robinson, R., Danielson, U. and Snaith, M. (1998). **Road maintenance management: Concepts and systems**. London: Macmillan.

Routimo, M., Salo, M. and Tuusa, H., (2007). Comparison of Voltage-Source and Current–Sourced Shunt Active Power Filters. In **IEEE Trans. Power Electronics**. 22(2): 636-643.

Samuel, P., Gupta, R. and Chandra, D. (2009). A study on the theory of instantaneous reactive power. In **IEEE Power Eng. Soc. Gen. Meeting. Canada** : IEEE Press.

Sao, C.K., Lehn, P.W., Iravani, M.R. and Martinez, J.A. (2002). A benchmark system for digital time-domain simulation of a pulse-width-modulated D-STATCOM. In **Power Delivery, IEEE Transactions on**. 17(4): 1113 – 1120.

Selvajyothi, K. and Janakiraman, P. A., (2010). Reduction of voltage harmonics in single phase inverters using composite observers. In **IEEE Trans. Power Del**. 18(4): 1302 – 1309.

Sharmeela, C., Uma, G. and Mohan, M.R. (2005). Multi-level distribution STATCOM for voltage sag and swell reduction. In **Proc. IEEE Power Engineering Society General Meeting**. (pp. 1303-1307). New York : IEEE Press.

Shukai Xu, Qiang Song, Yongqiang Zhu, and Wenhua Liu. (2005). Development of a D-STATCOM Prototype Based on Cascade Inverter with Isolation Transformer for Unbalanced Load Compensation. In **Industrial Technology, 2005. ICIT 2005. IEEE International Conference on**. (pp. 1051-1056). New York : IEEE Press.

Shukla, A., Ghosh, A. and Joshi, A. (2005). A hysteresis current controlled flying capacitor multilevel inverter based DSTATCOM. In **Proc of IEEE Power Engineering Society General Meeting**. (pp.857-864). New York : IEEE Press.

Singh, B. Adya, A., Mittal, A.P. and Gupta, J.R.P. (2005). Modeling and control of DSTATCOM for three-phase, four-wire distribution systems. In **Industry Applications Conference, 2005. Fourtieth IAS Annual Meeting. Conference Record of the 2005**. (pp. 2428- 2434). New York : IEEE Press.

Singh, B., Adya, A., Mittal, A.P. and Gupta, J.R.P., (2006). Analysis, simulation and control of DSTATCOM in three-phase, four-wire isolated distribution systems. In **Proc. IEEE Power India Conf**. New York: IEEE Press.

Singh, B., Adya, A., Mittal, A. P., Gupta, J. R. P. and Singh, B. N. (2006). Application of DSTATCOM for Mitigation of Voltag Sag for Motor Loads in Isolated Distribution Systems. In **IEEE ISIE, Montreal, Quebec**. (pp. 1806-1811). New York : IEEE Press.

Singh, B. and Jitendra Solanki. (2006). A Comparative Study of Control Algorithms for DSTATCOM for Load Compensation. In **Industrial Technology, 2006. ICIT 2006. IEEE International Conference on**. (pp. 1492-1497). New York : IEEE Press.

Singh, B. and Kansal, G. K. (2008). Solid State Voltage and Frequency Controller for a Stand Alone Wind Power Generating System. In **IEEE Trans. on Power Electronics**. 23(3): 1170-1177.

Singh, B. and Kansal, G. K. (2008). Voltage and Frequency Controller for a Three-Phase Four-Wire Autonomous Wind Energy Conversion System. In **IEEE Trans on Energy Conversion**. 23(2): 509-518.

Singh, B., Kasal, G., Chandra, A. and Haddad, K. A. (2007). Battery Based Voltage and Frequency Controller for Parallel Operated Isolated Asynchronous Generators. In **Proc. IEEE Int. Symp. on Ind. Elect**. (pp. 883-888). New York : IEEE Press.

Singh, B., Murthy, S. S. and Gupta, S. (2004). Analysis and Design of STATCOM-Based Voltage Regulator for Self-Excited Induction Generators. In **IEEE Transactions on Energy Conversion**. 19(4): (783-790).

Singh, B., Saha, R., Chandra, A. and Al-Haddad, K., (2009). Static Synchronous Compensators (STATCOM) : A review. IET Power Electron. In **IET Power Electron**. 2(4): 297- 324.

Singh, B., Solanki, J. and Verma, V. (2005). Neural Network Based Control of DSTATCOM with Rating Reduction for Three-Phase, Four-Wire System. In **Proc. Conf. IEEE- PEDS'05**. (pp. 920-925): New York : IEEE Press.

Somsai, K. and Kulworawanichpong, T. (2008). Modeling, simulation and control of D-STATCOM using ATP/EMTP. In **Harmonics and Quality of Power, 2008. ICHQP 2008. 13th International Conference on**. (pp. 1-4). New York : IEEE Press.

Sun, J., Czarkowski, D. and Zabar, Z. (2002).Voltage flicker mitigation using PWM-based distribution STATCOM.In **Proc. IEEE PES Summer Meeting**. (pp.616-621). New York : IEEE Press.

Tan, Y. L, (1999). Analysis of line compensation by shunt connected FACTs controllers: a comparison between SVC and STATCOM. In **IEEE power Eng. Rev**. 19(8): 7-58.

Vechiu, I., Curea, O. and Camblong, H. (2010). Transient Operation of a Four-Leg Inverter for Autonomous Applications With Unbalanced Load. In **IEEE Transactions on Power Electronics**. 25(2): 399-407.

Wang, Y.P., Hur, D.R., Chung, H.H., Watson, N.R., Arrilaga, J. and Matair, S.S (2000). A genetic algorithms approach to design an optimal PI controller for static VAr compensator. In **Int. Conf. Power System Technology (PowerCon 2000)**. (pp. 1557-1562).

Watanabe, E.H., Stephan, R.M. and Aredes, M. (1993). New concepts of instantaneous active and reactive powers inelectrical systems with generic loads. In **Power Delivery, IEEE Transactions on**. 8(2): 697-703.

Willems, J.L. (1992). A new interpretation of the Akagi-Nabae power components for nonsinusoidal three-phase situations. In **Instrumentation and Measurement, IEEE Transactions on**. 41(4): 523 – 527.

Xiao-ping Yang, Y., Yan-Xiao Zhang, Z. and Yan-ru, Z. (2008). Three–phase four-wire DSTATCOM based on a three-dimensional PWM algorithm. In **Proc Int. Conf. Electric. Utility Deregulation and Restructuring and Power Technologies**. (pp. 2061-2066).

Zhu, J. and MOmoh, J.A. (1998). Optimal Var pricing and Var placement using analytic hierarchical process. In **Electric Power Systems Research, Elsevier Science**. 48(1): (11– 17).

APPENDIX A

VALIDATION OF THE MATHERMATICS MODEL

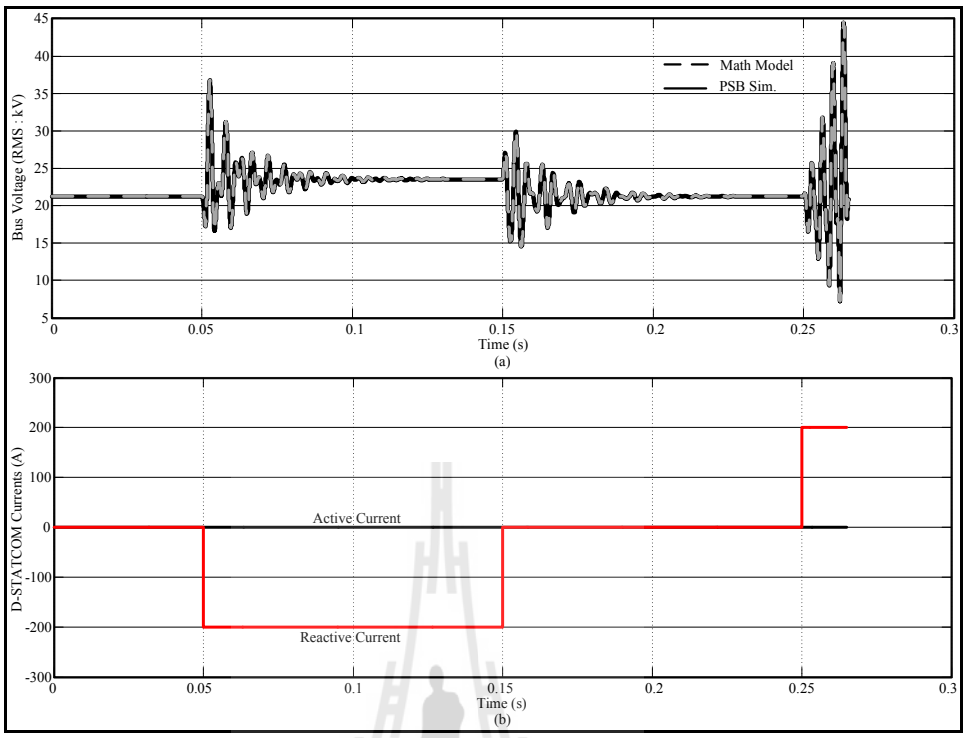

Figure A.1 Validation of the mathematic model of the equations (3.10) – (3.16)

Figure A.1 compare the responses of the AC bus voltage of the mathematic model in equations (3.10) – (3.16) and the model that is created on the SIMULINK/MATLAB as shown in Figure 8.3. The D-STATCOM active and reactive currents are selected as the inputs while the AC bus voltage is selected as the output. As can be seen in Figure A.1, the AC bus voltage responses of both mathematic

model and SIMULINK/MATLAB model are the same. Meanwhile, the responses of the DC voltage and currents of mathematic model in equations (5.15) – (5.14) and (6.9) – (6.18) are compared with those of the SIMULINK/MATLAB model in Figure 8.3. The D-STATACOM DC voltage and currents are the outputs with the voltage commands on *dq* axis are the inputs. The DC voltage and currents responses of these models are very close to each other.

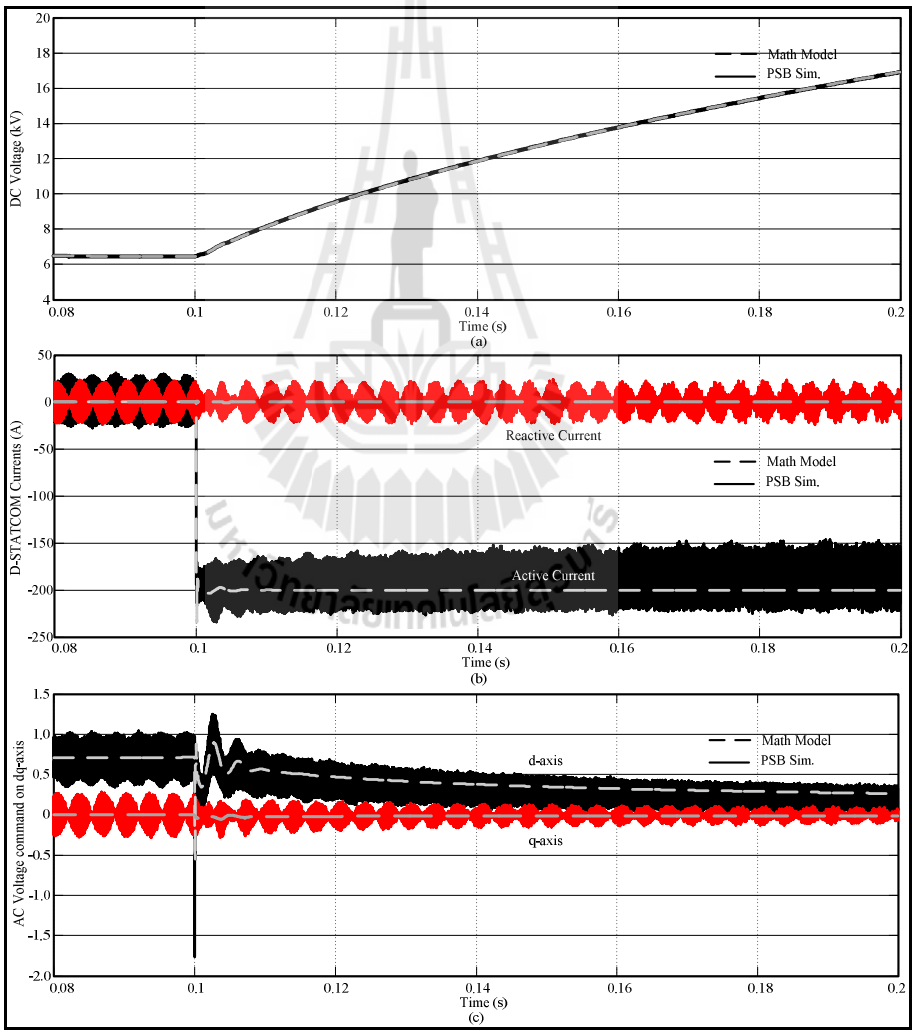

Figure A.2 Validation of the mathematic model of the equations (5.15) – (5.14) and (6.9) – (6.18)

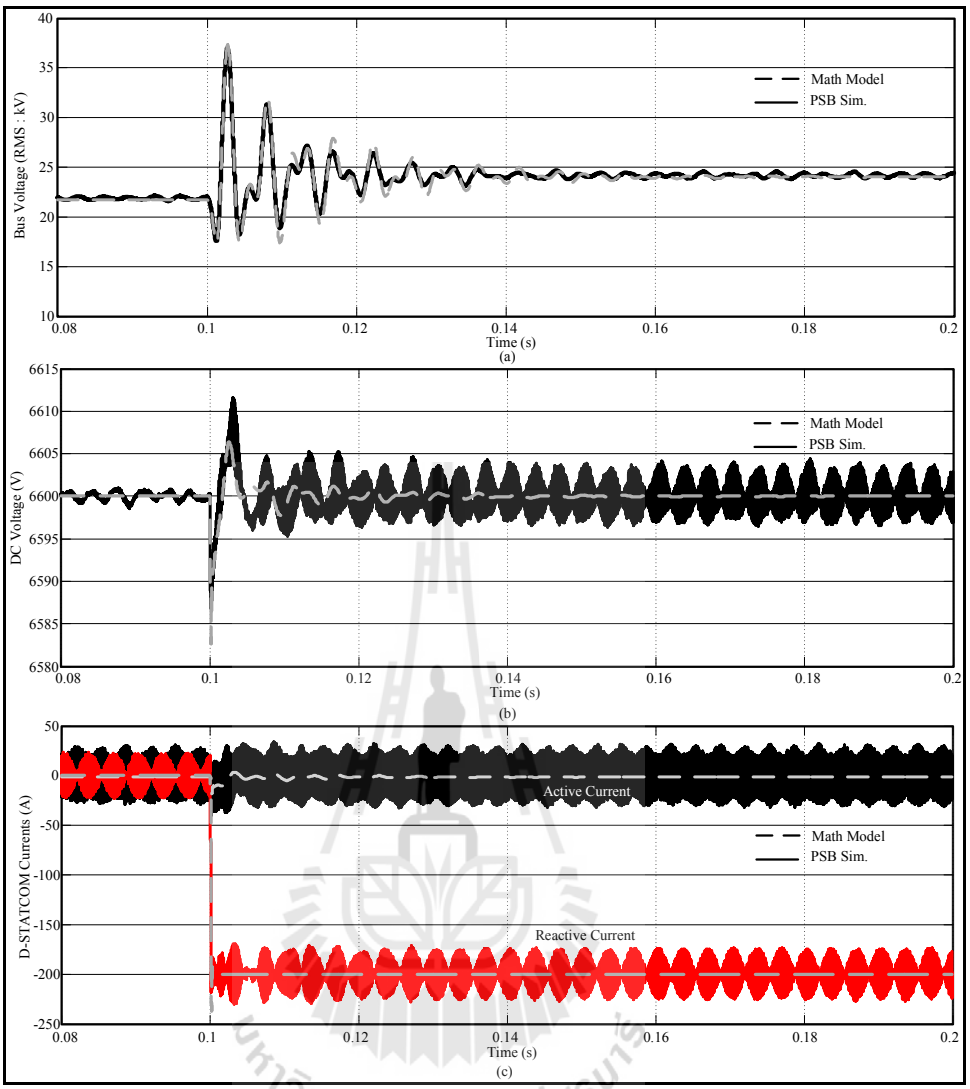

Figure A.3 Validation of the mathematic model of the equations (7.1) – (7.28)

Figure A.3 demonstrate the dynamic responses of DC voltage and current control of the mathematic model in equations (7.1) – (7.28) and SIMULINK/MATLAB model in Figure 8.3. It is seen that, the responses of both mathematic and SIMULINK/MATLAB models are very close to each other. In addition, the results of D-STATCOM and its control system for the load voltage control on the mathematic and SIMULINK/MATLAB simulations are illustrated and

compared in Figure A.4. As can be seen in this figure, the results show that the responses of both mathematic and SIMULINK/MATLAB simulations are similar.

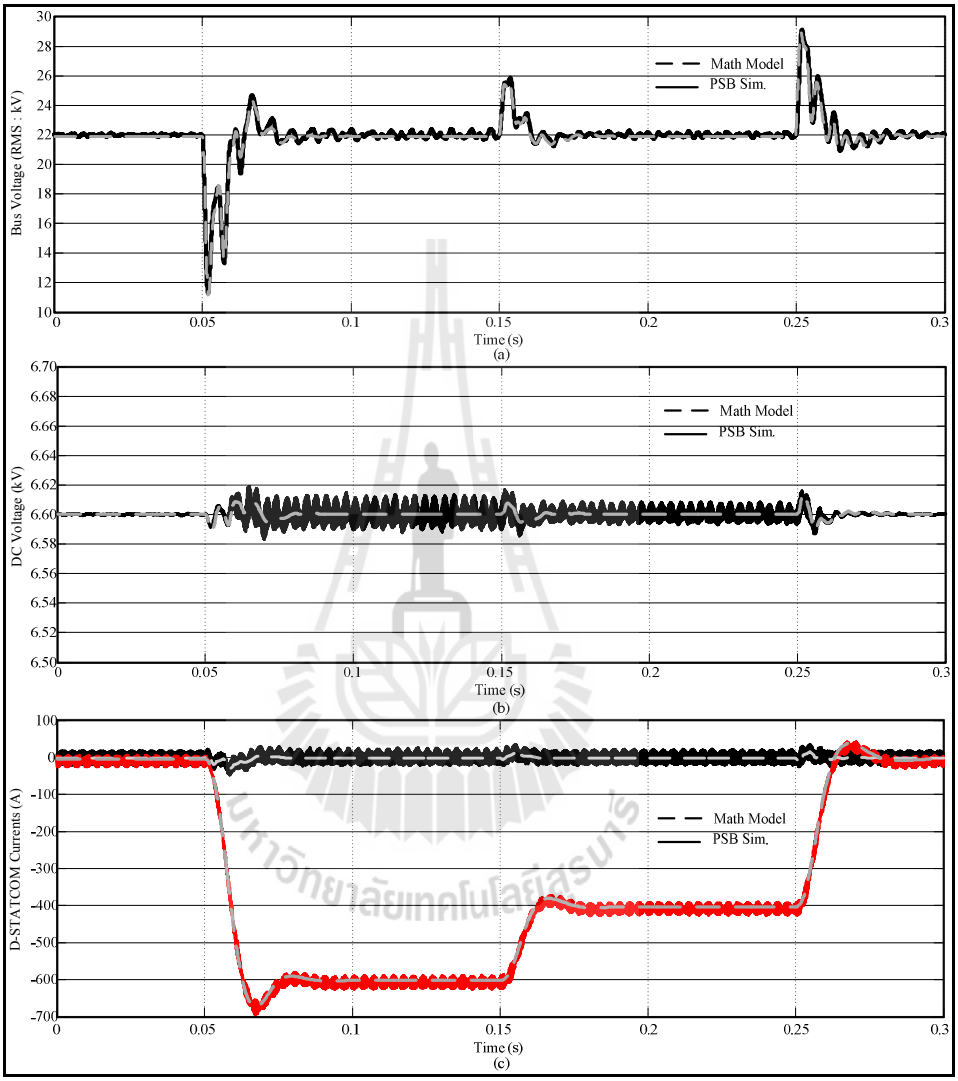

Figure A.4 Validation of the mathematic model of the distribution system with the D-STATCOM and its control system

APPENDIX B

DESIGN OF D-STATCOM

According to the steady state analysis of the distribution system that discussed in Chapter 3 with the system parameters as shown in Chapter 8, the sizes of D-STATCOM for the load voltage regulation are obtained and shown in Table 8.1 and Table 8.2. The maximum size in these cases is 13.82 *MVar* that it is selected to used in Chapter 8. The components rating of this D-STATCOM that are calculated on the secondary side of the coupling transformer (22 / 2.2 *kV*) as follows:

The compensation current:

$$I_f(A) = \frac{Q_{D-STATCOM}}{\sqrt{3}V_t} = \frac{13.82(MVar)}{\sqrt{3}\times 2.2(kV)} = 6281.8A$$

The DC bus voltage:

$$V_{dc} = \frac{2\sqrt{2}\left(\frac{V_t}{\sqrt{3}}\right)}{m_a} = \frac{2\sqrt{2}\left(\frac{2.2(kV)}{\sqrt{3}}\right)}{0.55} = 6.532kV$$

The AC inductor:

$$L_f = \frac{\left(\frac{\sqrt{3}}{2}\right)m_a V_{dc}}{6.a.f_s i_{cr(p-p)}} = \frac{\left(\frac{\sqrt{3}}{2}\right)\times 0.55\times 6.532(kV)}{6\times 1.2\times 5(kHz)\times 628.18(A)} = 0.1376mH$$

APPENDIX C

PUBLICATIONS

Publications

Somsai, K. ; Kulworawanichpong, T. ; Voraphonpiput, N. (2011). **Effects of Maximum Loading Ability and Minimum Voltage Source on Voltage Regulation by Using D-STATCOM**, Accepted to be published by *The International Review on Modelling ans Simulations* Vol 4, No. 5. pp. 2410-2416.

Somsai, K. ; Kulworawanichpong, T. ; Voraphonpiput, N. (2012). **Steady-state Modeling and Analysis of Distribution STATCOM**. Accepted to be published by *The Wulfenia Journal* Vol. 19, No. 10. pp. 281-307.

Somsai, K. ; Kulworawanichpong, T. ; Voraphonpiput, N. (2012). **Design of DC Voltage Control for D-STATCOM**. Accepted to be published by *The World Academy of Science, Engineering and Technology*. Issue. 71, pp. 420-426.

Somsai, K. ; Voraphonpiput, N. ; Kulworawanichpong, T. (2013). **Loop Shaping Control of Distribution STATCOM**. Accepted to be published by *The International Journal of Control and Automation* Vol. 6. No. 1. pp. 87-104.

Somsai, K. ; Voraphonpiput, N. ; Kulworawanichpong, T. (2013). **Symmetrical Optimum Design of Compensating Current and DC Voltage Controllers for D-STATCOM**. Accepted to be published by *The International Journal of Control and Automation* Vol. x. No. x. pp. xxx-xxx.

Somsai, K., Oonsivilai, A., Srikaew, A. and Kulworawanichpong, T. (2007). **Optimal PI controller design and simulation of a static var compensator using MATLAB's SIMULINK**. *In Proceedings of the 7th WSEAS International Conference on POWER SYSTEMS* (pp 30-35). Beijing, China : WSEAS.

Somsai, K. ; Kulworawanichpong, T. (2008). **Modeling, simulation and control of D-STATCOM using ATP/EMTP**. *In Proceedings of the 13th International Conference on Harmonics and Quality of Power (ICHQP 2008)*. Wollongong, NSW: IEEE.

Somsai, K. ; Kulworawanichpong, T. (2010). **Instantaneous power control of D-STATCOM with consideration of power factor correction**. *In Proceedings of the International Conference on Electrical Engineering/Electronics, Computer, Telecommunications and Information Technology (ECTI 2010)*. Thailand : ECTI.

Somsai, K. ; Kulworawanichpong, T. ; Voraphonpiput, N. (2012). **Steady-State Performance of D-STATCOM for Load Voltage Regulation**. *In Proceedings of the Power and Energy Engineering Conference (APPEEC), 2012 Asia-Pacific*. Shanghai, China: IEEE.

Somsai, K. ; Kulworawanichpong, T. ; Voraphonpiput, N. (2012). **Design of Decoupling Current Control with Symmetrical Optimum Method for D-STATCOM**. *In Proceedings of the Power and Energy Engineering Conference (APPEEC), 2012 Asia-Pacific*. Shanghai, China: IEEE.

International Journal of Control and Automation
Vol. 6, No. 1, February, 2013

Loop Shaping Control of Distribution STATCOM

Kittaya Somsai[1], Nitus Voraphonpiput[2] and Thanatchai Kulworawanichpong[1*]

[1]*School of Electrical Engineering, Suranaree University of Technology, Nakhon Ratchasima, Thailand*
[2]*Power Purchase Division, Electric Generating Authority of Thailand, Bangkok, Thailand*
** Corresponding Author, e-mail: thanatchai@gmail.com*

Abstract

This paper presents the system modeling and control design for the load voltage regulation using distribution static compensators (D-STATCOMs). The decoupling control based on the dq reference frame with the symmetrical optimum method is applied to design the D-STATCOM current and DC voltage controllers. The modeling strategy similar to that used for the field-oriented control of three-phase AC machines is employed to model the distribution system integrating with the D-STATCOM and its control circuit. This derived model is used for the load voltage controller design based on the linearized technique, called classical loop shaping method. A simplified 11-kV, 2-bus test power system is employed for simulation. Satisfactory results obtained by simulating the proposed model are compared with those obtained by the switching control of D-STATCOM power circuit created in MATLAB's Power System Blockset. As a result, the effectiveness of proposed model is verified. This design gave satisfactory responses to guarantee at least 3 dB of the gain margin and 40° of the phase margin.

Keywords: *D-STATCOM, voltage regulation, decoupling control, symmetrical optimum, classical loop shaping*

1. Introduction

In a power distribution system, voltage sag contributes more than 80% of power quality (PQ) problems that exist in power systems [1–2]. It is caused by a fault in the utility system, a fault within the customer's facility or a large increase of the load current, like starting a motor or transformer energizing, operation of process controllers; programmable logic controllers (PLC), adjustable speed drive (ASD) and robotics [1], and used of high intensity discharge lamps [3].

Controlled reactive power sources are commonly used for load voltage regulation in presence of disturbances like voltage sag. Due to their high control bandwidth, D-STATCOMs, based on three-phase pulse width modulation voltage source converters, have been proposed for this application [3–7]. For a fast control, the D-STATCOM is usually modeled using the *dq* axis theory for balanced three-phase systems, which allows definition of instantaneous reactive current and instantaneous magnitude of phase voltages [8]. In addition, the current controller design is developed using a rotating *dq* frame of reference that offers higher accuracy than the stationary frame techniques [9].

International Journal of Control and Automation
Vol. 6, No. 1, February, 2013

Most literatures on the D-STATCOM and STATCOM control concentrates in control of the output current and DC voltage regulation for a given reactive current reference. The current decoupling control based on the *dq* reference frame received considerable attention in [10–12]. To alleviate the interaction between the active and reactive currents, a feed-forward control loop with reactive current deviations as the input was introduced to compensate for the DC voltage drop [13]. In addition, an alternative approach using a linearized state space model in the D-STATCOM and STATCOM control design was proposed in [14–15]. For control design, a small signal model of the distribution system was derived by transforming the equivalent system impedance to the *dq* frame rotating at the power frequency in steady state, thereby imposing a limitation on the dynamic response [16].

In this paper, the D-STATCOM current and DC voltage decoupling control based on the *dq* reference frame are used and the proportional gain and integral time of PI controllers are also with its design. This derived model is used for the load voltage controller design based on some linearized technique, called classical loop shaping method. By using MATLAB for adjusting the transfer function to satisfy the loop shaping specifications, the controller's parameters and the stability margins for an inductive *RL* load with various operating conditions can be obtained. Performance of the proposed model and the controller design were verified using computer simulation performed in SIMULINK/MATLAB. In addition, the simulation results of the proposed model and the PSB in SIMULINK/MATLAB are compared in order to verify the proposed model.

2. Modeling of Power Distribution Systems

The system considered here is a simplified model of a load served by an electric power distribution system. The D-STATCOM is connected in parallel with the load. The distribution system with the D-STATCOM and its per-phase equivalent circuit are shown in Figure 1 and Figure 2, respectively. The system consists of the source modeled as an infinite bus with inductive source impedance, the load modeled by a series RL circuit, the D-STATCOM modeled as a controllable current source, and coupling capacitor. The coupling capacitor is used as a harmonic filter or fixed compensation capacitors connected in parallel with the load.

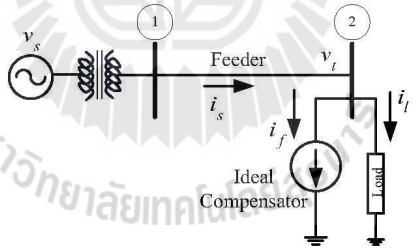

Figure 1. Distribution System with D-STATCOM

International Journal of Control and Automation
Vol. 6, No. 1, February, 2013

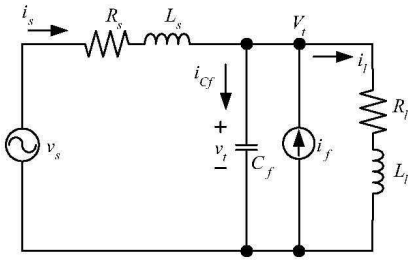

Figure 2. Per-phase Equivalent Circuit

2.1. Modeling with an Inductive *RL* Load

For an inductive load, *RL* load, it assumes that the source, the load and the D-STATCOM are balanced. Hence, the system dynamics can be described as:

$$L_s \frac{di_{s,abc}}{dt} = -R_s i_{s,abc} - v_{t,abc} + v_{s,abc} \quad (1)$$

$$C_f \frac{dv_{t,abc}}{dt} = -\frac{v_{t,abc}}{R_l} + i_{s,abc} + i_{f,abc} \quad (2)$$

Here, $i_{s,abc}$, $i_{f,abc}$, $v_{s,abc}$ and $v_{t,abc}$ are vectors consisting of individual phase quantities denoted in Figure 2, R_l is a load resistance, X_l is a load reactance, L_s is a source inductance, R_s is a source resistance, and C_f is a coupling capacitor. Under the assumption that zero sequence components are not presented, (1) – (2) can be transformed to an equivalent two-phase system by applying the following three-to-two phase transformation:

$$v_{s,xy} = v_{sa}e^{j0} + v_{sb}e^{j2\pi/3} + v_{sc}e^{j4\pi/3} \quad (3)$$

Where the complex number, $v_{s,xy} \triangleq v_{sx} + jv_{sy}$. This is followed by the following rotational transformation:

$$v_{s,dq} \triangleq v_{sd} + jv_{sq} = e^{-j\theta}v_{s,xy} \quad (4)$$

Applying the transformations, (1) – (2) can be written as:

$$C_f \dot{v}_{td} = -i_{ld} + \omega C_f v_{tq} + i_{sd} + i_{fd} \quad (5)$$

$$C_f \dot{v}_{tq} = -i_{lq} - \omega C_f v_{td} + i_{sq} + i_{fq} \quad (6)$$

$$L_l \dot{i}_{ld} = -R_l i_{ld} + \omega L_l i_{lq} + v_{td} \quad (7)$$

$$L_l \dot{i}_{lq} = -R_l i_{lq} - \omega L_l i_{ld} + v_{tq} \quad (8)$$

Where $\omega \triangleq \frac{d\theta}{dt}$ is to be designed and also be a function of time.

International Journal of Control and Automation
Vol. 6, No. 1, February, 2013

2.2. Choice of the Reference Frame

We choose the dq reference frame which is similar to that used for field-oriented control of three phase AC machines. Thus, angle θ used in (4) is defined by $\theta = \tan^{-1}(v_{ty}/v_{tx})$. This implies that

$$v_{tq} \equiv 0 \rightarrow \dot{v}_{tq} = 0 \tag{9}$$

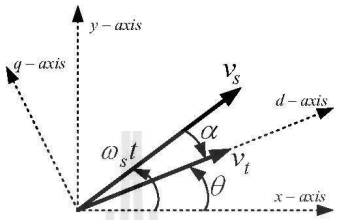

Figure 3. Orientation of Reference Frames

Defining $\alpha = \theta - \omega_s t$, where ω_s is the power frequency, we get $v_{s,dq} = V_s.e^{-j\alpha}$, where V_s is the magnitude of the supply voltage. The relative orientation of the vectors $v_{t,dq}$, $v_{s,dq}$ and the reference frame are shown in Figure 3. The system equations for the RL load can now be rewritten as:

$$L_s\dot{i}_{sd} = -R_s i_{sd} + \omega L_s i_{sq} - v_{td} + V_s \cos\alpha \tag{10}$$
$$L_s\dot{i}_{sq} = -R_s i_{sq} - \omega L_s i_{sd} - V_s \sin\alpha \tag{11}$$
$$C_f\dot{v}_{td} = -i_{ld} + i_{sd} + i_{fd} \tag{12}$$
$$L_l\dot{i}_{ld} = -R_l i_{ld} + \omega L_l i_{lq} + v_{td} \tag{13}$$
$$L_l\dot{i}_{lq} = -R_l i_{lq} - \omega L_l i_{ld} \tag{14}$$
$$\dot{\alpha} = \omega - \omega_s \tag{15}$$
$$\omega = \frac{-i_{lq}+i_{sq}+i_{fq}}{C_f v_{td}} \tag{16}$$

Where (16) is derived by using (9). This should be note that ω varies with time and is different from ω_s. Since $v_{tq} \equiv 0$, v_{td} represents the instantaneous magnitude of the phase voltages $v_{t,abc}$, while i_{fq} denotes the instantaneous reactive current supplied by the D-STATCOM. In addition, in the absence of negative sequence components, all the state variables in (10) – (15) is constant in steady state. Thus, this balanced three-phase system is effectively transformed into an equivalent DC system and its control problem is therefore simplified. (16) defines ω for the RL load. Thus, (10) – (16) define the system which can be used to design a controller.

International Journal of Control and Automation
Vol. 6, No. 1, February, 2013

3. D-STATCOM Modeling and Control

3.1. D-STATCOM Modeling

The basic circuit diagram and control of the D-STATCOM system are shown in Figure 4. It consists of a three-phase voltage source converter (VSC), an interfacing inductor, a DC link capacitor, and its control system. The VSC is connected to the network through a transformer and the interfacing inductor which are also used to filter high-frequency components of compensating currents. The inductance L_f in this figure represents the leakage inductance of the transformer and the interfacing inductor. The switching losses of the converter and the copper losses of the transformer are represented by a resistance R_f. In this paper, the D-STATCOM is used for load voltage regulation by injecting appropriate reactive power. Therefore, the control systems of the D-STATCOM consist of current control, DC voltage control, and AC voltage control. The primary control objective is to rapidly regulate the reactive current i_{fq} to the reference value (i_{fq}^*) which is generated by a load voltage controller. A secondary control objective is to keep the DC voltage at a desired value. It assumes that the internal dynamics of the D-STATCOM are slower than the switching period of the converter [16], so the D-STATCOM dynamics can be written as:

$$L_f \frac{di_{f,abc}}{dt} = -R_f i_{f,abc} - v_{t,abc} + v_{st,abc} \tag{17}$$

$$C_{dc}\dot{v}_{dc} = -\frac{v_{dc}}{R_d} - v_{st,abc}^T i_{f,abc} \tag{18}$$

Here, v_{dc} is the D-STATCOM's DC voltage, v_{st} is the D-STATCOM's output AC voltage, i_f is the D-STATCOM's output current, v_t is the load voltage, while the subscript "*abc*" implies three-phase vectors consisting of individual phase quantities. Parameters in these equations are DC link capacitance, C_{dc}, and capacitor leakage resistance, R_d. After applying the three-phase to two-phase transformation given by (3) followed by the rotational transformation of (4), the D-STATCOM dynamics can be rewritten as:

$$L_f \dot{i}_{fd} = -R_f i_{fd} + \omega L_f i_{fq} - v_{td} + k_p u_d v_{dc} \tag{19}$$

$$L_f \dot{i}_{fq} = -R_f i_{fq} - \omega L_f i_{fd} + k_p u_q v_{dc} \tag{20}$$

$$C_{dc}\dot{v}_{dc} = -\frac{v_{dc}}{R_d} - \frac{3}{2}k_p u_d i_{fd} - \frac{3}{2}k_p u_q i_{fq} \tag{21}$$

Where ω has been previously defined in (16), v_{dc}, i_{fd} and i_{fq} represent the state variables of the D-STATCOM, k_p is a constant value depending on the type of converters and transformer ratio, while u_d and u_q are the control inputs.

International Journal of Control and Automation
Vol. 6, No. 1, February, 2013

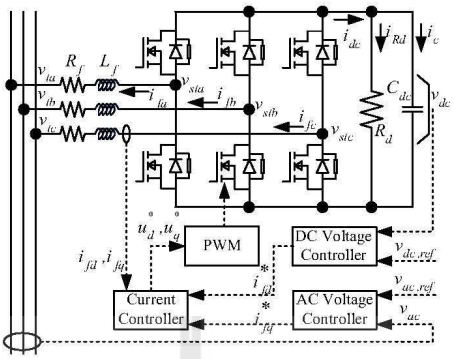

Figure 4. Basic Circuit Diagram and Control of the D-STATCOM System

3.2. D-STATCOM Modeling

The equations in (19) and (20) are used for designing the D-STATCOM current controller. These equations clearly show that the D-STATCOM output currents are induced by its output voltage modulation. However, the current control of the converter on the *dq* reference frame is a two-input two-output system with cross coupling between active and reactive currents. To eliminate the cross coupling effect, a decoupling control based on the *dq* reference frame is introduced where the proportional-plus-integral (PI) regulators are used to control the D-STATCOM currents in this work. The current control structure for the D-STATCOM and the D-STATCOM output current are detailed in Figure 5. The D-STATCOM output AC voltage, v_{st}, is generated by the VSC with pulse width modulation (PWM) and the D-STATCOM output voltage commands, u_d^* and u_q^*, are the inputs. The VSC with PWM can be simplified as $\frac{k_p v_{dc}}{sT_d+1}$ where T_d is the dead time.

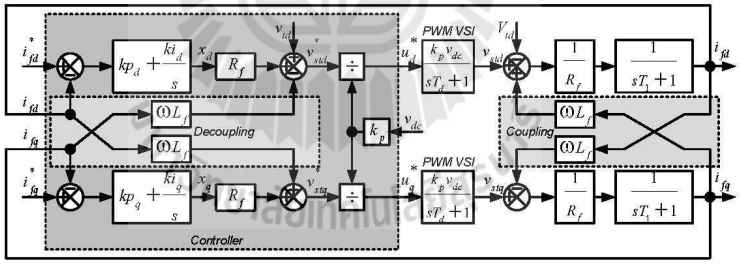

Figure 5. Current Control Structure for the D-STATCOM

3.3. DC Voltage Control (DC Link Voltage Control)

The secondary control objective is to keep v_{dc} around its reference. This objective cannot be achieved directly by u_d through (21) as there might be possibility of i_{fd} going to zero during a transient. However, v_{dc} can be controlled indirectly by adjusting i_{fd}. For designing the DC voltage controller, (21) is used. Although, v_{dc} can be controlled by varying i_{fd}, i_{fq} still affects v_{dc} through $u_q i_{fq}$ of (21). To eliminate this effect, the controller with decoupling, $u_q i_{fq}$, is applied where the proportional-plus-integral (PI) regulators are used to control the DC voltage. The DC voltage control structure and the D-STATCOM DC voltage are demonstrated in Fig. 6. The active current command i_{fd}^*, accounting for the DC voltage regulation, can be generated by the DC voltage controller with the DC voltage deviation as its input. The i_{fd}^* is used as the input of the current control, $G_{c,i}(s)$, then the controlled active current results in the regulation of the D-STATCOM's DC link voltage.

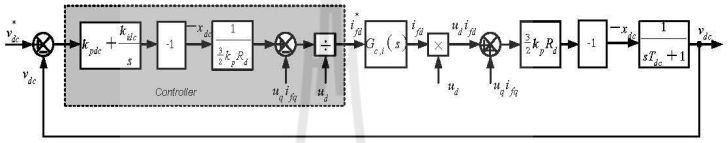

Figure 6. DC Voltage Control Structure and the D-STATCOM dc Voltage

The PI controller parameters depend on the parameters of the closed-loop transfer function, natural frequency (ω_0), damping coefficient (ζ), and pole value (p). In general, ω_0 and ζ characterize the desired system behavior and they are fixed, while the pole value can be chosen. Specific pole values can be imposed by using supplementary conditions. In this paper, the conditions for choosing the pole value refer to the symmetrical optimum method that is described in [17] and [18], which simplify expressions of the PI parameters. The goal is to find the pole value of the closed-loop transfer function which satisfies the assumptions of the symmetrical optimum method around ω_0 for the transfer function of the open-loop system.

4. Load Voltage Control using the Loop Shaping Method

Based on the distribution system model described in the previous section, we are now to design the load voltage controller. In addition, the D-STATCOM model and its control were integrated with the power distribution system for designing the load voltage controller. From the current control with decoupling as shown in Figure 5, the control inputs, u_d and u_q, of the D-STATCOM dynamics in (19) – (21) can be written as:

$$u_d = \frac{1}{k_p v_{dc}}\left[kp_d R_f\left(i_{fd}^* - i_{fd}\right) + ki_d R_f f_d - \omega L_f i_{fq} + v_{td}\right] \quad (22)$$

$$u_q = \frac{1}{k_p v_{dc}}\left[kp_q R_f\left(i_{fq}^* - i_{fq}\right) + ki_q R_f f_q + \omega L_f i_{fd}\right] \quad (23)$$

International Journal of Control and Automation
Vol. 6, No. 1, February, 2013

While the active current command i_{fd}^{*} can be derived from the DC voltage control with decoupling as shown in Figure 6 as:

$$i_{fd}^{*} = \frac{1}{u_d}\left[\frac{-kp_{dc}}{\frac{3}{2}k_p R_d}(v_{dc}^{*} - v_{dc}) - \frac{ki_{dc}}{\frac{3}{2}k_p R_d}v_d - u_q i_{fq}\right] \tag{24}$$

Where $\omega L_f i_{fq}$, $\omega L_f i_{fd}$ and $u_q i_{fq}$ are the decoupling terms of the current control and the DC voltage control, respectively. In addition, the dynamic equations of the current control and the DC voltage control that were integrated with the system can be written as:

$$\dot{f}_d = i_{fd}^{*} - i_{fd} \tag{25}$$

$$\dot{f}_q = i_{fq}^{*} - i_{fq} \tag{26}$$

$$\dot{v}_d = v_{dc}^{*} - v_{dc} \tag{27}$$

Therefore, the distribution system model in (10) – (16), the D-STATCOM dynamics in (19) – (21) and the dynamic equations of the D-STATCOM controllers in (22) – (27) can be used to form a set of state equations to design the load voltage controller for the *RL* load. For designing the load voltage controller, the load voltage v_{td} is chosen as the output of the system with the reactive current command i_{fq}^{*} as the control input. However, these state equations are a set of nonlinear differential equations. To investigate the dynamic performance of these systems, linear approximation is applied. Linearization of these systems around a specified operating point that described in [19] gives a set of linear equations for the inductive *RL* load as shown in (28).

$$\frac{d}{dt}\begin{bmatrix}\Delta v_{td}\\ \Delta i_{sd}\\ \Delta i_{sq}\\ \Delta i_{fd}\\ \Delta i_{fq}\\ \Delta v_{dc}\\ \Delta\alpha\\ \Delta f_d\\ \Delta f_q\\ \Delta v_d\\ \Delta i_{ld}\\ \Delta i_{lq}\end{bmatrix} = \begin{bmatrix} 0 & k_{isd1} & 0 & k_{ifd1} & 0 & 0 & 0 & 0 & 0 & 0 & k_{ild1} & 0\\ k_{vtd2} & k_{isd2} & k_{isq2} & 0 & k_{ifq2} & 0 & k_{\alpha 2} & 0 & 0 & 0 & 0 & k_{ilq2}\\ k_{vtd3} & k_{isd3} & k_{isq3} & 0 & k_{ifq3} & 0 & k_{\alpha 3} & 0 & 0 & 0 & 0 & k_{ilq3}\\ k_{vtd4} & 0 & k_{isq4} & k_{ifd4} & k_{ifq4} & k_{vdc4} & 0 & k_{fd4} & k_{fq4} & k_{vd4} & 0 & k_{ilq4}\\ 0 & 0 & 0 & 0 & k_{ifq5} & 0 & 0 & 0 & k_{fq5} & 0 & 0 & 0\\ k_{vtd6} & 0 & k_{isq6} & k_{ifd6} & k_{ifq6} & k_{vdc6} & 0 & k_{fd6} & k_{fq6} & k_{vd6} & 0 & k_{ilq6}\\ k_{vtd7} & 0 & k_{isq7} & 0 & k_{ifq7} & 0 & 0 & 0 & 0 & 0 & 0 & k_{ilq7}\\ 0 & 0 & k_{isq8} & k_{ifd8} & k_{ifq8} & k_{vdc8} & 0 & 0 & k_{fq8} & k_{vd8} & 0 & k_{ilq8}\\ 0 & 0 & 0 & 0 & k_{ifq9} & 0 & 0 & 0 & 0 & 0 & 0 & 0\\ 0 & 0 & 0 & 0 & 0 & k_{vdc10} & 0 & 0 & 0 & 0 & 0 & 0\\ k_{vtd11} & 0 & k_{isq11} & 0 & k_{ifq11} & 0 & 0 & 0 & 0 & 0 & k_{ild11} & k_{ilq11}\\ k_{vtd12} & 0 & k_{isq12} & 0 & k_{ifq12} & 0 & 0 & 0 & 0 & 0 & k_{ild12} & k_{ilq12}\end{bmatrix}\begin{bmatrix}\Delta v_{td}\\ \Delta i_{sd}\\ \Delta i_{sq}\\ \Delta i_{fd}\\ \Delta i_{fq}\\ \Delta v_{dc}\\ \Delta\alpha\\ \Delta f_d\\ \Delta f_q\\ \Delta v_d\\ \Delta i_{ld}\\ \Delta i_{lq}\end{bmatrix} + \begin{bmatrix}0\\0\\0\\b_{ifd}\\b_{ifq}\\b_{vdc}\\0\\b_{fd}\\b_{fq}\\0\\0\\0\end{bmatrix}\Delta i_{fq}^{*} \tag{28}$$

Table 1. Parameters of the Power Distribution System and the D-STATCOM

Distribution power system parameters	
Nominal source voltage (V_s)	12.81 kV
Desired load voltage magnitude (v_{td}^*)	11.00 kV
Source resistance and inductance (R_s and L_s)	1 Ω and 10 mH
Load resistance and inductance (R_l and L_l)	10 Ω and 10 mH
System frequency (f_s)	50 Hz
D-STATCOM parameters	
Coupling capacitor (C_f)	50 μF
Interfacing resistance and inductance (R_f and L_f)	0.1 Ω and 10 mH
Constant value of converter (k_p)	0.55
DC link voltage (v_{dc})	30 kV
DC link capacitance (C_{dc})	200 μF
Capacitor leakage resistance (R_d)	61.273 $k\Omega$
Switching frequency (f_{sw})	10 kHz

Base on the parameters of the distribution system and the D-STATCOM as shown in Table 1 and the D-STATCOM controllers as described in the previous section, the operating points of the systems can be obtained as shown in Table 2. Bode plots of the transfer function $\frac{\Delta v_{td}(s)}{\Delta i_{fq}^*(s)}$ for the linearized system of (28) with the operating point as shown in Table 2 is shown in Figure 7.

Table 2. Operating Points of the System

V_s (kV)	12.81 (1.0 pu.)	11.53 (0.9 pu.)	10.25 (0.8 pu.)	8.97 (0.7 pu.)
i_{fq0} (A)	0	-463.22	-960.10	-1516.0
v_{td0} (kV)	11.00	11.00	11.00	11.00
i_{sd0} (A)	1002.08	1004.03	1010.46	1022.98
i_{sq0} (A)	-143.97	321.48	818.35	1374.25
i_{fd0} (A)	-0.89	-2.84	-9.27	-21.79
v_{dc0} (kV)	30	30	30	30
α_0 (red)	-0.237	-0.306	-0.400	-0.537
f_{d0} (A)	0	0	0	0
f_{q0} (A)	0	0	0	0
v_{d0} (kV)	0	0	0	0
i_{ld0} (A)	1001.19	1001.19	1001.19	1001.19
i_{lq0} (A)	-314.53	-314.53	-314.53	-314.53

International Journal of Control and Automation
Vol. 6, No. 1, February, 2013

The bode plots of the transfer function for various operating conditions corresponding to a different value of i_{fq}, are also shown in Figure 7. Remarkably, the system dynamic in (28) gives non-minimum phase.

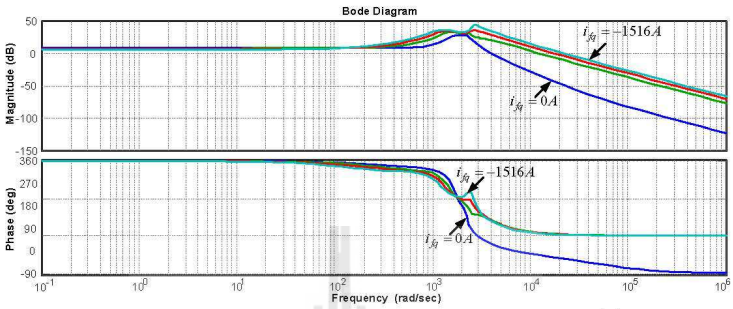

Figure 7. Bode Plots of the Transfer Function $\frac{\Delta v_{td}(s)}{\Delta i^*_{fq}(s)}$

4.1. Linear Controller Design using the Loop Shaping Method

The load voltage control is a single-input, single-output (SISO) control system with the load voltage v_{td} chosen as the output of the system and the reactive current command i^*_{fq} as the control input. For SISO systems, the classical loop shaping concept is a basis for designing the load voltage controller. The unity-feedback SISO system is depicted in Figure 8 where $P(s)$ represents the plant transfer function and $C(s)$ represents the controller transfer function. The signals $r(t)$, $d_i(t)$, $d_o(t)$, and $n(t)$ are reference input, input disturbance, output disturbance, and sensor noise, respectively. The signal $y(t)$ is the output, $e(t)$ is the tracking error, and $u(t)$ is the control input. The definitions of the open-loop transfer function $L(s)$, the sensitivity function $S(s)$, and the complementary sensitivity function $T(s)$ are:

$$L(s) = P(s)C(s) \quad (29)$$
$$S(s) = [1 + L(s)]^{-1} \quad (30)$$
$$T(s) = L(s)[1 + L(s)]^{-1} \quad (31)$$

The classical loop shaping is a design procedure that explicitly involves the shaping or the adjustment of the magnitude or loop-gain of the open-loop transfer function, $L(s)$, within a desired frequency spectrum. There are three basic types of loop shaping specifications, which are imposed in a different frequency [20]. i) At low frequencies we require $|L(j\omega)|$ to be large, so that $|S(j\omega)|$ is small and $T(j\omega) \approx 1$. This ensures good command tracking, and low sensitivity to plant variations, two of the most important benefits of the feedback. ii) At high frequencies we require $|L(j\omega)|$ to be small, so that $|T(j\omega)|$ is small. This ensures that the output $y(t)$ will be relatively insensitive to the sensor noise $n(t)$, and that the system will remain closed-loop stable in the appearance of plant variations at these frequencies. iii) $L(j\omega)$

should not drop-off too quickly near the crossover frequency to avoid internal instability. The specifications for the load voltage control performance in this paper are as follow:

1) Zero steady state tracking error.

2) At least 40 dB of disturbance rejection at low frequency.

3) The output $y(t)$ must be relatively insensitive to the sensor noise $n(t)$ at high frequency.

4) The gain margin should be greater than 3 dB and the phase margin should be greater than 40°.

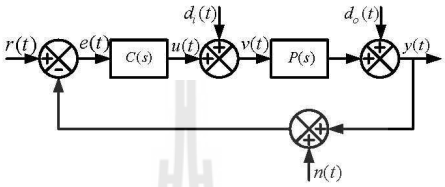

Figure 8. Block Diagram of a Unity Feedback SISO System

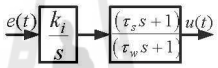

Figure 9. Designed Controller for the Load Voltage Control

Table 3. Controller Parameters and the Stability Margins

5.1) Current and DC voltage control without decoupling			
$v_s\ (kV)$	11.53	10.25	8.97
$i_{fq}\ (A)$	-463	-960	-1516
$v_{td}\ (kV)$	11.00	11.00	11.00
k_i	110	70	30
τ_s	0.00024	0.00024	0.00024
τ_w	0.002	0.002	0.002
GM(dB)	6.75	5.26	4.43
PM(deg)	41.2	42.5	45.0
5.2) Current and DC voltage control with decoupling			
$v_s\ (kV)$	11.53	10	8.97
$i_{fq}\ (A)$	-463	-960	-1516
$v_{td}\ (kV)$	11.00	11.00	11.00
k_i	110	70	30
τ_s	0.00024	0.00024	0.00024
τ_w	0.002	0.002	0.002
GM(dB)	5.94	4.31	3.68
PM(deg)	42.0	44.9	49.2

International Journal of Control and Automation
Vol. 6, No. 1, February, 2013

To satisfy the specifications 1) and 2) requires an integral action in the controller. In addition, the load voltage control gives non-minimum phase, so that the lag compensator is used for satisfying the specifications 3) and 4). The designed controller for the load voltage control is shown in Figure 9. By using MATLAB for adjusting the open-loop transfer function, $L(j\omega)$, to satisfy the loop shaping specifications described above, the controller parameters and the stability margins for the inductive RL load with various operating conditions corresponding to a different value of i_{fq} are obtained and presented in Table 3. The bode plots of the plant, desired controller, and the open-loop system including the plant augmented with the desired controller when the source voltage is 0.7 per-unit are demonstrated in Figure 10 whereas the root locus of the closed-loop system are shown in Figure 11.

In Figure 10, the bode plots for the inductive RL load, shows that $|L(j\omega)|$ is greater than 40 dB at low frequency while at high frequency, $|L(j\omega)|$ is small. The gain margin of the control loop is 3.68 dB at 487 rad/s and the phase margin is 49.2° at 122 rad/s, therefore specifications 1) – 4) are satisfied. In accordance with the root locus of the closed-loop system shown in Figure 11, all the closed-loop poles are on the left-half of the complex plane (LHP). Thus, the closed-loop system of the inductive RL load is stable.

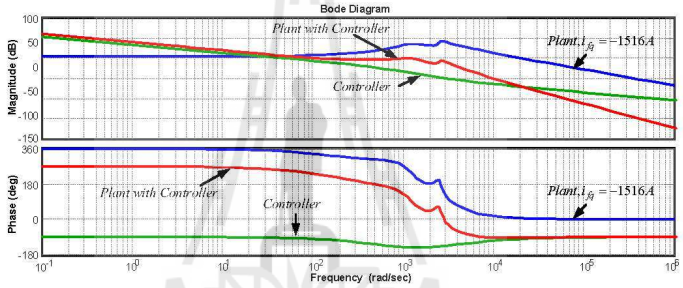

Figure 10. Open-loop System Including the Plant with the Desired Controller

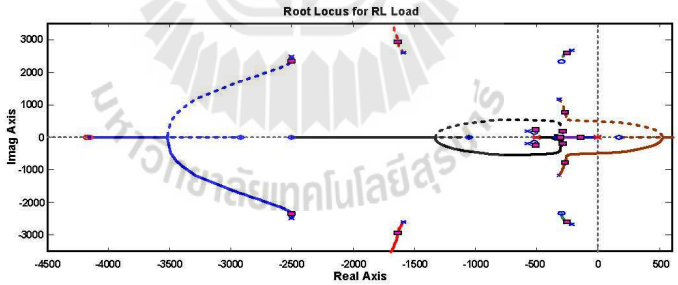

Figure 11. Root Locus of the Closed-loop System

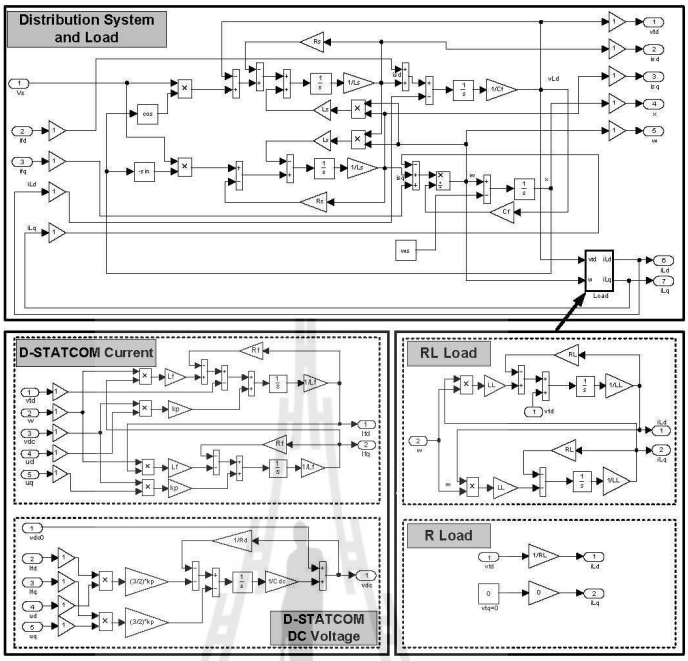

Figure 12. Test Power System and its Controllers in MATLAB Simulink

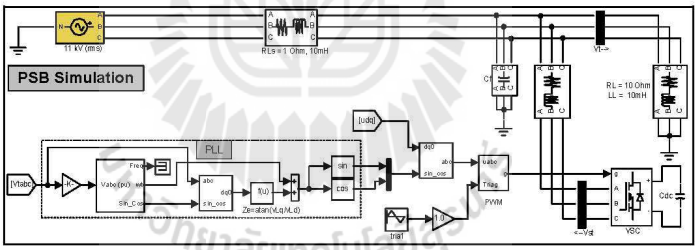

Figure 13. D-STATCOM System using MATLAB Power System Blockset (PSB)

5. Simulation Results and Discussion

The proposed D-STATCOM mathematical model, as summarized in (28), and its control were integrated with the power distribution system and the load voltage controller. This test system was formulated and therefore simulated in MATLAB

International Journal of Control and Automation
Vol. 6, No. 1, February, 2013

Simulink. The load voltage controller described in Section 4 provides the reactive current reference signal, i_{fq}^{*}, to the D-STATCOM controller while the active current reference signal, i_{fd}^{*}, is generated by the DC voltage controller. Other reference input to the D-STATCOM control is the desired constant DC voltage, v_{dc}^{*}.

The compensating current and DC voltage control schemes shown in Figures 5 and 6 are applied. The D-STATCOM model is integrated with the power distribution system and the load are shown in Figure 12 as created in SIMULINK/MATLAB. Simulation results for this integrated system when the source voltage are dropped to 0.9 pu., 0.8 pu. and 0.7 pu., are presented for the inductive *RL* load.

To verify the accuracy of the proposed D-STATCOM simulation, the similar task was also conducted by using MATLAB power system blockset (PSB) for simulating the D-STATCOM test system in power-electronic switching model. This can be summarized as shown in Figure 13.

With the load voltage controller designed using the classical loop shaping method, the stability margins (*i.e.*, both gain margin and phase margin) can be simply achieved to satisfy the specification. The response of the designed controller shows a good performance and preferable stability margins. Figure 14 shows the responses of the load voltage to the decreased source voltages down to 0.9 pu., 0.8 pu., and 0.7 pu., respectively. When considering the sag of the source voltage at 0.9 pu., we can see that the load voltage reaches its reference within 0.01 s. whilst the sags at 0.8 pu. and 0.7 pu. take longer time to recover, within 0.02 s.

Additionally, the responses of the load voltage control with and without the decoupling are compared. As can be seen, the load voltage controller with the decoupling gives better dynamic responses. It is because smaller settling time is experienced when the source voltage is decreased at 0.9 pu., 0.8 pu., and 0.7 pu., respective. Clearly, Figure 15 shows that the responses of the DC voltage for the D-STATCOM controllers with the decoupling also have smaller settling time and overshoot than that without the decoupling. In comparison, the simulation results show that the voltage controller with the decoupling is conservative and gives better performances.

Moreover, Figures 16 – 18 compares the dynamic responses of the load voltage, the DC voltage, and the D-STATCOM's currents of the proposed model and the PSB simulation. As a result, the responses of both simulations are thereby justifying the proposed model and the controller design.

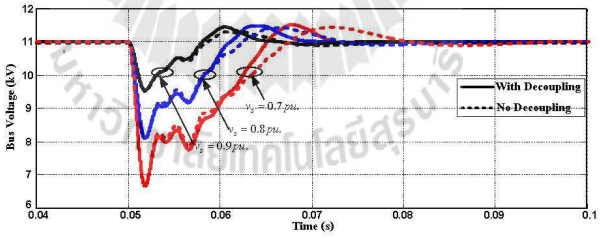

Figure 14. Load Voltage Responses

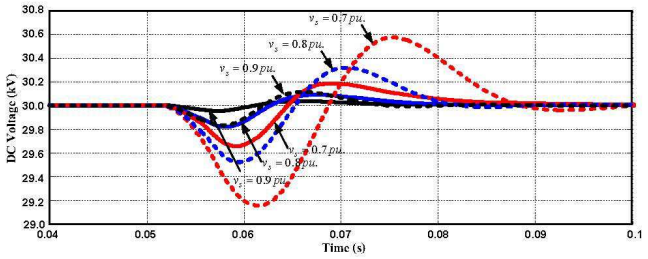

Figure 15. DC Voltage Responses

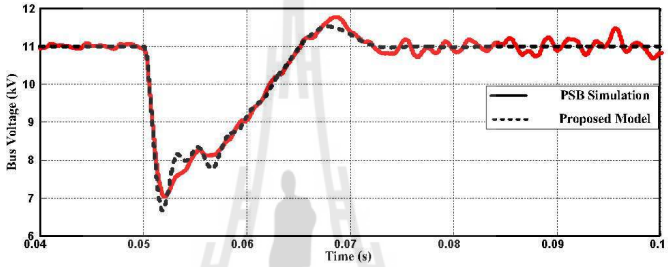

Figure 16. Comparisons for the Responses of the Load Voltage

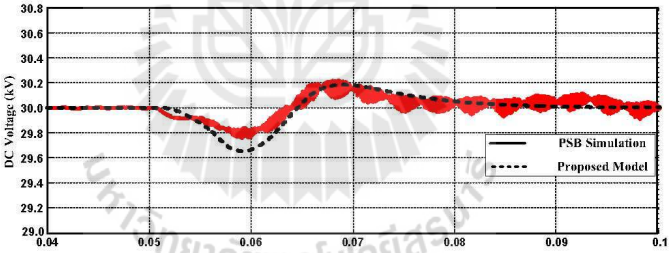

Figure 17. Comparisons for the Responses of the DC Voltage

International Journal of Control and Automation
Vol. 6, No. 1, February, 2013

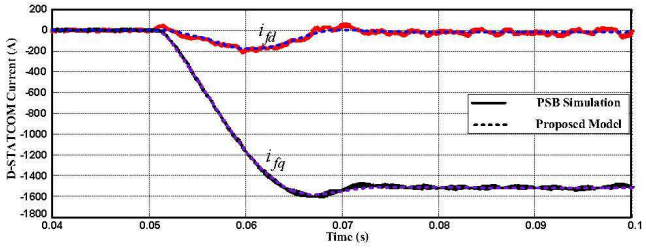

Figure 18. Comparison for the Responses of the D-STATCOM Current

6. Conclusion

This paper illustrates the system modeling and control design for the load voltage regulation using D-STATCOM. The D-STATCOM currents and DC voltage decoupling control based on the *dq* reference frame are used with the symmetrical optimum method to obtain the parameters of the PI controllers. This derived model is used for the load voltage controller design based on the linearized technique, called the classical loop shaping method. Performance of the propose model and the controller design are verified by using computer simulation performed in SIMULINK/MATLAB. The results show that the load voltage controller including the D-STATCOM controllers with the decoupling control has a good performance and sufficient stability margins. In addition, the simulation results obtained by using the proposed model in the frequency domain are compared with those acquired from MATLAB's Simulink - Power System Blockset to confirm the accuracy of this simulation.

Acknowledgements

One of the authors, Mr. Kittaya Somsai, would like to thank the office of the Higher Education Commission, Thailand for supporting a grant fund under the program Strategic Scholarships for Frontier Research Network for the Joint Ph.D Program Thai Doctoral degree for this research.

References

[1] R. C. Dugan, M. F. McGranaghan and H. Wayne Beaty, "Electrical Power System Quality", McGraw-Hill **(1996)**.
[2] A. Ghosh and G. Ledwich, "Power quality enhancement using custom power devices", Kluwer Academic, Massachusetts, **(2002)**.
[3] P. S. Sensarma, K. R. Padiya and V. Ramanarayanan, "Analysis and Performance Evaluation of a Distribution STATCOM for Compensating Voltage Fluctuations", IEEE Trans. Power Del. vol. 16, no. 2, **(2001)**, pp. 259 – 264.
[4] P. Rao, M. L. Crow and Z. Yang, "STATCOM control for power system voltage control applications", IEEE Trans. Power Del., vol. 15, no. 4, **(2000)**, pp. 1311 – 1317.
[5] K. R. Padiyar and A. M. Kulkarni, "Design of reactive current and voltage controller of static condenser", Electric Power Energy System, vol. 19, no. 6, **(1997)**, pp. 397 – 410.
[6] C. Hochgraf and R. H. Lasseter, "Statcom controls for operation with unbalanced voltages", IEEE Trans. Power Del., vol. 13, no. 2, **(1998)**, pp. 538 – 544.
[7] C. Chen and G. Joos, "Series and shunt active power conditioners for compensating distribution system faults", Canadian Conferences on Electrical Computer Engineering **(2000)** March 7 – 10, pp. 1182 – 1186.

[8] C. Schauder and H. Mehta, "Vector analysis and control of advanced static VAr compensators", IEE – Gen. Transm. Distrib., **(1993)**, pp. 299 – 306.
[9] E. Acha, V. G. Agelidis, O. Anaya-Lara and T. J. E. Miller, "Power Electronic control in Electrical system", Reed Educational and Professional, Oxford **(2002)**.
[10] C. Schauder, M. Gernhardt, E. Stacey, T. Lemak, L. Gyugyi, T. W. Cease and A. Edris, "Development of ±100 MVAr static condenser for voltage control of transmission systems", IEEE Trans. Power Del., vol. 10, no. 3, **(1995)**, pp. 1486 – 1496.
[11] W. -L. Chen, W. -G. Liang and H. -S. Gau, "Design of a mode decoupling STATCOM for voltage control of wind-driven induction generator systems", IEEE Trans. Power Del., vol. 25, no. 3, **(2010)**, pp. 1758 – 1767.
[12] M. G. Molina and P. E. Mercado, "Control design and simulation of DSTATCOM with energy storage for power quality improvements", IEEE/PES Transmission & Distribution Conf. Exposition, Latin America, TDC '06, **(2006)** August 15-18, pp. 1 – 7.
[13] G. G. Pablo and G. C. Aurelio, "Control system for a PWM-based STATCOM", IEEE Trans. Power Del., vol. 15, no. 4, **(2000)**, pp. 1252 – 1257.
[14] C. K. Sao, P. W. Lehn, M. R. Iravani and J. A. Martinez, "A benchmark system for digital time-domain simulation of a pulse-width-modulated D-STATCOM", IEEE Trans. Power Del., vol. 17, no. 4, **(2002)**, pp. 1113 – 1120.
[15] P. W. Lehn and M. R. Iravani, "Experimental evaluation of STATCOM closed loop dynamics", IEEE Trans. Power Del., vol. 13, no. 4, **(1998)**, pp. 1378 – 1384.
[16] A. Jain, K. Joshi, A. Behal and N. Mohan, "Voltage regulation with STATCOMs: modeling, control and results", IEEE Trans. Power Del., vol. 21, no. 2, **(2006)**, pp. 726 – 735.
[17] M. P. Kazmierkowski, R. Krishnan and F. Blaabjerg, "Control in power electronics selected problems", Elsevier Science, California **(2002)**.
[18] F. Frohr and F. Orttenburger, "Introduction to electronic control engineering", Second Wiley Eastern Reprint, New Delhi **(1992)**
[19] J. D'Azzo and H. Houpis, "Linear control system analysis and design: conventional and modern", McGraw-Hill, New York **(1995)**.
[20] C. Barratt and S. Boyd, "Interactive Loop-Shaping Design of MIMO Controllers", IEEE Symposium on Computer Aided Control System Design, Napa, California **(1992)** March, pp. 76 – 81.

Authors

Kittaya Somsai

Kittaya Somsai received the B.Eng degree in Electrical Engineering from Rajamangala University of Technology Thanyaburi (RMUTT) and the M.Eng degree in Electrical Engineering from King Mongkut's Institute of Technology North Bangkok (KMITNB), THAILAND in 2003 and 2005 respectively. He is currently working toward the Ph.D. degree. He is currently researching on Power System Control, Custom Power Device (CPD) and Flexible AC Transmission Systems (FACTS).

Nitus Voraphonpiput

Nitus Voraphonpiput received his B.Eng, M.Eng and Ph.D.Eng in Electrical Engineering from King Mongkut's Institute of Technology North Bangkok (KMITNB), THAILAND in 1993, 1998 and 2007 respectively. He is an engineer in charge of Power Purchase Agreement Division, Electricity Generating Authority of Thailand (EGAT). His current research interests on Power System Control and Flexible AC Transmission Systems (FACTS).

International Journal of Control and Automation
Vol. 6, No. 1, February, 2013

Thanatchai Kulworawanichpong

Thanatchai Kulworawanichpong is an associate professor of the School of Electrical Engineering, Institute of Engineering, Suranaree University of Technology, Nakhon Ratchasima, THAILAND. He received B.Eng. with first-class honour in Electrical Engineering from Suranaree University of Technology, Thailand (1997), M.Eng. in Electrical Engineering from Chulalongkorn University, Thailand (1999), and Ph.D. in Electronic and Electrical Engineering from the University of Birmingham, United Kingdom (2003). His fields of research interest include a broad range of power systems, power electronic, electrical drives and control, optimization and artificial intelligent techniques. He has joined the school since June 1998 and is currently a leader in Power System Research, Suranaree University of Technology, to supervise and co-supervise over 15 postgraduate students.

BIOGRAPHY

Mr. Kittaya Somsai is a lecturer at the Department of Electrical Engineering, Sakon Nakhon Campus, Rajamangala University of Technology Isan, Thailand. He received a B.E. in Electrical Engineering from Rajamangala University of Technology and a M.E. in Electrical Engineering from King Mongkut's Institute of Technology North Bangkok. He was a holder of the Thai government scholarship. His interests include FACT and custom power devices.